

Electronic Thesis and Dissertation Repository

---

9-16-2020 3:30 PM

# Effects of Oxidative Modifications on the Structure and Non-Canonical Functions of Cytochrome c Studied by Mass Spectrometry

Victor Yin, *The University of Western Ontario*

Supervisor: Konermann, Lars, *The University of Western Ontario*

A thesis submitted in partial fulfillment of the requirements for the Doctor of Philosophy degree in Chemistry

© Victor Yin 2020

Follow this and additional works at: <https://ir.lib.uwo.ca/etd>

 Part of the [Analytical Chemistry Commons](#), and the [Structural Biology Commons](#)

---

## Recommended Citation

Yin, Victor, "Effects of Oxidative Modifications on the Structure and Non-Canonical Functions of Cytochrome c Studied by Mass Spectrometry" (2020). *Electronic Thesis and Dissertation Repository*. 7332.

<https://ir.lib.uwo.ca/etd/7332>

This Dissertation/Thesis is brought to you for free and open access by Scholarship@Western. It has been accepted for inclusion in Electronic Thesis and Dissertation Repository by an authorized administrator of Scholarship@Western. For more information, please contact [wlsadmin@uwo.ca](mailto:wlsadmin@uwo.ca).

## Abstract

The peroxidase activity of the mitochondrial protein cytochrome *c* (cyt *c*) plays a critical role in triggering programmed cell death, or apoptosis. However, the native structure of cyt *c* should render this activity impossible due to the lack of open iron coordination sites at its heme cofactor. Despite its key biological importance, the molecular mechanisms underlying this structure-function mismatch remain enigmatic. The work detailed in this dissertation fills this knowledge gap by using mass spectrometry (MS) to decipher the central role that protein oxidative modifications and their associated structural changes play in activating the peroxidase function of cyt *c*.

Chapter 2 uses a suite of MS-based experiments to identify and characterize oxidative modifications in cyt *c* caused by the oxidant and canonical peroxidase substrate, H<sub>2</sub>O<sub>2</sub>. In doing so, we unravel the critical role that these *in situ* structural changes play in triggering the peroxidase activity of the protein via alteration of the coordination environment. Serendipitously, we also discover that certain functionally important oxidative modifications, particularly on Lys, can elude detection when using conventional bottom-up MS approaches. However, by applying top-down MS we could successfully detect these modifications.

Chapter 3 re-examines a popular and purportedly well-characterized model system for peroxidase-activated cyt *c*: cyt *c* treated with chloramine-T. By combining top-down MS with sample fractionation techniques, we uncover that this model system is in fact comprised of a broad ensemble of structurally and functionally distinct species. These species can be differentiated by the extent of oxidation at key Lys residues, which previously went undetected.

Chapter 4 expands on the previous chapters by probing the causal factors underpinning the production of oxidative modification products at Lys and other residues. We discover that Lys oxidation is catalyzed by the endogenous heme cofactor, while other transformations (e.g. Met oxidation) proceed via direct interaction with the oxidant.

Chapter 5 utilizes oxidized cyt *c* as a model system to test the compatibility of protein stability measurements in the gas phase to their counterparts in solution. Unlike many other protein systems, we discover that oxidized cyt *c* shows opposing stability trends in solution and in the gas phase.

**Keywords:** mass spectrometry, cytochrome *c*, peroxidase, protein oxidation, oxidative damage, ion mobility spectrometry.

## Summary for Lay Audience

Proteins are large molecules comprised of amino acids that play important roles in many aspects of biology. Proteins adapt a variety of functions, depending on their structure. Cytochrome *c* (cyt *c*) is a protein found in the mitochondria of cells that normally functions as an electron transporter, which is possible because of the iron-containing heme group in cyt *c*. Cyt *c* also has an alternative function (as a peroxidase), which plays a key role in triggering programmed cell death, or apoptosis. Despite this importance, it is poorly understood how cyt *c* can have peroxidase function despite structural features that should render it inactive. In this dissertation, we use mass spectrometry (MS) to study how oxidants can interact with cyt *c*, altering its structure and accommodating its peroxidase function.

We first studied the effects of the oxidant hydrogen peroxide (H<sub>2</sub>O<sub>2</sub>) on the structure and function of cyt *c* (Chapter 2). We uncovered that cyt *c* is extensively modified by H<sub>2</sub>O<sub>2</sub>. Using MS, we determined that these oxidative modifications cause structural changes near the heme that enable peroxidase function. A key finding was that oxidation of one type of amino acid, lysine, was critical.

We next focused on another oxidant, chloramine-T (CT) (Chapter 3). CT-treated cyt *c* has long been a popular model system for studying apoptosis and is thought to be simple and well-characterized. Using a combination of MS and purification techniques, we discovered that CT-treated cyt *c* is actually a mixture of structurally and functionally distinct species. The main difference between these species was the presence of lysine oxidation at key positions on the protein.

We then explored the processes underlying the formation of oxidative modifications in cyt *c* (Chapter 4). We determined that the heme plays a key role in producing lysine oxidation, while other amino acids (e.g. methionine) were oxidized independently of the heme group.



Finally, we used oxidized cyt *c* to compare the differences in protein stability using MS versus conventional spectroscopic techniques in solution (Chapter 5). Unlike many other proteins, we found that oxidized cyt *c* showed opposing stability trends in these two types of measurements.

## Co-Authorship Statement

The works described in chapters 2, 3, and 5 are published in the following respective articles:

Yin, V.; Shaw, G. S.; Konermann, L. Cytochrome *c* as a Peroxidase: Activation of the Precatalytic Native State by H<sub>2</sub>O<sub>2</sub>-Induced Covalent Modifications. *J. Am. Chem. Soc.* **2017**, *139* (44), 15701–15709. doi: 10.1021/jacs.7b07106. Reproduced with permission. © 2017 American Chemical Society.

Yin, V.; Mian, S. H.; Konermann, L. Lysine Carbonylation Is a Previously Unrecognized Contributor to Peroxidase Activation of Cytochrome *c* by Chloramine-T. *Chem. Sci.* **2019**, *10* (8), 2349–2359. doi: 10.1039/C8SC03624A. Reproduced with permission from the Royal Society of Chemistry.

Yin, V.; Konermann, L. Probing the Effects of Heterogeneous Oxidative Modifications on the Stability of Cytochrome *c* in Solution and in the Gas Phase. *J. Am. Soc. Mass Spectrom.* **2020**. In press. doi: 10.1021/jasms.0c00089. Reproduced with permission. © 2020 American Chemical Society.

The work described in Chapter 4 is incorporated into the following article:

Yin, V.; Holzschere, D; Konermann, L. Delineating Heme-Mediated versus Direct Protein Oxidation in Peroxidase-Activated Cytochrome *c* by Top-Down Mass Spectrometry. Submitted.

The original drafts of each article were written by the author. Subsequent edits were performed in collaboration between the author and Dr. Lars Konermann. The  $^1\text{H}$ -NMR spectra described in Chapter 2 were collected by Dr. Gary Shaw. A portion of the experimental work in Chapter 4 was performed in collaboration with Derek Holzscherer, under direct supervision by the author. All other experimental work and data analysis were performed by the author.

## Acknowledgements

As the cliché goes: “*it takes a village to raise a child*”. While I cannot possibly hope to get through everyone who has supported me up until this point, I will attempt to do this statement some justice.

First and foremost, I would like to thank my research supervisor, Prof. Lars Konermann. It is needless to say that without his support, none of this work would have been possible. As a fresh graduate student in Lars’s research group, while full of boundless curiosity and enthusiasm, I was certainly lacking in any competency or know-how. I credit Lars with not only providing me with the technical skills to conduct research, but also instilling in me the mindset necessary to be an effective researcher.

I would also like to thank all the members of the Konermann Lab (and beyond) with whom I’ve been fortunate to have the opportunity to work with. Since I joined, the group has always fostered a positive environment – slow to judge, quick to help – and for that I will always be grateful. I am also grateful to my friends and colleagues in the broader research community for their support and camaraderie.

I will always be indebted to my parents, who left everything behind in the hopes of a better life for them and their children in Canada. Without their sacrifices, I certainly would not be here today. As the first person in my family to even have a chance to go to college, let alone get a graduate degree, I hope that everything has been worthwhile.

Last, but certainly not least, I would like to thank my better half, Angel, for her seemingly endless patience and love, and for making me want to be a better person and a better scientist. Thank you.

# Table of Contents

<b>Abstract.....</b>	<b>ii</b>
<b>Summary for Lay Audience.....</b>	<b>iv</b>
<b>Co-Authorship Statement .....</b>	<b>vi</b>
<b>Acknowledgements .....</b>	<b>viii</b>
<b>Table of Contents .....</b>	<b>ix</b>
<b>List of Symbols and Abbreviations .....</b>	<b>xv</b>
<b>Chapter 1. Introduction.....</b>	<b>1</b>
<b>1.1. Protein Structure and Function .....</b>	<b>1</b>
<b>1.2. Cytochrome <i>c</i> .....</b>	<b>2</b>
<b>1.3. Protein Oxidation .....</b>	<b>6</b>
<b>1.4. Common Methods for Studying Protein Structure.....</b>	<b>7</b>
1.4.1. Optical Spectroscopy .....	7
1.4.2. High-Resolution Structural Techniques.....	8
<b>1.5. Mass Spectrometry and Associated Techniques.....</b>	<b>9</b>
1.5.1. Electrospray Ionization Mass Spectrometry (ESI-MS) .....	10
1.5.2. Mass Spectrometers for Protein Analysis.....	11
1.5.3. Ion Mobility Spectrometry.....	14
<b>1.6. ESI-MS Experiments for Studying Protein Structure .....</b>	<b>16</b>

1.6.1. Primary Structure: Sequencing .....	16
1.6.2. Higher Order Structure: Covalent Labeling Experiments .....	18
1.6.3. Higher Order Structure: Native Mass Spectrometry.....	19
<b>1.7. Scope of Thesis.....</b>	<b>20</b>
<b>1.8. References .....</b>	<b>22</b>
<b>Chapter 2. Elucidation of an H<sub>2</sub>O<sub>2</sub>-Induced, <i>In Situ</i> Activation Mechanism of the Peroxidase Activity of Cytochrome <i>c</i> .....</b>	<b>34</b>
<b>2.1. Introduction .....</b>	<b>34</b>
<b>2.2. Materials and Methods .....</b>	<b>37</b>
2.2.1. Materials. ....	37
2.2.2. Optical Spectroscopy. ....	37
2.2.3. Protein Samples. ....	37
2.2.4. NMR Spectroscopy.....	38
2.2.5. Mass Spectrometry. ....	38
<b>2.3. Results and Discussion .....</b>	<b>39</b>
2.3.1. Peroxidase Kinetics.....	39
2.3.2. Spectroscopic Evidence for H <sub>2</sub> O <sub>2</sub> -Induced Structural Changes. ....	43
2.3.3. H <sub>2</sub> O <sub>2</sub> -Induced Modifications Probed by Mass Spectrometry. ....	46
2.3.4. Peptide Mapping of Oxidation Patterns.....	47
2.3.5. Chemical Deconvolution. ....	52

2.3.6. Top-down MS.....	57
2.3.7. Peroxidase Activation Mechanism of Cyt <i>c</i> .....	61
<b>2.4. Conclusions .....</b>	<b>63</b>
<b>2.5. References .....</b>	<b>64</b>
<b>Chapter 3. Lysine Carbonylation as a Previously Unrecognized Contributor to Peroxidase Activation of Cytochrome <i>c</i> in Oxidants Other than H<sub>2</sub>O<sub>2</sub> .....</b>	<b>70</b>
<b>3.1. Introduction .....</b>	<b>70</b>
<b>3.2. Methods.....</b>	<b>74</b>
3.2.1. Materials.....	74
3.2.2. Preparation of CT-cyt <i>c</i> .....	74
3.2.3. Optical Spectroscopy.....	74
3.2.4. Mass Spectrometry.....	75
<b>3.3. Results and Discussion .....</b>	<b>76</b>
3.3.1. Chloramine-T-induced Met80 Oxidation.....	76
3.3.2. SCX Fractionation and Optical Characterization.....	76
3.3.3. Peroxidase Activity of CT-cyt <i>c</i> Fractions.....	81
3.3.4. SCX Fractions Represent Specific Proteoforms.....	82
3.3.5. Top-Down CID-IM-MS for Proteoform-Selective Analysis.....	86
3.3.6. Mapping of LysCHO Sites.....	91
3.3.7. LC-MS/MS Peptide Mapping Revisited.....	94

3.3.8. Mechanism of CT-induced Peroxidase Activation.....	96
<b>3.4. Conclusions .....</b>	<b>100</b>
<b>3.5. References .....</b>	<b>102</b>
<b>Chapter 4. Delineating Heme-Mediated versus Direct Protein Oxidation Pathways in Peroxidase-Activated Cytochrome c .....</b>	<b>107</b>
<b>4.1. Introduction .....</b>	<b>107</b>
<b>4.2. Methods .....</b>	<b>111</b>
4.2.1. Materials.....	111
4.2.2. Mass Spectrometry.....	111
4.2.3. Heme Removal: Preparation of aposs-cyt <i>c</i> .....	111
4.2.4. CT-induced Oxidation and GRT Labeling.....	112
<b>4.3. Results and Discussion .....</b>	<b>115</b>
4.3.1. Effects of CT-Induced Oxidation.....	115
4.3.2. Oxidation Site Mapping.....	118
4.3.3. Confirming LysCHO Sites by GRT Labeling.....	121
4.3.4. Confirming Heme Catalysis Using MP11.....	125
<b>4.4. Conclusions .....</b>	<b>128</b>
<b>4.5. References .....</b>	<b>130</b>



<b>Chapter 5. Probing the Effects of Heterogeneous Oxidative Modifications on the Stability of Cytochrome <i>c</i> in Solution and in the Gas Phase.....</b>	<b>135</b>
<b>5.1. Introduction .....</b>	<b>135</b>
<b>5.2. Materials and Methods .....</b>	<b>138</b>
5.2.1. Materials. ....	138
5.2.2. Protein Oxidation.....	139
5.2.3. Thermal Unfolding. ....	139
5.2.4. Mass Spectrometry. ....	140
<b>5.3. Results and Discussion .....</b>	<b>141</b>
5.3.1. Chromatographic Separation of Proteoforms. ....	141
5.3.2. Stability of CT-cyt <i>c</i> in Solution.....	143
5.3.3. ESI Charge States of CT-cyt <i>c</i> .....	145
5.3.4. Native ESI Gas Phase Conformations of CT-cyt <i>c</i> .....	147
5.3.5. Gas Phase Stability of CT-cyt <i>c</i> .....	147
5.3.6. Proteoform-Resolved CIU Analysis. ....	151
<b>5.4. Conclusions .....</b>	<b>154</b>
<b>5.5. References .....</b>	<b>156</b>
<b>Chapter 6. Summary and Future Work .....</b>	<b>161</b>
<b>6.1. Summary .....</b>	<b>161</b>
<b>6.2. Future Work .....</b>	<b>162</b>

6.2.1. Peroxidase Activation <i>In Vivo</i> .....	162
6.2.2. Cyt <i>c</i> / Cardiolipin Interactions.....	163
6.2.3. Oxidation Mapping in Other Systems .....	163
<b>6.3. References .....</b>	<b>165</b>
<b>Appendix I – Permissions .....</b>	<b>167</b>
<b>Curriculum Vitae .....</b>	<b>170</b>

## List of Symbols and Abbreviations

BIRD	blackbody infrared dissociation
CD	circular dichroism
CE	collision energy
CEM	chain ejection model
CID	collision-induced dissociation
CIU	collision-induced unfolding
CL	cardiolipin
CRM	charged residue model
cryo-EM	cryo-electron microscopy
CT	chloramine-T
cyt <i>c</i>	cytochrome <i>c</i>
DC	direct current
DNPH	dinitrophenylhydrazine
DTT	dithiothreitol
ESI	electrospray ionization
<i>fox</i>	fraction oxidized
FPOP	fast photochemical oxidation of proteins
GRT	Girard's reagent T
HDX-MS	hydrogen-deuterium exchange mass spectrometry
HOS	higher order structure
HRP	horseradish peroxidase
IM	ion mobility
IMS	ion mobility spectrometry
LC	liquid chromatography
LC/MS	liquid chromatography mass spectrometry
LysCHO	carbonylated lysine, amino adipic semialdehyde
<i>m/z</i>	mass-to-charge ratio
MALDI	matrix-assisted laser desorption/ionization

MetO	methionine sulfoxide
MP11	microperoxidase-11
MS	mass spectrometry
MS/MS	tandem mass spectrometry
MW	molecular weight
NMR	nuclear magnetic resonance
NOESY	Nuclear Overhauser Effect Spectroscopy
PDB	Protein Data Bank
QqQ-MS	triple quadrupole mass spectrometer
Q-TOF	quadrupole time-of-flight
R6G	rhodamine 6G
RF	radio frequency
ROS	reactive oxygen species
RR	resonance Raman
SCX	strong cation exchange chromatography
SID	surface-induced dissociation
TM	melting temperature
TWIG	traveling wave ion guide
TWIMS	traveling wave ion mobility spectrometry
UV-Vis	ultraviolet-visible
XL-MS	cross-linking mass spectrometry
XRD	X-ray diffraction
$z$	charge
$\Omega$	collision cross-section
$\Omega/z$	collision cross-section-to-charge ratio

# Chapter 1. Introduction

## 1.1. Protein Structure and Function

Proteins are biological macromolecules composed of a linear polymer of  $\alpha$ -amino acids. These building blocks are linked via amide bonds between the amine and carboxylate groups of consecutive residues (Figure 1-1). Each monomer can be one of 20 proteogenic amino acids, which differ by their side chain moiety.

Proteins are involved in virtually every aspect of biological function.<sup>1</sup> This enormous versatility is possible due to the vast multitude of possible three-dimensional structures that can arise from a polypeptide chain. A hallmark of proteins is their propensity to fold into highly ordered structures; the overall conformation is determined by their sequence, as well as the chemical environment surrounding the protein (pH, ionic strength, chemical modifications, etc.).<sup>2</sup> Some proteins may also incorporate non-amino acid elements, known as co-factors. These co-factors can associate with the protein through noncovalent or covalent interactions. A central tenet of structural biology is that the function of a protein is dictated by its structure.

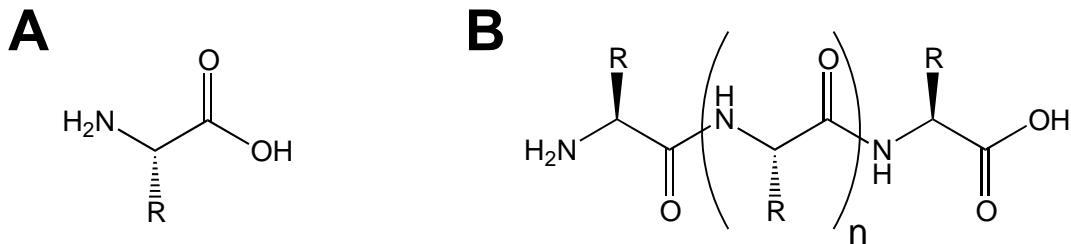


**Figure 1-1.** Generic chemical structures of (A)  $\alpha$ -amino acids and (B) polypeptides. Different sidechains, R, give rise to each of the different amino acid residues.

One phenomenon that is of growing interest is the ability of some proteins to perform multiple, sometimes radically different functions, often termed protein “moonlighting”.<sup>3,4</sup> Typically, such proteins are known for a primary, canonical function, but have been found to also perform other, non-canonical functions. Some of this moonlighting is possible without an accompanying change in structure (e.g. when different functions are linked to different domains of the protein). Other cases require a change in conformation that may be triggered by an altered chemical environment (e.g. cellular location, pH, post-translational modifications, ligand-binding, etc.).

## **1.2. Cytochrome *c***

One protein that exhibits moonlighting functionality is cytochrome *c* (cyt *c*), a highly conserved,<sup>5</sup> 12 kDa heme-containing protein (or hemeprotein) normally found in the intermembrane space of mitochondria.<sup>6</sup> The *c*-type heme cofactor of cyt *c* is covalently bound to the protein through thioether linkages to Cys14 and Cys17. In the native protein the iron center is hexa-coordinated, with four dative bonds from nitrogens in the porphyrin ring, one from the imidazole side chain of His18, and another from the thioether sulfur of Met80 (Figure 1-2). The canonical function of cyt *c* is to act as an electron carrier between complexes III and IV in the respiratory electron transport chain, cycling between the Fe(II) and Fe(III) oxidation states.<sup>7,8</sup> However, cyt *c* also possesses a moonlighting function as a peroxidase.<sup>9-12</sup>

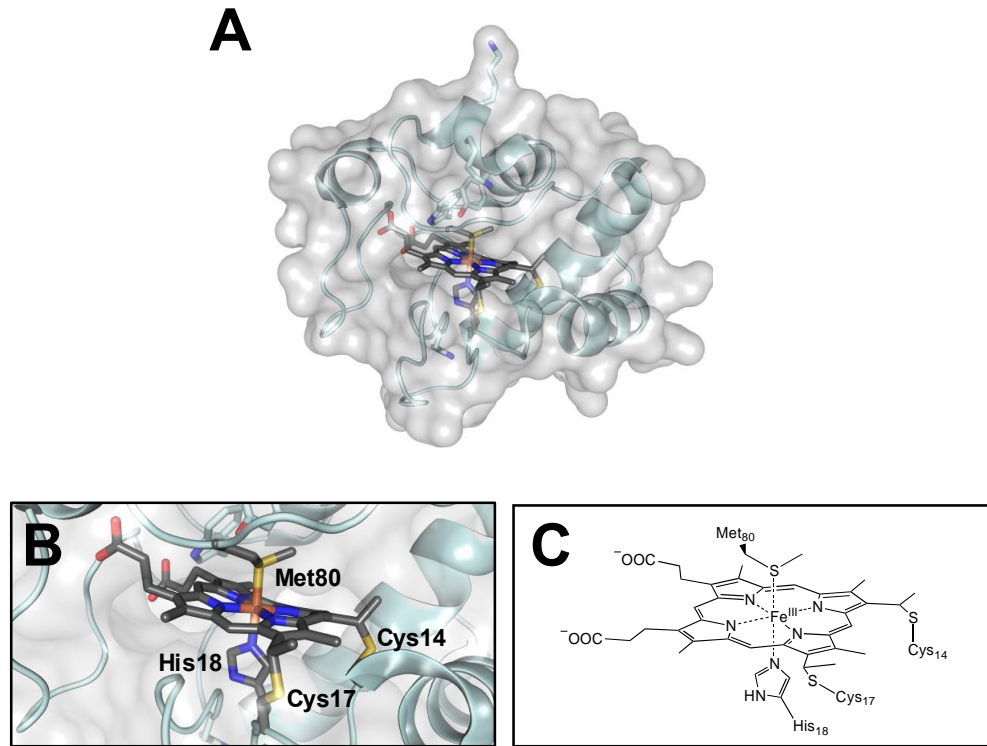


**Figure 1-2.** (A): Crystal structure of cyt *c* (equine, PDB: 1HRC)<sup>13</sup>; (B): Magnified view of the heme center; (C) Schematic representation of the heme center.

Peroxidases are a class of heme proteins that catalyze the oxidation of substrates using H<sub>2</sub>O<sub>2</sub>, with the most well-known example being horseradish peroxidase (HRP).<sup>14</sup> In this capacity, cyt *c* was found to play a crucial role in apoptosis (programmed cell death) by catalyzing the peroxidation of membrane lipids (via formation of lipid radicals and subsequent non-enzymatic reaction with molecular oxygen).<sup>15</sup> This process increases the permeability of the mitochondrial membrane and allows the passage of cyt *c* into the cytoplasm, where interactions between cyt *c* and apoptotic factors initiate apoptosis.<sup>16–20</sup> Although the precise mechanism is not fully understood, it is generally thought that cyt *c* exhibits peroxidase activity in a manner similar to that of other peroxidases by catalyzing the heterolytic cleavage of H<sub>2</sub>O<sub>2</sub> via cycling between Fe(III) and Fe(IV) oxidation states (Figure 1-3).<sup>14</sup> There is also some evidence that cyt *c* may also be able to catalyze homolytic H<sub>2</sub>O<sub>2</sub> cleavage to directly produce hydroxyl radicals ( $\cdot$ OH).<sup>21,22</sup>

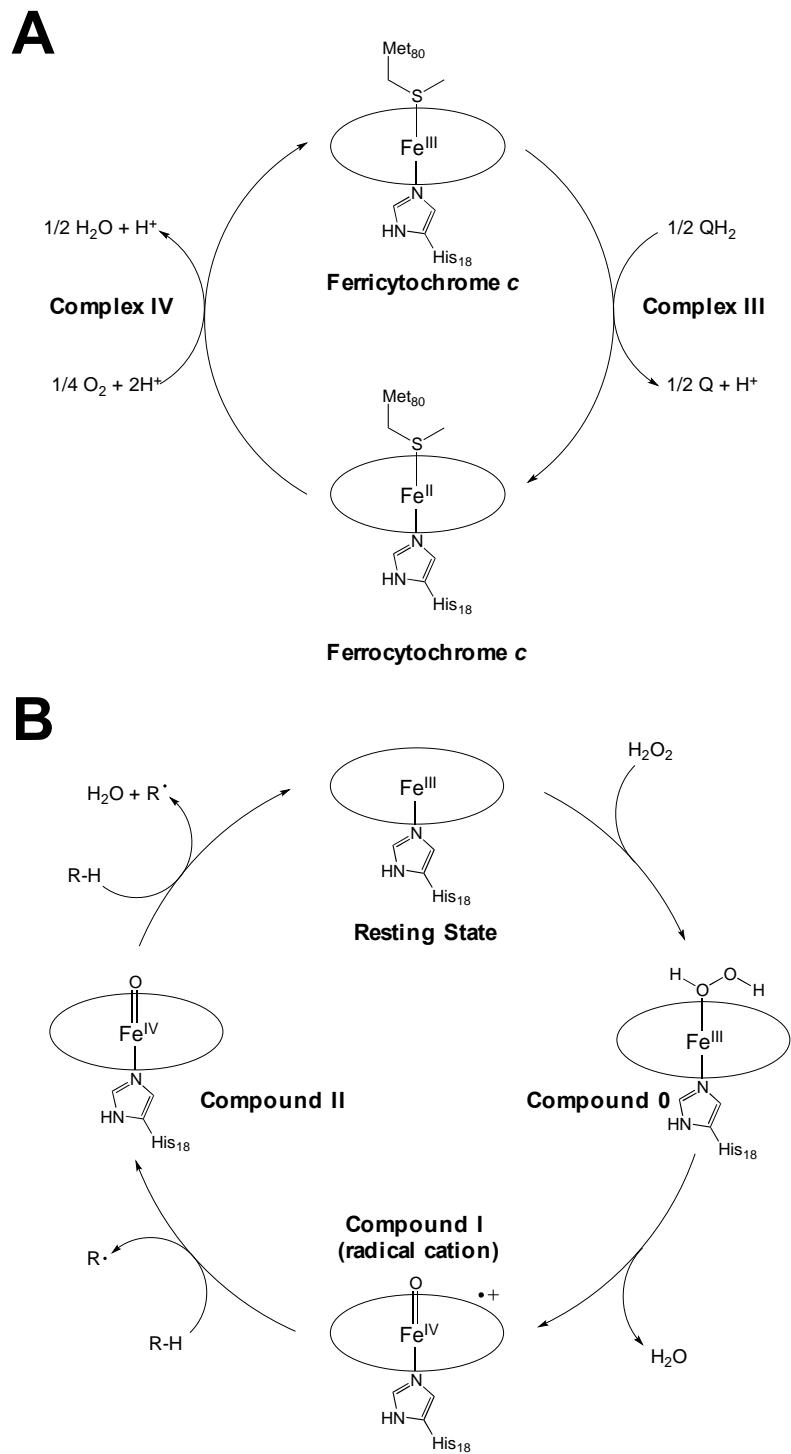


**Figure 1-3.** Functions of cyt *c*. (A) electron carrier function. (B) peroxidase function based on the mechanism for classical peroxidases.<sup>14</sup> The porphyrin ring is represented here as a disc. The produced radical species may undergo further reactions with molecular oxygen to form various oxidized products.



Regardless of the mechanistic details, all proposed explanations of cyt *c* peroxidase activity require an Fe(III) species with an open distal coordinate site that can bind H<sub>2</sub>O<sub>2</sub>, in line with HRP and other peroxidases.<sup>14</sup> In the native conformation of cyt *c*, this distal site is occupied by Met80 (Figure 1-2C). As such, numerous studies have explored how an assortment of protein-ligand interactions, post-translational modifications, and/or mutations can promote dissociation of the Met80-Fe bond, and how this may trigger the functional switch from an electron carrier to a peroxidase.<sup>10-12,23-29</sup> Studies *in vivo* have shown that cyt *c* mutants lacking Met80 show increased peroxidase activity and promoted release of cyt *c* into the cytoplasm from the mitochondria.<sup>30</sup> Other studies have shown that binding to anionic lipid molecules such as cardiolipin,<sup>31-33</sup> as well as certain post-translational modifications (e.g. Tyr74 nitration)<sup>34</sup>, result in changes of the coordination environment that are correlated with increased peroxidase activity. One of the most-studied alternate cyt *c* forms is the so-called “alkaline conformer”, where a lysine residue (likely Lys72/73) is the 6th ligand in place of Met80.<sup>35-37</sup> Unexpectedly, the alkaline conformer exhibits enhanced peroxidase activity, despite also lacking an open coordination site to bind H<sub>2</sub>O<sub>2</sub>.<sup>26,38</sup>

Despite decades of research studying the various effectors of the peroxidase activity of cyt *c*, a long-standing enigma is that cyt *c*, in its native state hexacoordinate state, is peroxidase-active.<sup>9</sup> While there have been some attempts to address this paradox in both the native state and the alkaline conformer (e.g. partial pentacoordinate occupancy via conformational fluctuations)<sup>39,40</sup>, the phenomenon remains poorly understood.

### 1.3. Protein Oxidation

Exposure of proteins and other biomolecules to reactive oxygen species (ROS) such as  $\text{H}_2\text{O}_2$ ,  $\cdot\text{OH}$ , and  $\cdot\text{O}_2^-$  is an unavoidable consequence of aerobic cellular respiration.<sup>41,42</sup> ROS can induce covalent (oxidative) modifications, many of which have pronounced effects on protein structure and function. Accumulation of oxidized protein is correlated with disease states related to aging<sup>43-45</sup> and neurodegeneration.<sup>46-52</sup> Proteins at high risk of oxidation (e.g. redox-active metalloenzymes) are thought to have evolved protective mechanisms to mitigate these deleterious effects (e.g. controlled electron hole hopping).<sup>53-55</sup> Aside from their negative consequences, protein oxidative modifications also play important roles in cell signalling and in regulating the cellular response to oxidative stress.<sup>56-58</sup>

A wide variety of protein oxidation products exist for almost every amino acid residue.<sup>59-62</sup> The most common oxidation targets are the sulfur-containing (Cys, Met) and aromatic (Trp, Tyr, Phe) residues. Oxidation of these residues typically results in the incorporation of one or more oxygen atoms, producing a series of  $+n\text{O}$  modifications.<sup>61,62</sup> The residues Cys and Tyr can also oxidatively dimerize to form cystine<sup>63</sup> and dityrosine<sup>64,65</sup>, respectively. Mass spectrometry is commonly used to detect these oxidative modifications due to their characteristic changes in mass.<sup>61,62</sup>

Another class of protein oxidative modifications are carbonylation products, in which a reactive carbonyl (i.e. ketone or aldehyde) is produced.<sup>46,62</sup> These types of modifications are often studied by applying spectroscopic and/or antibody-based quantitative assays that utilize the reactivity these moieties with 2,4-dinitrophenylhydrazine (DNPH) or other hydrazines.<sup>66,67</sup> Glu and Lys are the most common targets of protein carbonylation,<sup>68</sup> although carbonylation at other residues are also known.<sup>62</sup>

## 1.4. Common Methods for Studying Protein Structure

### 1.4.1. Optical Spectroscopy

Optical spectroscopy utilizes the interactions between photons and chemical matter to glean information on various physical and chemical properties of a system.<sup>69</sup> In the context of studying protein structure, two common optical techniques are circular dichroism (CD) spectroscopy and fluorescence spectroscopy.

CD spectroscopy takes advantage of the chirality of proteins and their constituent L-amino acids.<sup>70</sup> When interacting with circularly polarized light (which can be either left- or right-handed) chiral molecules will absorb each of these two components to a different degree. The difference between these two absorbances produces the CD signal. For proteins, far-UV photons (ca. 190 – 250 nm) are typically used, corresponding to  $\pi \rightarrow \pi^*$  and  $n \rightarrow \pi^*$  electronic transitions of backbone amide groups.<sup>71</sup> As the CD transitions are sensitive to the three-dimensional arrangement of the polypeptide backbone,<sup>72</sup> each type of secondary structure (e.g.  $\alpha$ -helix,  $\beta$ -sheet) gives rise to characteristic CD signals. The secondary structure content of a protein can be estimated by fitting experimental CD spectra to a linear combination of the “pure” basis spectra.<sup>73</sup> Due to its convenience and sensitivity to changes in secondary structure, CD spectroscopy is often used in protein folding studies.<sup>74</sup> Protein unfolding curves can be generated by plotting CD signals at a given wavelength as a function of temperature or denaturant concentration.<sup>75</sup> Various thermodynamic parameters can be extracted from these experiments.<sup>76</sup>

Fluorescence spectroscopy utilizes the capacity for some chromophores to emit light (fluoresce) following irradiation. Fluorescence spectroscopy offers the advantages of high sensitivity and low background intensity, thereby providing very high S/N ratios.<sup>77</sup> For protein studies, the fluorescence of intrinsic tryptophan residues is commonly utilized.<sup>78,79</sup> Upon irradiation at 280 nm, these residues fluoresce at ca. 350 nm. Both the intensity and wavelength of the emission are a sensitive probe for the tryptophan microenvironment.<sup>79</sup> Polar environments (e.g. solvent exposure) induce a red shift in the emission wavelength, whereas hydrophobic environments (e.g. the protein core) induce a blue shift. Fluorescence quenching can also be used to provide proximity information.<sup>80</sup>

UV/vis spectroscopy of most proteins does not provide much structural information. However, the heme cofactor is itself a chromophore that absorbs strongly in the visible range, enabling several optical analyses unique to hemeproteins in this range of the electromagnetic spectrum.<sup>81</sup> The positions and relative intensities of the heme absorption bands (e.g. the Soret band at ca. 400 nm and the Q band at ca. 550 nm) are affected by changes in ligation state of the heme iron.<sup>82</sup> This strong absorbance also renders the use of resonance Raman (RR) spectroscopy viable.<sup>83</sup> RR spectroscopy is a variant of Raman spectroscopy that exploits the ability of highly absorbing electronic transitions to greatly enhance the intensity of Raman scattering. Raman spectroscopy probes the vibronic structure of system, and thereby provides insight into the environment surrounding the heme iron.<sup>84</sup>

#### **1.4.2. High-Resolution Structural Techniques**

A number of biophysical techniques allow the determination of protein structures with atomic (or near-atomic) resolution. Nuclear magnetic resonance (NMR) spectroscopy provides structural information from direct solution phase measurements, whereas X-ray diffraction (XRD) and cryo-electron microscopy (cryo-EM) obtain structure from measurements in the solid-state.

NMR spectroscopy utilizes nuclear spin transitions to obtain chemical information on a molecule.<sup>85</sup> Samples are placed in a strong external magnetic field, which causes the nuclear spin states to become non-degenerate (the Zeeman effect). A series of radio frequency (RF) pulses can then be applied to excite the nuclear spins. The energies of these transitions (usually reported as chemical shifts) are sensitive to the chemical environment of each nucleus. Typical NMR spectroscopy workflows for protein structure determination employ a series of multi-dimensional experiments that together first establish atomic connectivity.<sup>85-87</sup> Afterwards, Nuclear Overhauser Effect Spectroscopy (NOESY) experiments are performed that provide distance constraints between various nuclei.<sup>88-90</sup> By combining these constraints with chemical shift information, model protein structures can be built using molecular mechanics force fields.<sup>91,92</sup> Protein NMR spectroscopy

typically requires the use of isotopically enriched protein (e.g.  $^{14}\text{N} \rightarrow ^{15}\text{N}$ ,  $^{12}\text{C} \rightarrow ^{13}\text{C}$ ,  $^1\text{H} \rightarrow ^2\text{H}$ ) and high protein concentrations to mitigate the inherently low sensitivity of the technique.<sup>85</sup>

XRD utilizes the diffraction patterns of an ordered (crystalline) material to obtain structural information.<sup>93</sup> To perform XRD, a sample of interest must first be crystallized, after which it is subjected to X-ray radiation. The scattering of these X-rays by the electrons of each atom produce a characteristic diffraction pattern, from which the three-dimensional electron density map can be determined. Both bonding and atomic coordinates can be inferred from the electron density at a resolution ca. 1 Å (or even slightly lower).<sup>94</sup> A major limitation of XRD is the immense difficulty in growing protein crystals of sufficiently high-quality.<sup>95</sup>

Cryo-EM is a high-resolution imaging technique that utilizes an electron beam to elucidate protein structures.<sup>96,97</sup> Samples are prepared by first spreading solubilized protein across a grid. This is followed by flash-freezing to form a thin layer of vitreous ice embedded with protein.<sup>98</sup> The sample is then imaged by electron microscopy. By combining images from many viewing angles and protein orientations, three-dimensional protein structures can be reconstructed. Although sub-Å resolution is theoretically obtainable via cryo-EM, a number of practical challenges (e.g. sample integrity, detector efficiency) currently preclude this limit from being reached.<sup>98</sup>

## 1.5. Mass Spectrometry and Associated Techniques

Mass spectrometry (MS) is an analytical technique that measures the mass-to-charge ratio ( $m/z$ ) of analyte ions in the gas phase. The  $m/z$  provides information on the chemical composition of a molecule. In comparison to other analytical techniques, MS has the advantages of high sensitivity and low sample consumption. The basic design of a mass spectrometer includes three primary components: 1) an ion source that converts analytes to ions, 2) a mass analyzer that differentiates ions by  $m/z$ , and 3) a detector to record the ions.

Due to the plethora of options in these three components, an assortment of instrumental designs are possible, with specific designs tailored to the types of analytes being studied.

### 1.5.1. Electrospray Ionization Mass Spectrometry (ESI-MS)

In the context of protein analysis, the most commonly used ionization technique is electrospray ionization (ESI), although other techniques (e.g. matrix-assisted laser desorption/ionization, MALDI) are also available.<sup>99</sup> ESI is particularly well-suited for proteins and other biological macromolecules.<sup>100–102</sup> In ESI, an analyte solution is introduced into a conductive capillary, and a high positive voltage (although negative voltages are used for some applications) is applied. A Taylor cone is formed at the capillary tip, from which charged, analyte-containing droplets are emitted.<sup>103–105</sup> After a number of fission and desolvation events, gaseous charged analytes are eventually produced, which can then be introduced into the mass spectrometer.<sup>106,107</sup> The ESI process generally produces multiply charged, protonated species of the form  $[M+zH]^{z+}$ , where  $M$  is the molecular weight of the neutral analyte, and  $z$  corresponds to the number of excess protons, i.e. the charge state.

Several models have been proposed to describe the process in which proteins emerge from charged ESI droplets.<sup>104</sup> Globular, native proteins are thought to follow the charged residue model (CRM).<sup>108,109</sup> In the CRM, the protein remains solvated within the droplet core while excess water and/or charge is shed by evaporation or fission events. This process continues until the protein ion is fully desolvated. Under these “native ESI” conditions, the observed protein charge state ( $z_R$ ) can be approximated by the Rayleigh limit of an equivalently sized ESI droplet<sup>110</sup>

$$z_R = \frac{8\pi}{e} \sqrt{\epsilon_0 \gamma r^3} \quad (1.1)$$

where  $e$  is the elementary charge,  $\epsilon_0$  is the vacuum permittivity,  $\gamma$  is the surface tension, and  $r$  is the droplet radius.

In contrast to their native counterparts, unfolded proteins tend to exhibit much higher charge states.<sup>111–113</sup> The chain ejection model (CEM) has been proposed to explain this behavior.<sup>114–116</sup> In the CEM, the unfolded protein chain migrates to the surface of the ESI droplet, where Coulombic repulsion promotes the gradual ejection of the protein chain off of the droplet surface. Electrostatic forces promote the migration of H<sup>+</sup> from the ESI droplet to the nascent chain, until the highly charged protein is eventually fully ejected from the ESI droplet.

ESI-MS offers several advantages for protein analysis. Firstly, ESI represents a “soft” ionization technique, in that covalent bonds are not broken by the ionization process. This is in contrast to “harsh” ionization techniques such as electron impact<sup>117</sup> where analytes often fragment. Under properly optimized conditions, even non-covalent interactions can be retained during ESI, allowing ESI-MS to provide direct information on protein-ligand<sup>118,119</sup> and protein-protein<sup>120–123</sup> interactions. Secondly, ESI-MS is amenable to a very broad mass range ( $\sim 10^2 - 10^6$  Da); small molecular weight (MW) analytes are not obscured by chemical noise as is the case with MALDI<sup>124</sup>, while large MW analytes become multiply charged ( $z \gg 1$ ), lowering the observed  $m/z$  to levels tractable for common mass analyzers. Thirdly, ESI can be easily coupled with liquid chromatography (LC), facilitating the analysis of complex biological protein mixtures, e.g. for proteomic applications.<sup>125–128</sup>

### **1.5.2. Mass Spectrometers for Protein Analysis**

For the analysis of proteins and other biomolecules, tandem mass spectrometry (MS/MS) experiments are often essential. In MS/MS, ions are fragmented in the gas phase, and the mass spectrum of the fragment ions is monitored to obtain information on chemical structure.<sup>129</sup> The prototypical example of a tandem mass spectrometer for biomolecular analysis is a triple quadrupole mass spectrometer (QqQ-MS).<sup>130</sup> Quadrupoles are devices, composed of two pairs of parallel conductive rods, that can act as ion mass filters.<sup>131,132</sup> Depending on the RF and direct current (DC) voltages applied to the rods, only specific

$m/z$  values successfully traverse the quadrupole, while other species are filtered out. These voltages can be ramped, allowing a range of  $m/z$  values to be swept across to generate a mass spectrum. Quadrupoles can also be operated as broadband (“RF-only”) ion guide, allowing ions of all  $m/z$  to traverse through the device. A QqQ-MS is composed of three quadrupoles (Q1, q2, and Q3) that are arranged sequentially (Figure 1-4A).

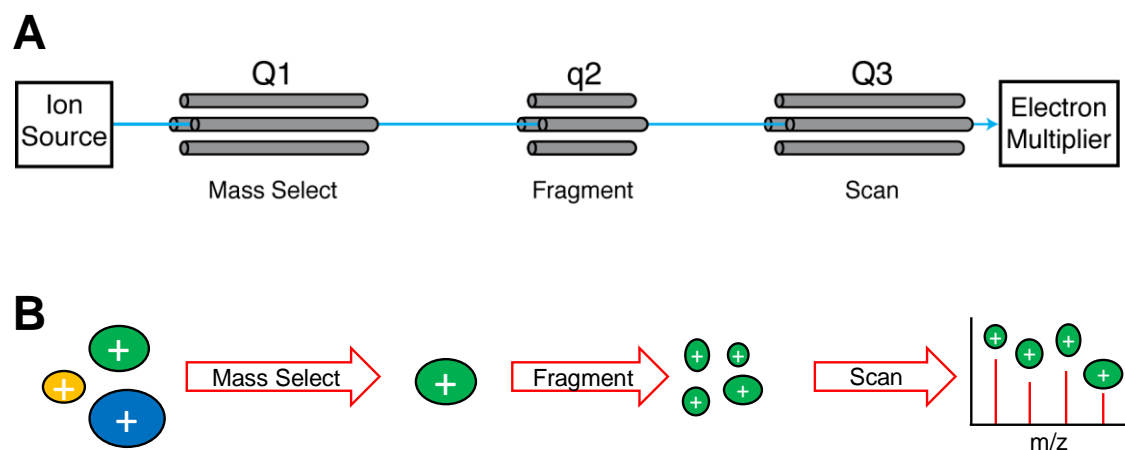


**Figure 1-4.** (A) Schematic diagram of a QqQ-MS. Each quadrupole is labeled according to its standard function in MS/MS. The ion path is shown in blue. (B) Illustration of a standard MS/MS experiment. Analyte ions are shown as coloured ovals. The ion depicted in green is the target of MS/MS analysis.



A multitude of MS/MS experiments can be performed using a QqQ-MS.<sup>133</sup> In the archetypal MS/MS experiment (fragment ion scan, Figure 1-4B), Q1 is used as a mass filter to select an ion of interest to be fragmented (called the “precursor ion”). Next, q2 is used as a fragmentation cell to activate the ion. Collision-induced dissociation (CID) is the most commonly used fragmentation technique, although other activation methods (e.g. electron- or photon-based) have also been developed.<sup>134</sup> For CID experiments, q2 is filled with an inert gas such as Ar. A potential difference is then applied across q2, accelerating the analyte ion through the collision gas. Repeated collisions between the analyte and background gas results in vibrational heating of the analyte until fragmentation occurs. Q3 is then scanned across the  $m/z$  range to generate a mass spectrum of the produced fragment ions. Finally, the ions are detected. An electron multiplier is typically used for this purpose, which detects ions by converting ion impact events to electrical signals which are subsequently amplified.<sup>135</sup> The output of this experiment is a mass spectrum of all fragment ions produced by a particular precursor ion (i.e. a tandem mass spectrum).

Many modern tandem mass spectrometers are derived from the basic QqQ-MS design.<sup>133</sup> Common alterations replace Q3 with a higher resolution mass analyzer. One such configuration is a quadrupole time-of-flight (Q-TOF) mass spectrometer, where Q3 is replaced with a time-of-flight (TOF) mass analyzer.<sup>136,137</sup> A TOF measures  $m/z$  by first applying a high voltage pulse that accelerates the ions. The ions are then allowed to traverse a field-free region. The amount of time,  $t_{flight}$ , for an ion to traverse this region can be related to  $m/z$  by

$$t_{flight} = \frac{D}{\sqrt{Ede}} \times \sqrt{\frac{m}{z}} \quad (1.2)$$

where  $D$  is the length of the field-free region,  $E$  is the strength of the initial electric field, and  $d$  is the length of the region where the accelerating field is applied.<sup>138</sup> The resolution of a TOF can be greatly enhanced by the use of an ion mirror (a reflectron) to correct for variability in the initial ion energies.<sup>139</sup>

A contemporary example of a Q-TOF design is the commercially available SYNAPT family of mass spectrometers manufactured by Waters (Figure 1-5).<sup>140–142</sup> In the SYNAPT platform, Q1 remains essentially unchanged, while the q2 quadrupole is replaced with a series of three traveling wave ion guides (TWIGs) in the so-called “TriWave” cell.<sup>143</sup> The first and third TWIGs are functionally similar to a typical collision cell, while the central cell is configured to allow traveling wave ion mobility experiments to be performed.

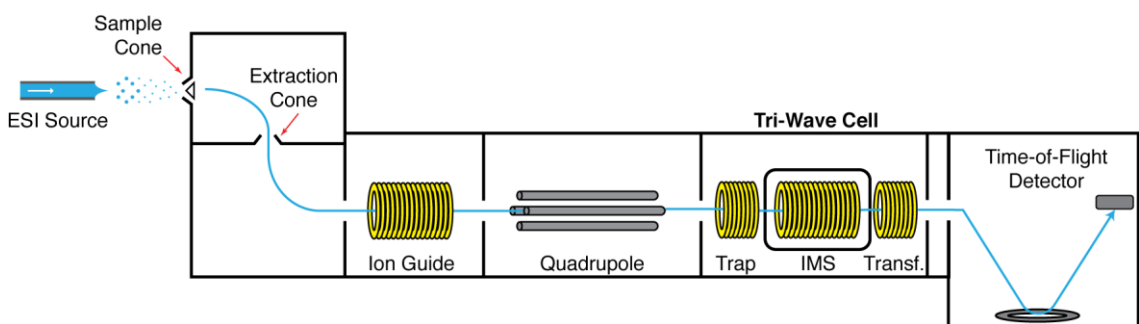


**Figure 1-5.** Representative schematic diagram of the Waters SYNAPT ESI-MS systems used in this work. The ion path is shown in blue.

### 1.5.3. Ion Mobility Spectrometry

Ion mobility spectrometry (IMS) is a gas-phase technique that provides information on the conformation (shape) of an analyte.<sup>144</sup> In IMS, ions enter a cell filled with neutral gas (e.g. He or N<sub>2</sub>), and an electric field is applied across the cell. As ions traverse the cell, collisions with the neutral gas impede their movement. Ions with a larger collision cross section ( $\Omega$ ) experience more collisions (drag) from the background gas than ions with a smaller  $\Omega$ , and thus take longer to traverse the cell. IMS separates ions by collisional cross section-to-charge ratio ( $\Omega/z$ ).<sup>145</sup> If the applied electric field is uniform (as in traditional drift tube IMS),  $\Omega$  can be directly calculated from the drift time ( $t_d$ ) via the Mason-Schamp equation.<sup>146</sup>

Traveling wave ion mobility spectrometry (TWIMS) is a type of IMS that utilizes a series of traveling DC waves to push ions (Figure 1-6), instead of employing a uniform electric field.<sup>143</sup> In TWIMS, separation occurs when ions experience sufficient drag from the background gas to “roll over” the DC wave, impeding their movement until the next wave arrives. Many such roll over events take place as ions travel through the TWIMS device. Unlike drift tube IMS,  $\Omega$  cannot be directly calculated from the TWIMS drift time. Instead, TWIMS measurements must be empirically calibrated to determine  $\Omega$  using the relationship

$$\frac{\Omega}{z} = F \times t_d^B \quad (1.3)$$

where  $F$  and  $B$  are experimentally obtained by performing TWIMS measurements on standards where  $\Omega$  is already known.<sup>147,148</sup>

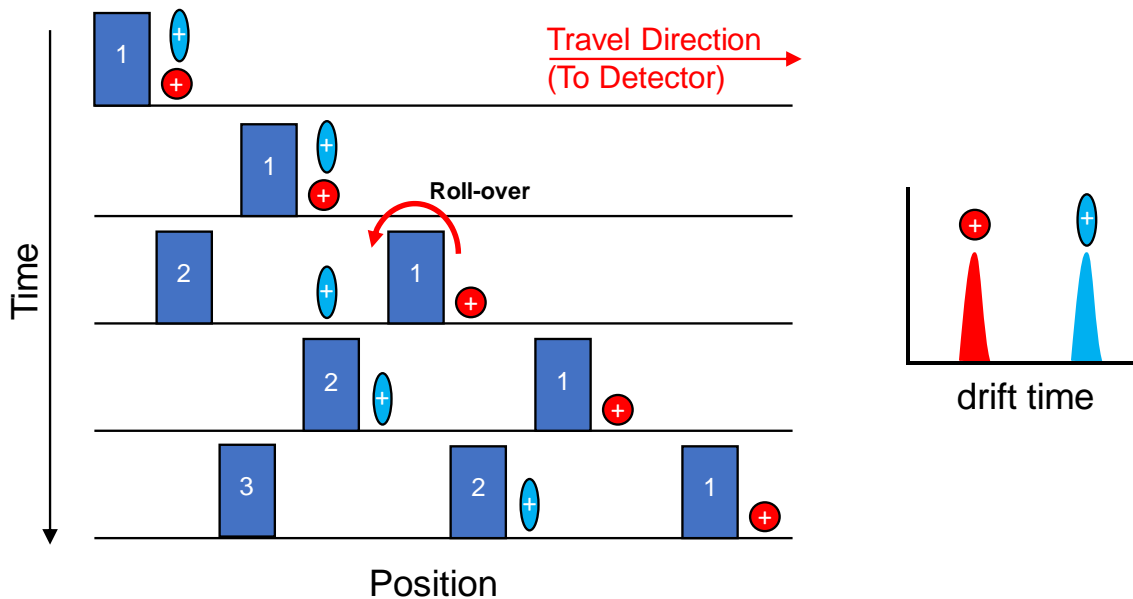


**Figure 1-6.** Illustration of TWIMS. Left: a series of traveling DC waves (blue blocks, numbered) push ions from left to right across the IMS cell. For equally charged ions, ions with a larger  $\Omega$  (light blue ion) will experience more roll-over events (e.g. third row) compared to ions with a smaller  $\Omega$  (red ion). Right: the resulting ion mobilogram from this process.

## 1.6. ESI-MS Experiments for Studying Protein Structure

A versatile toolbox of MS-based techniques has been developed for studying protein structure.<sup>102</sup> These techniques can be loosely assigned to two categories: those that probe primary structure (i.e. sequencing), and those that probe higher order structure (HOS). Of the latter class, a distinction can be drawn on how higher order structural information is encoded into the mass domain for MS detection, either by 1) covalent labeling of solution phase structures, or 2) preserving HOS into the gas phase.

### 1.6.1. Primary Structure: Sequencing

The primary structure of a protein is given by its amino acid sequence.<sup>1</sup> As every amino acid (except Leu/Ile) has a unique mass, MS/MS offers a convenient method to determine the sequence of a peptide or protein.<sup>149</sup> These experiments rely on the fact that MS/MS activation predominantly results in fragmentation along the polypeptide backbone.<sup>150</sup> The amino acid sequence can thus be determined from a tandem mass spectrum by the mass differences between successive fragment ions. Similarly, protein modifications (e.g. post-translational modifications, oxidative modifications) can be localized in an MS/MS experiment by looking for mass differences that do not correspond to those of the unmodified amino acids.<sup>151</sup> The exact location of cleavage along the backbone depends on the MS/MS activation method used.<sup>152</sup> For CID, fragmentation primarily occurs across backbone amide bonds<sup>153</sup> to produce a series of fragment ions denoted as *b*-ions if they contain the N-terminus, or *y*-ions if they contain the C-terminus.<sup>154-156</sup> Each fragment is numbered according to its proximity to their respective terminus (Figure 1-7).

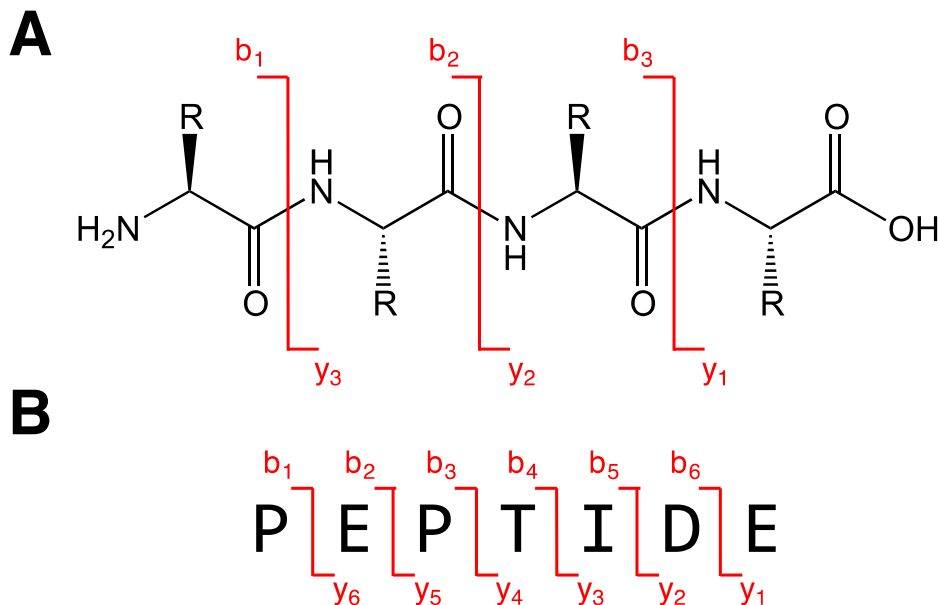


**Figure 1-7.** CID fragmentation of a polypeptide. Each position is labeled with its corresponding *b/y*-ion notation. (A) Generic polypeptide structure overlaid with possible CID fragmentation positions. (B) An alternative representation of MS/MS cleavage patterns using the heptapeptide Pro-Glu-Pro-Thr-Ile-Asp-Glu.

As the fragmentation efficiency and other factors worsen with increasing polypeptide length, proteins are often subjected to enzymatic proteolysis to produce smaller peptides prior to MS/MS.<sup>157</sup> This is termed the *bottom-up* MS approach. Alternatively, it is also possible to perform MS/MS directly on intact proteins without proteolysis, termed the *top-down* MS approach.<sup>158–160</sup> Due to its high demands on instrument performance and challenging data analysis, top-down MS is comparatively less utilized. However, top-down MS experiments provide information not easily obtainable by the bottom-up approach, such as combinatorial relationships between different PTMs. This enables characterization of protein proteoforms, i.e. the specific molecular form of a protein.<sup>161</sup> In addition, top-down can probe individual proteoforms in a mixture (versus the ensemble measurements inherent to the bottom-up approach).<sup>162–164</sup>

### 1.6.2. Higher Order Structure: Covalent Labeling Experiments

Typical MS experiments are performed under conditions where protein HOS is lost (e.g. acidified solvent, digestion into peptides), precluding their interrogation. One approach, collectively referred to as covalent labeling, circumvents this issue by first treating the protein with a reagent that chemically modifies the protein in a way such that the pattern of modifications on the protein sequence encodes information on its HOS.<sup>165</sup> Even if the protein structure is disrupted after labeling, the location of the chemical modifications do not change. These labels can then be detected and localized by MS(/MS), thereby allowing protein HOS to be probed through changes in the mass spectrum. Different labeling techniques have developed to probe each level of protein HOS.

The basic form of a covalent labeling experiment is protein footprinting.<sup>166</sup> In these experiments, protein is exposed to a solution containing a labeling reagent. These reagents may be residue-specific (e.g. iodoacetamide for Cys residues)<sup>167,168</sup> or be broadly reactive (e.g. radical species such as  $\cdot\text{OH}$ ).<sup>61,169,170</sup> Only residues accessible to the reagent (i.e. the solvent-exposed protein surface) are labeled, whereas residues buried within the protein are protected and do not react. These experiments provide information on the protein tertiary structure. To study quaternary structure, a variant of protein footprinting known as crosslinking mass spectrometry (XL-MS) employing bifunctional labeling reagents can be used.<sup>171-173</sup> These reagents consist of two reactive labeling moieties that are covalently linked by an inert spacer with a well-defined length. Upon reaction with the protein, the locations of the labels serve as a “molecular ruler” that provides a distance constraint between the two labeled sites. The topology of proteins and protein complexes can therefore be mapped by the locations of crosslinks.<sup>174</sup> XL-MS is often used in conjunction with other biophysical techniques (e.g. cryo-EM) to provide additional constraints for structural refinement.<sup>175,176</sup>

Hydrogen-deuterium exchange mass spectrometry (HDX-MS) is another popular form of covalent labeling.<sup>177–182</sup> In HDX-MS, protein is exposed to heavy water (D<sub>2</sub>O), which gradually replaces labile hydrogens (1 Da) with deuterium (2 Da). The rate and locations of deuterium uptake is sensitive to dynamic changes in hydrogen-bonding networks. As many of these exchange processes are extremely fast, conventional HDX-MS monitors only the slow-exchanging amide hydrogens of the polypeptide backbone, thereby providing information on protein secondary structure. HDX-MS differs substantially from the protein footprinting techniques described above in that the incorporated deuterium is labile and readily dissociable.<sup>183–185</sup> Specialized workflows (e.g. acidic proteolysis<sup>186,187</sup>, low-temperature chromatography<sup>188</sup>, rapid analysis) must therefore be adapted. Challenges also arise in localizing HDX-MS at the residue level due to the mobile nature of deuterium in collisionally heated protein or peptide ions (“scrambling”).<sup>189–192</sup> Nevertheless, these limitations are greatly outweighed by the wealth of information gleaned by HDX-MS, particularly regarding protein folding<sup>193–195</sup> and dynamics.<sup>196</sup>

### **1.6.3. Higher Order Structure: Native Mass Spectrometry**

Protein HOS can also be directly measured by ESI-MS if experimental conditions that promote the preservation of the native protein structure during ionization and subsequent transfer into the gas phase are implemented. This approach is often referred to as native MS<sup>123</sup> and/or “gas phase structural biology”.<sup>197</sup> Information such as protein-ligand<sup>198,199</sup> or protein complex stoichiometry<sup>120,200,201</sup> is readily obtainable from the ion masses observed in native mass spectra. Moreover, the charge state distribution can provide insight into protein tertiary structure.<sup>113,196</sup>

A variety of gas-phase techniques can be performed in conjunction with native MS. One particularly powerful example is native IMS, from which protein shape/conformation can be inferred via  $\Omega$  measurements.<sup>202,203</sup> This can provide a great deal of information on the HOS of a protein, especially when compared against calculated  $\Omega$  values of candidate structures.<sup>204,205</sup> The observation that  $\Omega$  values measured by native IMS are fairly

consistent with their condensed phase counterparts have bolstered the view that native-like protein structures can be retained in the gas phase.<sup>206,207</sup> Native IMS can also monitor changes in  $\Omega$  as a protein is unfolded in the gas phase, forming the basis of collision-induced unfolding (CIU) experiments.<sup>208</sup> In CIU, native protein ions are purposely disrupted (e.g. by increasing energy in the collision cell). By plotting  $\Omega$  as a function of ion activation, these CIU profiles can be interpreted in an analogous manner to unfolding curves in solution (e.g. monitored by CD spectroscopy), providing thermodynamic information.

## 1.7. Scope of Thesis

The structural basis underlying the peroxidase activity of cyt *c* remains poorly understood. One key aspect that remains unexplored is the potential role of protein oxidative modifications in the peroxidase activity of cyt *c*. It is known that prolonged incubation of cyt *c* with the oxidant (and canonical peroxidase substrate)  $\text{H}_2\text{O}_2$  results in deactivation of the protein, suggesting that some form of  $\text{H}_2\text{O}_2$ -induced protein modification must be occurring.<sup>209–212</sup> However, the chemical nature of these modifications and their structural implications have not yet been elucidated. We hypothesize that early oxidation events could initially enhance the protein's peroxidase function.

In Chapter 2, we characterize  $\text{H}_2\text{O}_2$ -induced oxidative modifications in cyt *c* by applying a suite of MS-based experiments. In doing so, we unravel the critical role that these *in situ* structural changes play in initially triggering the peroxidase activity of the protein before eventual inactivation occurs. Through this work, we serendipitously discover that certain functionally important oxidative modifications (e.g. on Lys) tend to elude detection when using conventional analytical approaches. We propose that these modifications may be severely under-reported in the literature.



Chapter 3 explores this postulate by conducting studies on cyt *c* treated with chloramine-T, a popular and purportedly well-characterized model system for peroxidase-activated cyt *c*. We confirm that the previously unreported oxidation of Lys also occurs here, and we uncover that this model system is actually a complex ensemble of structurally (and functionally) distinct species that differ by the severity of oxidation.

Chapter 4 expands on the previous chapters by probing the causal factors underpinning the production of specific oxidative modification products. We uncover the role of heme-mediated catalysis in the formation of certain protein oxidative modifications in cyt *c*, while other transformations proceed via direct interaction with the oxidant.

Chapter 5 utilizes oxidatively-modified cyt *c* to address the comparability of MS-derived gas-phase stability measurements to their classical solution phase counterparts. Unlike many other systems, we discover that oxidized cyt *c* shows *divergent* stability behaviour, i.e. destabilization in solution vs. stabilization in the gas phase.

## 1.8. References

- (1) Voet, D. V. 2nd ed.; John Wiley & Sons, 2004.
- (2) Lesk, A. M. Oxford Press, 2001.
- (3) Jeffery, C. J. *Trends Genet.* **2003**, *19* (8), 415–417.
- (4) Huberts, D. H. E. W.; van der Klei, I. J. *Biochim. Biophys. Acta - Mol. Cell Res.* **2010**, *1803* (4), 520–525.
- (5) Margoliash, E. *Proc. Natl. Acad. Sci.* **1963**, *50* (4), 672.
- (6) Neupert, W. *Annu. Rev. Biochem.* **1997**, *66* (1), 863–917.
- (7) Bertini, I.; Gray, H. B.; Stiefel, E. I.; Valentine, J. S. University Science Books, 2007.
- (8) Alvarez-Paggi, D.; Hannibal, L.; Castro, M. A.; Oviedo-Rouco, S.; Demicheli, V.; Tórtora, V.; Tomasina, F.; Radi, R.; Murgida, D. H. *Chem. Rev.* **2017**, *117* (21), 13382–13460.
- (9) Radi, R.; Thomson, L.; Rubbo, H.; Prodanov, E. *Arch. Biochem. Biophys.* **1991**, *288* (1), 112–117.
- (10) Kagan, V. E.; Bayır, H. A.; Belikova, N. A.; Kapralov, O.; Tyurina, Y. Y.; Tyurin, V. A.; Jiang, J.; Stoyanovsky, D. A.; Wipf, P.; Kochanek, P. M.; Greenberger, J. S.; Pitt, B.; Shvedova, A. A.; Borisenko, G. *Free Radic. Biol. Med.* **2009**, *46* (11), 1439–1453.
- (11) Hüttemann, M.; Pecina, P.; Rainbolt, M.; Sanderson, T. H.; Kagan, V. E.; Samavati, L.; Doan, J. W.; Lee, I. *Mitochondrion* **2011**, *11* (3), 369–381.
- (12) Hannibal, L.; Tomasina, F.; Capdevila, D. A.; Demicheli, V.; Tórtora, V.; Alvarez-Paggi, D.; Jemmerson, R.; Murgida, D. H.; Radi, R. *Biochemistry* **2016**, *55* (3), 407–428.
- (13) Bushnell, G. W.; Louie, G. V.; Brayer, G. D. *J. Mol. Biol.* **1990**, *214* (2), 585–595.
- (14) Dunford, H. B. 2nd ed.; John Wiley & Sons: Hoboken, N.J., 2010.
- (15) Kagan, V. E.; Tyurin, V. A.; Jiang, J.; Tyurina, Y. Y.; Ritov, V. B.; Amoscato, A. A.; Osipov, A. N.; Belikova, N. A.; Kapralov, A. A.; Kini, V.; Vlasova, I. I.; Zhao, Q.; Zou, M.; Di, P.; Svistunenko, D. A.; Kurnikov, I. V.; Borisenko, G. G. *Nat. Chem. Biol.* **2005**, *1* (4), 223–232.
- (16) Liu, X.; Kim, C. N.; Yang, J.; Jemmerson, R.; Wang, X. *Cell* **1996**, *86* (1), 147–157.

- (17) Li, P.; Nijhawan, D.; Budihardjo, I.; Srinivasula, S. M.; Ahmad, M.; Alnemri, E. S.; Wang, X. *Cell* **1997**, *91* (4), 479–489.
- (18) Yu, X.; Acehan, D.; Menetret, J. F.; Booth, C. R.; Ludtke, S. J.; Riedl, S. J.; Shi, Y.; Wang, X.; Akey, C. W. *Structure* **2005**, *13* (11), 1725–1735.
- (19) Acehan, D.; Jiang, X.; Morgan, D. G.; Heuser, J. E.; Wang, X.; Akey, C. W. *Mol. Cell* **2002**, *9* (2), 423–432.
- (20) Mendez, D. L.; Akey, I. V.; Akey, C. W.; Kranz, R. G. *Biochemistry* **2017**, *56* (22), 2766–2769.
- (21) Barr, D. P.; Mason, R. P. *J. Biol. Chem.* **1995**, *270* (21), 12709–12716.
- (22) Aguila, S.; Vidal-Limon, A. M.; Alderete, J. B.; Sosa-Torres, M.; Vazquez-Duhalt, R. *J. Mol. Catal. B-Enzym.* **2013**, 85–86, 187–192.
- (23) Cassina, A. M.; Hodara, R.; Souza, J. M.; Thomson, L.; Castro, L.; Ischiropoulos, H.; Freeman, B. A.; Radi, R. *J. Biol. Chem.* **2000**, *275* (28), 21409–21415.
- (24) Chen, Y.-R.; Deterding, L. J.; Sturgeon, B. E.; Tomer, K. B.; Mason, R. P. *J. Biol. Chem.* **2002**, *277* (33), 29781–29791.
- (25) Ying, T.; Wang, Z.-H.; Lin, Y.-W.; Xie, J.; Tan, X.; Huang, Z.-X. *Chem. Commun.* **2009**, No. 30, 4512–4514.
- (26) Garcia-Heredia, J. M.; Diaz-Quintana, A.; Salzano, M.; Orzaez, M.; Perez-Paya, E.; Teixeira, M.; De la Rosa, M. A.; Diaz-Moreno, I. *J. Biol. Inorg. Chem.* **2011**, *16* (8), 1155–1168.
- (27) Capdevila, D. A.; Alvarez-Paggi, D.; Castro, M. A.; Tortora, V.; Demicheli, V.; Estrin, D. A.; Radi, R.; Murgida, D. H. *Chem. Commun.* **2014**, *50* (20), 2592–2594.
- (28) Paul, S. S.; Sil, P.; Haldar, S.; Mitra, S.; Chattopadhyay, K. *J. Biol. Chem.* **2015**, *290* (23), 14476–14490.
- (29) Paul, S. S.; Sil, P.; Chakraborty, R.; Haldar, S.; Chattopadhyay, K. *Biochemistry* **2016**.
- (30) Godoy, L. C.; Muñoz-Pinedo, C.; Castro, L.; Cardaci, S.; Schonhoff, C. M.; King, M.; Tórtora, V.; Marín, M.; Miao, Q.; Jiang, J. F.; Kapralov, A.; Jemmerson, R.; Silkstone, G. G.; Patel, J. N.; Evans, J. E.; Wilson, M. T.; Green, D. R.; Kagan, V. E.; Radi, R.; Mannick, J. B. *Proc. Natl. Acad. Sci.* **2009**, *106* (8), 2653–2658.
- (31) Belikova, N. A.; Vladimirov, Y. A.; Osipov, A. N.; Kapralov, A. A.; Tyurin, V. A.; Potapovich, M. V.; Basova, L. V.; Peterson, J.; Kurnikov, I. V.; Kagan, V. E. *Biochemistry* **2006**, *45* (15), 4998–5009.

- (32) Hanske, J.; Toffey, J. R.; Morenz, A. M.; Bonilla, A. J.; Schiavoni, K. H.; Pletneva, E. V. *Proc. Natl. Acad. Sci.* **2012**, *109* (1), 125–130.
- (33) Ascenzi, P.; Coletta, M.; Wilson, M. T.; Fiorucci, L.; Marino, M.; Polticelli, F.; Sinibaldi, F.; Santucci, R. *IUBMB Life* **2015**, *67* (2), 98–109.
- (34) Abriata, L. A.; Cassina, A.; Tortora, V.; Marin, M.; Souza, J. M.; Castro, L.; Vila, A. J.; Radi, R. *J. Biol. Chem.* **2009**, *284* (1), 17–26.
- (35) Rosell, F. I.; Ferrer, J. C.; Mauk, A. G. *J. Am. Chem. Soc.* **1998**, *120* (44), 11234–11245.
- (36) Assfalg, M.; Bertini, I.; Dolfi, A.; Turano, P.; Mauk, A. G.; Rosell, F. I.; Gray, H. B. *J. Am. Chem. Soc.* **2003**, *125* (10), 2913–2922.
- (37) Zaidi, S.; Hassan, M. I.; Islam, A.; Ahmad, F. *Cell. Mol. Life Sci.* **2014**, *71* (2), 229–255.
- (38) Amacher, J. F.; Zhong, F. F.; Lisi, G. P.; Zhu, M. Q.; Alden, S. L.; Hoke, K. R.; Madden, D. R.; Pletneva, E. V. *J. Am. Chem. Soc.* **2015**, *137* (26), 8435–8449.
- (39) Karsisiotis, A. I.; Deacon, O. M.; Wilson, M. T.; Macdonald, C.; Blumenschein, T. M. A.; Moore, G. R.; Worrall, J. A. R. *Sci. Rep.* **2016**, *6*, 30447.
- (40) Deacon, O. M.; Karsisiotis, A. I.; Moreno-Chicano, T.; Hough, M. A.; Macdonald, C.; Blumenschein, T. M. A.; Wilson, M. T.; Moore, G. R.; Worrall, J. A. R. *Biochemistry* **2017**, *56* (46), 6111–6124.
- (41) Turrens, J. F. *J. Physiol.* **2003**, *552* (2), 335–344.
- (42) Murphy, M. P. *Biochem. J.* **2008**, *417* (1), 1–13.
- (43) Berlett, B. S.; Stadtman, E. R. *J. Biol. Chem.* **1997**, *272* (33), 20313–20316.
- (44) Fan, X.; Zhang, J.; Theves, M.; Strauch, C.; Nemet, I.; Liu, X.; Qian, J.; Giblin, F. J.; Monnier, V. M. *J. Biol. Chem.* **2009**, *284* (50), 34618–34627.
- (45) de Graff, A. M. R.; Hazoglou, M. J.; Dill, K. A. *Structure* **2016**, *24* (2), 329–336.
- (46) Dalle-Donne, I.; Giustarini, D.; Colombo, R.; Rossi, R.; Milzani, A. *Trends Mol. Med.* **2003**, *9* (4), 169–176.
- (47) Dalle-Donne, I.; Scaloni, A.; Giustarini, D.; Cavarra, E.; Tell, G.; Lungarella, G.; Colombo, R.; Rossi, R.; Milzani, A. *Mass Spectrom. Rev.* **2005**, *24* (1), 55–99.
- (48) Sultana, R.; Boyd-Kimball, D.; Poon, H. F.; Cai, J.; Pierce, W. M.; Klein, J. B.; Markesbery, W. R.; Zhou, X. Z.; Lu, K. P.; Butterfield, D. A. *Neurobiol. Aging* **2006**, *27* (7), 918–925.

- (49) Sevcsik, E.; Trexler, A. J.; Dunn, J. M.; Rhoades, E. *J. Am. Chem. Soc.* **2011**, *133* (18), 7152–7158.
- (50) Martins, D.; English, A. M. *Redox Biol.* **2014**, *2*, 632–639.
- (51) Pedersen, J. T.; Chen, S. W.; Borg, C. B.; Ness, S.; Bahl, J. M.; Heegaard, N. H. H.; Dobson, C. M.; Hemmingsen, L.; Cremades, N.; Teilum, K. *J. Am. Chem. Soc.* **2016**, *138* (12), 3966–3969.
- (52) Radi, R. *Proc. Natl. Acad. Sci.* **2018**, *115* (23), 5839.
- (53) Gray, H. B.; Winkler, J. R. *Proc. Natl. Acad. Sci.* **2015**, *112* (35), 10920–10925.
- (54) Kathiresan, M.; English, A. M. *Chem. Sci.* **2017**, *8* (2), 1152–1162.
- (55) Kathiresan, M.; English, A. M. *J. Am. Chem. Soc.* **2018**, *140* (38), 12033–12039.
- (56) Thannickal, V. J.; Fanburg, B. L. *Am. J. Physiol.-Lung Cell. Mol. Physiol.* **2000**, *279* (6), L1005–L1028.
- (57) Lee, J.-W.; Helmann, J. D. *Nature* **2006**, *440* (7082), 363–367.
- (58) Giorgio, M.; Trinei, M.; Migliaccio, E.; Pelicci, P. G. *Nat. Rev. Mol. Cell Biol.* **2007**, *8* (9), 722–728.
- (59) E. R. Stadtman. *Annu. Rev. Biochem.* **1993**, *62* (1), 797–821.
- (60) Levine, R. L.; Stadtman, E. R. *Mol. Aging* **2001**, *36* (9), 1495–1502.
- (61) Xu, G.; Chance, M. R. *Chem. Rev.* **2007**, *107* (8), 3514–3543.
- (62) Møller, I. M.; Rogowska-Wrzesinska, A.; Rao, R. S. P. *J. Proteomics* **2011**, *74* (11), 2228–2242.
- (63) Go, Y.-M.; Jones, D. P. *Free Radic. Biol. Med.* **2011**, *50* (4), 495–509.
- (64) Giulivi, C.; Davies, K. J. A. In *Methods in Enzymology*; Academic Press, 1994; Vol. 233, pp 363–371.
- (65) Giulivi, C.; Davies, K. J. A. *J. Biol. Chem.* **2001**, *276* (26), 24129–24136.
- (66) Luo, S.; Wehr, N. B. *Redox Rep.* **2009**, *14* (4), 159–166.
- (67) Yan, L.-J. *Curr. Protoc. Protein Sci.* **2009**, *56* (1), 14.4.1–14.4.28.
- (68) Requena, J. R.; Chao, C.-C.; Levine, R. L.; Stadtman, E. R. *Proc. Natl. Acad. Sci. U. S. A.* **2001**, *98* (1), 69–74.
- (69) Parson, W. W. Springer Berlin Heidelberg, 2015; pp 1–29.

- (70) Greenfield, N. J. *Nat. Protoc.* **2006**, *1* (6), 2876–2890.
- (71) Beychok, S. *Science* **1966**, *154* (3754), 1288.
- (72) Sreerama, N.; Woody, R. W. In *Methods in Enzymology*; Academic Press, 2004; Vol. 383, pp 318–351.
- (73) Sreerama, N.; Woody, R. W. *Anal. Biochem.* **2000**, *287* (2), 252–260.
- (74) Greenfield, N. J. *Nat. Protoc.* **2006**, *1* (6), 2527–2535.
- (75) Becktel, W. J.; Schellman, J. A. *Biopolymers* **1987**, *26* (11), 1859–1877.
- (76) Swint, L.; Robertson, A. D. *Protein Sci.* **1993**, *2* (12), 2037–2049.
- (77) Lakowicz, J. R. Springer US, 2006; pp 1-26.
- (78) Chen, Y.; Barkley, M. D. *Biochemistry* **1998**, *37* (28), 9976–9982.
- (79) Ghisaidoobe, A. B. T.; Chung, S. J. *Int. J. Mol. Sci.* **2014**, *15* (12), 22518–22538.
- (80) Yuan, T.; Weljie, A. M.; Vogel, H. J. *Biochemistry* **1998**, *37* (9), 3187–3195.
- (81) Gouterman, M. *J. Mol. Spectrosc.* **1961**, *6*, 138–163.
- (82) Dolphin, D. Elsevier Science, 2012.
- (83) Spiro, T. G. In *Advances in Protein Chemistry*; Anfinsen, C. B., Edsall, J. T., Richards, F. M., Eds.; Academic Press, 1985; Vol. 37, pp 111–159.
- (84) Smulevich, G.; Mauro, J. M.; Fishel, L. A.; English, A. M.; Kraut, J.; Spiro, T. G. *Biochemistry* **1988**, *27* (15), 5477–5485.
- (85) Cavanagh, J.; Fairbrother, W. J.; Palmer III, A. G.; Skelton, N. J. Elsevier, 1995.
- (86) Grzesiek, S.; Bax, A. *J. Am. Chem. Soc.* **1992**, *114* (16), 6291–6293.
- (87) Grzesiek, S.; Bax, A. *J. Magn. Reson.* **1992**, *99* (1), 201–207.
- (88) Marion, D.; Driscoll, P. C.; Kay, L. E.; Wingfield, P. T.; Bax, A.; Gronenborn, A. M.; Clore, G. M. *Biochemistry* **1989**, *28* (15), 6150–6156.
- (89) Marion, D.; Kay, L. E.; Sparks, S. W.; Torchia, D. A.; Bax, A. *J. Am. Chem. Soc.* **1989**, *111* (4), 1515–1517.
- (90) Zuiderweg, E. R. P.; Fesik, S. W. *Biochemistry* **1989**, *28* (6), 2387–2391.
- (91) Bax, A. *Annu. Rev. Biochem.* **1989**, *58* (1), 223–256.

- (92) Cornilescu, G.; Delaglio, F.; Bax, A. *J. Biomol. NMR* **1999**, *13* (3), 289–302.
- (93) Drenth, J. Springer Science & Business Media, 2007.
- (94) Smyth, M. S.; Martin, J. H. *J. Mol. Pathol.* **2000**, *53* (1), 8.
- (95) Ilari, A.; Savino, C. In *Bioinformatics*; Springer, 2008; pp 63–87.
- (96) Frank, J. Oxford University Press, 2006.
- (97) Frank, J. *Q. Rev. Biophys.* **2009**, *42* (3), 139–158.
- (98) Milne, J. L. S.; Borgnia, M. J.; Bartesaghi, A.; Tran, E. E. H.; Earl, L. A.; Schauder, D. M.; Lengyel, J.; Pierson, J.; Patwardhan, A.; Subramaniam, S. *FEBS J.* **2013**, *280* (1), 28–45.
- (99) Patel, R. *Clin. Chem.* **2013**, *59* (2), 340–342.
- (100) Fenn, J.; Mann, M.; Meng, C.; Wong, S.; Whitehouse, C. *Science* **1989**, *246* (4926), 64.
- (101) Kaltashov, I. A.; Eyles, S. J. In *Mass Spectrometry in Structural Biology and Biophysics*; John Wiley & Sons, Inc., 2012; pp 52–88.
- (102) Konermann, L.; Vahidi, S.; Sowole, M. A. *Anal. Chem.* **2014**, *86* (1), 213–232.
- (103) Kebarle, P.; Verkerk, U. H. *Mass Spectrom. Rev.* **2009**, *28* (6), 898–917.
- (104) Konermann, L.; Ahadi, E.; Rodriguez, A. D.; Vahidi, S. *Anal. Chem.* **2013**, *85* (1), 2–9.
- (105) Konermann, L.; Metwally, H.; Duez, Q.; Peters, I. *Analyst* **2019**, *144* (21), 6157–6171.
- (106) Cech, N. B.; Enke, C. G. *Mass Spectrom. Rev.* **2001**, *20* (6), 362–387.
- (107) Nguyen, S.; Fenn, J. B. *Proc. Natl. Acad. Sci.* **2007**, *104* (4), 1111.
- (108) Dole, M.; Mack, L. L.; Hines, R. L.; Mobley, R. C.; Ferguson, L. D.; Alice, M. B. *J. Chem. Phys.* **1968**, *49* (5), 2240–2249.
- (109) McAllister, R. G.; Metwally, H.; Sun, Y.; Konermann, L. *J. Am. Chem. Soc.* **2015**, *137* (39), 12667–12676.
- (110) Rayleigh, Lord. *Lond. Edinb. Dublin Philos. Mag. J. Sci.* **1882**, *14* (87), 184–186.
- (111) Mirza, U. A.; Cohen, S. L.; Chait, B. T. *Anal. Chem.* **1993**, *65* (1), 1–6.

- (112) Konermann, L.; Rosell, F. I.; Mauk, A. G.; Douglas, D. J. *Biochemistry* **1997**, *36* (21), 6448–6454.
- (113) Konermann, L.; Douglas, D. J. *Biochemistry* **1997**, *36* (40), 12296–12302.
- (114) Konermann, L.; Rodriguez, A. D.; Liu, J. *Anal. Chem.* **2012**, *84* (15), 6798–6804.
- (115) Ahadi, E.; Konermann, L. *J. Phys. Chem. B* **2012**, *116* (1), 104–112.
- (116) Metwally, H.; Duez, Q.; Konermann, L. *Anal. Chem.* **2018**, *90* (16), 10069–10077.
- (117) Märk, T. D.; Dunn, G. H. Springer Vienna, 2013.
- (118) El-Hawiet, A.; Kitova, E. N.; Liu, L.; Klassen, J. S. *J. Am. Soc. Mass Spectrom.* **2010**, *21* (11), 1893–1899.
- (119) Ishii, K.; Noda, M.; Uchiyama, S. *Biophys. Physicobiology* **2016**, *13*, 87–95.
- (120) Heck, A. J. R.; van den Heuvel, R. H. H. *Mass Spectrom. Rev.* **2004**, *23* (5), 368–389.
- (121) Hernández, H.; Robinson, C. V. *Nat. Protoc.* **2007**, *2* (3), 715–726.
- (122) Heck, A. J. R. *Nat. Methods* **2008**, *5* (11), 927–933.
- (123) Leney, A. C.; Heck, A. J. R. *J. Am. Soc. Mass Spectrom.* **2017**, *28* (1), 5–13.
- (124) Krutchinsky, A. N.; Chait, B. T. *J. Am. Soc. Mass Spectrom.* **2002**, *13* (2), 129–134.
- (125) Aebersold, R.; Goodlett, D. R. *Chem. Rev.* **2001**, *101* (2), 269–296.
- (126) Aebersold, R.; Mann, M. *Nature* **2003**, *422* (6928), 198–207.
- (127) Han, X.; Aslanian, A.; Yates, J. R. *Anal. Tech.* **2008**, *12* (5), 483–490.
- (128) Nilsson, T.; Mann, M.; Aebersold, R.; Yates, J. R.; Bairoch, A.; Bergeron, J. J. M. *Nat. Methods* **2010**, *7* (9), 681–685.
- (129) McLafferty, F. W. *Science* **1981**, *214* (4518), 280–287.
- (130) Yost, R. A.; Enke, C. G. *Anal. Chem.* **1979**, *51* (12), 1251–1264.
- (131) March, R. E. *J. Mass Spectrom.* **1997**, *32* (4), 351–369.
- (132) Dawson, P. H. Elsevier, 2013.
- (133) Dass, C. John Wiley & Sons, 2007; Vol. 16.
- (134) Sleno, L.; Volmer, D. A. *J. Mass Spectrom.* **2004**, *39* (10), 1091–1112.



- (135) Dubois, F.; Knochenmuss, R.; Zenobi, R.; Brunelle, A.; Deprun, C.; Le Beyec, Y. *Rapid Commun. Mass Spectrom.* **1999**, *13* (9), 786–791.
- (136) Morris, H. R.; Paxton, T.; Dell, A.; Langhorne, J.; Berg, M.; Bordoli, R. S.; Hoyes, J.; Bateman, R. H. *Rapid Commun. Mass Spectrom.* **1996**, *10* (8), 889–896.
- (137) Shevchenko, A.; Chernushevich, I.; Ens, W.; Standing, K. G.; Thomson, B.; Wilm, M.; Mann, M. *Rapid Commun. Mass Spectrom.* **1997**, *11* (9), 1015–1024.
- (138) Guilhaus, M. In *Encyclopedia of Analytical Science (Second Edition)*; Worsfold, P., Townshend, A., Poole, C., Eds.; Elsevier: Oxford, 2005; pp 412–423.
- (139) Mamyrin, B. A. *Int. J. Mass Spectrom.* **2001**, *206* (3), 251–266.
- (140) Thalassinou, K.; Slade, S. E.; Jennings, K. R.; Scrivens, J. H.; Giles, K.; Wildgoose, J.; Hoyes, J.; Bateman, R. H.; Bowers, M. T. *Spec. Issue Honour Dudley H Williams* **2004**, *236* (1), 55–63.
- (141) Pringle, S. D.; Giles, K.; Wildgoose, J. L.; Williams, J. P.; Slade, S. E.; Thalassinou, K.; Bateman, R. H.; Bowers, M. T.; Scrivens, J. H. *Int. J. Mass Spectrom.* **2007**, *261* (1), 1–12.
- (142) Giles, K.; Williams, J. P.; Campuzano, I. *Rapid Commun. Mass Spectrom.* **2011**, *25* (11), 1559–1566.
- (143) Giles, K.; Pringle, S. D.; Worthington, K. R.; Little, D.; Wildgoose, J. L.; Bateman, R. H. *Rapid Commun. Mass Spectrom.* **2004**, *18* (20), 2401–2414.
- (144) Eiceman, G. A.; Karpas, Z.; Hill Jr, H. H. CRC press, 2013; pp 1-36.
- (145) Bohrer, B. C.; Merenbloom, S. I.; Koeniger, S. L.; Hilderbrand, A. E.; Clemmer, D. E. *Annu. Rev. Anal. Chem.* **2008**, *1* (1), 293–327.
- (146) McDaniel, E. W.; Mason, E. A. Wiley, 1988.
- (147) Sun, Y.; Vahidi, S.; Sowole, M. A.; Konermann, L. *J. Am. Soc. Mass Spectrom.* **2016**, *27* (1), 31–40.
- (148) Hinnenkamp, V.; Klein, J.; Meckelmann, S. W.; Balsaa, P.; Schmidt, T. C.; Schmitz, O. *J. Anal. Chem.* **2018**, *90* (20), 12042–12050.
- (149) Mann, M.; Højrup, P.; Roepstorff, P. *Biol. Mass Spectrom.* **1993**, *22* (6), 338–345.
- (150) Coon, J. J.; Syka, J. E. P.; Shabanowitz, J.; Hunt, D. F. *BioTechniques* **2005**, *38* (4), 519–523.
- (151) Witze, E. S.; Old, W. M.; Resing, K. A.; Ahn, N. G. *Nat. Methods* **2007**, *4* (10), 798–806.

- (152) Syka, J. E. P.; Coon, J. J.; Schroeder, M. J.; Shabanowitz, J.; Hunt, D. F. *Proc. Natl. Acad. Sci. U. S. A.* **2004**, *101* (26), 9528.
- (153) Mitchell Wells, J.; McLuckey, S. A. In *Methods in Enzymology*; Academic Press, 2005; Vol. 402, pp 148–185.
- (154) Roepstorff, P.; Fohlman, J. *Biomed. Mass Spectrom.* **1984**, *11* (11), 601.
- (155) Biemann, K. *Methods Enzymol.* **1990**, *193*, 886–887.
- (156) Chu, I. K.; Siu, C.-K.; Lau, J. K.-C.; Tang, W. K.; Mu, X.; Lai, C. K.; Guo, X.; Wang, X.; Li, N.; Xia, Y.; Kong, X.; Oh, H. B.; Ryzhov, V.; Tureček, F.; Hopkinson, A. C.; Siu, K. W. M. *Spec. Issue Biol. Cation Radic. Ion-Electron Ion-Ion Interact.* **2015**, *390*, 24–27.
- (157) Chait, B. T. *Science* **2006**, *314* (5796), 65.
- (158) Han, X.; Jin, M.; Breuker, K.; McLafferty, F. W. *Science* **2006**, *314* (5796), 109.
- (159) Chen, B.; Brown, K. A.; Lin, Z.; Ge, Y. *Anal. Chem.* **2018**, *90* (1), 110–127.
- (160) Lermyte, F.; Tsybin, Y. O.; O'Connor, P. B.; Loo, J. A. *J. Am. Soc. Mass Spectrom.* **2019**, *30* (7), 1149–1157.
- (161) Smith, L. M.; Kelleher, N. L.; Linial, M.; Goodlett, D.; Langridge-Smith, P.; Ah Goo, Y.; Safford, G.; Bonilla\*, L.; Kruppa, G.; Zubarev, R.; Rontree, J.; Chamot-Rooke, J.; Garavelli, J.; Heck, A.; Loo, J.; Penque, D.; Hornshaw, M.; Hendrickson, C.; Pasa-Tolic, L.; Borchers, C.; Chan, D.; Young\*, N.; Agar, J.; Masselon, C.; Gross\*, M.; McLafferty, F.; Tsybin, Y.; Ge, Y.; Sanders\*, I.; Langridge, J.; Whitelegge\*, J.; Marshall, A.; The Consortium for Top Down Proteomics. *Nat. Methods* **2013**, *10* (3), 186–187.
- (162) Toby, T. K.; Fornelli, L.; Kelleher, N. L. *Annu. Rev. Anal. Chem.* **2016**, *9* (1), 499–519.
- (163) Patrie, S. M. In *Modern Proteomics – Sample Preparation, Analysis and Practical Applications*; Mirzaei, H., Carrasco, M., Eds.; Springer International Publishing: Cham, 2016; pp 171–200.
- (164) Schaffer, L. V.; Millikin, R. J.; Miller, R. M.; Anderson, L. C.; Fellers, R. T.; Ge, Y.; Kelleher, N. L.; LeDuc, R. D.; Liu, X.; Payne, S. H.; Sun, L.; Thomas, P. M.; Tucholski, T.; Wang, Z.; Wu, S.; Wu, Z.; Yu, D.; Shortreed, M. R.; Smith, L. M. *PROTEOMICS* **2019**, *19* (10), 1800361.
- (165) Fabris, D.; Yu, E. T. *J. Mass Spectrom.* **2010**, *45* (8), 841–860.
- (166) Liu, X. R.; Zhang, M. M.; Gross, M. L. *Chem. Rev.* **2020**, *120* (10), 4355–4454.

- (167) Smythe, C. V. *J. Biol. Chem.* **1936**, *114* (3), 601–612.
- (168) Anson, M. L. *J. Gen. Physiol.* **1940**, *23* (3), 321–331.
- (169) Hambly, D. M.; Gross, M. L. *J. Am. Soc. Mass Spectrom.* **2005**, *16* (12), 2057–2063.
- (170) Hambly, D.; Gross, M. *Int. J. Mass Spectrom.* **2007**, *259* (1–3), 124–129.
- (171) Leitner, A.; Walzthoeni, T.; Kahraman, A.; Herzog, F.; Rinner, O.; Beck, M.; Aebersold, R. *Mol. Amp Cell. Proteomics* **2010**, *9* (8), 1634.
- (172) Leitner, A.; Faini, M.; Stengel, F.; Aebersold, R. *Trends Biochem. Sci.* **2016**, *41* (1), 20–32.
- (173) O'Reilly, F. J.; Rappsilber, J. *Nat. Struct. Mol. Biol.* **2018**, *25* (11), 1000–1008.
- (174) Liu, F.; Rijkers, D. T. S.; Post, H.; Heck, A. J. R. *Nat. Methods* **2015**, *12* (12), 1179–1184.
- (175) Rappsilber, J. *J. Struct. Biol.* **2011**, *173* (3), 530–540.
- (176) Schmidt, C.; Urlaub, H. *Curr. Opin. Struct. Biol.* **2017**, *46*, 157–168.
- (177) Hamuro, Y.; Coales, S. J.; Southern, M. R.; Nemeth-Cawley, J. F.; Stranz, D. D.; Griffin, P. R. *J. Biomol. Tech. JBT* **2003**, *14* (3), 171–182.
- (178) Maier, C. S.; Deinzer, M. L. In *Methods in Enzymology*; Academic Press, 2005; Vol. 402, pp 312–360.
- (179) Wales, T. E.; Engen, J. R. *Mass Spectrom. Rev.* **2006**, *25* (1), 158–170.
- (180) Marcsisin, S. R.; Engen, J. R. *Anal. Bioanal. Chem.* **2010**, *397* (3), 967–972.
- (181) Konermann, L.; Pan, J.; Liu, Y.-H. *Chem. Soc. Rev.* **2011**, *40* (3), 1224–1234.
- (182) Masson, G. R.; Jenkins, M. L.; Burke, J. E. *Expert Opin. Drug Discov.* **2017**, *12* (10), 981–994.
- (183) Resing, K. A.; Hoofnagle, A. N.; Ahn, N. G. *J. Am. Soc. Mass Spectrom.* **1999**, *10* (8), 685–702.
- (184) Hoofnagle, A. N.; Resing, K. A.; Ahn, N. G. In *MAP Kinase Signaling Protocols*; Seger, R., Ed.; Humana Press: Totowa, NJ, 2004; pp 283–298.
- (185) Zhang, Z.; Smith, D. L. *Protein Sci.* **1993**, *2* (4), 522–531.
- (186) Rosa, J. J.; Richards, F. M. *J. Mol. Biol.* **1979**, *133* (3), 399–416.

- (187) Englander, J. J.; Rogero, J. R.; Englander, S. W. *Anal. Biochem.* **1985**, *147* (1), 234–244.
- (188) Wu, Y.; Engen, J. R.; Hobbins, W. B. *J. Am. Soc. Mass Spectrom.* **2006**, *17* (2), 163–167.
- (189) Jørgensen, T. J. D.; Gårdsvoll, H.; Ploug, M.; Roepstorff, P. *J. Am. Chem. Soc.* **2005**, *127* (8), 2785–2793.
- (190) McLafferty, F. W.; Guan, Z.; Haupts, U.; Wood, T. D.; Kelleher, N. L. *J. Am. Chem. Soc.* **1998**, *120* (19), 4732–4740.
- (191) Ferguson, P. L.; Pan, J.; Wilson, D. J.; Dempsey, B.; Lajoie, G.; Shilton, B.; Konermann, L. *Anal. Chem.* **2007**, *79* (1), 153–160.
- (192) Ferguson, P. L.; Konermann, L. *Anal. Chem.* **2008**, *80* (11), 4078–4086.
- (193) Pan, J.; Han, J.; Borchers, C. H.; Konermann, L. *Anal. Chem.* **2010**, *82* (20), 8591–8597.
- (194) Englander, S. W.; Mayne, L.; Kan, Z.-Y.; Hu, W. *Annu. Rev. Biophys.* **2016**, *45* (1), 135–152.
- (195) Yao, Z.; Tito, P.; Robinson, C. V. In *Methods in Enzymology*; Academic Press, 2005; Vol. 402, pp 389–402.
- (196) Eyles, S. J.; Kaltashov, I. A. *Methods* **2004**, *34* (1), 88–99.
- (197) Marcoux, J.; Robinson, C. V. *Structure* **2013**, *21* (9), 1541–1550.
- (198) Ganem, B.; Li, Y. T.; Henion, J. D. *J. Am. Chem. Soc.* **1991**, *113* (16), 6294–6296.
- (199) Katta, V.; Chait, B. T. *J. Am. Chem. Soc.* **1991**, *113* (22), 8534–8535.
- (200) Loo, J. A. *J. Mass Spectrom.* **1995**, *30* (1), 180–183.
- (201) Loo, J. A. *Mass Spectrom. Rev.* **1997**, *16* (1), 1–23.
- (202) Ruotolo, B. T.; Benesch, J. L. P.; Sandercock, A. M.; Hyung, S.-J.; Robinson, C. V. *Nat. Protoc.* **2008**, *3* (7), 1139–1152.
- (203) Uetrecht, C.; Rose, R. J.; van Duijn, E.; Lorenzen, K.; Heck, A. J. R. *Chem. Soc. Rev.* **2010**, *39* (5), 1633–1655.
- (204) Mesleh, M. F.; Hunter, J. M.; Shvartsburg, A. A.; Schatz, G. C.; Jarrold, M. F. *J. Phys. Chem.* **1996**, *100* (40), 16082–16086.

- (205) Ewing, S. A.; Donor, M. T.; Wilson, J. W.; Prell, J. S. *J. Am. Soc. Mass Spectrom.* **2017**, 28 (4), 587–596.
- (206) Jurneczko, E.; Barran, P. E. *Analyst* **2011**, 136 (1), 20–28.
- (207) Lanucara, F.; Holman, S. W.; Gray, C. J.; Eyers, C. E. *Nat. Chem.* **2014**, 6 (4), 281–294.
- (208) Dixit, S. M.; Polasky, D. A.; Ruotolo, B. T. *Curr. Opin. Chem. Biol.* **2018**, 42, 93–100.
- (209) Florence, T. M. *J. Inorg. Biochem.* **1985**, 23 (2), 131–141.
- (210) Villegas, J. A.; Mauk, A. G.; Vazquez-Duhalt, R. *Chem. Biol.* **2000**, 7 (4), 237–244.
- (211) Kim, N. H.; Jeong, M. S.; Choir, S. Y.; Kang, J. H. *Mol. Cells* **2006**, 22 (2), 220–227.
- (212) Stocks, B. B.; Konermann, L. *J. Mol. Biol.* **2010**, 398 (2), 362–373.

## Chapter 2. Elucidation of an H<sub>2</sub>O<sub>2</sub>-Induced, *In Situ* Activation Mechanism of the Peroxidase Activity of Cytochrome *c*

### 2.1. Introduction

Cytochrome *c* (cyt *c*) is a highly conserved 12 kDa heme protein that transfers electrons in the respiratory chain. Cyt *c* can also catalyze the H<sub>2</sub>O<sub>2</sub>-induced oxidation of a wide range of substrates.<sup>1-3</sup> This peroxidase activity has attracted considerable attention due to its role during apoptosis (programmed cell death).<sup>4-9</sup> A key apoptotic pathway involves the production of H<sub>2</sub>O<sub>2</sub> in mitochondria.<sup>10,11</sup> Cyt *c* utilizes this H<sub>2</sub>O<sub>2</sub> to catalyze the oxidation of cardiolipin in the mitochondrial membrane.<sup>4,5,12-14</sup> The damaged membrane allows the release of pre-apoptotic factors into the cytoplasm, ultimately resulting in cell death.<sup>4,6,7,15</sup> Like other peroxidases,<sup>16-18</sup> cyt *c* follows a mechanism where H<sub>2</sub>O<sub>2</sub> reacts with the Fe(III) resting state to produce “Compound I”, with a Fe(IV)=O heme and an adjacent radical. Subsequent H abstraction from organic substrates regenerates the resting state.<sup>19</sup> Reactions of the newly formed radicals with O<sub>2</sub> then yield stable oxidation products.<sup>20,21</sup> This cycle usually consumes external substrates, but it also oxidizes the protein and causes gradual deactivation.<sup>22-25</sup>

Classical peroxidases have a five-coordinate heme, where the sixth (distal) site is vacant or occupied by loosely bound water.<sup>16,18,26</sup> This five-coordinate structure allows for Fe-H<sub>2</sub>O<sub>2</sub> interactions which are required for initiating the catalytic cycle.<sup>6,8,13,14,26-28</sup> Native cyt *c* is six-coordinate, with Met80 as distal ligand (Figure 2-1A).<sup>29</sup> It thus seems paradoxical that cyt *c* would be peroxidase-active.<sup>14,30-33</sup> A possible explanation invokes transiently formed five-coordinate conformers.<sup>2,33-40</sup> Rupture of the distal Met80-Fe bond by unfolding,<sup>8,37</sup> chemical,<sup>2,31,32,35,41,42</sup> or mutational<sup>6,14,28,30,36,41,43-45</sup> modifications enhances peroxidase activity.

The proximal His18-Fe contact in cyt *c* is quite robust, while the 70-85 Ω loop is flexible<sup>39</sup> and allows various distal ligation scenarios.<sup>2,46</sup> Basic pH produces “alkaline” conformers with Lys72, 73 or 79 as distal ligand (Figure 2-1B).<sup>33,40,42,47,48</sup> This transition can be pushed into the neutral range by various means<sup>2,35,42,46,49</sup> that include Tyr67 modifications.<sup>44,46,50</sup> Similarly, cardiolipin binding<sup>13,51,52</sup> causes displacement of Met80 by Lys or His.<sup>12,34,53,54</sup>

It is counterintuitive that the aforementioned non-native conformers show enhanced peroxidase activity, considering their apparent lack of a vacant sixth coordination site.<sup>6,13,26-28,35,42,49,55</sup> Once again, catalysis may be facilitated by transiently populated five-coordinate forms.<sup>2,33-40</sup> However, alkaline iron ligation by Lys is more stable than the native Met80-Fe bond.<sup>31,35,39,46</sup> Alkaline conformers should thus have a lower peroxidase activity than native cyt *c*, which is opposite to the observed behavior.<sup>15,35,42,49,55,56</sup> Overall, it remains unclear why native cyt *c* and other six-coordinate variants possess apparent peroxidase activity.

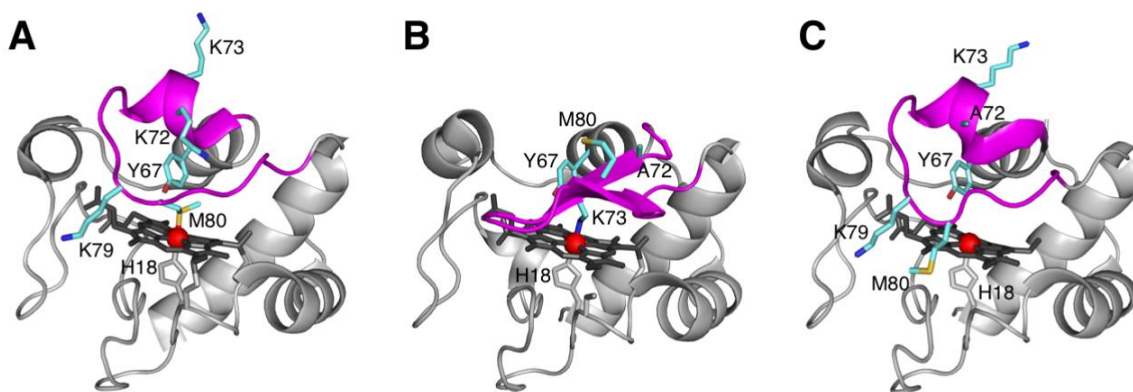


**Figure 2-1.** Cyt *c* crystal structures. The 70-85 Ω-loop is depicted in magenta, key residues are highlighted in cyan, iron is displayed in red. (A) Native equine wild-type with Met80-Fe ligation (PDB 1HRC).<sup>29</sup> (B) Alkaline conformer with Lys73-Fe ligation (yeast K72A/T78C/K79G/C102S, PDB 4Q5P).<sup>35</sup> (C) Distally de-ligated form (yeast K72A/C102S, PDB 4MU8).<sup>14</sup>

Some catalyzed reactions (unrelated to peroxidases) exhibit an initial lag phase. Such behavior can have different mechanistic origins, but it often reflects the *in situ* activation of a pre-catalyst.<sup>57-59</sup> Intriguingly, a lag phase is also seen for cyt *c*-catalyzed peroxidase reactions.<sup>14,40,60</sup> The possible implications of this phenomenon have received surprisingly little attention. Cyt *c* kinetic analyses usually discard lag phase data, while focusing on the subsequent steady-state regime.<sup>14,44,54,61</sup> Contrary to prevailing views, there is a possibility that native cyt *c* does *not* exhibit substantial peroxidase activity, and that a potent peroxidase is formed only after H<sub>2</sub>O<sub>2</sub>-induced modifications. Such activated cyt *c* would likely be five-coordinate, as seen in certain peroxidase-enhanced mutants (Figure 2-1C).<sup>14</sup> The occurrence of an H<sub>2</sub>O<sub>2</sub>-induced activation step would imply that investigations conducted in the absence of H<sub>2</sub>O<sub>2</sub> are unsuitable for deciphering the properties of peroxidase-active cyt *c*.

Here we address the issues outlined above by performing time-resolved experiments on the consequences of H<sub>2</sub>O<sub>2</sub>-cyt *c* interactions. We interrogate H<sub>2</sub>O<sub>2</sub>-induced structural changes by coupling catalase quenching assays with spectroscopic techniques, as well as mass spectrometry (MS)-based peptide mapping, covalent labeling, and top-down assays. Our data suggest that unmodified cyt *c* exhibits minimal peroxidase activity. H<sub>2</sub>O<sub>2</sub> causes highly selective covalent modifications that produce five-coordinate proteoforms with enhanced peroxidase activity. These findings resolve the apparent structure-function mismatch by uncovering a previously unrecognized H<sub>2</sub>O<sub>2</sub>-induced activation process.



## 2.2. Materials and Methods

### 2.2.1. Materials.

Horse heart ferri-cyt *c*, guaiacol (o-methoxyphenol)<sup>62</sup>, chloramine-T (N-chloro-4-toluol-sulfonamide)<sup>63</sup>, and Girard's reagent T (GRT, carboxymethyl-trimethylammonium-hydrazide chloride)<sup>64</sup> were from Sigma (St. Louis, MO). Unless specified otherwise, solutions contained 10  $\mu\text{M}$  cyt *c* in 65 mM aqueous potassium phosphate buffer at pH 7.4. The  $\text{H}_2\text{O}_2$  concentration employed here (500  $\mu\text{M}$ , unless noted otherwise) falls within the range used for earlier assays<sup>14,40,60</sup> and is physiologically relevant as the mitochondrial  $\text{H}_2\text{O}_2$  concentration can reach  $\sim 10^{-4}$  M at the onset of apoptosis.<sup>11</sup> All experiments were conducted at  $22 \pm 2$  °C.

### 2.2.2. Optical Spectroscopy.

UV-Vis spectra were acquired on a Cary-100 instrument (Varian, Mississauga, ON). For measurements at 695 nm the protein concentration was raised to 40  $\mu\text{M}$ . Peroxidase kinetics were measured by tracking the oxidation of 9 mM guaiacol in the presence of 1  $\mu\text{M}$  cyt *c*. Reaction rates ( $\mu\text{M}$  guaiacol oxidized  $\text{s}^{-1}$ ) were determined<sup>62</sup> with  $\epsilon_{470} = 26.6 \text{ mM}^{-1} \text{ cm}^{-1}$  for the tetraguaiacol product. Circular dichroism (CD) spectra were recorded on a J-810 spectropolarimeter (JASCO, Easton, MD). For probing  $\text{H}_2\text{O}_2$ -induced structural changes, UV-Vis data were recorded on-line (20 s per spectrum). CD scans were slower ( $\sim 20$  min per spectrum), requiring quenching of the samples with 0.1  $\mu\text{M}$  catalase prior to data acquisition.

### 2.2.3. Protein Samples.

For MS, 100  $\mu\text{L}$  aliquots were removed from the reaction mixture at selected time points, followed by catalase quenching. NMR samples were prepared identically, but in  $\text{D}_2\text{O}$ . In addition, NMR samples were concentrated to 100  $\mu\text{M}$  using 10 kDa MWCO centrifuge filters (Millipore, Etobicoke, ON). Carbonyl labeling was performed by incubating 10  $\mu\text{M}$  cyt *c* in buffer with 80 mM GRT<sup>65</sup> for 3 hours at room temperature. The reaction was halted by exchange into GRT-free buffer using 10 kDa MWCO filters.

#### 2.2.4. NMR Spectroscopy.

<sup>1</sup>H-NMR data were collected at 25°C using a Varian Inova 600 MHz spectrometer using a spectral width of 50,000 Hz and an acquisition time of 0.4 s. 2,2-dimethyl-2-silapetane-5-sulphonate served as internal reference. A weak pre-saturation pulse was applied during the 0.1 s recycle delay to suppress the residual water signal. Data were zero filled to 132 K, processed using line broadening factors of 2.5 or 10 Hz, and baseline corrected.

#### 2.2.5. Mass Spectrometry.

MS was performed on a Synapt G2 ESI mass spectrometer coupled to a UPLC (Waters, Milford, MA). Intact cyt *c* was analyzed using a C4 desalting column. For top-down MS/MS, 16+ ions were quadrupole selected, followed by CID in Ar. [Fe(III) cyt *c* + 15H]<sup>16+</sup> isotope distributions<sup>66</sup> were simulated using ProteinProspector (UCSF). Tryptic peptides were generated using MS-grade modified trypsin (Promega, Madison, WI) in a 50:1 cyt *c*/trypsin ratio. Digests were incubated overnight at 37°C. Peptides were analyzed by LC/MS using a C18 column. Peptides were identified using data-dependent acquisition and MS<sup>E</sup>. For quantitating oxidative modifications in tryptic peptides 2.5 μM bradykinin was added to each sample as internal standard after digestion.<sup>67</sup> Normalized peptide intensities  $N(t)$  were calculated as a function of H<sub>2</sub>O<sub>2</sub> incubation time  $t$  as  $N(t) = I(t) / I_{brad}$ , where  $I(t)$  is the signal intensity of an unmodified tryptic peptide at time  $t$ , and  $I_{brad}$  is the bradykinin intensity. In analogous fashion,  $N_{contr}$  data were generated for unoxidized control samples. The extent of oxidation can then be expressed as “fraction oxidized”,  $fox(t) = (1 - [N(t)/N_{contr}])$ .<sup>67</sup> Monitoring the depletion of unoxidized peptides ensures robust  $fox$  data even if some of the products are difficult to detect.<sup>67</sup>

## 2.3. Results and Discussion

### 2.3.1. Peroxidase Kinetics.

The peroxidase activity of *cyt c* can be probed by monitoring the oxidation of chromophoric substrates such as guaiacol in the presence of  $\text{H}_2\text{O}_2$ .<sup>1,28,35,62,68</sup> Without catalyst there was no evidence of product formation, whereas oxidation proceeded readily after *cyt c* addition (Figure 2-2, black trace). The guaiacol kinetics exhibited three stages (Figure 2-2, red trace): (i) a lag phase during which the rate gradually increased from ~zero, (ii) a linear steady-state region, and (iii) a region during which the rate declined. The third stage reflects oxidative deactivation of *cyt c* (Figure 2-3).<sup>23,24</sup> Lowering the  $\text{H}_2\text{O}_2$  concentration slowed the overall progression (Figure 2-4). A lag phase was also seen for the oxidation of substrates other than guaiacol (Figure 2-5).

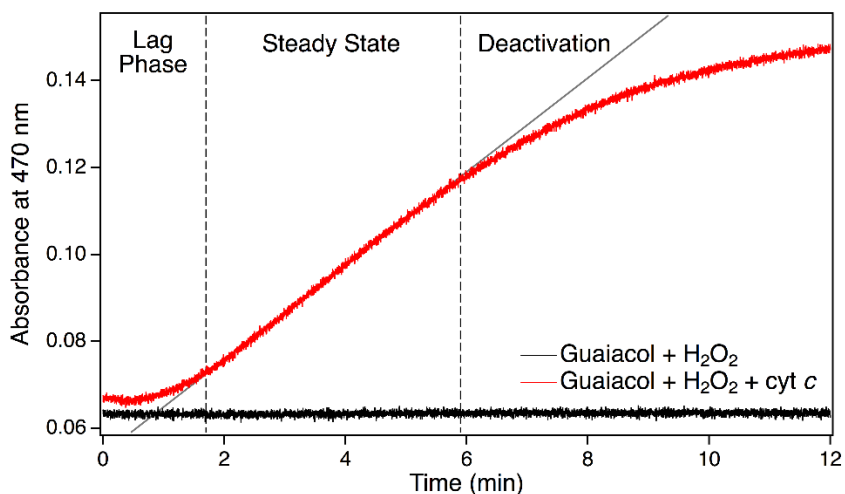


**Figure 2-2.** Peroxidase activity of *cyt c* measured by guaiacol oxidation (9 mM) in the presence of 500  $\mu\text{M}$   $\text{H}_2\text{O}_2$  in phosphate buffer at pH 7.4. A fit to the linear region (solid gray line) yields a reaction rate of 0.027  $\mu\text{M s}^{-1}$ .

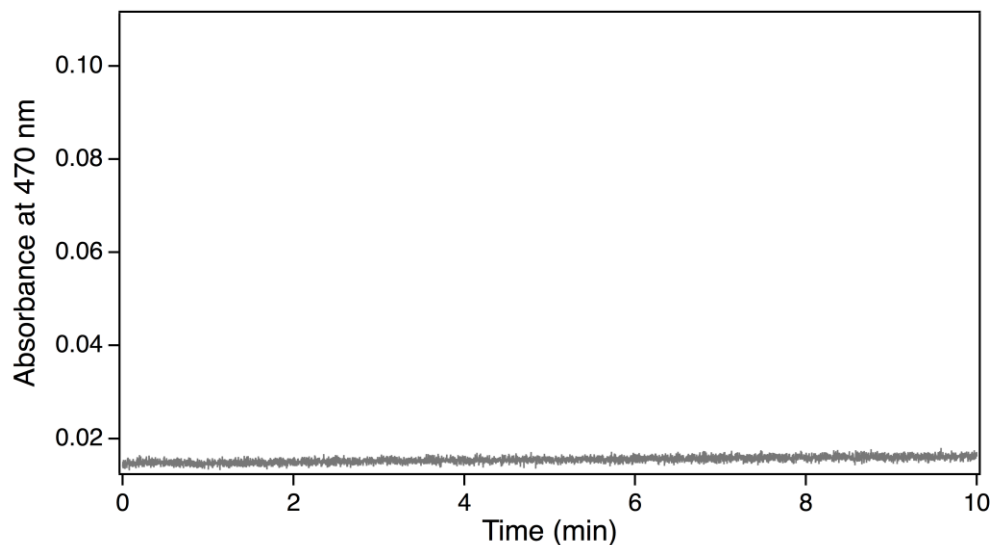


**Figure 2-3.** Peroxidase activity of *cyt c* measured after pre-incubation of the protein with 500  $\mu\text{M}$   $\text{H}_2\text{O}_2$  for 15 min, prior to addition of guaiacol. No product formation is detectable under these conditions as a result of oxidative self-degradation.

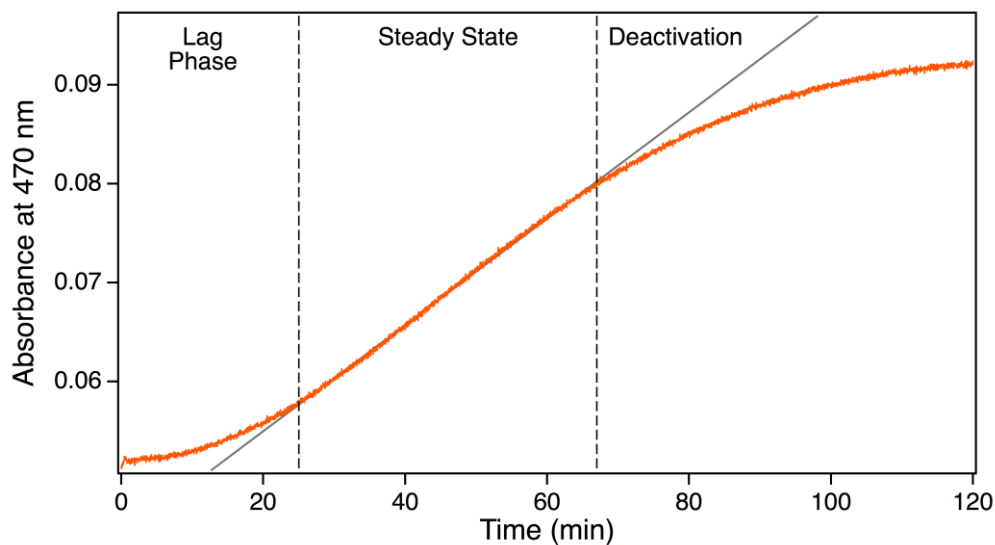


**Figure 2-4.** Peroxidase activity of *cyt c* measured by probing the oxidation of guaiacol as in Figure 2-2 but in the presence of 50  $\mu\text{M}$   $\text{H}_2\text{O}_2$  instead of 500  $\mu\text{M}$ . A fit to the linear region (solid black line) yields a reaction rate of 0.0013  $\mu\text{M s}^{-1}$ .

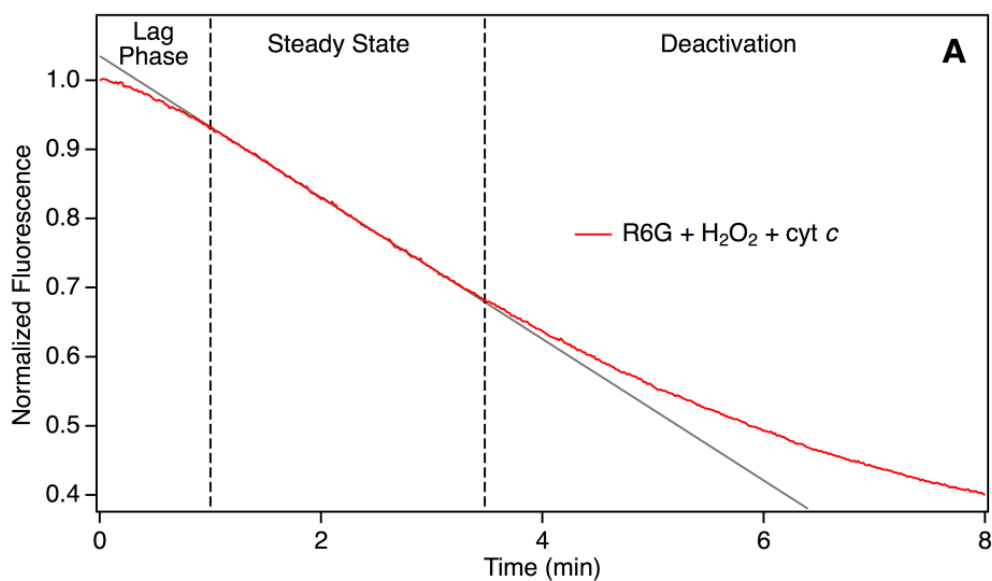


**Figure 2-5.** Peroxidase activity of cyt *c* probed by fluorescence bleaching of 10  $\mu$ M rhodamine 6G (R6G) in the presence of 500  $\mu$ M H<sub>2</sub>O<sub>2</sub>. A three-stage kinetic progression similar to that of guaiacol is observed (see Figure 2-2). Fluorescence experiments were performed on a Fluorolog-3 fluorimeter (Horiba Jobin Yvon; Edison, NJ), using an excitation wavelength of 526 nm, and an emission wavelength of 555 nm.

A lag phase in the peroxidase kinetics of cyt *c* has been reported previously,<sup>14,40,60</sup> but this phenomenon has received very little attention. One study<sup>60</sup> attributed the lag phase to Fe(II) → Fe(III) conversion, but this scenario can be excluded for the Fe(III) samples used here (Figure 2-6). We nonetheless agree with the basic conclusion of ref. 60 that the lag phase suggests some form of pre-catalyst activation.<sup>57-59</sup> Figure 2-2 and Figure 2-5 still leave room for alternative explanations, but when considering the MS data discussed below it will become clear that covalent modifications are indeed required for converting cyt *c* to an active peroxidase.

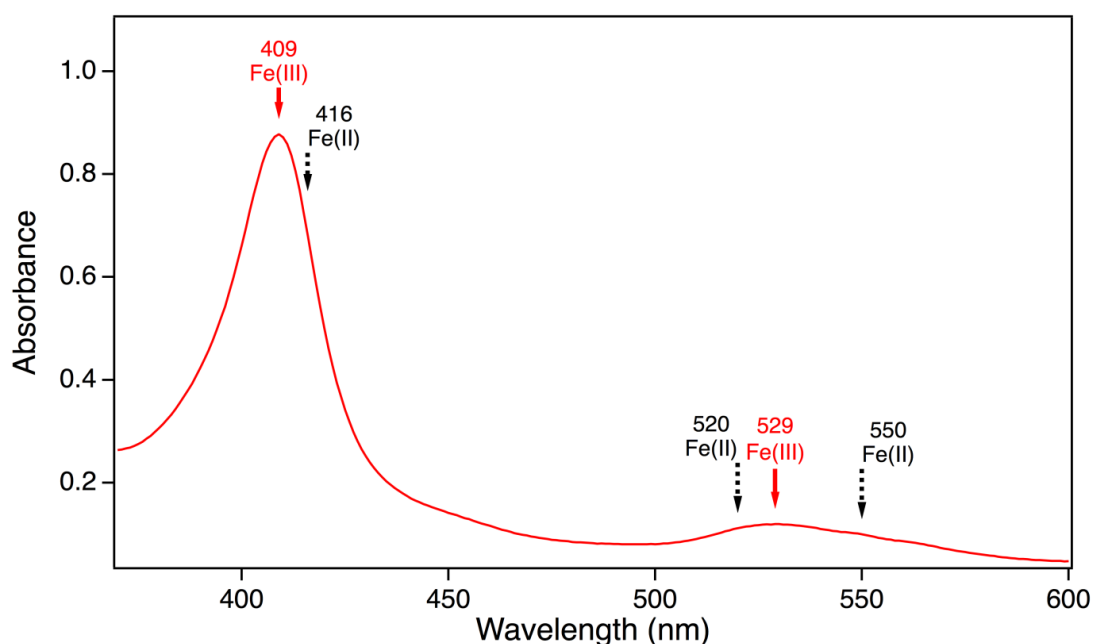


**Figure 2-6.** UV-Vis absorption spectrum of cyt *c* used in this work, prior to H<sub>2</sub>O<sub>2</sub> exposure. These data confirm the oxidation state of the heme iron as Fe(III). The measured spectral maxima (red) are consistent with literature values for the Fe(III) form, whereas there is no match with the peak positions expected for Fe(II) cyt *c* (black).<sup>1,2</sup>

### 2.3.2. Spectroscopic Evidence for H<sub>2</sub>O<sub>2</sub>-Induced Structural Changes.

Upon exposing cyt *c* to H<sub>2</sub>O<sub>2</sub> the CD amplitude at 222 nm decreased by ~30% within 20 min, implying a loss in  $\alpha$ -helicity (Figure 2-7A).<sup>69</sup> A Soret shift from 409 nm to 406 nm indicated alterations in the heme environment, while a declining Soret intensity was caused by heme degradation (Figure 2-7B).<sup>23,24,70,71</sup> Disappearance of the 695 nm band (A<sub>695</sub>)<sup>72</sup> revealed rupture of the Met80-Fe bond (Figure 2-7C). A<sub>695</sub> declined more rapidly than the Soret peak, implying that the loss of Met80 ligation is triggered by events other than heme degradation.

An important question is whether the loss of Met80 ligation is followed by the formation of alternative distal contacts. <sup>1</sup>H-NMR allows fingerprinting the Fe environment due to paramagnetic proton shifts.<sup>40,42,46,73,74</sup> After 5 min in H<sub>2</sub>O<sub>2</sub> several <sup>1</sup>H signals associated with native cyt *c* had significantly dropped in intensity, including those of Met80 (Figure 2-8). This matches the UV-Vis-detected loss of Met80-Fe ligation (Figure 2-7C). The NMR spectra provided no evidence for alternative Fe ligation scenarios, e.g. distal Lys contacts would cause conspicuous peaks in the 12-25 ppm range.<sup>46,74</sup> No such signals were apparent in our NMR data, nor was there evidence that other ligands replace Met80. It is concluded that H<sub>2</sub>O<sub>2</sub> triggers the formation of conformers with a vacant sixth coordination site. Considering that peroxidases require a five-coordinate heme,<sup>6,8,13,14,26-28</sup> our spectroscopic data strongly suggest that the peroxidase activity of cyt *c* arises from five-coordinate species produced in the presence of H<sub>2</sub>O<sub>2</sub>.

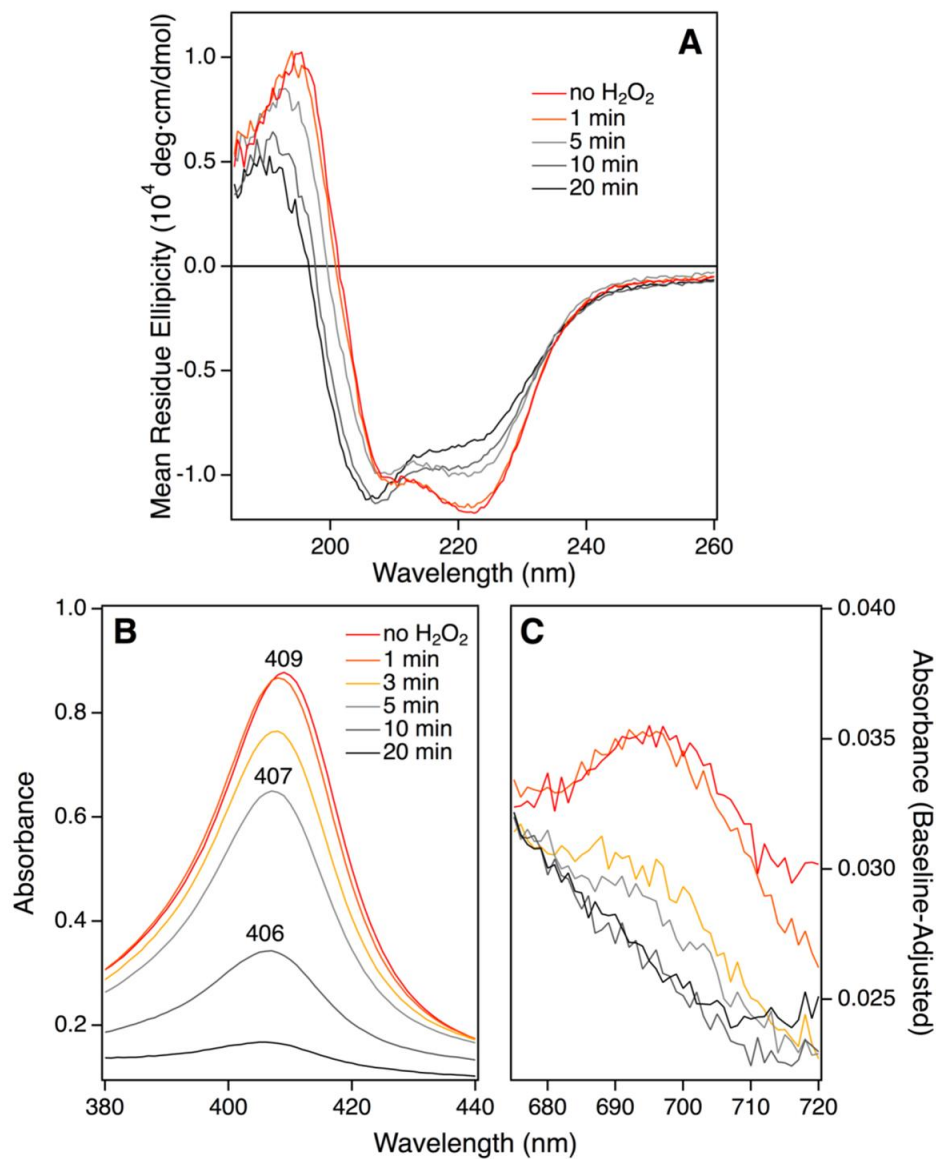


**Figure 2-7.** Spectroscopic evidence for *cyt c* time-dependent structural changes in 500  $\mu\text{M}$   $\text{H}_2\text{O}_2$ . (A) Far-UV CD spectra. (B) UV-Vis absorption spectra of the heme Soret band. (C) Absorption spectra of the A695 band, which reports on the Met80-Fe interaction. For better visualization spectra in panel C were baseline shifted such that they all had the same absorbance at 670 nm.



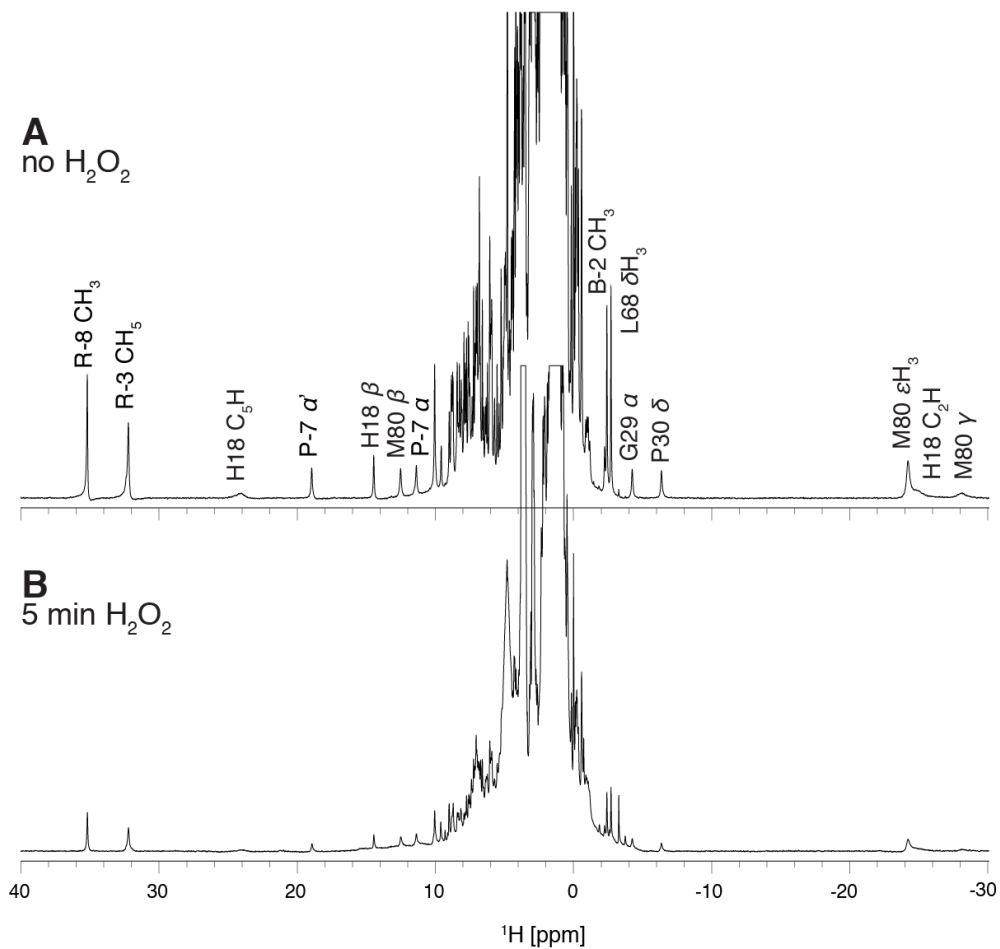


**Figure 2-8.**  $^1\text{H}$ -NMR spectra of cyt *c*. (A) No  $\text{H}_2\text{O}_2$  added. (B) After 5 min of incubation in  $500\ \mu\text{M}$   $\text{H}_2\text{O}_2$  and subsequent catalase quenching. Peaks were assigned and denoted according to Feng *et al.*<sup>73</sup> A global loss in signal intensity after  $\text{H}_2\text{O}_2$  incubation is consistent with partial heme degradation, as also confirmed by optical data of Figure 2-7.

### 2.3.3. H<sub>2</sub>O<sub>2</sub>-Induced Modifications Probed by Mass Spectrometry.

Intact protein mass spectra acquired during H<sub>2</sub>O<sub>2</sub> incubation revealed a gradually declining signal amplitude (Figure 2-9A-D), concomitant with dramatic peak broadening (Figure 2-9E-H). The  $t = 0$  spectrum displayed a single major isotope distribution corresponding to unmodified cyt *c*, denoted as “M0” in Figure 2-9E. After 10 min the mass distribution was split into numerous signals, arising from covalent oxidative modifications (M1, M2, M3, ..., Figure 2-9F-H). The spacing between successive  $M_i$  species corresponded to mass differences of 14 - 16 Da. Similar patterns have previously been reported for other proteins after exposure to different types of oxidants.<sup>22,32,75,76</sup>

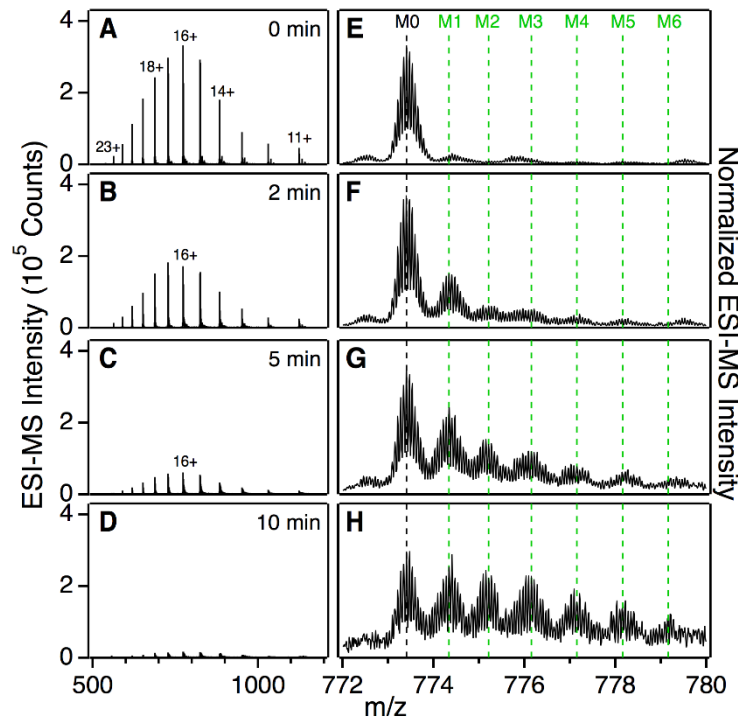


**Figure 2-9.** (A-D): Cyt *c* mass spectra acquired after varying H<sub>2</sub>O<sub>2</sub> incubation times. (E-H): 16+ charge state region. M0 denotes unmodified protein. M1, M2, .... refers to oxidatively modified forms. Protein (10 μM) and H<sub>2</sub>O<sub>2</sub> (500 μM) were incubated in phosphate buffer at pH 7.4.

#### 2.3.4. Peptide Mapping of Oxidation Patterns.

LC-MS was applied to monitor H<sub>2</sub>O<sub>2</sub>-induced modifications via analyses of tryptic peptides. The resulting  $f_{OX}$  data (Figure 2-10) were visualized as color maps (Figure 2-11). T13-T15 (residues 61-79) consistently stood out as the most heavily oxidized region. This region covers the distal side of the heme, i.e. the catalytically active region. Considering the critical role of the Met80-Fe bond for catalytic activity,<sup>8,32,41,56,77</sup> it might have been expected that the Met-80 containing T16 would be most strongly oxidized. However, T16 generally showed lower  $f_{OX}$  than T13-T15 (Figure 2-11).

H<sub>2</sub>O<sub>2</sub>-induced modifications were further characterized by subjecting tryptic peptides to tandem MS (Figure 2-12). Detected oxidation sites included Tyr48 (+16), Trp58 (+16,+32), Met80 (+16,+32) and a +32 Da shift within residues 33-35 (His-Gly-Leu). T5 could not be probed due to the heterogeneity of heme degradation products.<sup>23,24,70,71</sup> Surprisingly, we were unable to detect T13-T15 oxidation products after *cyt c* incubation in H<sub>2</sub>O<sub>2</sub>. Chymotrypsin and GluC were tested as alternative proteases, but the results were inconclusive (data not shown). Oxidized T13-T15 peptides were readily observable after alternative treatments were performed as controls (Figure 2-13). This implies that H<sub>2</sub>O<sub>2</sub> causes specific T13-T15 modifications that interfere with MS detection. The nature of these modifications will be discussed below.

The H<sub>2</sub>O<sub>2</sub>-induced oxidation patterns of Figure 2-11 are very different from those observed after exposing *cyt c* to free ·OH in bulk solution.<sup>78</sup> In the latter case, oxidation primarily affects solvent-accessible residues.<sup>20</sup> In contrast, modifications formed under the conditions of the current work are heme-catalyzed,<sup>19</sup> such that buried sites adjacent to the porphyrin are particularly prone to oxidation.<sup>22-25</sup> Free ·OH is not involved in these peroxidase processes.<sup>19</sup>

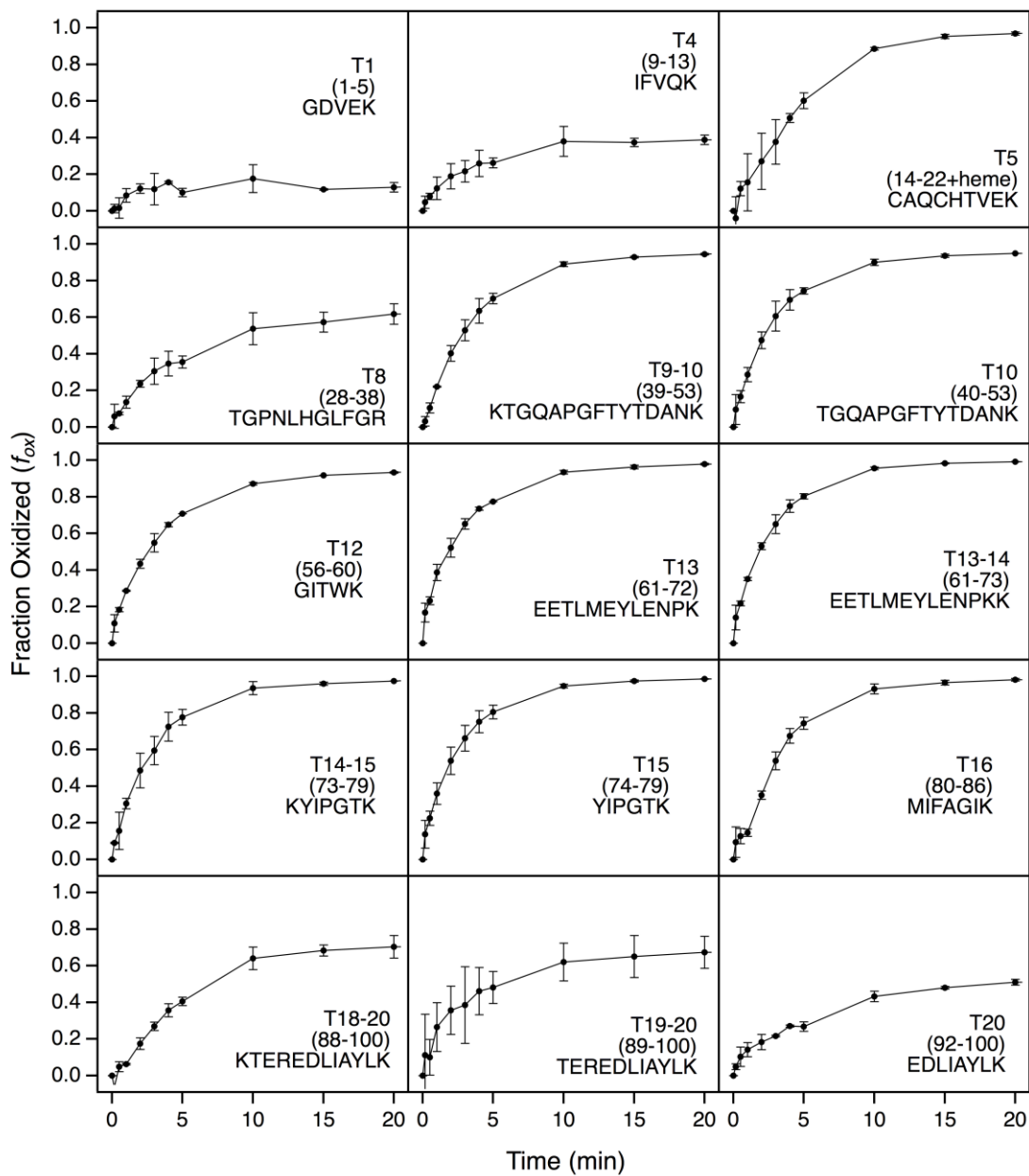


**Figure 2-10.** Fraction oxidized ( $f_{ox}$ ) plots of tryptic cyt *c* peptides following incubation in 500  $\mu$ M  $H_2O_2$  and catalase quenching. Standard deviations of two replicates are depicted as error bars.

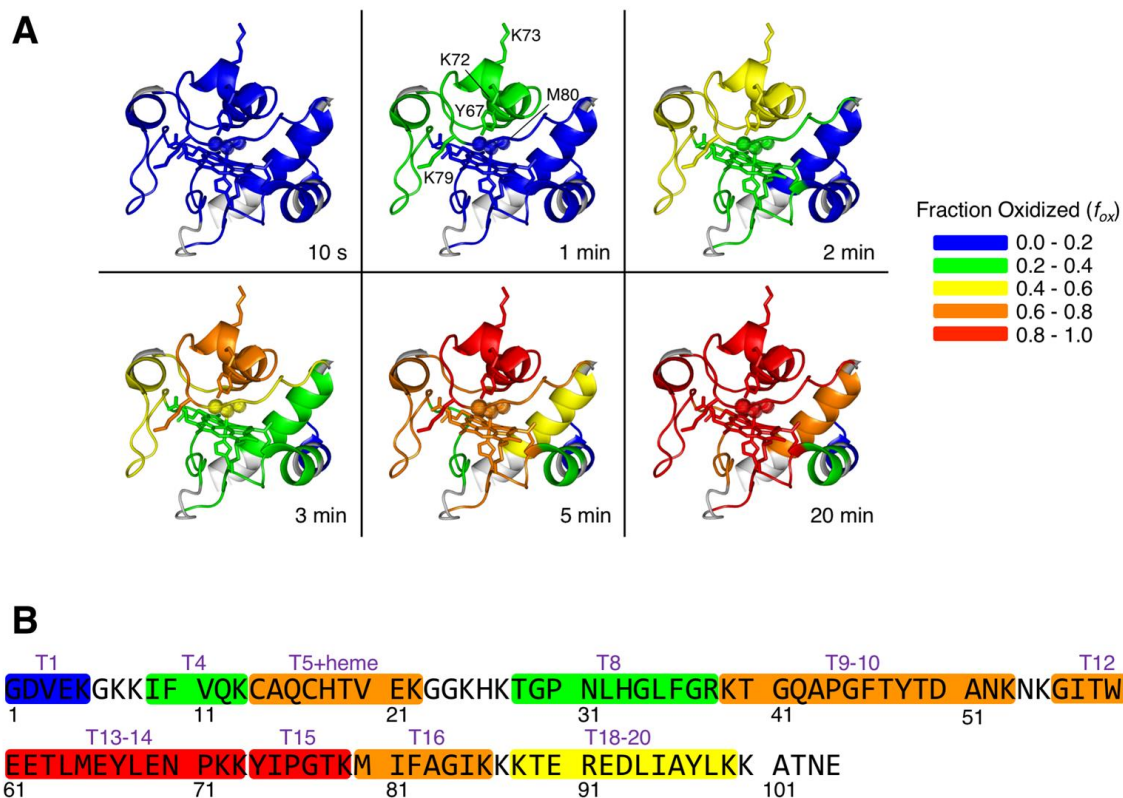


**Figure 2-11.** (A) Tryptic peptide mapping, displaying the extent of oxidative modifications as a function of H<sub>2</sub>O<sub>2</sub> incubation time. Colors indicate the fraction oxidized,  $f_{ox}$ , ranging from blue (little oxidation) to red (heavily oxidized). Met80 is highlighted as spheres. Regions for which no structural data were obtained are colored grey (sequence coverage 89%). (B)  $f_{ox}$  data for  $t = 5$  min mapped to the cyt *c* sequence. Detected tryptic peptides are annotated as T1, T4, etc. Peptides T9-10, T13-14, and T18-20 arise from missed cleavage sites. T5 includes the heme.

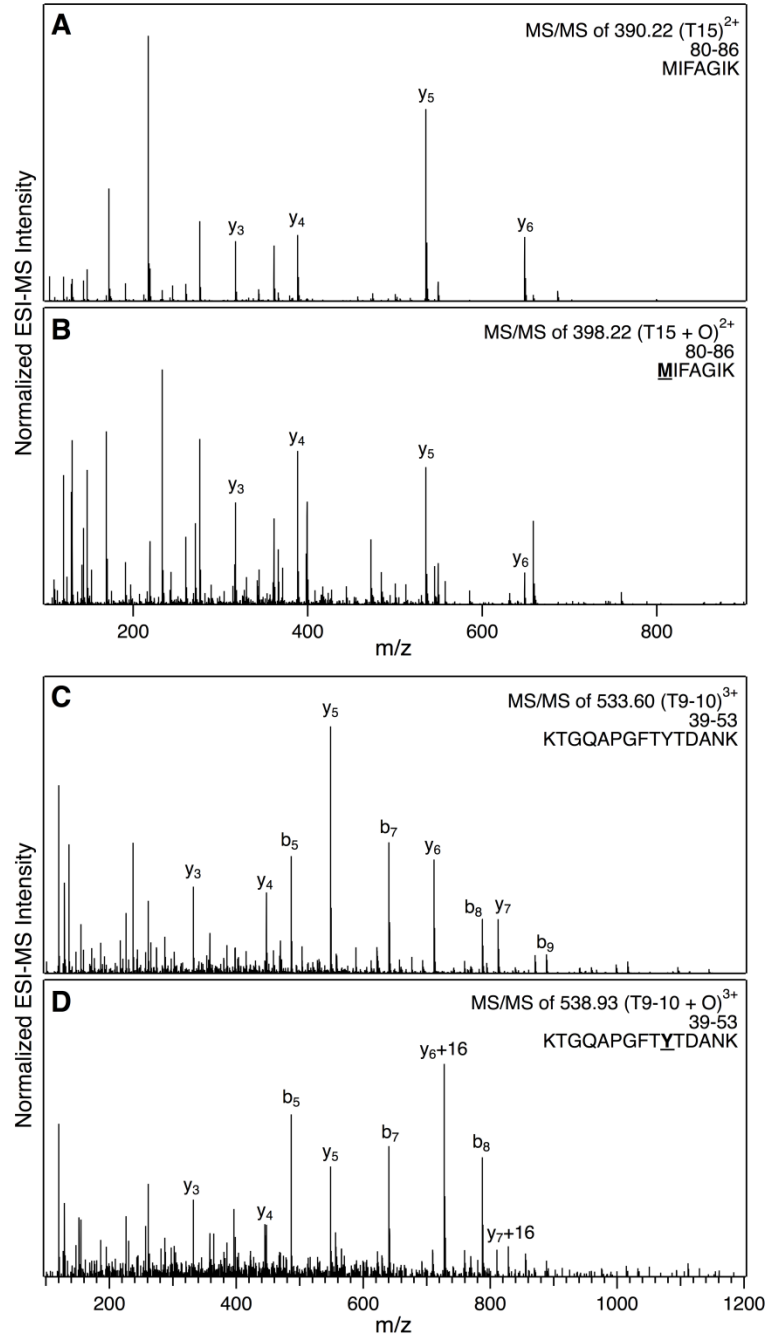


**Figure 2-12.** Representative tandem mass spectra of tryptic peptides, illustrating the identification of oxidation sites. MS/MS data of oxidized peptides were obtained after 30 min of *cyt c* incubation in 500  $\mu$ M H<sub>2</sub>O<sub>2</sub>, followed by tryptic digestion. (A) Unmodified T15. (B) T15 oxidized at Met80 (MetO formation, +16 Da, bold/underlined). (C) Unmodified T9-10. (D) T9-10 oxidized at Tyr48 (+16 Da, bold/underlined).

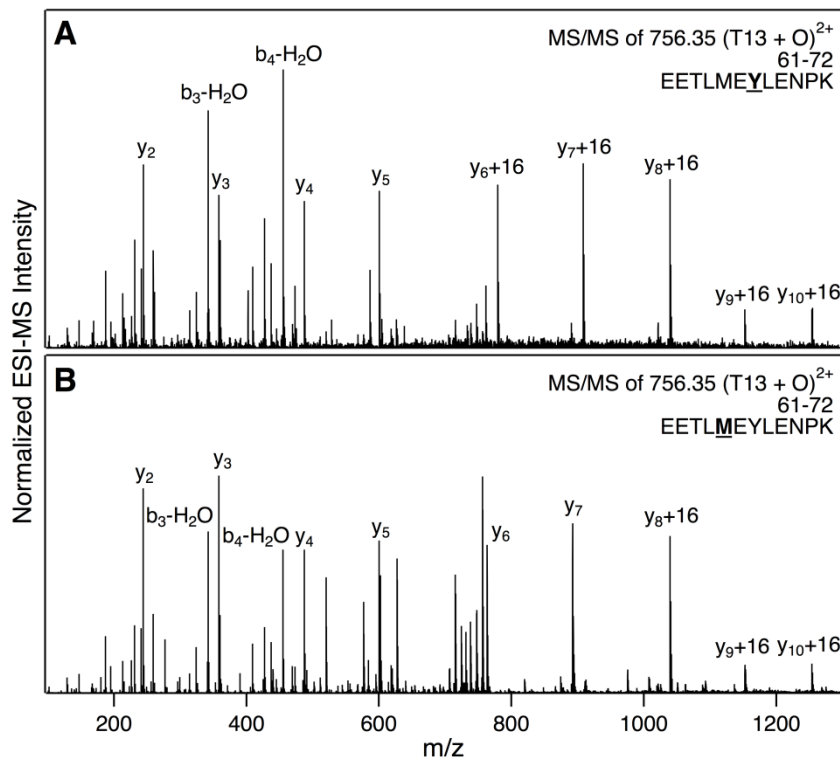


**Figure 2-13.** Representative tandem mass spectra of tryptic cyt *c* peptides obtained in control experiments. (A): Y67 oxidation (+16 Da) generated after incubation of pre-digested tryptic peptides in H<sub>2</sub>O<sub>2</sub> (30 min). (B) M65 oxidation (+16 Da) generated after cyt *c* oxidation using chloramine-T.<sup>56</sup> Chloramine-T treatment was performed by adding 2.5 mM of the oxidant to buffered protein solution, followed by room temperature incubation for 1 hour. Reactions were stopped by exchange into phosphate buffer using 10 kDa MWCO centrifuge filters that were spun 3 times, each cycle being 15 minutes at 10 kG.

### 2.3.5. Chemical Deconvolution.

Several mechanistic aspects can be uncovered by examining the intact protein mass envelope. Figure 2-14A-C displays the mass distribution of unmodified *cyt c*. Oxidative modifications M1, M2, ... formed upon H<sub>2</sub>O<sub>2</sub> exposure are highlighted in Figure 2-14D. The M1 population is of key interest because it carries the initial modifications. The M1 isotope envelope was ~50% wider than that of unmodified *cyt c*, and the center of M1 was shifted roughly -2 Da relative to a hypothetical [*cyt c* + O] species (Figure 2-14E). These characteristics imply that M1 encompasses different oxidation products with slightly different masses.

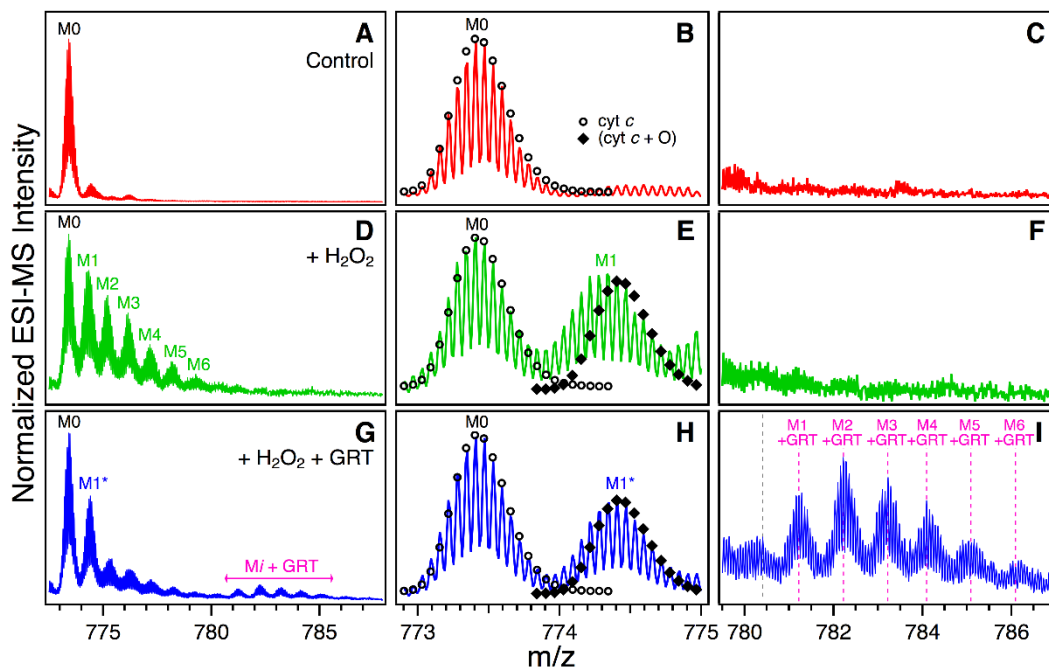


**Figure 2-14.** Mass spectra of the 16+ charge state for unmodified *cyt c* (A-C), after 5 min in H<sub>2</sub>O<sub>2</sub> (D-F), and after 5 min in H<sub>2</sub>O<sub>2</sub> with subsequent GRT labeling (G-I). Column 2 shows close-ups of the region comprising M0 (unmodified protein) and M1 (first modification peak), with simulated isotope envelopes for *cyt c* and [*cyt c* + O]. Column 3 shows the GRT-labeled M<sub>i</sub> forms. Carbonyl-depleted M1 after GRT labeling is denoted as M1\* (panel H).



Chemical deconvolution was applied to tackle the heterogeneity of the H<sub>2</sub>O<sub>2</sub>-treated protein. GRT selectively tags reactive carbonyl groups formed by oxidation (i.e. not those of endogenous amides or carboxylates, Figure 2-15).<sup>64,65,79,80</sup> By shifting carbonylated species into a mass range that differs from that of non-carbonylated forms, GRT labeling reveals proteins carrying other types of modifications. Without H<sub>2</sub>O<sub>2</sub> treatment *cyt c* did not incorporate GRT (Figure 2-16D). In contrast, extensive GRT labeling took place for M1, M2, ... formed in the presence of H<sub>2</sub>O<sub>2</sub> (Figure 2-14I). This observation reveals that H<sub>2</sub>O<sub>2</sub> causes *cyt c* carbonylation, consistent with immunological data.<sup>81</sup> The extent of carbonylation increased with H<sub>2</sub>O<sub>2</sub> exposure time (Figure 2-16). Reaction products M1, M2, ... tagged with one or two GRT moieties were clearly discernible in the spectra (Figure 2-14I, Figure 2-17). The relatively low signal intensity of these products likely reflects the aggregation propensity of carbonylated proteins.<sup>82</sup>

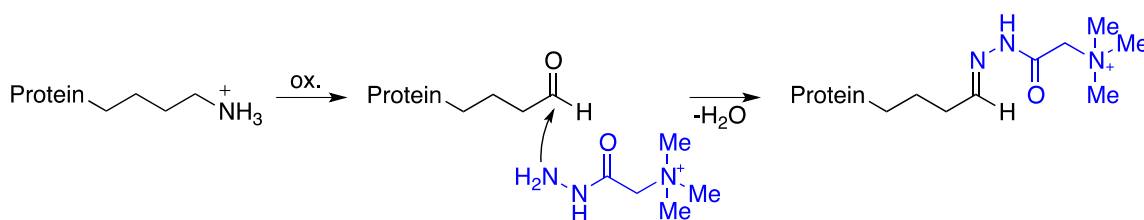


**Figure 2-15.** Assay for Lys carbonylation, i.e. oxidative deamination to aminoaldehyde,  $\Delta m = -1.032$  Da. Covalent attachment of the hydrazide-containing label, Girard's Reagent T (GRT) takes place via Schiff base formation. This results in  $\Delta m/z = +112.063$ , when going from a Lys<sup>+</sup>-containing reactant to the GRT-labeled product. The quaternary ammonium group adds a permanent cationic moiety to facilitate MS detection.

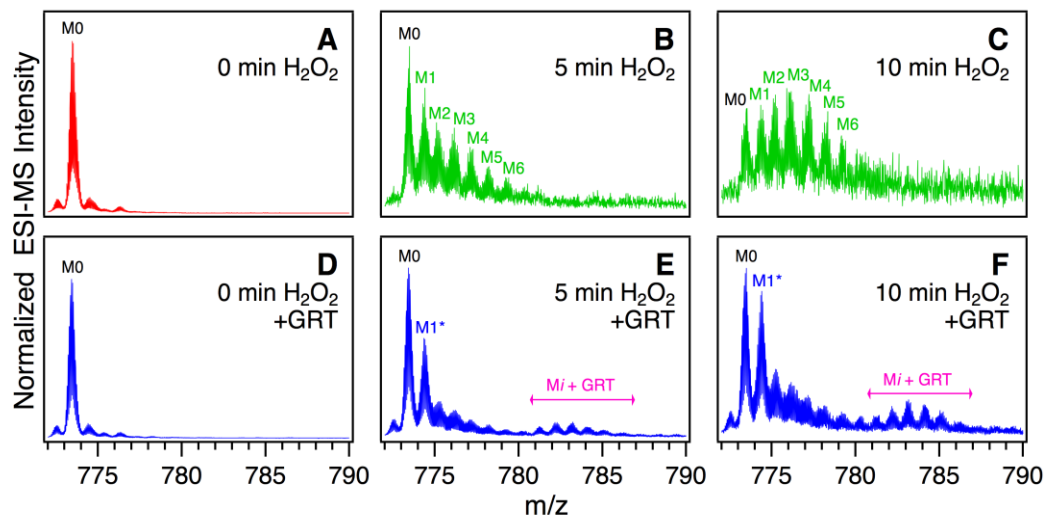


**Figure 2-16.** Intact protein mass spectra of cyt *c* (16+) following H<sub>2</sub>O<sub>2</sub> incubation and subsequent labeling with GRT. (A) unmodified cyt *c*. (B, C) After increasing lengths of H<sub>2</sub>O<sub>2</sub> incubation. (D) – (F) show spectra of the corresponding samples after GRT labeling. Note that GRT labeling is detectable only after H<sub>2</sub>O<sub>2</sub> exposure, reflecting the formation of reactive carbonyl groups.

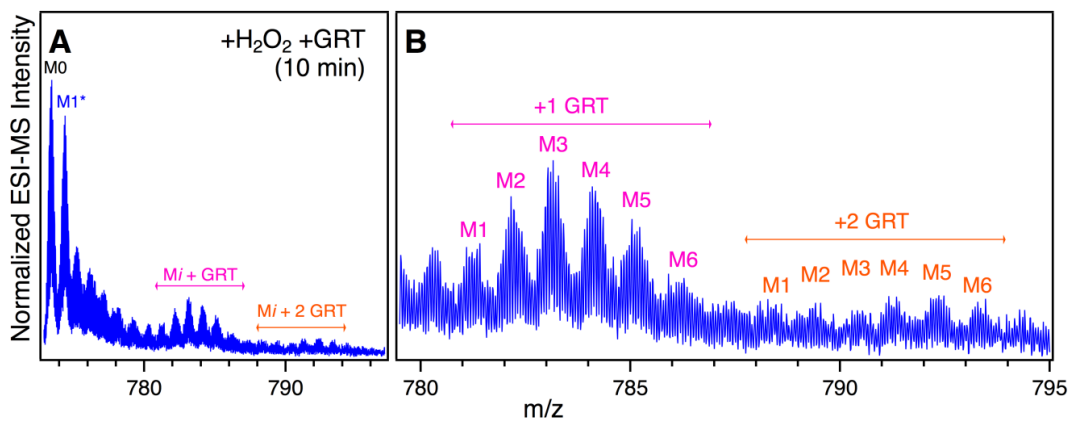


**Figure 2-17.** Mass spectral data for cyt *c* following 10 min incubation in 500  $\mu$ M H<sub>2</sub>O<sub>2</sub> and subsequent GRT labeling. The populations of singly and doubly-adducted GRT are highlighted in magenta and orange, respectively. (A) Overview of the 16+ range. (B) Expanded view of the *m/z* range corresponding to GRT addition.

In addition to unmodified cyt *c* (M0), carbonyl-depleted cyt *c* showed “M1” as the only major signal (Figure 2-14G). The centroid of this carbonyl-depleted M1 (Figure 2-14H) was shifted by roughly +2 Da relative to the original M1 (Figure 2-14E). We will refer to this sub-population as M1\*. Comparison with a simulated isotope envelope reveals that M1\* primarily consists of proteins with the composition [cyt *c* + O] (Figure 2-14H).

The aforementioned findings demonstrate that M1 (Figure 2-14E) comprises [cyt *c* + O], along with carbonylated species that are 1 to 2 Da lower in mass. Lys conversion to amino adipic semialdehyde ( $R-CH_2-NH_2 \rightarrow R-CHO$ ) is the only documented carbonylation pathway with a mass shift of -1 Da.<sup>20,79</sup> Thus, we propose that M1 contains [cyt *c* + O] where 0, 1, or 2 of the 19 Lys side chains have undergone carbonylation. Tyr dimerization (-2 Da)<sup>83</sup> and other crosslinking modifications<sup>20,79</sup> in M1 can be excluded, because they would not convey GRT reactivity. Thus, the various oxidative modifications detected by peptide mapping (at Tyr48, Trp58, Met80 etc., see above) must reside in the more highly oxidized species  $M_i$ , with  $i > 1$ . Likely, these highly oxidized species are also subject to Tyr dimerization, as suggested in previous work.<sup>81,83</sup>

Figure 2-14 also provides information regarding the temporal sequence of oxidation events. [cyt *c* + O] is susceptible to carbonylation, seen from disappearance of -1 and -2 Da mass shifts by GRT labeling, and from the formation of [M1+GRT] and [M1+2GRT] (Figure 2-14I, Figure 2-16). In contrast, M0 is effectively inert against carbonylation, evident from the fact that neither H<sub>2</sub>O<sub>2</sub> nor GRT treatment affect the M0 mass distribution (Figure 2-14E, H), and from the lack of a discernible [M0 + GRT] signal in Figure 2-14I. Hence, carbonylation occurs *after* an initial +O modification.

The carbonyl-depleted and the carbonylated sub-populations show major differences in their degree of self-oxidation, which serves as a proxy for the level of peroxidase activity (Figure 2-18). The carbonyl-depleted sub-population is dominated by M1\* (incorporation of a single oxygen, Figure 2-18A). In contrast, carbonylated cyt *c* has its maximum at [M2+GRT] with major contributions from [M3+GRT] and beyond (with 2, 3, ... incorporated oxygens, Figure 2-18B). The fact that carbonylated cyt *c* exhibits more

extensive self-oxidation, implies that carbonylation enhances peroxidase activity relative to unmodified *cyt c* and [*cyt c* + O]. In other words, Figure 2-18 provides unequivocal proof that chemical modifications cause peroxidase activation of *cyt c*, i.e. the transition of a low activity catalyst to the active enzyme. Our data imply that this activation follows a sequential mechanism, with incorporation of a single oxygen as the initial step. The [*cyt c* + O] formed in this way retains a low peroxidase activity, similar to that of the unmodified protein. Peroxidase activation takes place upon subsequent carbonylation.

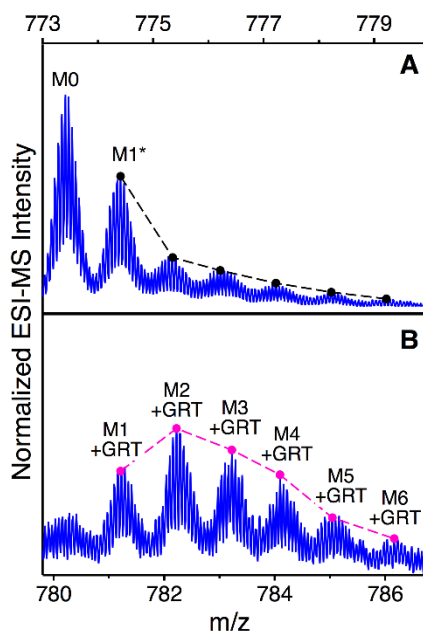


**Figure 2-18.** Comparison of oxidation patterns after 5 min in  $\text{H}_2\text{O}_2$  followed by GRT labeling, (A) The carbonyl-depleted protein is dominated by M0 and M1\*. Other oxidation peaks have very low intensity. (B) The carbonyl-containing population exhibits a dramatically elevated oxidation level. Peak maxima of oxidatively modified species are highlighted, annotation is as in Figure 2-14.

### 2.3.6. Top-down MS.

To pinpoint the initial [cyt *c* + O] modification(s) we performed top-down experiments, i.e. tandem MS without prior protein digestion (Figure 2-19).<sup>84</sup> This approach allowed the interrogation of specific species within the heterogeneous mix formed during H<sub>2</sub>O<sub>2</sub> exposure. Top-down data (see Figure 2-20 for full spectra) were acquired for three precursor ions, the M0 unmodified control (Figure 2-14B), M1 (Figure 2-14E), and carbonyl-depleted M1\* (Figure 2-14H). The *b* and *y* fragments provided complete sequence coverage (Figure 2-19A). Dissociation of both M1 and M1\* resulted in unmodified C-terminal fragments up to *y*<sub>37</sub>, whereas a +16 Da shift was seen from *y*<sub>38</sub> onwards (Figure 2-19B). This pattern identifies Tyr67 as the oxidation site in [cyt *c* + O]. Other oxidation sites were absent, revealing that M1\* is just a single proteoform. The top-down identification of Tyr67 oxidation is also consistent with the peptide data of Figure 2-11, which mapped the most prevalent early modification to residues 61-79.

Unfortunately, top-down fragmentation did not reveal the nature of carbonylation sites, as none of the M1 fragments displayed mass shifts related to Lys carbonylation (or other non-Tyr67 oxidation events). GRT labeling revealed that M1 represents a mix of carbonylated and non-carbonylated species. Evidently, the fragmentation of carbonylated proteins was suppressed in our top-down experiments. We attribute this effect to the inability of carbonylated Lys to bear charge, thereby inhibiting the gas phase dissociation of amide bonds<sup>85,86</sup> or favoring dissociation pathways that do not conform to canonical *b/y* patterns.<sup>87</sup> Peptide mapping using trypsin, chymotrypsin, and GluC was applied as outlined above, but unfortunately those experiments also did not yield direct information regarding the location of carbonylation sites.

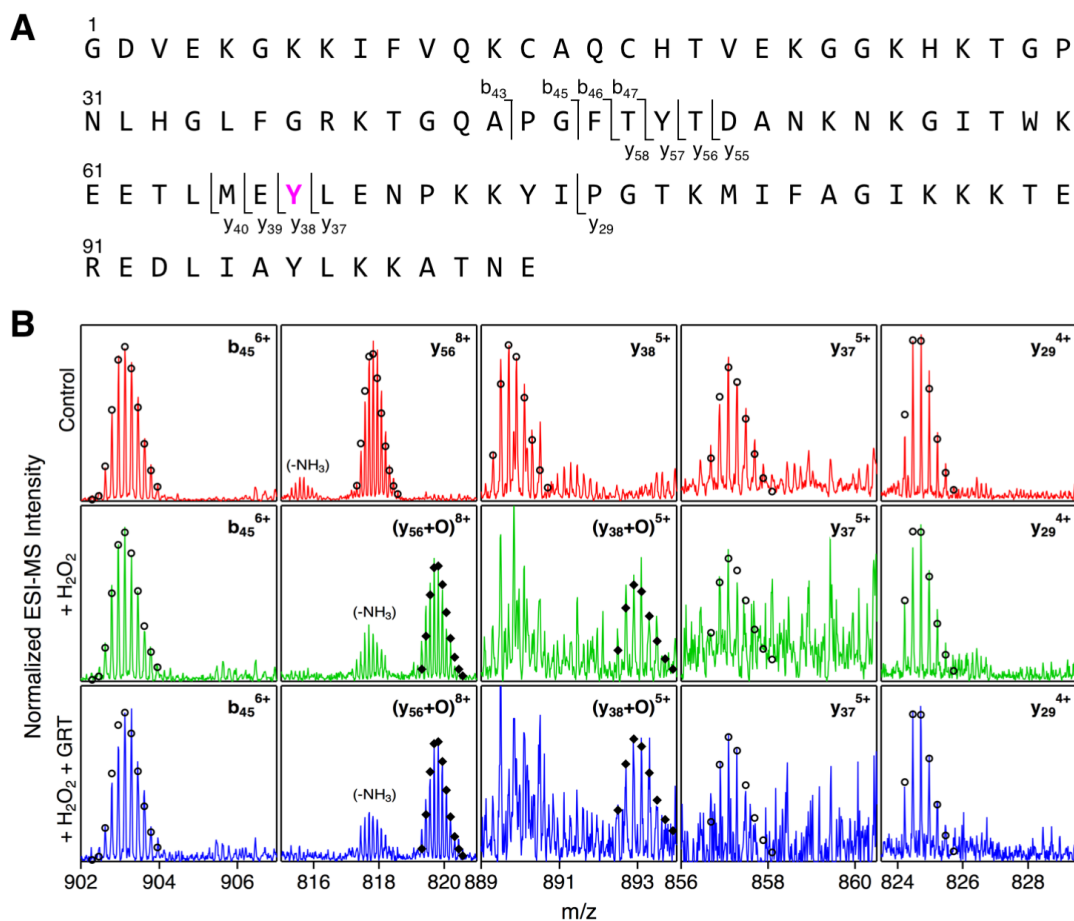


**Figure 2-19.** Top-down MS/MS data produced by CID of cyt  $c^{16+}$ . (A) Sequence with observed fragmentation sites. (B) Representative ion signals after fragmentation of M0 (unmodified protein,  $m/z$  773.5, top row), M1 (first modification peak, center row,  $m/z$  774.4), and M1\* (first modification peak after GRT labeling,  $m/z$  774.5). Peaks are labeled following standard  $b$  and  $y$  ion notation. Each panel also shows a simulated isotope distribution, corresponding to either the unmodified protein (circles) or the +O species (diamonds). The +O Da modification can be assigned to Y67.

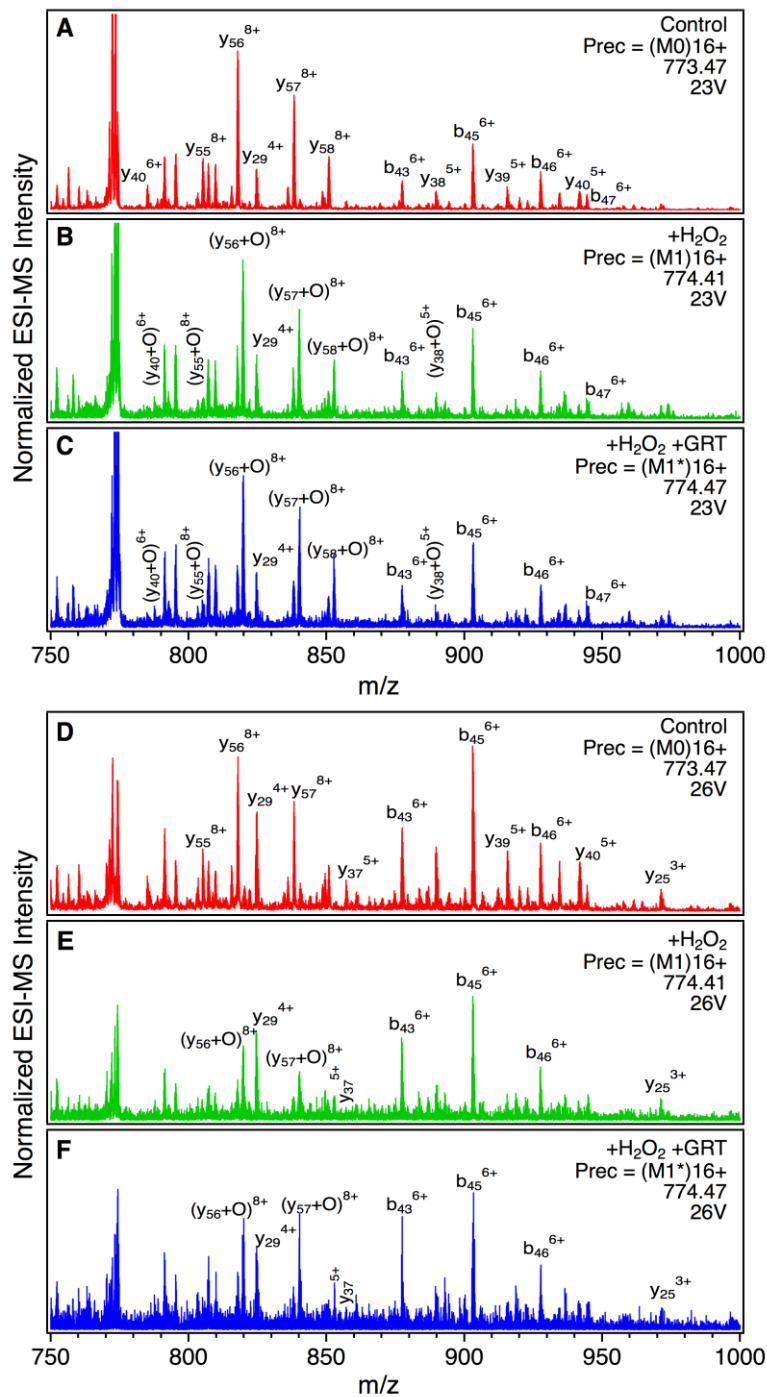


**Figure 2-20.** Complete top-down tandem mass spectra produced by CID of cytochrome  $c^{16+}$ . The data of Figure 2-19 are a subset of the spectra shown here. (A) Spectrum obtained after fragmentation of (A) M0, (B) M1, and (C) M1\* at a collision voltage of 23 V. Panels (D) – (F) show spectra obtained for the same precursor ions, but at a slightly elevated collision voltage of 26 V.

Despite our inability to directly identify the nature of carbonylation sites in M1, there is evidence to suggest that Lys72/73 are primarily affected. Carbonylation of these residues explains the lack of detectable oxidized peptides in the T13-T15 region. Specifically, the high  $f_{ox}$  of T15 at early times (Figure 2-11) likely reflects a missed tryptic cleavage due to Lys73 carbonylation. Also, Lys72/Lys73 are known to adopt positions close to the heme in “alkaline” cyt *c*,<sup>2,40,42,44,46-50</sup> particularly after Tyr67 modifications.<sup>35</sup> The proximity to the reactive iron makes Lys72/Lys73 prime candidates for oxidative modifications. Consistent with this view, the spectroscopic properties of H<sub>2</sub>O<sub>2</sub>-activated cyt *c* (at  $t \approx 5$  min, Figure 2-7) are close to those of “alkaline” Tyr67Arg cyt *c*.<sup>46</sup> Similarities include a Soret maximum at 406 nm, the shape of the CD spectrum with a minimum at  $\sim 206$  nm, and loss of A695. The 406 nm Soret signal is compatible with distal ligation by OH<sup>-</sup>/H<sub>2</sub>O (after H<sub>2</sub>O<sub>2</sub>-activation) or by Lys (for Tyr67Arg).<sup>35</sup>

It is instructive to consider the viability of alternative scenarios, where M1 represents a mix of two independently formed products, i.e. [cyt *c* + O] (Tyr67 oxidized, +16 Da) and [cyt *c* + O - 2H] (aliphatic ketone, +14 Da). In such a case Figure 2-18 would imply that the +14 Da species is highly prone to self-oxidation, whereas Tyr67 oxidation protects the protein against additional modifications. It is difficult to envision such a scenario because (i) Tyr67 modifications generally enhance (rather than inhibit) peroxidase activity.<sup>35,44,46,50</sup> (ii) If Tyr67 were to inhibit self-oxidation M1\* should accumulate after extended H<sub>2</sub>O<sub>2</sub> exposure, in contradiction with the spectra of Figure 2-9. (iii) +14 Da products are generally disfavored relative to other modifications,<sup>20,79</sup> while Lys carbonylation is highly prevalent during metal-catalyzed oxidation.<sup>88</sup> (iv) The top-down detection of +14 Da modifications should be straightforward; our data did not provide any evidence of such species. All these points argue against the presence of +14 Da modifications in M1, reinforcing the view that Tyr67 oxidation leads to an on-pathway intermediate (M1\*) that undergoes subsequent Lys carbonylation to form M1.



### 2.3.7. Peroxidase Activation Mechanism of Cyt *c*.

From the data presented above we can propose a model for the H<sub>2</sub>O<sub>2</sub>-induced peroxidase activation of cyt *c* (Figure 2-21). The native state M0 has low peroxidase activity because the distal coordination site is occupied by Met80, restricting interactions of the iron center with H<sub>2</sub>O<sub>2</sub>. The initial modification en route towards the active state is Tyr67 oxidation (to 3,4- or 2,4-dihydroxyphenylalanine<sup>20</sup>). This reaction likely takes place in a heme-catalyzed fashion,<sup>89</sup> facilitated by transient opening events of the 70-85 Ω loop (Figure 1) which represents the most dynamic cyt *c* region.<sup>39</sup> A Tyr67 radical formed in the presence of H<sub>2</sub>O<sub>2</sub><sup>89,90</sup> may be an intermediate of this oxidation step. Tyr67 modifications are known to destabilize the Met80-Fe bond due to involvement of the Tyr side chain in packing interactions and H-bonding. These conditions favor distal heme ligation by Lys72/73.<sup>44,46,50</sup> Our data suggest that an analogous ligand displacement takes place after Tyr67 oxidation, producing M1\* where Lys72/73 compete with Met80 for iron ligation. M1\* transiently accumulates to no more than ~10% of the total protein population (Figure 2-18). The lack of discernible Lys-specific <sup>1</sup>H-NMR signals (Figure 2-8) indicates that iron contacts with Lys72/73 in the M1\* state remain fluctuational, while the proximity of Lys72/73 to the redox-active heme triggers carbonylation. Carbonylated Lys is no longer capable of iron ligation, leaving behind a vacant distal coordination site. The five-coordinate M1 produced in this way represents the nascent peroxidase-active state of cyt *c*. Peroxidase activity is likely retained while additional oxidation events affect Met80, Tyr48, Trp58 and other residues (corresponding to M2, M3, ...). Activity is gradually lost as more and more of the protein is affected by oxidation.

The modification steps of Figure 2-21 require access of H<sub>2</sub>O<sub>2</sub> and O<sub>2</sub> to the protein interior. We envision that this access is provided by conformational fluctuations, as noted above.<sup>39</sup> Such fluctuations will be particularly important for facilitating the initial steps, i.e. M0 → M1\* → M1. Previous studies already noted the importance of dynamics for the peroxidase activity of cyt *c*,<sup>2,33-38,40</sup> but the role ascribed to these fluctuations here is different from that envisioned earlier. Other studies implied that native state fluctuations *per se* might produce a five-coordinate population that is entirely responsible for the “native state” peroxidase activity. Our observations demonstrate that the peroxidase

activity of unmodified native cyt *c* is low, and that significant substrate turnover takes place only after carbonylation.

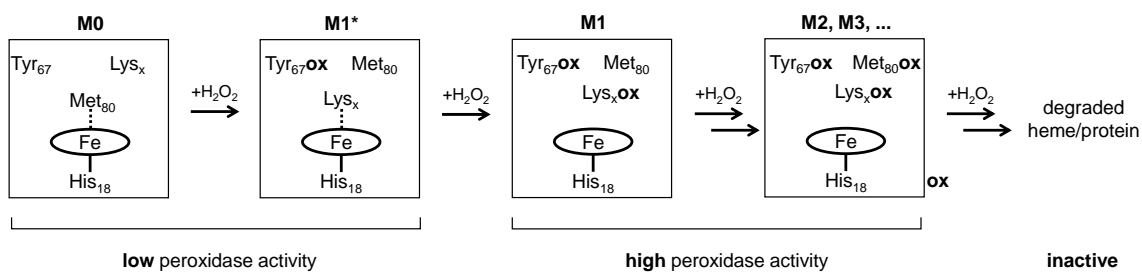


**Figure 2-21.** Proposed model for the H<sub>2</sub>O<sub>2</sub>-induced peroxidase activation of cyt *c*. MS-detected proteoforms are denoted along the top. Dotted lines in M0 and M1\* indicate occasional opening of distal contacts due to protein conformational fluctuations, allowing for Fe-H<sub>2</sub>O<sub>2</sub> interactions that are required for activation (oxygen incorporation into Tyr<sub>67</sub>, carbonylation of Lys<sub>x</sub>). M1, M2, ... represent peroxidase-active species where Fe-H<sub>2</sub>O<sub>2</sub> contacts are greatly facilitated because the distal coordination site is vacant. The nature of “Lys<sub>x</sub>” could not be determined with absolute certainty in this study, but our data indicate that it corresponds to Lys<sub>72</sub> and/or Lys<sub>73</sub>.

## 2.4. Conclusions

Previous studies did not comprehensively answer the question why native cyt *c*, with its six-coordinate iron, possesses apparent peroxidase activity. The present work resolves this conundrum by attributing much of the peroxidase activity to five-coordinate species formed in the presence of H<sub>2</sub>O<sub>2</sub>. The conversion from a pre-catalyst to peroxidase-active cyt *c* is consistent with the observation of a lag phase during substrate oxidation.<sup>14,40,60</sup>

Various reasons may have contributed to the fact that the H<sub>2</sub>O<sub>2</sub>-induced activation of cyt *c* has been overlooked in the past. Many earlier studies characterized wild type and mutant proteins *ex situ*, without considering the possibility of H<sub>2</sub>O<sub>2</sub>-induced, functionally relevant alterations. Also, H<sub>2</sub>O<sub>2</sub> produces a mix of transient proteoforms that are difficult to characterize by most techniques. Here we approached the problem from a new angle by interrogating catalase-quenched samples in a time-resolved fashion using optical techniques and MS.

It is tempting to speculate on the implications of our findings for the role of cyt *c* during apoptosis. Our *in vitro* data suggest that cyt *c* within mitochondria might also adopt its peroxidase-active state only after oxidative modifications. Specifically, cardiolipin-bound cyt *c* with Lys or His ligation<sup>12,34,53,54</sup> likely does not represent a form that is highly peroxidase-active. Instead, these hexa-coordinate species may be analogous to M1\* (Figure 8), requiring oxidative modifications to free up the distal coordination site prior to becoming an active catalyst. Similarly, engineered six-coordinate constructs might enter the sequence of Figure 2-21 at the M1\* stage, skipping the initial oxidation event, and thereby providing an explanation for their enhanced apparent peroxidase activity.<sup>6,13,26-28,35,42,49,55</sup>

## 2.5. References

- (1) Vazquez-Duhalt, R., *J. Mol. Catal. B* **1999**, *7*, 241-249.
- (2) Hannibal, L.; Tomasina, F.; Capdevila, D. A.; Demicheli, V.; Tórtora, V.; Alvarez-Paggi, D.; Jemmerson, R.; Murgida, D. H.; Radi, R., *Biochemistry* **2016**, *55* (3), 407-428.
- (3) Dunford, H. B., *Peroxidases and Catalases: Biochemistry, Biophysics, Biotechnology, and Physiology*. 2nd ed. ed.; John Wiley & Sons: Hoboken, N.J, 2010.
- (4) Kagan, V. E.; Tyurin, V. A.; Jiang, J.; Tyurina, Y. Y.; Ritov, V. B.; Amoscato, A. A.; Osipov, A. N.; Belikova, N. A.; Kapralov, A. A.; Kini, V.; Vlasova, I. I.; Zhao, Q.; Zou, M.; Di, P.; Svistunenko, D. A.; Kurnikov, I. V.; Borisenko, G. G., *Nat. Chem. Biol.* **2005**, *1* (4), 223-232.
- (5) Jiang, X.; Wang, X., *Annu. Rev. Biochem.* **2004**, *73* (1), 87-106.
- (6) Godoy, L. C.; Muñoz-Pinedo, C.; Castro, L.; Cardaci, S.; Schonhoff, C. M.; King, M.; Tórtora, V.; Marín, M.; Miao, Q.; Jiang, J. F.; Kapralov, A. A.; Jemmerson, R.; Silkstone, G. G.; Patel, J. N.; Evans, J. E.; Wilson, M. I. T.; Green, D. R.; Kagan, V. E.; Radi, R.; Mannick, J. B., *Proc. Natl. Acad. Sci. U.S.A.* **2009**, *106* (8), 2653-2658.
- (7) Yu, X.; Acehan, D.; Menetret, J. F.; Booth, C. R.; Ludtke, S. J.; Riedl, S. J.; Shi, Y.; Wang, X.; Akey, C. W., *Structure* **2005**, *13* (11), 1725-35.
- (8) Bren, K. L.; Raven, E. L., *Science* **2017**, *356* (6344), 1236-1236.
- (9) Mara, M. W.; Hadt, R. G.; Reinhard, M. E.; Kroll, T.; Lim, H.; Hartsock, R. W.; Alonso-Mori, R.; Chollet, M.; Glowonia, J. M.; Nelson, S.; Sokaras, D.; Kunnus, K.; Hodgson, K. O.; Hedman, B.; Bergmann, U.; Gaffney, K. J.; Solomon, E. I., *Science* **2017**, *356* (6344), 1276-1280.
- (10) Lee, S.; Tak, E.; Lee, J.; Rashid, M. A.; Murphy, M. P.; Ha, J.; Kim, S. S., *Cell Res.* **2011**, *21* (5), 817-834.
- (11) Giorgio, M.; Trinei, M.; Migliaccio, E.; Pelicci, P. G., *Nat. Rev. Mol. Cell Biol.* **2007**, *8* (9), 722A-728.
- (12) Bradley, J. M.; Silkstone, G.; Wilson, M. T.; Cheesman, M. R.; Butt, J. N., *J. Am. Chem. Soc.* **2011**, *133* (49), 19676-19679.
- (13) Abe, M.; Niibayashi, R.; Koubori, S.; Moriyama, I.; Miyoshi, H., *Biochemistry* **2011**, *50* (39), 8383-8391.

- (14) McClelland, L. J.; Mou, T.-C.; Jeakins-Cooley, M. E.; Sprang, S. R.; Bowler, B. E., *Proc. Natl. Acad. Sci. U.S.A.* **2014**, *111* (18), 6648-6653.
- (15) Kitt, J. P.; Bryce, D. A.; Minter, S. D.; Harris, J. M., *J. Am. Chem. Soc.* **2017**.
- (16) Veitch, N. C., *Phytochem.* **2004**, *65*, 249-259.
- (17) Rodriguez Maranon, M. J.; Mercier, D.; van Huystee, R. B.; Stillman, M. J., *Biochem. J.* **1994**, *301* ( Pt 2), 335-341.
- (18) Volkov, A. N.; Nicholls, P.; Worrall, J. A. R., *Biochim. Biophys. Acta.* **2011**, *1807* (11), 1482-1503.
- (19) Lawrence, A.; Jones, C. M.; Wardman, P.; Burkitt, M. J., *J. Biol. Chem.* **2003**, *278* (32), 29410-29419.
- (20) Xu, G.; Chance, M. R., *Chem. Rev.* **2007**, *107*, 3514-3543.
- (21) Von Sonntag, C.; Schuchmann, H. P., *Angew. Chem.-Int. Edit. Engl.* **1991**, *30* (10), 1229-1253.
- (22) Kathiresan, M.; English, A. M., *Chem. Sci.* **2017**, *8* (2), 1152-1162.
- (23) Florence, T. M., *J. Inorg. Biochem.* **1985**, *23*, 131-141.
- (24) Villegas, J. A.; Mauk, A. G.; Vazquez-Duhalt, R., *Chem. Biol.* **2000**, *7* (4), 237-244.
- (25) Gray, H. B.; Winkler, J. R., *Proc. Natl. Acad. Sci. U. S. A.* **2015**, *112* (35), 10920-10925.
- (26) Hersleth, H.-P.; Ryde, U.; Rydberg, P.; Görbitz, C. H.; Andersson, K. K., *J. Inorg. Biochem.* **2006**, *100* (4), 460-476.
- (27) Diederix, R. E. M.; Ubbink, M.; Canters, G. W., *ChemBioChem* **2002**, *3*, 110-112.
- (28) Wang, Z.-H.; Lin, Y.-W.; Rosell, F. I.; Ni, F.-Y.; Lu, H.-J.; Yang, P.-Y.; Tan, X.-S.; Li, X.-Y.; Huang, Z.-X.; Mauk, A. G., *ChemBioChem* **2007**, *8* (6), 607-609.
- (29) Bushnell, G. W.; Louie, G. V.; Brayer, G. D., *J. Mol. Biol.* **1990**, *214*, 585-595.
- (30) Moreno-Beltran, B.; Guerra-Castellano, A.; Diaz-Quintana, A.; Del Conte, R.; Garcia-Maurino, S. M.; Diaz-Moreno, S.; Gonzalez-Arzola, K.; Santos-Ocana, C.; Velazquez-Campoy, A.; De la Rosa, M. A.; Turano, P.; Diaz-Moreno, I., *Proc. Natl. Acad. Sci. U. S. A.* **2017**, *114* (15), E3041-E3050.
- (31) Capdevila, D. A.; Oviedo Rouco, S.; Tomasina, F.; Tortora, V.; Demicheli, V.; Radi, R.; Murgida, D. H., *Biochemistry* **2015**, *54*, 7491-7504.

- (32) Chen, Y.-R.; Deterding, L. J.; Sturgeon, B. E.; Tomer, K. B.; Mason, R. P., *J. Biol. Chem.* **2002**, *277* (33), 29781-29791.
- (33) Nold, S. M.; Lei, H.; Mou, T.-C.; Bowler, B. E., *Biochemistry* **2017**, *56*, 3358–3368.
- (34) Milazzo, L.; Tognaccini, L.; Howes, B. D.; Sinibaldi, F.; Piro, M. C.; Fittipaldi, M.; Baratto, M. C.; Pogni, R.; Santucci, R.; Smulevich, G., *Biochemistry* **2017**, *56* (13), 1887-1898.
- (35) Amacher, J. F.; Zhong, F. F.; Lisi, G. P.; Zhu, M. Q.; Alden, S. L.; Hoke, K. R.; Madden, D. R.; Pletneva, E. V., *J. Am. Chem. Soc.* **2015**, *137* (26), 8435-8449.
- (36) Karsisiotis, A. I.; Deacon, O. M.; Wilson, M. T.; Macdonald, C.; Blumenschein, T. M. A.; Moore, G. R.; Worrall, J. A. R., *Sci Rep* **2016**, *6*, 30447.
- (37) Diederix, R. E. M.; Ubbink, M.; Canters, G. W., *Biochemistry* **2002**, *41*, 13067-13077.
- (38) Sutin, N.; Yandell, J. K., *J. Biol. Chem.* **1972**, *247* (21), 6932-6936.
- (39) Xu, Y.; Mayne, L.; Englander, S. W., *Nat. Struct. Biol.* **1998**, *5*, 774-778.
- (40) García-Heredia, J. M.; Díaz-Moreno, I.; Nieto, P. M.; Orzáez, M.; Kocanis, S.; Teixeira, M.; Pérez-Payá, E.; Díaz-Quintana, A.; De la Rosa, M. A., *Biochim. Biophys. Acta* **2010**, *1797* (6–7), 981-993.
- (41) Wang, Z.; Ando, Y.; Nugraheni, A. D.; Ren, C.; Nagao, S.; Hirota, S., *Mol. Biosyst.* **2014**, *10* (12), 3130-3137.
- (42) Abriata, L. A.; Cassina, A.; Tortora, V.; Marin, M.; Souza, J. M.; Castro, L.; Vila, A. J.; Radi, R., *J. Biol. Chem.* **2009**, *284* (1), 17-26.
- (43) Josephs, Tracy M.; Morison, Ian M.; Day, Catherine L.; Wilbanks, Sigurd M.; Ledgerwood, Elizabeth C., *Biochem. J.* **2014**, *458* (2), 259-265.
- (44) Tognaccini, L.; Ciaccio, C.; D'Oria, V.; Cervelli, M.; Howes, B. D.; Coletta, M.; Mariottini, P.; Smulevich, G.; Fiorucci, L., *J. Inorg. Biochem.* **2016**, *155*, 56-66.
- (45) Ciaccio, C.; Tognaccini, L.; Battista, T.; Cervelli, M.; Howes, B. D.; Santucci, R.; Coletta, M.; Mariottini, P.; Smulevich, G.; Fiorucci, L., *J. Inorg. Biochem.* **2017**, *169*, 86-96.
- (46) Gu, J.; Shin, D.-W.; Pletneva, E. V., *Biochemistry* **2017**, *56*, 2950–2966.
- (47) Assfalg, M.; Bertini, I.; Dolfi, A.; Turano, P.; Mauk, A. G.; Rosell, F. I.; Gray, H. B., *J. Am. Chem. Soc.* **2003**, *125*, 2913-2922.

- (48) Döpner, S.; Hildebrandt, P.; Rosell, F. I.; Mauk, A. G., *J. Am. Chem. Soc.* **1998**, *120*, 11246-11255.
- (49) Garcia-Heredia, J. M.; Diaz-Quintana, A.; Salzano, M.; Orzaez, M.; Perez-Paya, E.; Teixeira, M.; De la Rosa, M. A.; Diaz-Moreno, I., *J. Biol. Inorg. Chem.* **2011**, *16* (8), 1155-68.
- (50) Ying, T.; Wang, Z.-H.; Lin, Y.-W.; Xie, J.; Tan, X.; Huang, Z.-X., *Chem. Commun.* **2009**, (30), 4512-4514.
- (51) Kagan, V. E.; Bayır, H. A.; Belikova, N. A.; Kapralov, O.; Tyurina, Y. Y.; Tyurin, V. A.; Jiang, J.; Stoyanovsky, D. A.; Wipf, P.; Kochanek, P. M.; Greenberger, J. S.; Pitt, B.; Shvedova, A. A.; Borisenko, G. G., *Free Radic. Biol. Med.* **2009**, *46* (11), 1439-1453.
- (52) Serpas, L.; Milorey, B.; Pandiscia, L. A.; Addison, A. W.; Schweitzer-Stenner, R., *J. Phys. Chem. B* **2016**, *120*, 12219–12231.
- (53) Ranieri, A.; Millo, D.; Di Rocco, G.; Battistuzzi, G.; Bortolotti, C. A.; Borsari, M.; Sola, M., *J. Biol. Inorg. Chem.* **2015**, *20* (3), 531-540.
- (54) Yanamala, N.; Kapralov, A. A.; Djukic, M.; Peterson, J.; Mao, G. W.; Klein-Seetharaman, J.; Stoyanovsky, D. A.; Stursa, J.; Neuzil, J.; Kagan, V. E., *J. Biol. Chem.* **2014**, *289* (47).
- (55) Belikova, N. A.; Vladimirov, Y. A.; Osipov, A. N.; Kapralov, A. A.; Tyurin, V. A.; Potapovich, M. V.; Basova, L. V.; Peterson, J.; Kurnikov, I. V.; Kagan, V. E., *Biochemistry* **2006**, *45* (15), 4998-5009.
- (56) Capdevila, D. A.; Marmisolle, W. A.; Tomasina, F.; Demicheli, V.; Portela, M.; Radi, R.; Murgida, D. H., *Chem. Sci.* **2015**, *6* (1), 705-713.
- (57) Widegren, J. A.; Finke, R. G., *J. Mol. Catal. A* **2003**, *198* (1–2), 317-341.
- (58) Haw, J. F.; Song, W. G.; Marcus, D. M.; Nicholas, J. B., *Acc. Chem. Res.* **2003**, *36* (5), 317-326.
- (59) Wunder, S.; Lu, Y.; Albrecht, M.; Ballauff, M., *Acs Catalysis* **2011**, *1* (8), 908-916.
- (60) Radi, R.; Thomson, L. M.; Rubbo, H.; Prodanov, E., *Arch. Biochem. Biophys.* **1991**, *288* (1), 112-117.
- (61) Capdevila, D. A.; Alvarez-Paggi, D.; Castro, M. A.; Tortora, V.; Demicheli, V.; Estrin, D. A.; Radi, R.; Murgida, D. H., *Chem. Commun.* **2014**, *50* (20), 2592-2594.
- (62) Baldwin, D. A.; Marques, H. M.; Pratt, J. M., *J. Inorg. Biochem.* **1987**, *30*, 203-217.

- (63) Pande, J.; Kinnally, K.; Thallum, K. K.; Verma, B. C.; Myer, Y. P.; Rechsteiner, L.; Bosshard, H. R., *J. Protein Chem.* **1987**, *6* (4), 295-319.
- (64) Yang, Y.; Stella, C.; Wang, W. R.; Schoneich, C.; Gennaro, L., *Anal. Chem.* **2014**, *86* (10), 4799-4806.
- (65) Mirzaei, H.; Regnier, F., *J. Chromatogr. A* **2006**, *1134* (1-2), 122-133.
- (66) He, F.; Hendricksen, C. L.; Marshall, A. G., *J. Am. Soc. Mass Spectrom.* **2000**, *11*, 120-126.
- (67) Stocks, B. B.; Konermann, L., *Anal. Chem.* **2009**, *81*, 20-27.
- (68) Matsui, T.; Ozaki, S.-i.; Watanabe, Y., *J. Am. Chem. Soc.* **1999**, *121* (43), 9952-9957.
- (69) Chen, Y.; Yang, J. T.; Martinez, H. M., *Biochemistry* **1972**, *22*, 4120-4131.
- (70) Lan, W.; Wang, Z.; Yang, Z.; Ying, T.; Zhang, X.; Tan, X.; Liu, M.; Cao, C.; Huang, Z.-X., *PLoS ONE* **2014**, *9* (9), e107305.
- (71) Nagababu, E.; Rifkind, J. M., *Antioxid. Redox Signaling* **2004**, *6* (6), 967-978.
- (72) Kaminsky, L. S.; Miller, V. J.; Davison, A. J., *Biochemistry* **1973**, *12*, 2215-2221.
- (73) Feng, Y. Q.; Roder, H.; Englander, S. W., *Biophys. J.* **1990**, *57* (1), 15-22.
- (74) Russell, B. S.; Melenkivitz, R.; Bren, K. L., *Proc. Natl. Acad. Sci. U. S. A.* **2000**, *97* (15), 8312-8317.
- (75) Lim, J.; Vachet, R. W., *Anal. Chem.* **2004**, *76*, 3498-3504.
- (76) Gau, B. C.; Sharp, J. S.; Rempel, D. L.; Gross, M. L., *Anal. Chem.* **2009**, *81*, 6563-6571.
- (77) Birk, A. V.; Chao, W. M.; Liu, S. Y.; Soong, Y.; Szeto, H. H., *Biochim. Biophys. Acta* **2015**, *1847* (10), 1075-1084.
- (78) Stocks, B. B.; Konermann, L., *J. Mol. Biol.* **2010**, *398*, 362-373.
- (79) Møller, I. M.; Rogowska-Wrzesinska, A.; Rao, R. S. P., *J. Proteomics* **2011**, *74* (11), 2228-2242.
- (80) Artemenko, K.; Mi, J.; Bergquist, J., *Free Radical Res.* **2015**, *49* (5), 477-493.
- (81) Kim, N. H.; Jeong, M. S.; Choir, S. Y.; Kang, J. H., *Mol. Cells* **2006**, *22* (2), 220-227.
- (82) de Graff, A. M. R.; Hazoglou, M. J.; Dill, K. A., *Structure* **2016**, *24* (2), 329-336.



- (83) Tew, D.; Demontellano, P. R. O., *J. Biol. Chem.* **1988**, 263 (33), 17880-17886.
- (84) Siuti, N.; Kelleher, N. L., *Nat. Methods* **2007**, 4, 817-821.
- (85) Dongré, A. R.; Jones, J. L.; Somogyi, Á.; Wysocki, V. H., *J. Am. Chem. Soc.* **1996**, 118, 8365-8374.
- (86) Greer, S. M.; Holden, D. D.; Fellers, R.; Kelleher, N. L.; Brodbelt, J. S., *J. Am. Soc. Mass Spectrom.* **2017**, 28, 1587-1599.
- (87) Paizs, B.; Suhai, S., *Mass Spectrom. Rev.* **2005**, 24, 508-548.
- (88) Temple, A.; Yen, T.-Y.; Gronert, S., *J. Am. Soc. Mass Spectrom.* **2006**, 17, 1172-1180.
- (89) Kapralov, A. A.; Yanamala, N.; Tyurina, Y. Y.; Castro, L.; Samhan-Arias, A.; Vladimirov, Y. A.; Maeda, A.; Weitz, A. A.; Peterson, J.; Mylnikov, D.; Demicheli, V.; Tortora, V.; Klein-Seetharaman, J.; Radi, R.; Kagan, V. E., *Biochim. Biophys. Acta* **2011**, 1808 (9), 2147-2155.
- (90) Qian, S. Y.; Chen, Y.-R.; Deterding, L. J.; Fann, Y. C.; Chignell, C. F.; Tomer, K. B.; Mason, R. P., *Biochem. J.* **2002**, 363 (Pt 2), 281-288.

# Chapter 3. Lysine Carbonylation as a Previously Unrecognized Contributor to Peroxidase Activation of Cytochrome *c* in Oxidants Other than H<sub>2</sub>O<sub>2</sub>

## 3.1. Introduction

Cytochrome *c* (cyt *c*) is a 12 kDa mitochondrial heme protein whose primary role is to serve as an electron shuttle in the respiratory chain.<sup>1</sup> Cyt *c* also possesses a second biologically relevant function as a peroxidase.<sup>2-8</sup> Peroxidases catalyze the oxidation (H abstraction) of substrates in the presence of H<sub>2</sub>O<sub>2</sub>. Catalytic turnover involves heme cycling between the Fe(III) and Fe(IV)=O states.<sup>9</sup> The peroxidase activity of cyt *c* is critical for triggering apoptosis (programed cell death) via oxidation of the mitochondrial membrane lipid cardiolipin.<sup>7,10-12</sup> Apoptosis is an essential process, e.g. for suppressing tumor growth.<sup>13</sup>

Peroxidases require a pentacoordinated heme with a vacant distal coordination site where H<sub>2</sub>O<sub>2</sub> can bind, and where the Fe(IV)=O oxygen can be accommodated.<sup>14</sup> The heme in native cyt *c* is hexacoordinated, as the distal site is occupied by the Met80 sulfur (Figure 3-1).<sup>15</sup> Dissociation of this Met80-Fe contact is a mandatory prerequisite for converting cyt *c* into a peroxidase.<sup>14,16-17</sup> There are different ways to achieve displacement of the distal Met80, such as unfolding<sup>14, 16</sup> chemical<sup>5, 17-20</sup> or mutational modifications,<sup>4,7,18,21-26</sup> as well as cardiolipin binding.<sup>3,27-29</sup> Exposure to basic pH induces the formation of “alkaline” conformations where Lys72, 73 or 79 serve as distal ligands instead of Met80.<sup>20,30-34</sup> Chemical or mutational modifications can shift this alkaline transition into the neutral range.<sup>5,19-20,35-40</sup>

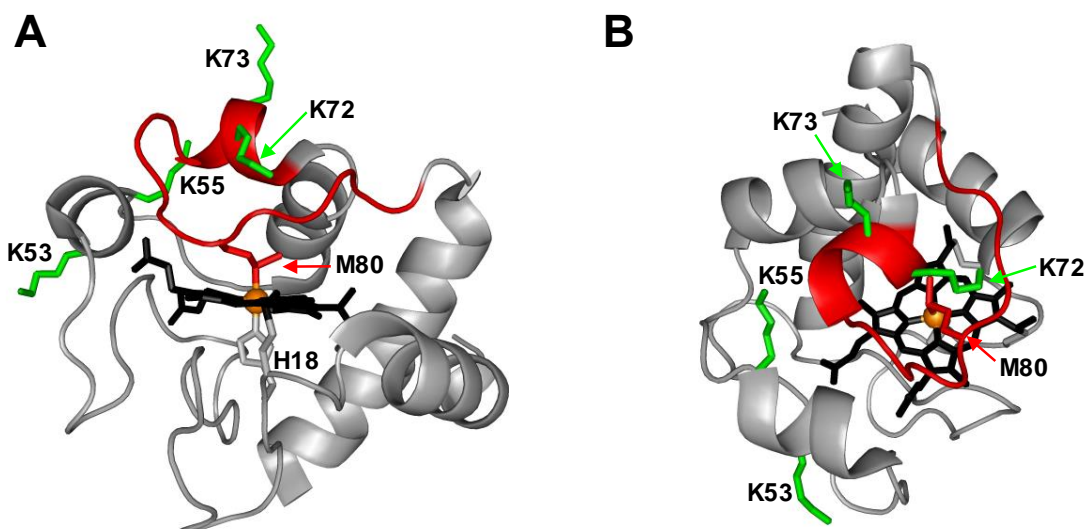


**Figure 3-1.** Crystal structure of equine cyt *c* (PDB 1HRC) with key residues highlighted. (A) Side view. (B) Top view. In the native state, the heme co-factor is ligated by Met80 and His18. Lys72/73 and Lys53/55 represent possible alternative distal ligands that may interact with Fe instead of Met80 under certain conditions. The flexible 71-85  $\Omega$  loop is shown in red.

We recently demonstrated<sup>41</sup> that H<sub>2</sub>O<sub>2</sub> converts native cyt *c* into an active peroxidase via a reaction sequence that starts with Tyr67 oxidation, followed by dissociation of the Met80-Fe contact. Subsequently, Lys72 or 73 occupy the distal coordination site. Carbonylation then abrogates the capability of Lys72/73 to serve as Fe ligands, thereby generating the free distal site that is required for an active peroxidase.<sup>41</sup> Lys carbonylation corresponds to the oxidation of the ε-amino group to an aldehyde (LysCHO, aminoadipic semialdehyde,  $\Delta M = -1$  Da).<sup>42-43</sup>

The most straightforward method to rupture the Met80-Fe bond is via Met oxidation to methionine sulfoxide (MetO). It is widely believed that this oxidative modification is sufficient for generating the open distal site that is required for peroxidase activation of cyt *c* *in vitro* and *in vivo*.<sup>17-18,37-38,44-47</sup> In other words, this Met80-centric view envisions a simple causal relationship between MetO formation and peroxidase activity.<sup>17-18,37-38,45-47</sup>

A key pillar of the Met80-centric view comes from work on chloramine-T (CT) oxidized cyt *c* (CT-cyt *c*). CT is a mild oxidizing agent<sup>48</sup> that transforms into other reactive species in aqueous solution.<sup>49</sup> Among these, OCl<sup>-</sup> appears to be mainly responsible for cyt *c* oxidation, evident from the fact that cyt *c* exposure to CT and to OCl<sup>-</sup> causes similar effects.<sup>17</sup> CT-cyt *c* is a potent peroxidase.<sup>17,37</sup> Several studies have shown that CT-cyt *c* carries a sulfoxide at both Met80 and Met65, while claiming that no other chemical modifications are present.<sup>17,48,50</sup> These claims go back to amino acid analyses conducted in the 1970s, which concluded that CT specifically oxidizes Met, while leaving all other residues unmodified (except for -SH groups, which are absent in cyt *c*).<sup>51</sup> Those early studies<sup>17,48,50-51</sup> cemented the widely held belief that Met80 oxidation, without any other covalent changes, generates an active peroxidase.<sup>17-18,37,45-47</sup> As a result, CT-cyt *c* has become a widely used model for peroxidase-activated cyt *c*.<sup>17,37-38,47</sup>

Considering the far-reaching implications of work in this area (including the role of *cyt c* in apoptosis and tumorigenesis),<sup>13</sup> it is imperative to fully understand the properties of CT-*cyt c*. Is it true that Met80 oxidation is sufficient for peroxidase activation? Is it true that MetO formation is the only CT-induced oxidative modification? Several lines of evidence hint at the involvement of additional factors. (1) Disruption of the Met80-Fe bond tends to produce “alkaline” ligation scenarios, where even at near-neutral pH the distal site becomes occupied by side chains such as Lys72/73.<sup>19,35-36,38</sup> These alternative ligation scenarios are promoted by the flexible nature of the 71-85  $\Omega$  loop (Figure 3-1).<sup>52-53</sup> Hence, it is not obvious why Met80 oxidation in itself would produce a vacant distal site that is required for peroxidase activity. (2) The purported strict selectivity of CT for Met is somewhat suspicious, considering that other oxidants can induce various modifications at different types of residues.<sup>54-58</sup> (3) Typical CT-*cyt c* literature protocols utilize strong cation exchange (SCX) chromatography, which separates proteins according to their positive surface charge. Surprisingly, CT-*cyt c* undergoes SCX fractionation into several distinct bands.<sup>37-38,47-48</sup> MetO formation does not directly affect charge. The fact that CT-*cyt c* produces several SCX fractions thus suggests that the protein might contain additional, hitherto unidentified modifications. The possible existence of such modifications and their implications for peroxidase activation have been ignored thus far in the literature.

In this work we critically examined the structure and function of CT-*cyt c*. Various mass spectrometry (MS) techniques were applied to characterize CT-induced covalent modifications in unprecedented detail. We were able to pinpoint previously unidentified features of the peroxidase activation process. Met80 oxidation alone was found to result in low peroxidase activity, because the distal site remained impeded by alkaline-like Lys ligation. Only after opening of the distal site by CT-induced LysCHO formation did the protein show higher levels of activity. Previous studies on CT-*cyt c* that assumed a “clean” MetO protein have - in all likelihood - inadvertently characterized samples that contained both MetO *and* LysCHO sites. Our findings argue against the prevailing notion that Met80 oxidation alone is sufficient for peroxidase activation. Instead, Lys carbonylation is a key peroxidase co-activator.

## **3.2.Methods**

### **3.2.1. Materials.**

Horse heart ferricyt *c*, H<sub>2</sub>O<sub>2</sub>, guaiacol (o-methoxyphenol), ammonium acetate, and chloramine-T (N-chloro-4-toluol-sulfonamide), were from Sigma Aldrich (St. Louis, MO). Solvents were from Fisher Scientific (Nepean, ON). Potassium phosphate was supplied by Caledon Laboratories (Georgetown, ON), and MS-grade modified trypsin was from Promega (Madison, WI). All experiments were conducted at 22 ± 2 °C.

### **3.2.2. Preparation of CT-cyt *c*.**

Treatment of cyt *c* with CT was performed as described,<sup>37</sup> with minor alterations. Briefly, a 5 mM aqueous solution of CT was added to 1 mM cyt *c* of (both in 50 mM Tris buffer, pH 8.4) in a 1:1 volume ratio and reacted at room temperature for 3 hours. The reaction was then halted by dialysis against 10 mM potassium phosphate (pH 7.4) using 10 kDa MWCO filters (EMD Millipore, Etobicoke, ON). The CT-cyt *c* produced in this way was either used directly or subjected to SCX chromatography using a 5 mL HiTrap sulfopropyl (SP) cartridge (GE Healthcare) on an ÄKTApurifier FPLC. The HiTrap SP column was conditioned as per manufacturer instructions, and proteins were loaded at 0.25 mL min<sup>-1</sup>. The column was then washed with H<sub>2</sub>O until the absorbance (280 nm) reached the pre-loading baseline. SCX elution was performed using a linear gradient of 500 mM ammonium acetate (pH 9) over 5 column volumes while collecting the eluent in 1 mL fractions.

### **3.2.3. Optical Spectroscopy.**

UV-Vis spectra were acquired on a Cary-100 spectrophotometer (Varian, Mississauga, ON). Soret measurement were performed on 10 µM protein solutions in 50 mM potassium phosphate buffer (pH 7.4). Absorbance measurements at 695 nm were performed at 40 µM protein. Peroxidase activity was measured as described<sup>59</sup> by tracking the oxidation of 9 mM guaiacol in the presence of 100 µM H<sub>2</sub>O<sub>2</sub>. Additional experiments were also conducted using 500 µM H<sub>2</sub>O<sub>2</sub>. This H<sub>2</sub>O<sub>2</sub> concentration range is in line with previous work,<sup>7, 32</sup> and it is comparable to physiological H<sub>2</sub>O<sub>2</sub> levels at the onset of

apoptosis.<sup>60</sup> In these assays the formation of tetraguaiacol was probed by UV-Vis at 470 nm.<sup>59</sup> All activity assays contained 1  $\mu\text{M}$  protein as determined by absorption measurements at the Soret maximum. Kinetic measurements at each  $\text{H}_2\text{O}_2$  concentration were repeated in triplicate. Circular dichroism (CD) spectra were recorded on a Jasco J-810 spectropolarimeter (JASCO, Easton, MD), on 10  $\mu\text{M}$  protein solutions in phosphate buffer (pH 7.4).

#### **3.2.4. Mass Spectrometry.**

MS experiments were performed on a Synapt G2 ESI quadrupole-time-of-flight instrument (Waters, Milford, MA) operated in resolution mode. The capillary, sample cone, and extraction cone voltages were set at +2.8 kV, 25 V, and 4 V, respectively. MS/MS experiments were performed using collision-induced dissociation (CID) with argon as collision gas. Protein samples for bottom-up MS experiments were prepared by overnight digestion using trypsin (50:1 protein/trypsin) at 37 °C, and subsequently analyzed by liquid chromatography – mass spectrometry (LC/MS) using a nanoACQUITY UPLC (Waters) with a C18 column. Samples for intact protein MS were prepared as 10  $\mu\text{M}$  solutions in a 50:50 solution of  $\text{H}_2\text{O}$ :ACN with 0.1% formic acid, and directly infused at 5  $\mu\text{L min}^{-1}$  using a syringe pump. For ion mobility-assisted top-down MS/MS experiments (top-down CID-IM-MS), 16+ protein ions were quadrupole-selected prior to CID in the trap collision cell. The collision energy used was 23 V for all samples. Ion mobility spectrometry (IMS) separation of CID products was performed in  $\text{N}_2$  buffer gas at a wave velocity of 350  $\text{m s}^{-1}$  and wave height of 13 V. Simulated isotope distributions were generated using ProteinProspector (UCSF). All simulated spectra correspond to the ferric (Fe(III)) state of cyt *c*.

### **3.3. Results and Discussion**

#### **3.3.1. Chloramine-T-induced Met80 Oxidation.**

The CT-cyt *c* used in this study was prepared using established procedures.<sup>37-38,47</sup> An initial characterization was conducted by subjecting unfractionated samples to a standard tryptic digestion/LC-MS/MS workflow. As expected, these assays revealed MetO formation (+16 Da) at Met80 and Met65, in line with earlier reports (Figure 3-2).<sup>17,37,46-47</sup> No other +16 Da modifications were detected. These observations appear to support the widely held belief that CT selectively oxidizes Met.<sup>17,48,50-51</sup> However, from the data discussed below it will be seen that standard mapping experiments (such as those of Figure 3-2) provide an incomplete view of the CT-induced oxidation events.

#### **3.3.2. SCX Fractionation and Optical Characterization.**

SCX elution profiles of CT-cyt *c* exhibited three major peaks (Figure 3-3A), consistent with previous observations.<sup>37-38,47-48</sup> Close examination of the highest intensity region revealed the presence of two partially overlapping signals (around 23 mL, equivalent to “peak B” in ref. 37). In total, therefore, SCX revealed the existence of four chromatographically distinguishable CT-cyt *c* forms. We will refer to these fractions as I, II, III, and IV in the order of decreasing retention. Fraction I had the largest retention volume, i.e. it interacted most strongly with the stationary phase, implying the most highly cationic character. The SCX behavior of fraction I was indistinguishable from that of unmodified cyt *c*. Conversely, fraction IV showed the weakest interaction with the stationary phase, i.e. proteins in this fraction carried the least amount of positive charge. From the  $A_{280}$  values in the SCX chromatograms, the relative abundance of fractions IV, III, II, and I can be estimated to be roughly 10%, 35%, 35%, and 20%, respectively. For subsequent experiments we isolated thin slices out of the chromatograms for targeted experiments on each fraction (Figure 3-3A).



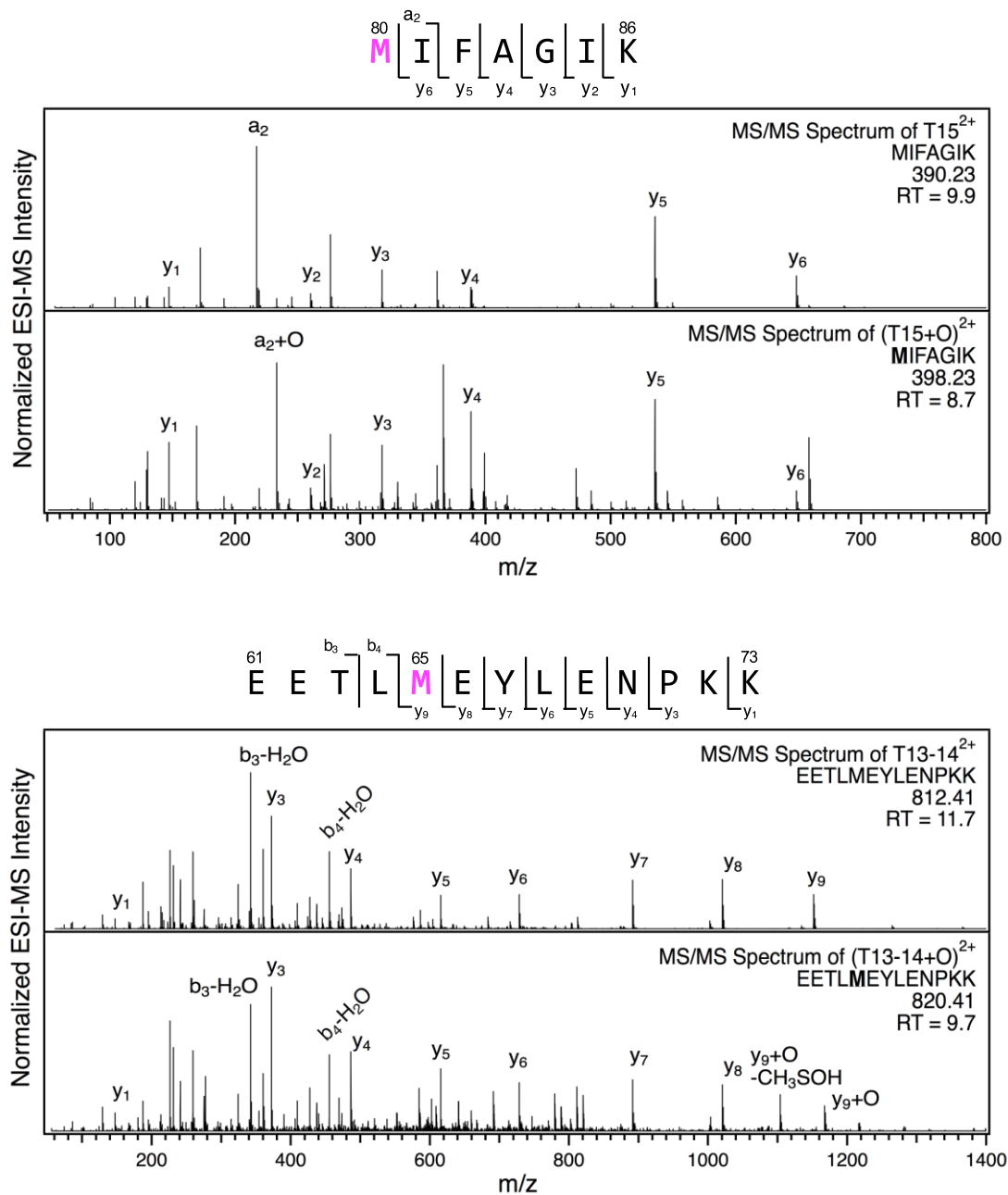


**Figure 3-2.** Tandem mass spectra of Met-containing tryptic peptides. In each panel, the top trace depicts the unmodified peptide, whereas the bottom trace depicts the MetO form. Top: peptide T15 (residues 80-86) reveals (+16 Da) at Met80. Bottom: peptide T13-14 (residues 61-73), with MetO formation at Met65. These experiments were conducted on unfractionated samples. i.e. without prior SCX chromatography.

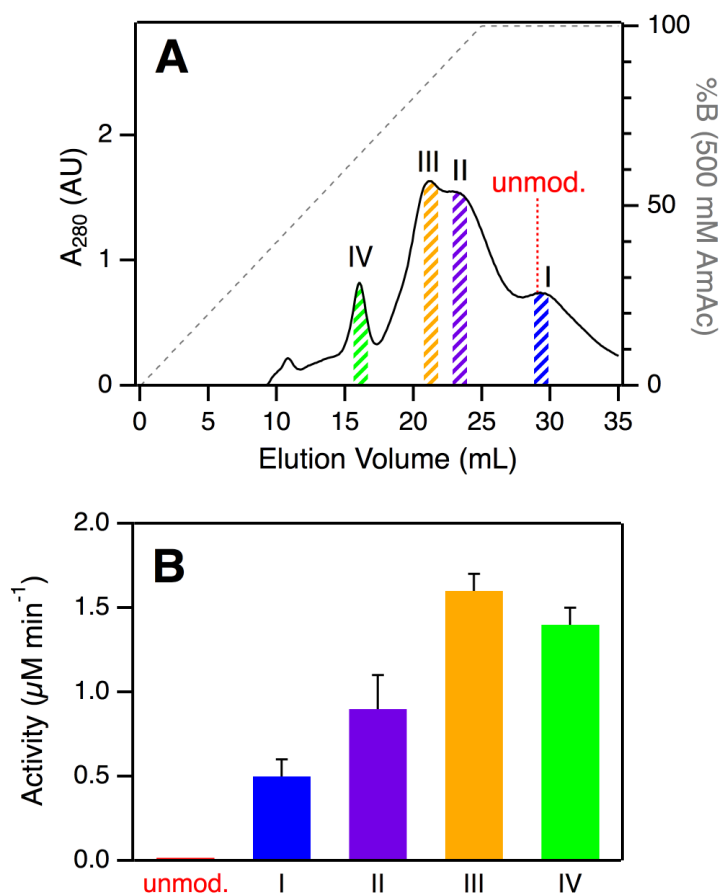


**Figure 3-3.** (A) Analysis of CT-cyt *c* by SCX chromatography. Four major species (I-IV) were discernible. Colored bars indicate collected fractions used for subsequent experiments. The elution volume of unmodified cyt *c* is indicated for comparison. (B) Peroxidase activity of CT-cyt *c* fractions measured in 100  $\mu\text{M}$   $\text{H}_2\text{O}_2$ . Error bars represent standard deviations of three independent experiments.

Optical spectra of the four CT-cyt *c* fractions were very similar to one another, but markedly different from those of unmodified cyt *c* (Figure 3-4). CT-cyt *c* showed a ~30% CD intensity loss at 222 nm, revealing some decrease of  $\alpha$ -helicity upon oxidation.<sup>61</sup> There was no concomitant increase in the random coil region (~200 nm), suggesting that CT-induced modifications did not cause unfolding, but transitions to alternative folded structures.<sup>61</sup> A blue shift of the UV-vis Soret band from 409 nm to ~405 nm indicated alterations in the heme environment. In addition, all CT-cyt *c* fractions exhibited loss of the 695 nm absorption band, signaling disruption of the Met80-Fe bond.<sup>62</sup>

In summary, the spectroscopic data of Figure 3-4 indicate the formation of non-native, structured conformers in the CT-treated samples. The CD spectra were similar to those of Lys-ligated alkaline cyt *c*.<sup>19,35-36</sup> The blue-shifted Soret band is reminiscent of alkaline cyt *c* as well.<sup>34,38</sup> Resonance Raman (RR) data in the literature showed Fraction I to be Lys-ligated, whereas the remaining fractions were reported to have an open (OH<sup>-</sup>/H<sub>2</sub>O coordinated) distal site.<sup>37</sup> All these observations support the view that CT-cyt *c* shares structural features with previously characterized alkaline cyt *c* conformers.<sup>19,34,36</sup> Recent NMR and EPR work by Zhong *et al.* arrived at an analogous conclusion.<sup>38</sup>

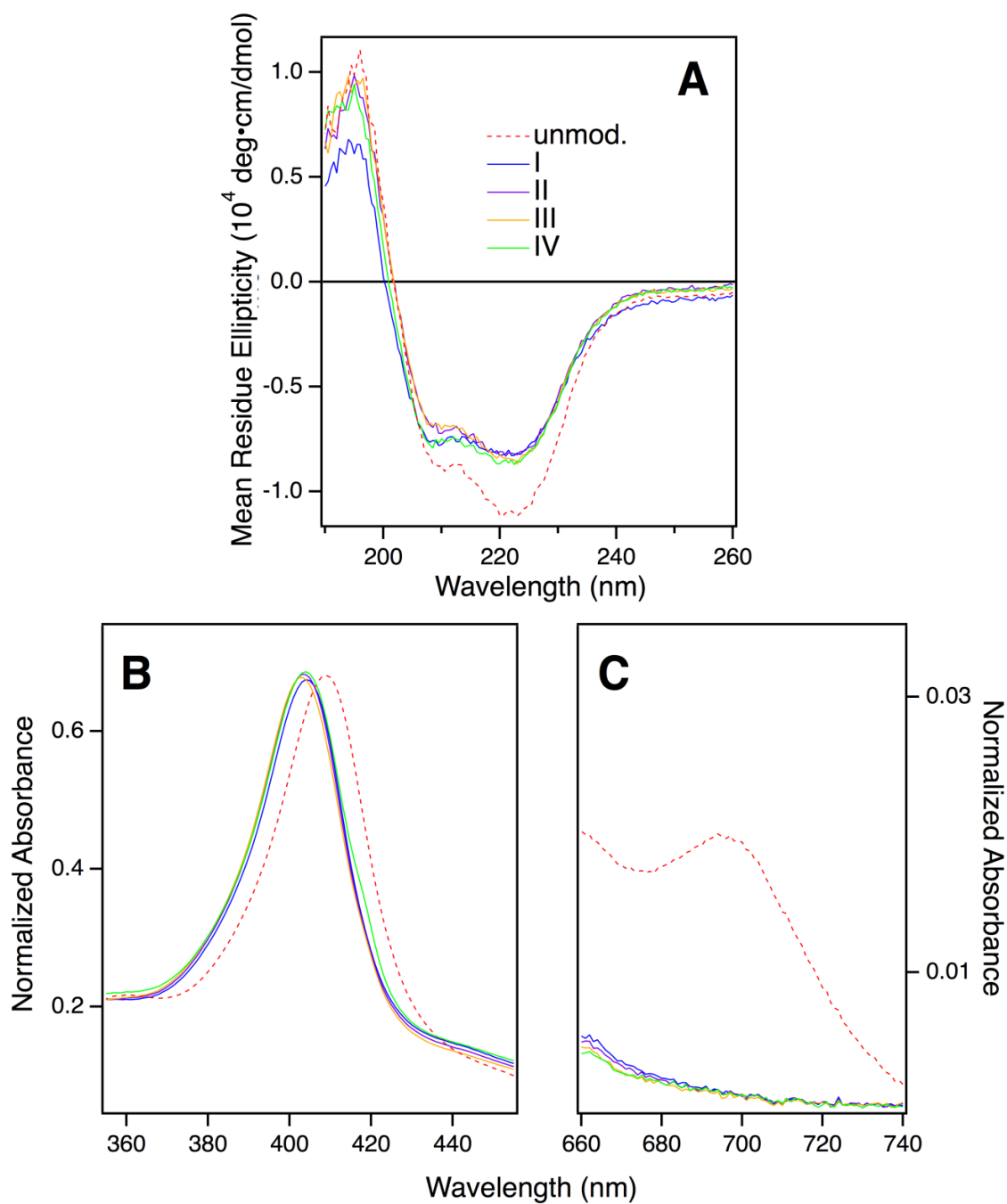


**Figure 3-4.** Optical spectroscopy of CT-cyt *c* fractions. All data was compared against unmodified cyt *c* controls (dashed red trace) (A) Far-UV CD spectra. (B) Soret UV/vis to probe heme coordination environment. (C) A695 UV/vis band, characteristic of the Fe-Met80 bond.

### 3.3.3. Peroxidase Activity of CT-cyt *c* Fractions.

Despite their similar CD and UV-Vis spectroscopic properties (Figure 3-4), the four CT-cyt *c* fractions exhibited very different levels of peroxidase activity. Kinetic measurements were performed in the presence of 100  $\mu\text{M}$   $\text{H}_2\text{O}_2$  (Figure 3-3B).<sup>59</sup> Fraction I showed a relatively low activity; that of fraction II was twofold higher, and for fraction III an additional  $\sim$ twofold increase was observed. Fractions III and IV had similar activities. For the low  $\text{H}_2\text{O}_2$  concentration of Figure 3-3B, turnover was barely detectable for unmodified cyt *c*. This activity trend can be summarized as follows: unmodified cyt *c* < fraction I < fraction II < fraction III  $\approx$  fraction IV. The same trend was observed when the experiments were repeated at a higher  $\text{H}_2\text{O}_2$  concentration of 500  $\mu\text{M}$ , where even untreated cyt *c* showed non-zero activity (data not shown).

A number of earlier studies implied that CT treatment of cyt *c* generates a homogeneous product that is oxidized only at Met80 and Met65.<sup>17,48,50</sup> The data presented here demonstrate that this view is not correct. Instead, CT-cyt *c* is a mixture of at least four species that can be separated by SCX (Figure 3-3A) and that exhibit different peroxidase activities (Figure 3-3B). While SCX fractionation of CT-cyt *c* has been demonstrated previously,<sup>37-38,47-48</sup> the chemical origin of this phenomenon and the associated activity differences remain unexplained. SCX separates proteins according to their cationic surface charge. CT-induced Met  $\rightarrow$  MetO conversion does not directly alter the ionic nature of the protein (Figure 3-5). Conformational factors could, in principle, contribute to the SCX fractionation.<sup>48</sup> However, the nearly indistinguishable CD and UV-Vis spectra point to similar overall structures for fractions I-IV (Figure 3-4), making conformational factors an unlikely culprit for the observed SCX behavior.

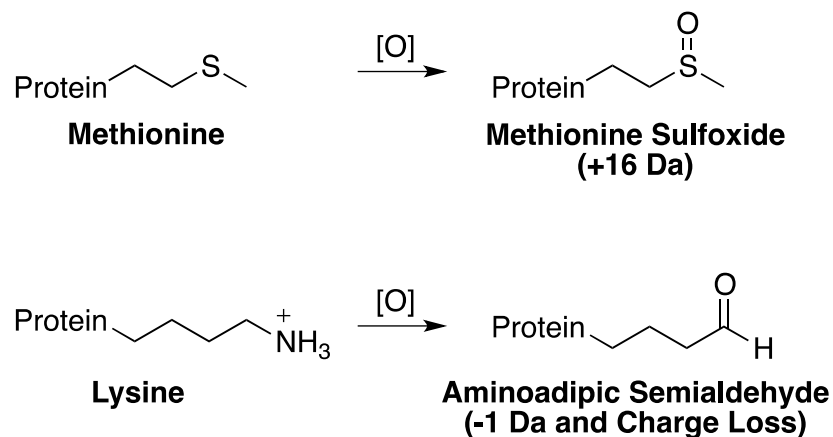


**Figure 3-5.** Structures of oxidation products of methionine (MetO, methionine sulfoxide) and lysine (LysCHO, amino adipic semialdehyde).

### 3.3.4. SCX Fractions Represent Specific Proteoforms.

For uncovering the origin of the SCX properties and activity differences of fractions I-IV we applied a range of MS methods. As an initial step, intact protein mass spectra were acquired (Figure 3-6). At first glance, the mass distributions of the four fractions appear to be almost identical, reminiscent of the optical data in Figure 3-4. Each spectrum in Figure 3-6 is dominated by two signals that are spaced +16 Da apart, as expected for MetO formation at Met80 and/or Met65. In addition, each fraction showed a low intensity signal close to the mass of unmodified *cyt c*. In Figure 3-6 these signals were annotated according to the number (0, 1, 2) of MetO formation events. This interpretation reflects the existing literature, which assumes that CT specifically targets Met80 and Met65 while leaving other residues unmodified.<sup>17,37-38,47-48,50-51</sup>

To test the viability of this simple MetO-centric interpretation we calculated theoretical isotope distributions for unmodified *cyt c*, a +16 Da variant (one MetO), and a +32 Da variant (two MetO). These theoretical distributions were superimposed on the experimental spectra (Figure 3-6, top row). Fraction I showed excellent agreement with the theoretical data. In contrast, fractions II, III, and IV exhibited gradually increasing mass defects, i.e. the measured peaks had a lower mass than expected. The magnitude of this discrepancy correlated with the SCX elution behavior: Fraction IV showed the largest discrepancy, while fraction I exhibited no discrepancy. The mismatch between experimental spectra and the theoretical “clean” +16 Da adducts implies that MetO formation is not the only type of covalent modification in fractions II-IV. Control experiments confirmed that mass discrepancies were already observable for unfractionated CT-*cyt c*, i.e. the observed effects were not an SCX-related artifact (Figure 3-7).

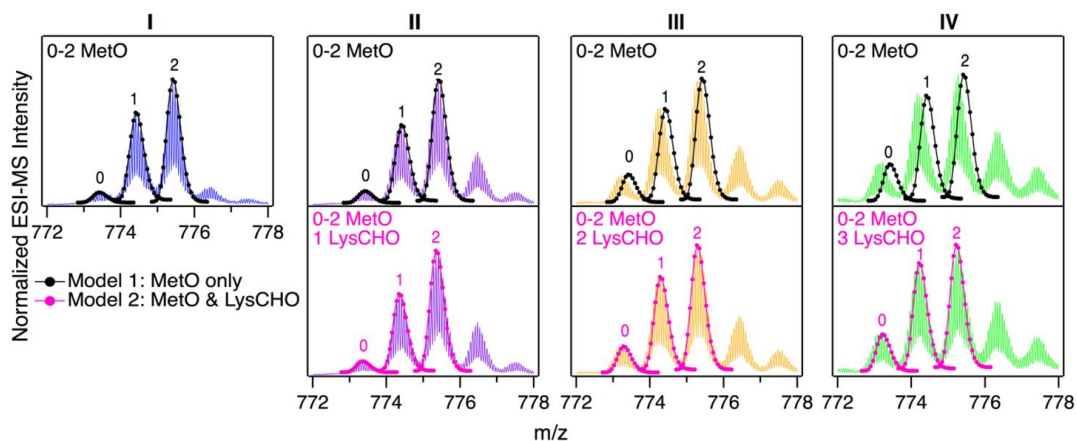


**Figure 3-6.** Intact protein mass spectra of CT-*cyt c* fractions I-IV, focusing on the 16+ charge state, which yielded the highest signal intensity. Labels 0, 1, or 2 above peaks refer to the number of MetO sites (+16 Da). Top: Black lines/dots represent theoretical isotope distributions for MetO formation. Bottom: Magenta lines/dots represent theoretical isotope distributions for MetO formation plus one, two, or three LysCHO formation events (Lys carbonylation, -1 Da). Top and bottom panels in each column show the same experimental data with different isotope models.

The missing piece of the puzzle that explains the properties of CT-cyt *c* is Lys carbonylation (Figure 3-5). This reaction is known to be facilitated by metal centers (i.e. heme in cyt *c*).<sup>43</sup> It involves a radical intermediate<sup>63</sup> that gets converted to  $\epsilon$ -hydroxylysine. Elimination of ammonia then produces LysCHO.<sup>64</sup> Each LysCHO formation event is accompanied by a -1 Da shift.<sup>41,64</sup> Compilations of known oxidative protein modifications reveals LysCHO formation to be the only process associated with a -1 Da shift.<sup>42-43</sup> The direct MS-based detection of LysCHO sites will be discussed below.

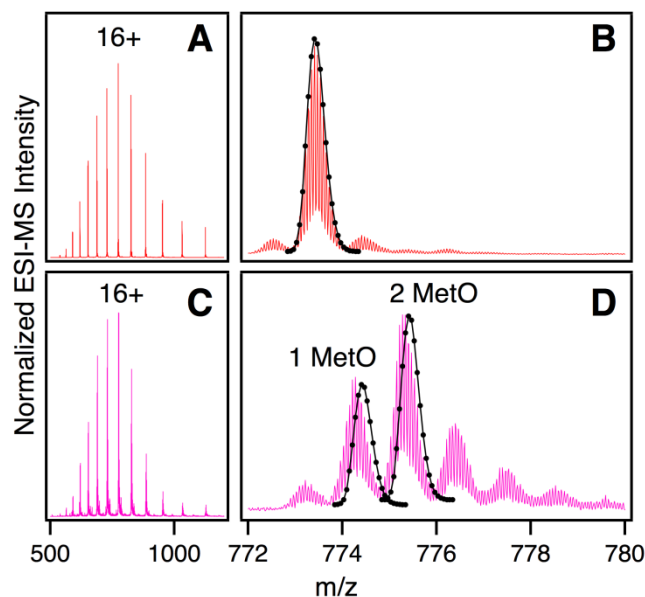


**Figure 3-7.** Intact protein ESI mass spectra of cyt *c* before (red) and after (magenta) CT treatment, but prior to SCX fractionation. Panels A and C depict the total charge state envelope, where panels B and D show a magnified view of the 16+ charge state. The data for unmodified cyt *c* are overlaid with a simulated isotopic distribution. The CT-cyt *c* mass spectrum is overlaid with simulated isotopic distributions for Met oxidation (+16 and +32 Da, respectively). Major discrepancies are observable between simulated and experimental isotopic envelopes for CT-cyt *c*. These discrepancies are caused by the presence of LysCHO sites under the conditions of C/D.



Returning to Figure 3-6, revised modeling of the mass spectra to account for a combination of MetO (+16 Da) and LysCHO formation (-1 Da) resulted in excellent agreement between experimental and simulated spectra for all fractions (Figure 3-6, bottom row). The isotope models suggest that fractions I, II, III, and IV carry 0, 1, 2, and 3 LysCHO groups, respectively. These modifications are in addition to MetO formation at Met80 and Met65.<sup>17,37-38,47-48,50-51</sup>

The different numbers of LysCHO groups provide an explanation for the SCX behavior of the four fractions. The SCX strategy used here separates proteins on the basis of their overall cationic charge; each LysCHO site reduces this charge by one unit.<sup>41-42,64</sup> In fraction I, the lack of Lys modifications causes the most positive surface charge, similar to that of unmodified cyt *c* (pI 9.6).<sup>65</sup> Hence, fraction I (and unmodified cyt *c*) interact most tightly with the SCX column, resulting in the largest elution volume (Figure 3-3A). On the other extreme, fraction IV with its three LysCHO has lost three positive charges, causing those proteins to interact most weakly with the column. The behavior of fractions II and III falls in-between these two extremes.

In summary, LysCHO formation accounts for the previously unexplained observation<sup>37-38,47-48</sup> that CT-cyt *c* can be fractionated by SCX. LysCHO has been shown to play a role in the peroxidase activation of cyt *c* by H<sub>2</sub>O<sub>2</sub>.<sup>41</sup> However, LysCHO formation in cyt *c* has not been reported for oxidizing agents other than H<sub>2</sub>O<sub>2</sub>. The number of LysCHO sites is the *only* detectable difference in the covalent structures of fractions I-IV, implying that LysCHO formation must be responsible for their different activities. Combining the information of Figure 3-3B and Figure 3-6, the peroxidase activity can be ranked according to the number of LysCHO: fraction I (0 LysCHO) < fraction II (1 LysCHO) < fraction III (2 LysCHO) ≈ fraction IV (3 LysCHO).

### 3.3.5. Top-Down CID-IM-MS for Proteoform-Selective Analysis.

Mapping of LysCHO sites poses significant analytical challenges.<sup>66</sup> Typical bottom-up MS assays struggle with this task due to LysCHO-induced interference with tryptic cleavage and losses of ionization/fragmentation efficiency.<sup>42,67-68</sup> Thus, it is not surprising that previous MS investigations failed to detect LysCHO in CT-cyt *c*.<sup>17-18,37-38,45-48,50-51</sup> To address these challenges we applied top-down MS/MS, i.e. gas phase fragmentation of undigested proteins.<sup>69</sup> Initial attempts were unsuccessful due to the complexity of the fragment ion spectra. This problem was solved by incorporating ion mobility (IM) spectrometry to provide an additional separation dimension, thereby implementing a “top-down CID-IM-MS” workflow (Figure 3-8). Similar experiments have previously been applied to simple model systems,<sup>70-72</sup> but this work marks the first time that such an approach was used for tracking unknown biologically relevant modifications.

For validation, top-down CID-IM-MS was initially applied to peak 1 of fraction I (which is devoid of LysCHO) to examine the initial MetO formation event (Figure 3-9). All C-terminal fragments starting at *y*<sub>25</sub> showed a +16 Da shift relative to unmodified cyt *c*. The *y*<sub>25</sub> to *y*<sub>24</sub> transition allowed the oxidation site to be identified as Met80 with single-residue resolution. The presence of other oxidation sites in peak 1 (including Met65) could be ruled out. Measurements on peak 2 (+32 Da) verified Met80 and Met65 as the only two oxidation sites in fraction I (Figure 3-10). Taken together, these data imply that CT-induced MetO formation is a sequential process, with Met80 as the initial oxidation target whereas Met65 is affected at a later stage.

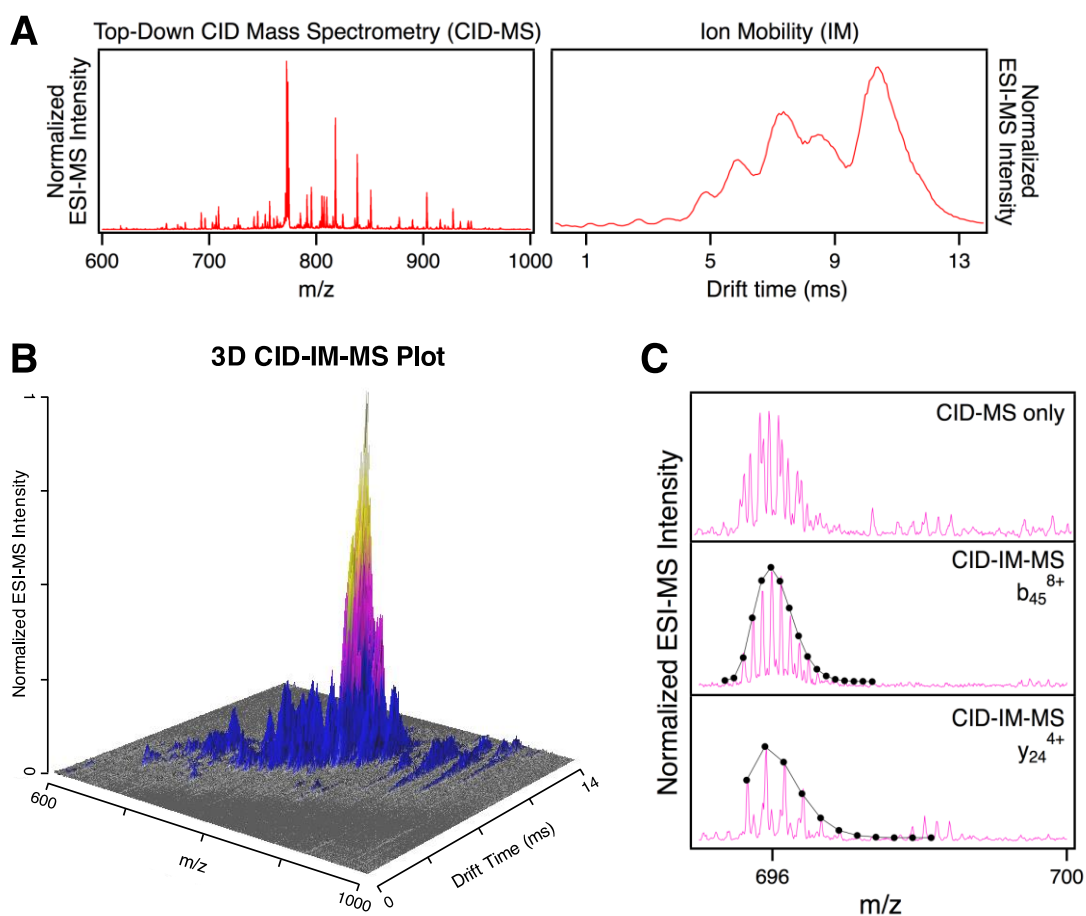


**Figure 3-8.** Principle of top-down CID-IM-MS experiments. (A) Fragmentation is initially achieved by precursor selection and CID in the trap collision cell of the Synapt G2, generating a complex mix of product ions. These fragment ions are then subjected to IMS, providing drift time information for each of the gas phase species, thereby adding a second dimension to the MS/MS spectrum (illustrated in panel B). (C) Representative example of peak assignments made possible by top-down CID-IM-MS of CT-cyt *c*. The initial MS/MS spectrum (top) shows signals that occupy the same  $m/z$  space; such the data cannot be interpreted. Using IMS, the complex multiplet can be separated into clean isotopic distributions: one corresponding to  $b_{45}^{8+}$ , and another to  $y_{24}^{4+}$ .

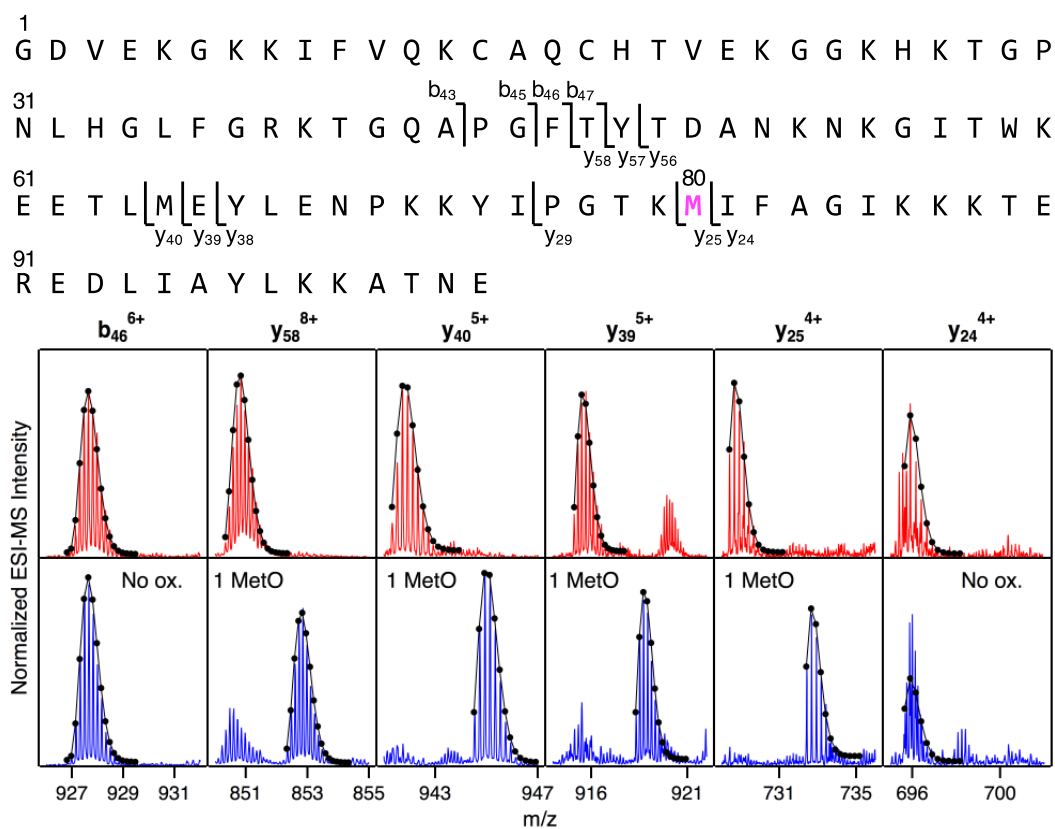


**Figure 3-9.** Top-down CID-IM-MS data that pinpoint MetO formation in fraction I. The sequence is shown along the top, with key fragments indicated. Bottom: Selected fragment ions from an unmodified control (red), and from peak 1 of fraction I (blue, see Figure 3-6). Lines/dots represent theoretical isotope distributions calculated for unmodified fragments (“no ox.”), or for MetO containing fragments. Met80 is the only covalent modification in peak 1 of fraction I.

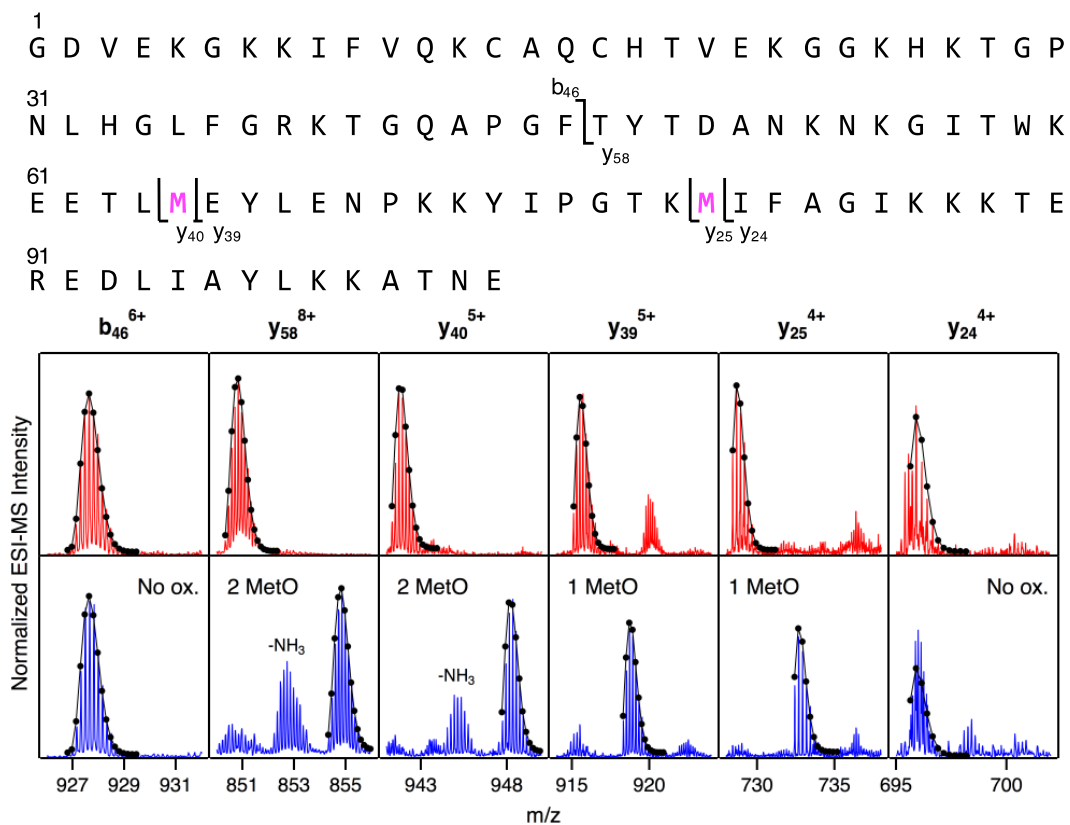


**Figure 3-10.** Representative CID-IM-MS fragment ions to determine the two sites of oxidation in peak 2 of fraction I (+32 Da). Top: Sequence of *cyt c*, with locations of diagnostic fragments labeled. Bottom: Representative fragment ions from an unmodified *cyt c* control (red) and fragment ions of peak 2 of fraction I (blue) overlaid with simulated isotopic envelopes, allowing mapping of the two +16 Da adducts to Met65 and Met80 with single-residue resolution for both.

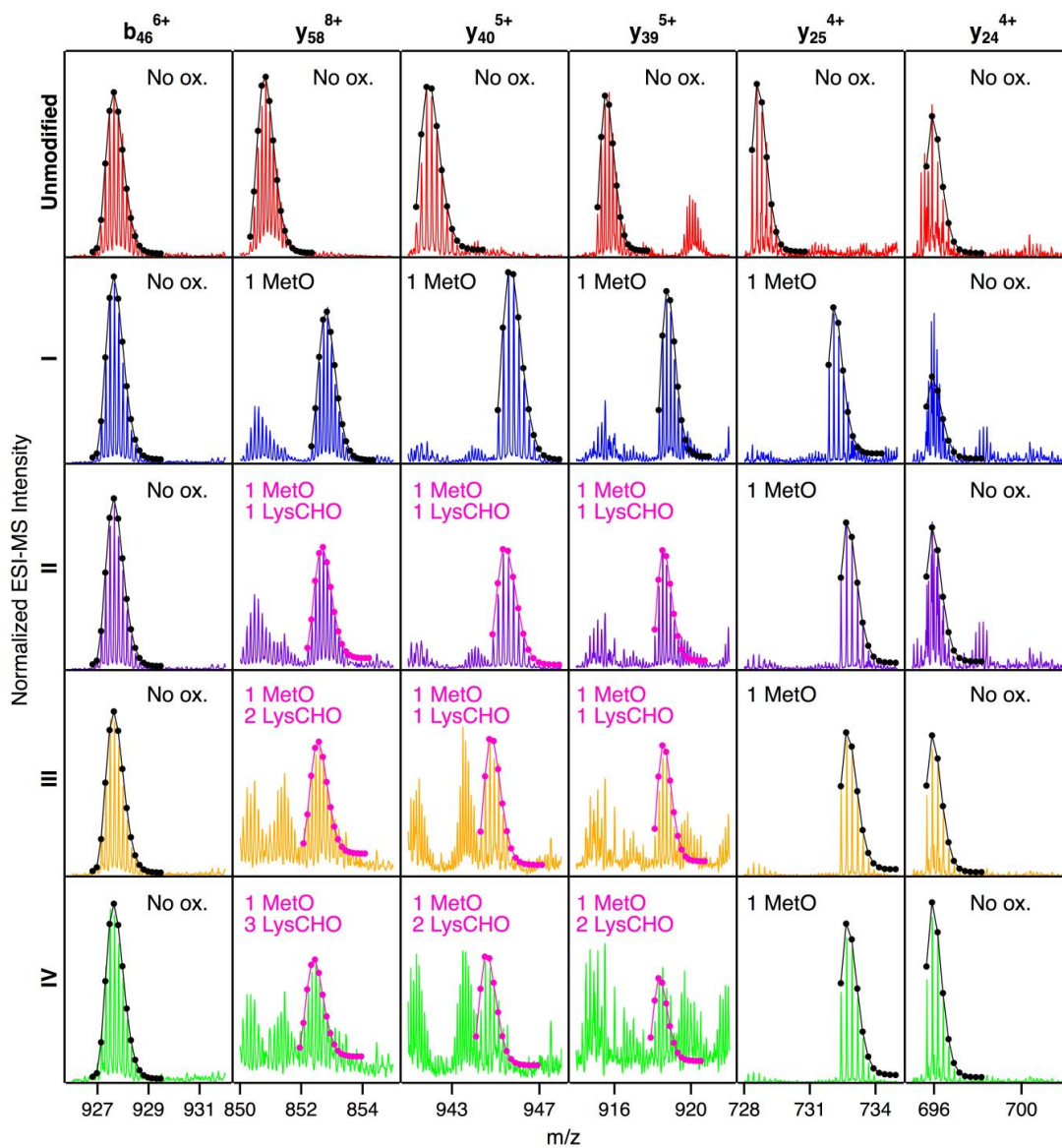


**Figure 3-11.** Diagnostic top-down CID-IM-MS fragment ions of peak 1 for all CT-cyt *c* fractions, highlighting the fact that in all fractions Met80 gets oxidized first. In other words, the first MetO signal in all fractions does *not* originate from heterogeneous Met65/80 oxidation. Each fragment ion is overlaid with a simulated isotopic envelope.

### 3.3.6. Mapping of LysCHO Sites.

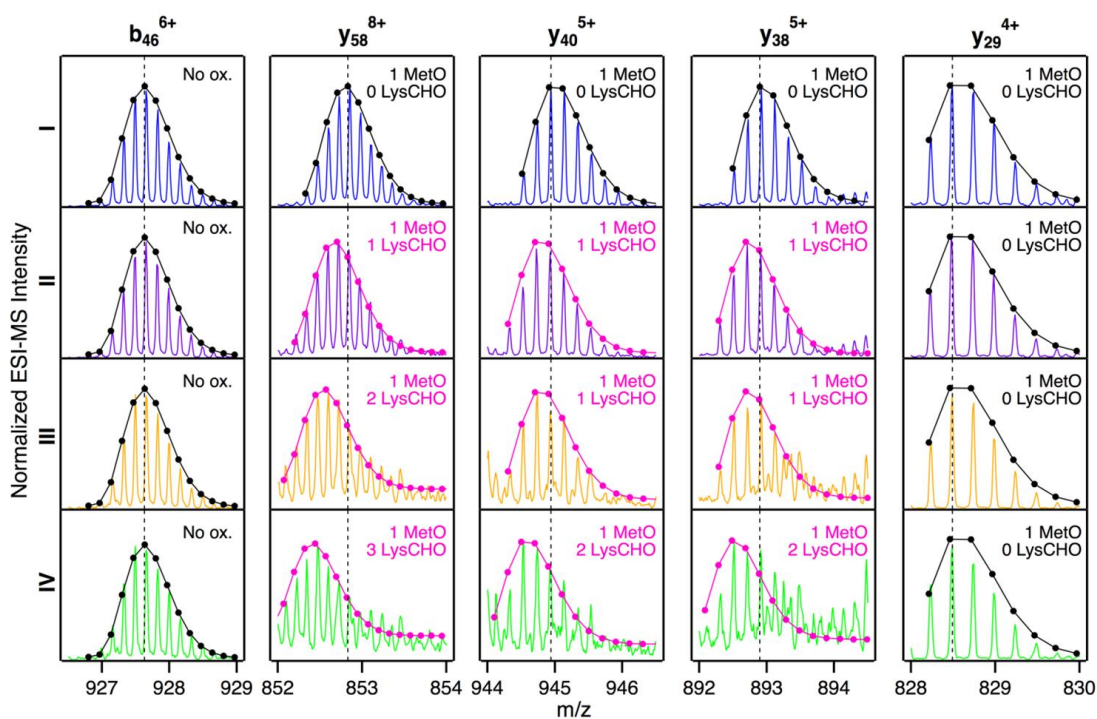
We next sought to identify the locations of LysCHO groups in fractions II, III, and IV by top-down CID-IM-MS. According to Figure 3-6, these fractions possess 1, 2, and 3 carbonylation sites, respectively. LysCHO sites can be identified from -1 Da mass shifts of fragment ions. The experiments were facilitated by the fact that, fortuitously, peak 1 in all fractions corresponded exclusively to MetO formation at Met80 (Figure 3-11). Thus, LysCHO sites in the various fractions could be mapped via comparisons with fraction I fragments. By using this internal reference, we could unequivocally rule out calibration errors as an explanation for the observed -1 Da shifts. Our assignments were further verified by simulated isotope distributions that were overlaid onto the experimental spectra.

Figure 3-12 reveals that for all fractions, N-terminal fragments up to b<sub>46</sub>, as well as C-terminal fragments up to y<sub>29</sub> were indistinguishable from those of fraction I. This finding confines *all* LysCHO sites to residues 47-75 which comprise five out of the total 19 Lys residues. In fraction II, y-ions from y<sub>38</sub> to y<sub>58</sub> showed a -1 Da shift. The y<sub>38</sub> to y<sub>29</sub> transition narrowed down the location of this modification to <sup>67</sup>YLENPKKYI<sup>75</sup>. Hence, the single LysCHO site in Fraction II is located on Lys72 or Lys73 (Figure 3-12, second row).

Fraction III also showed a y<sub>38</sub> to y<sub>29</sub> -1 Da transition, implying one LysCHO modification on Lys72/73. An additional transition took place between y<sub>40</sub> and y<sub>58</sub>, localizing the second LysCHO site to the region <sup>49</sup>TDANKNKGITWKEETLM<sup>65</sup>. Thus, the second modification site in Fraction III is located on Lys53, Lys55, or Lys60 (Figure 3-12, third row).

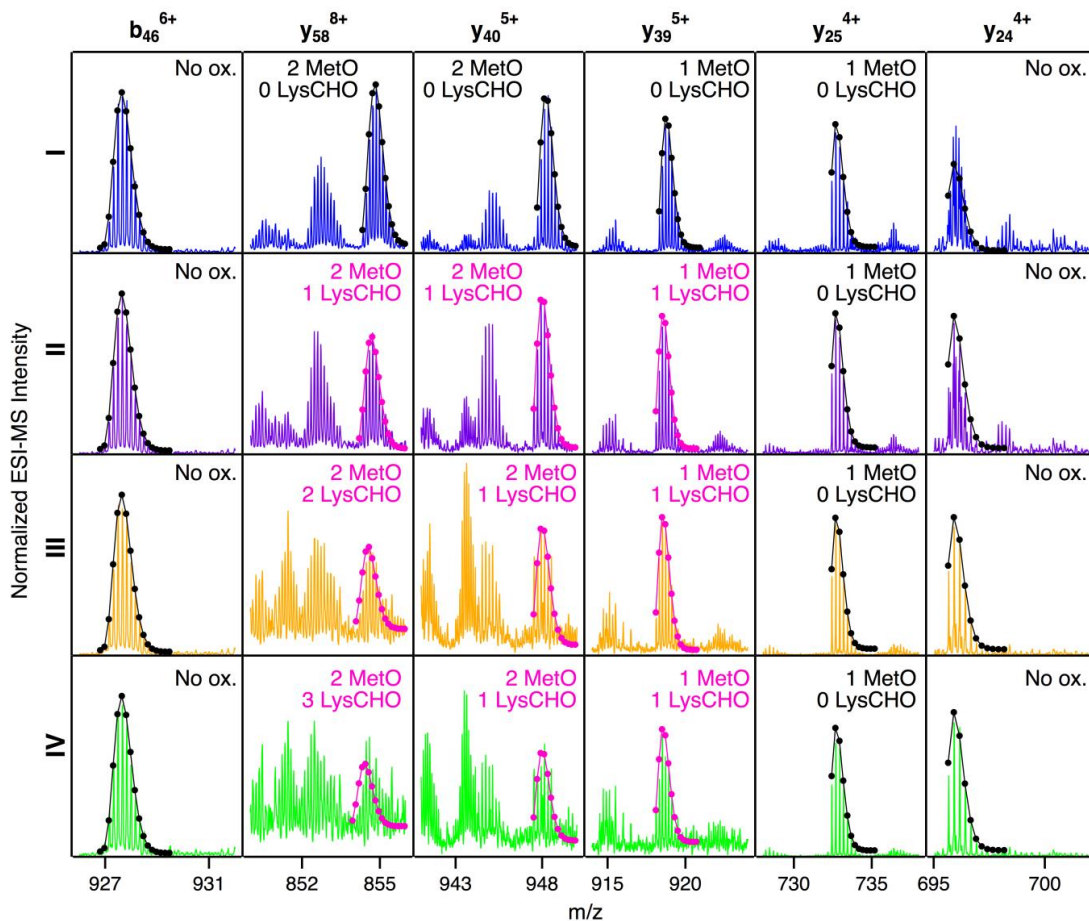
Pinpointing the three LysCHO sites in Fraction IV was complicated by diminished fragmentation efficiencies that translated into low S/N ratios. This phenomenon likely reflects the loss of protonation sites after LysCHO formation, keeping in mind that the proximity to H<sup>+</sup> sites favors b/y ion formation.<sup>73-75</sup> y<sub>58</sub> exhibited a mass shift of -3 Da (Figure 3-12, bottom row), confirming the presence of three LysCHO sites, as inferred from Figure 3-6. From the fragment ion mass shifts in Figure 3-12 (bottom row), the predominant modification pattern of fraction IV appears to be a single LysCHO in the

Lys53/55/60 range, plus two LysCHO at Lys72/73. However, we cannot rule out that the final LysCHO formation event also affects Lys53/55/60 to some extent. The similar peroxidase activities of fractions III and IV suggest that this third LysCHO is of minor functional importance. Experiments analogous to those of Figure 3-12 were conducted on peak 2 of each fraction, yielding LysCHO patterns similar to those of peak 1 (Figure 3-13).



**Figure 3-12.** Selected top-down CID-IM-MS ions generated by fragmentation of peak 1 from fractions I (blue), II (violet), III (orange), and IV (green). Each fragment ion is overlaid with its simulated isotopic envelope (lines/dots). Vertical dashed lines were included as visual aid to highlight LysCHO-related -1 Da mass shifts.





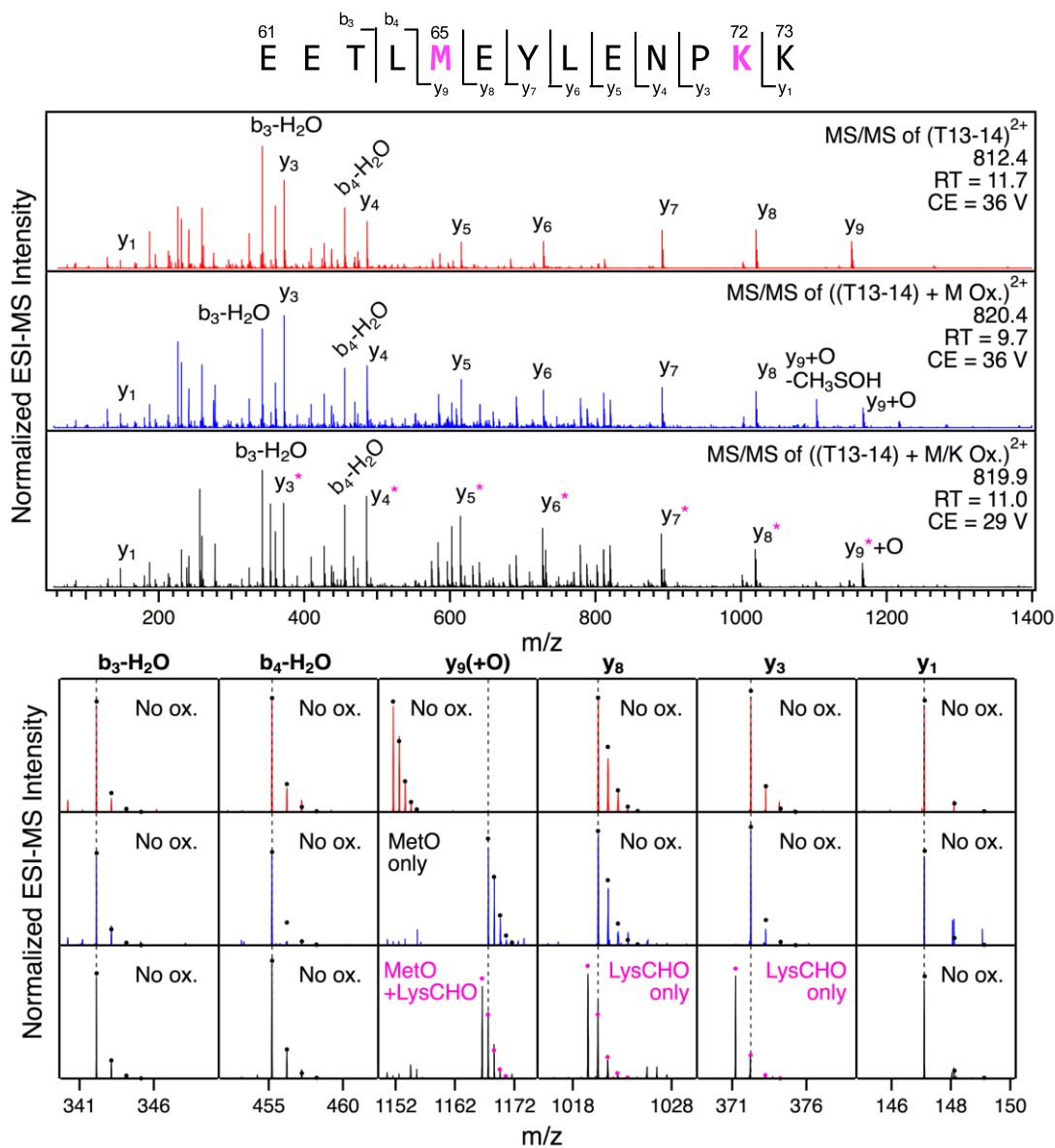
**Figure 3-13.** Diagnostic CID-IM-MS fragment ions of peak 2 for all four CT-cyt c fractions. Each fragment ion is overlaid with a simulated isotopic envelope. Met oxidation for all fractions can be mapped to Met65 and Met80, each with single-residue resolution. The location of LysCHO sites is consistent with the assignments derived for peak 1 (Figure 3-12), with some minor differences in fraction IV.

Figure 3-12 implies that CT-mediated LysCHO formation is a well-ordered process. Starting from LysCHO-free protein (fraction I), carbonylation initially affects Lys72/73 (fraction II). The next carbonylation event takes place in the Lys53/55/60 region, generating fraction III. The final LysCHO site may affect Lys72/73 or Lys53/55/60. As noted above, MetO formation is also a sequential process, initially affecting Met80 and subsequently Met65.

### **3.3.7. LC-MS/MS Peptide Mapping Revisited.**

The detection of LysCHO sites by top-down CID-IM-MS may seem at odds with previous studies on CT-cyt *c* that only found MetO formation.<sup>17,37-38,47</sup> In intact protein MS data the small (-1 Da) mass shifts associated with LysCHO formation are easily overlooked, unless the spectra are carefully scrutinized via isotope modeling (Figure 3-6). Similarly, LysCHO detection by traditional tryptic digestion LC-MS/MS (e.g. Figure 3-2) is difficult due to reduced fragmentation resulting from charge site loss, and suppression of tryptic cleavage.<sup>42,73-75</sup> These issues are exacerbated for the situation encountered here, where up to three LysCHO sites are confined to a fairly narrow sequence range (Lys53/55/60/72/73).

Armed with the information from top-down CID-IM-MS, we revisited the tryptic digestion LC-MS/MS workflow with careful optimization of experimental parameters. Gratifyingly, we were able to confirm carbonylation of Lys72 in the missed-cleavage peptide T13-14 (residues 61-73, Figure 3-14). Consistent with the data reported above, this LysCHO peptide was found in fractions II-IV, but not in fraction I. No other LysCHO sites were detected by LC-MS/MS. Thus, the top-down CID-IM-MS workflow is superior for this type of application, as it allowed the detection of all three carbonylation sites (Figure 3-12).



**Figure 3-14.** LC-MS/MS analysis of tryptic peptide T13-14 (<sup>61</sup>EETLMEYLENPK<sup>73</sup>) in unfractionated CT-cyt *c*. Three LC separated variants were interrogated: unmodified (red), with Met65 oxidation (blue), and with both Met65 oxidation and Lys72 carbonylation (black). Top: fragment ion spectra. Bottom: Magnified views of representative fragment ions, highlighting +16 Da (MetO) and -1 Da (LysCHO) mass shifts. Ions denoted with an asterisk contain the LysCHO site. Simulated isotopic envelopes are shown as circles. Much lower collision energies (CE) were required for adequate fragmentation of the carbonylated peptide.

### 3.3.8. Mechanism of CT-induced Peroxidase Activation.

The data of this work provide a clear view of the sequential CT-induced events that convert cyt *c* into an active peroxidase. This mechanism, summarized in Figure 3-15, is governed by the undisputed fact that peroxidase activity requires the distal coordination site to be accessible.<sup>14,16-17</sup> Unmodified (native) cyt *c* has the lowest peroxidase-activity of all the forms studied here because its distal ligation site is blocked by Met80. Very slow substrate turnover under these conditions may take place as the result of conformational fluctuations<sup>52-53</sup> that occasionally disrupt the Met80-Fe bond.<sup>40-41,76</sup>

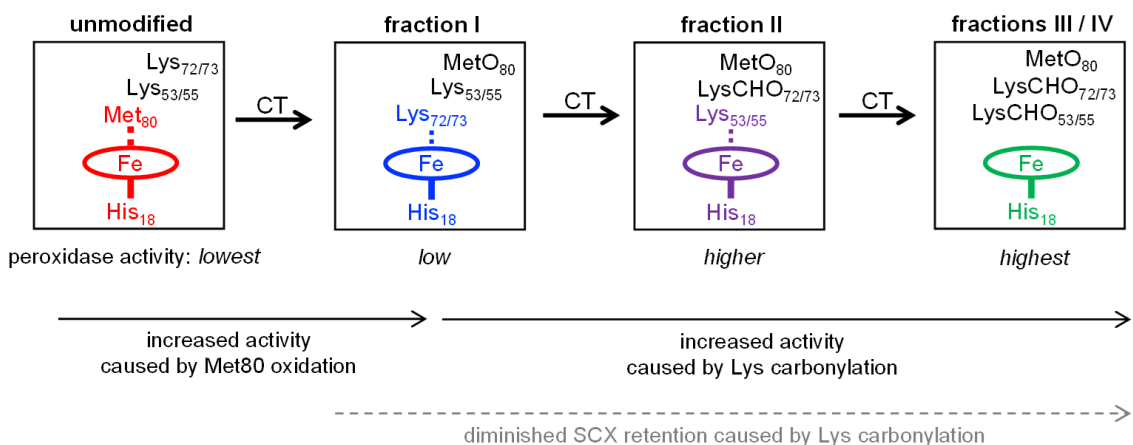


**Figure 3-15.** Model of CT-induced peroxidase activation of cyt *c*. SCX fractions I-IV exhibit different activity due to distal ligation changes. In unmodified cyt *c* the distal ligation site is blocked by Met80. In fraction I MetO formation has displaced Met80 from the heme iron, and distal ligation is provided by Lys<sub>72/73</sub>. In fraction II carbonylation of Lys<sub>72/73</sub> causes a transition to distal ligation by Lys<sub>53/55</sub>. In fractions III and IV the heme has an open coordination site because carbonylation has abrogated the capability of Lys<sub>72/73</sub> and Lys<sub>53/55</sub> to act as distal ligands. Peroxidase activity increases from left to right, concomitant with increased accessibility of the distal ligation site. Dashed lines indicate Fe coordination bonds that can transiently open as a result of protein conformational fluctuations.

CT-induced oxidation of Met80 generates fraction I, an “alkaline” conformer where Lys72 or Lys73 has moved into the ligation site previously occupied by Met80. This ligation switch is supported by RR data<sup>37</sup> as well as NMR and EPR experiments.<sup>38</sup> While the enhanced peroxidase activity of alkaline Lys-Fe conformers is well documented,<sup>38</sup> the origin of this effect is somewhat unclear because transient opening of the Lys-Fe contact takes place more slowly than for Met-Fe.<sup>34,77</sup> Likely, the enhanced activity of fraction I is not caused by hexacoordinated Lys-Fe species *per se*, but by pentacoordinated structures that are part of the fraction I ensemble.<sup>14,38</sup> RR spectra are consistent with this interpretation, suggesting the presence of ~15% pentacoordinated protein in the predominantly Lys-Fe coordinated fraction I (“peak A” in Figure S13 of ref. 37). Other factors may contribute to the peroxidase activity of Lys-ligated cyt *c* as well,<sup>41</sup> one of these is the increased heme pocket volume which facilitates substrate access.<sup>19,77</sup>

As the next step in Figure 3-15, carbonylation abrogates the iron ligating capability of Lys72/73, thereby generating fraction II. Fraction II still does not represent a genuine pentacoordinated conformer, evident from the fact that subsequent Lys53/55 carbonylation further enhances peroxidase activity (our MS data suggested the possible participation of Lys60, but we exclude this residue for reasons outlined below). Our data are thus consistent with a scenario where Lys53/55 participate in iron ligation in fraction II. However, these Lys53/55-Fe contacts must be quite labile, evident from the fact that fraction II has a higher activity than both fraction I and unmodified cyt *c* (Figure 3-3B). Carbonylation of Lys53/55 subsequently produces fraction III which possesses a permanently open distal site and shows the highest peroxidase activity. RR data confirm that fraction III is pentacoordinated, as expected for a functional peroxidase.<sup>37</sup> A final carbonylation event produces fraction IV which retains both an open distal site and peroxidase activity.

The essential point in the activation cascade of Figure 3-15 is that CT-induced Met80 oxidation only results in a moderate level of peroxidase activity, because the distal site remains congested by Lys ligation. Subsequent CT-induced LysCHO formation frees up the distal site, thereby producing a genuine pentacoordinated heme. Previous work attributed the peroxidase activity of CT-cyt *c* exclusively to MetO formation,<sup>17-18,37-38,44-47</sup>

failing to recognize the occurrence and mechanistic significance of Lys carbonylation. Our data reveal that MetO formation only represents an initial step en route toward peroxidase-activated CT-cyt *c*. Lys carbonylation represents a co-activator that boosts the activity by a factor of ~4 (fractions III/IV) relative to the MetO-only form (fraction I, see Figure 3-3).

The model of Figure 3-15 provides a simple explanation for the correlation between the activity of the CT-cyt *c* fractions and their SCX behavior: both factors are directly tied to the number of LysCHO sites. When accounting for the SCX fractionation behavior, one has to remember that while the protein interacts with the anionic stationary phase, it may adopt structures and ligation scenarios that differ from the bulk solution conformations of Figure 3-15.<sup>78</sup>

The ability of cyt *c* to adopt various distal ligation scenarios is consistent with the foldon model that dissects the protein into regions of different stability (Figure 3-16).<sup>52</sup> The gray and red foldons (40-57 and 71-85  $\Omega$  loops, respectively) show the highest flexibility.<sup>52</sup> Not surprisingly, the alternative Fe ligands identified above are located in these two flexible regions, i.e. Lys72/73 (red) and Lys53/55 (gray). Opening of gray<sup>79</sup> and red<sup>53</sup> has previously been linked to alkaline conformers. The flexibility of gray and red also governs the CT-induced transitions outlined in Figure 3-15. In native cyt *c* the red foldon is anchored by the Met80-Fe linkage.<sup>52-53,79</sup> Our data suggest that MetO formation sterically perturbs this (already labile)<sup>52</sup> region, thereby triggering rearrangements that allow Lys72/73 to move into the distal site.<sup>53</sup> The foldon hierarchy dictates that red can only open up when gray is already unfolded.<sup>52-53,79</sup> Hence, after carbonylation of Lys72/73, the plasticity of the unfolded gray foldon will allow Lys53/55 to move into the vacated distal site. Our MS data suggest that Lys60 could also participate in Fe ligation, but its placement in the relatively rigid yellow foldon renders such a scenario less likely (Figure 3-16).

Our data do not provide evidence for carbonylation of Lys79. In principle, this residue represents another possible ligand that might block access to the iron after Met80 oxidation.<sup>38</sup> However, evidence for such Lys79-Fe contacts comes primarily from work on K72A yeast *iso-1* cyt *c* which has coordination propensities that are different from those of

the horse wild type studied here.<sup>38</sup> Our findings suggest that Lys79-Fe contacts do not play a major role in Met80-oxidized horse cyt *c*, such that peroxidase activation is attainable without Lys79 carbonylation.

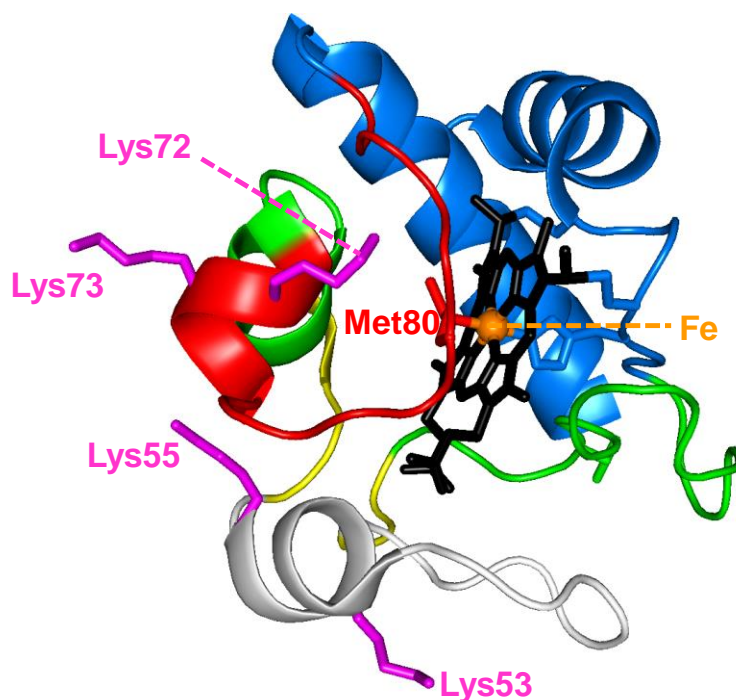


**Figure 3-16.** Foldon structure of cyt *c*. Colors indicate the propensity to undergo transient unfolding: gray (least stable) > red > yellow > green > blue (most stable). Also shown are Lys side chains (magenta) that can act as distal Fe ligands during CT-induced peroxidase activation. Lys72/73 are in the “red” foldon (second-least stable, 71-85  $\Omega$  loop). Lys53/55 are in the “gray” foldon (least stable, 40-57  $\Omega$  loop). On the basis of our MS results the participation of Lys60 (not shown) in heme ligation cannot be ruled out, but the positioning of Lys60 in the relatively rigid “yellow” foldon renders such a scenario less likely. N.B.: Various terms have been used for the gray foldon; these include “N”, “nested yellow”, “N-yellow”, “infrared”, and “black”.<sup>52,53,79</sup>

### 3.4. Conclusions

Our discovery of multiple, previously unreported carbonylation events in CT-cyt *c* calls into question the prevailing Met80-centric view of peroxidase activation, according to which oxidation of Met80 alone is sufficient for turning cyt *c* into a pentacoordinated peroxidase.<sup>17-18,37-38,44-45,47-48</sup> The conclusions from a number of those reports have relied on the alleged fidelity of CT for specific Met oxidation. Several studies pooled the highest intensity region in the SCX chromatogram, assuming that samples obtained in this way represent the expected “clean” MetO species.<sup>37-38,47-48</sup> Our data strongly suggest that such samples correspond to fractions II/III, with oxidation at Met80, Met65, *and* with LysCHO sites in the Lys72/73 and Lys53/55 range. Carbonylation of these samples enhances their peroxidase activity almost fourfold relative to fraction I, which represents the true MetO-only species (Figure 3-3, Figure 3-6). It appears that past studies inadvertently studied carbonylated CT-cyt *c* proteoforms, misattributing some of the carbonylation-induced effects to MetO formation.

Previous studies on CT-cyt *c* yielded conflicting results, according to whether the distal site is open,<sup>37</sup> or occupied by Lys.<sup>38</sup> The present work helps resolve these discrepancies. CT-cyt *c* comprises multiple species with different coordination patterns (Figure 3-15). Thus, any results will depend on the precise experimental conditions used for isolating protein from the CT-cyt *c* reaction mixture.

Only four out of the 19 Lys residues in cyt *c* were identified as possible carbonylation sites. In native cyt *c* these four residues are relatively close to the distal face of the heme, which represents the site of peroxidase catalysis (Figure 3-1). Considering that all 19 Lys residues are solvent-exposed (Figure 3-17), the spatial selectivity of LysCHO formation rules out diffusion-mediated oxidation events, where modifications are governed by solvent accessibility.<sup>55</sup> It instead appears that LysCHO formation is heme-dependent.<sup>43,58</sup> This line of thought bolsters our conclusions, as carbonylation of Lys53/55/72/73 confirms the capability of these residues to come in direct contact with the heme by serving as alternative Fe ligands (Figure 3-15).



There are certain parallels, but also differences between the CT-induced peroxidase activation of cyt *c* studied here, and the H<sub>2</sub>O<sub>2</sub>-induced activation that we explored earlier.<sup>41</sup> The initial transformation triggered by H<sub>2</sub>O<sub>2</sub> is oxidation of Tyr67, while this residue remains unmodified during CT exposure. Peroxidase activation by both CT and H<sub>2</sub>O<sub>2</sub> involves sequential modifications and transiently populated alkaline conformers, ultimately producing a vacant distal site. One key difference is that CT-induced activation relies on MetO formation for disruption of the Met80-Fe bond (Figure 3-15). In contrast, H<sub>2</sub>O<sub>2</sub> causes this bond to break as a result of Tyr67 oxidation, without Met80 oxidation. The reasons underlying the different initial reactivities of the two oxidants remain to be fully explored. Likely, H<sub>2</sub>O<sub>2</sub> oxidation of Tyr67 proceeds with catalysis by the iron center,<sup>43</sup> whereas CT can oxidize Met without heme involvement.<sup>51</sup> A common feature of CT and H<sub>2</sub>O<sub>2</sub>-induced activation is LysCHO formation which prevents the distal site from being blocked by Lys side chains. It is likely that LysCHO formation plays a similar role for the conversion of cyt *c* into an apoptotic peroxidase under other conditions, e.g. after cardiolipin binding<sup>3,27-29</sup> *in vitro* and *in vivo*. However, this hypothesis remains to be verified experimentally.

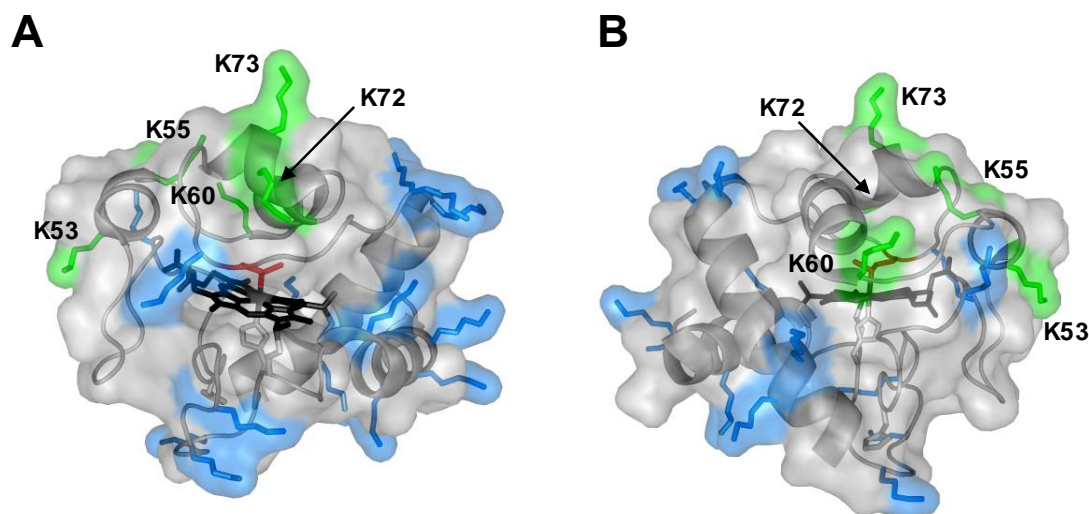


**Figure 3-17.** Crystal structure of native cyt *c* (PDB: 1HRC) depicting all 19 Lys residues. Sites of Lys carbonylation are shown in green and labeled. All other Lys are shown in blue. (A) Front view. (B) Back view.

### 3.5. References

- (1) Alvarez-Paggi, D.; Hannibal, L.; Castro, M. A.; Oviedo-Rouco, S.; Demicheli, V.; Tórtora, V.; Tomasina, F.; Radi, R.; Murgida, D. H., *Chem. Rev.* **2017**, *117* (21), 13382-13460.
- (2) Radi, R.; Thomson, L. M.; Rubbo, H.; Prodanov, E., *Arch. Biochem. Biophys.* **1991**, *288* (1), 112-117.
- (3) Kagan, V. E.; Bayır, H. A.; Belikova, N. A.; Kapralov, O.; Tyurina, Y. Y.; Tyurin, V. A.; Jiang, J.; Stoyanovsky, D. A.; Wipf, P.; Kochanek, P. M.; Greenberger, J. S.; Pitt, B.; Shvedova, A. A.; Borisenko, G. G., *Free Rad. Biol. Med.* **2009**, *46* (11), 1439-1453.
- (4) Godoy, L. C.; Muñoz-Pinedo, C.; Castro, L.; Cardaci, S.; Schonhoff, C. M.; King, M.; Tórtora, V.; Marín, M.; Miao, Q.; Jiang, J. F.; Kapralov, A. A.; Jemmerson, R.; Silkstone, G. G.; Patel, J. N.; Evans, J. E.; Wilson, M. I. T.; Green, D. R.; Kagan, V. E.; Radi, R.; Mannick, J. B., *Proc. Natl. Acad. Sci. U.S.A.* **2009**, *106* (8), 2653-2658.
- (5) Hannibal, L.; Tomasina, F.; Capdevila, D. A.; Demicheli, V.; Tórtora, V.; Alvarez-Paggi, D.; Jemmerson, R.; Murgida, D. H.; Radi, R., *Biochemistry* **2016**, *55* (3), 407-428.
- (6) Liptak, M. D.; Fagerlund, R. D.; Ledgerwood, E. C.; Wilbanks, S. M.; Bren, K. L., *J. Am. Chem. Soc.* **2011**, *133* (5), 1153-1155.
- (7) McClelland, L. J.; Mou, T.-C.; Jeakins-Cooley, M. E.; Sprang, S. R.; Bowler, B. E., *Proc. Natl. Acad. Sci. U.S.A.* **2014**, *111* (18), 6648-6653.
- (8) Jenkins, C. M.; Yang, K.; Liu, G.; Moon, S. H.; Dilthey, B. G.; Gross, R. W., *J. Biol. Chem.* **2018**, *293* (22), 8693-8709.
- (9) Veitch, N. C., *Phytochem.* **2004**, *65*, 249-259.
- (10) Kitt, J. P.; Bryce, D. A.; Minter, S. D.; Harris, J. M., *J. Am. Chem. Soc.* **2017**.
- (11) Oemer, G.; Lackner, K.; Muigg, K.; Krumschnabel, G.; Watschinger, K.; Sailer, S.; Lindner, H.; Gnaiger, E.; Wortmann, S. B.; Werner, E. R.; Zschocke, J.; Keller, M. A., *Proc. Natl. Acad. Sci. U.S.A.* **2018**, *115* (16), 4158-4163.
- (12) Belikova, N. A.; Vladimirov, Y. A.; Osipov, A. N.; Kapralov, A. A.; Tyurin, V. A.; Potapovich, M. V.; Basova, L. V.; Peterson, J.; Kurnikov, I. V.; Kagan, V. E., *Biochemistry* **2006**, *45* (15), 4998-5009.
- (13) Wong, R. S. Y., *J. Exp. Clin. Cancer Res.* **2011**, *30*.

- (14) Diederix, R. E. M.; Ubbink, M.; Canters, G. W., *Biochemistry* **2002**, *41*, 13067-13077.
- (15) Bushnell, G. W.; Louie, G. V.; Brayer, G. D., *J. Mol. Biol.* **1990**, *214*, 585-595.
- (16) Bren, K. L.; Raven, E. L., *Science* **2017**, *356* (6344), 1236-1236.
- (17) Chen, Y.-R.; Deterding, L. J.; Sturgeon, B. E.; Tomer, K. B.; Mason, R. P., *J. Biol. Chem.* **2002**, *277* (33), 29781-29791.
- (18) Wang, Z.; Ando, Y.; Nugraheni, A. D.; Ren, C.; Nagao, S.; Hirota, S., *Mol. Biosyst.* **2014**, *10* (12), 3130-3137.
- (19) Amacher, J. F.; Zhong, F. F.; Lisi, G. P.; Zhu, M. Q.; Alden, S. L.; Hoke, K. R.; Madden, D. R.; Pletneva, E. V., *J. Am. Chem. Soc.* **2015**, *137* (26), 8435-8449.
- (20) Abriata, L. A.; Cassina, A.; Tortora, V.; Marin, M.; Souza, J. M.; Castro, L.; Vila, A. J.; Radi, R., *J. Biol. Chem.* **2009**, *284* (1), 17-26.
- (21) Josephs, Tracy M.; Morison, Ian M.; Day, Catherine L.; Wilbanks, Sigurd M.; Ledgerwood, Elizabeth C., *Biochem. J.* **2014**, *458* (2), 259-265.
- (22) Karsisiotis, A. I.; Deacon, O. M.; Wilson, M. T.; Macdonald, C.; Blumenschein, T. M. A.; Moore, G. R.; Worrall, J. A. R., *Sci Rep* **2016**, *6*, 30447.
- (23) Moreno-Beltran, B.; Guerra-Castellano, A.; Diaz-Quintana, A.; Del Conte, R.; Garcia-Maurino, S. M.; Diaz-Moreno, S.; Gonzalez-Arzola, K.; Santos-Ocana, C.; Velazquez-Campoy, A.; De la Rosa, M. A.; Turano, P.; Diaz-Moreno, I., *Proc. Natl. Acad. Sci. U.S.A.* **2017**, *114* (15), E3041-E3050.
- (24) Tognaccini, L.; Ciaccio, C.; D'Oria, V.; Cervelli, M.; Howes, B. D.; Coletta, M.; Mariottini, P.; Smulevich, G.; Fiorucci, L., *J. Inorg. Biochem.* **2016**, *155*, 56-66.
- (25) Ciaccio, C.; Tognaccini, L.; Battista, T.; Cervelli, M.; Howes, B. D.; Santucci, R.; Coletta, M.; Mariottini, P.; Smulevich, G.; Fiorucci, L., *J. Inorg. Biochem.* **2017**, *169*, 86-96.
- (26) Wang, Z.-H.; Lin, Y.-W.; Rosell, F. I.; Ni, F.-Y.; Lu, H.-J.; Yang, P.-Y.; Tan, X.-S.; Li, X.-Y.; Huang, Z.-X.; Mauk, A. G., *ChemBioChem* **2007**, *8* (6), 607-609.
- (27) Abe, M.; Niibayashi, R.; Koubori, S.; Moriyama, I.; Miyoshi, H., *Biochemistry* **2011**, *50* (39), 8383-8391.
- (28) Serpas, L.; Milorey, B.; Pandiscia, L. A.; Addison, A. W.; Schweitzer-Stenner, R., *J. Phys. Chem. B* **2016**, *120*, 12219-12231.
- (29) Bradley, J. M.; Silkstone, G.; Wilson, M. T.; Cheesman, M. R.; Butt, J. N., *J. Am. Chem. Soc.* **2011**, *133* (49), 19676-19679.

- (30) Assfalg, M.; Bertini, I.; Dolfi, A.; Turano, P.; Mauk, A. G.; Rosell, F. I.; Gray, H. B., *J. Am. Chem. Soc.* **2003**, *125*, 2913-2922.
- (31) Nold, S. M.; Lei, H.; Mou, T.-C.; Bowler, B. E., *Biochemistry* **2017**, *56*, 3358–3368.
- (32) García-Heredia, J. M.; Díaz-Moreno, I.; Nieto, P. M.; Orzáez, M.; Kocanis, S.; Teixeira, M.; Pérez-Payá, E.; Díaz-Quintana, A.; De la Rosa, M. A., *Biochim. Biophys. Acta* **2010**, *1797* (6–7), 981-993.
- (33) Döpner, S.; Hildebrandt, P.; Rosell, F. I.; Mauk, A. G., *J. Am. Chem. Soc.* **1998**, *120*, 11246-11255.
- (34) Rosell, F. I.; Ferrer, J. C.; Mauk, A. G., *J. Am. Chem. Soc.* **1998**, *120* (44), 11234-11245.
- (35) Gu, J.; Shin, D.-W.; Pletneva, E. V., *Biochemistry* **2017**, *56*, 2950–2966.
- (36) Garcia-Heredia, J. M.; Diaz-Quintana, A.; Salzano, M.; Orzaez, M.; Perez-Paya, E.; Teixeira, M.; De la Rosa, M. A.; Diaz-Moreno, I., *J. Biol. Inorg. Chem.* **2011**, *16* (8), 1155-68.
- (37) Capdevila, D. A.; Marmisolle, W. A.; Tomasina, F.; Demicheli, V.; Portela, M.; Radi, R.; Murgida, D. H., *Chem. Sci.* **2015**, *6* (1), 705-713.
- (38) Zhong, F.; Pletneva, E. V., *Inorg. Chem.* **2018**, *57* (10), 5754-5766.
- (39) Capdevila, D. A.; Alvarez-Paggi, D.; Castro, M. A.; Tortora, V.; Demicheli, V.; Estrin, D. A.; Radi, R.; Murgida, D. H., *Chem. Commun.* **2014**, *50* (20), 2592-2594.
- (40) Deacon, O. M.; Svistunenko, D. A.; Moore, G. R.; Wilson, M. T.; Worrall, J. A. R., *Biochemistry* **2018**, *57* (29), 4276-4288.
- (41) Yin, V.; Shaw, G. S.; Konermann, L., *J. Am. Chem. Soc.* **2017**, *139*, 15701–15709.
- (42) Bachi, A.; Dalle-Donne, I.; Scaloni, A., *Chem. Rev.* **2013**, *113* (1), 596-698.
- (43) Møller, I. M.; Rogowska-Wrzesinska, A.; Rao, R. S. P., *J. Proteomics* **2011**, *74* (11), 2228-2242.
- (44) Lushington, G. H.; Cowley, A. B.; Silchenko, S.; Lukat-Rodgers, G. S.; Rodgers, K. R.; Benson, D. R., *Inorg. Chem.* **2003**, *42* (23), 7550-7559.
- (45) Birk, A. V.; Chao, W. M.; Liu, S. Y.; Soong, Y.; Szeto, H. H., *Biochim. Biophys. Acta* **2015**, *1847* (10), 1075-1084.
- (46) Nugraheni, A. D.; Ren, C. G.; Matsumoto, Y.; Nagao, S.; Yamanaka, M.; Hirota, S., *J. Inorg. Biochem.* **2018**, *182*, 200-207.

- (47) Parakra, R. D.; Kleffmann, G. N. L.; Jameson, T.; Ledgerwood, E. C., *Dalton Trans.* **2018**, 47, 9128-9135.
- (48) Pande, J.; Kinnally, K.; Thallum, K. K.; Verma, B. C.; Myer, Y. P.; Rechsteiner, L.; Bosshard, H. R., *J. Protein Chem.* **1987**, 6 (4), 295-319.
- (49) Mushran, S. P.; Agrawal, M. C.; Prasad, B., *J. Chem. Soc. B* **1971**, 0 (8), 1712-1714.
- (50) Michel, B.; Proudfoot, A. E. I.; Wallace, C. J. A.; Bosshard, H. R., *Biochemistry* **1989**, 28 (2), 456-462.
- (51) Shechter, Y.; Burstein, Y.; Patchornik, A., *Biochemistry* **1975**, 14 (20), 4497-4503.
- (52) Hu, W. B.; Kan, Z. Y.; Mayne, L.; Englander, S. W., *Proc. Natl. Acad. Sci. U.S.A.* **2016**, 113 (14), 3809-3814.
- (53) Maity, H.; Rumbley, J. N.; Englander, S. W., *Proteins* **2006**, 63 (2), 349-355.
- (54) Jones, L. M.; Sperry, J. B.; Carroll, J. A.; Gross, M. L., *Anal. Chem.* **2011**, 83, 7657-7661.
- (55) Xu, G.; Chance, M. R., *Chem. Rev.* **2007**, 107, 3514-3543.
- (56) Kathiresan, M.; English, A. M., *Chem. Sci.* **2017**, 8 (2), 1152-1162.
- (57) Sharp, J. S.; Becker, J. M.; Hettich, R. L., *Anal. Chem.* **2004**, 76, 672-683.
- (58) Bridgewater, J. D.; Lim, J.; Vachet, R. W., *Anal. Chem.* **2006**, 78, 2432-2438.
- (59) Baldwin, D. A.; Marques, H. M.; Pratt, J. M., *J. Inorg. Biochem.* **1987**, 30, 203-217.
- (60) Giorgio, M.; Trinei, M.; Migliaccio, E.; Pelicci, P. G., *Nat. Rev. Mol. Cell Biol.* **2007**, 8 (9), 722A-728.
- (61) Kelly, S. W.; Jess, T. J.; Price, N. C., *Biochim. Biophys. Acta* **2005**, 1751, 119-139.
- (62) Kaminsky, L. S.; Miller, V. J.; Davison, A. J., *Biochemistry* **1973**, 12, 2215-2221.
- (63) Chen, Y. R.; Chen, C. L.; Liu, X. P.; Li, H. T.; Zweier, J. L.; Mason, R. P., *Free Radic. Biol. Med.* **2004**, 37 (10), 1591-1603.
- (64) Requena, J. R.; Chao, C.-C.; Levine, R. L.; Stadtman, E. R., *Proc. Natl. Acad. Sci. U.S.A.* **2001**, 98 (1), 69-74.
- (65) Graf, M.; Garcia, R. G.; Watzig, H., *Electrophoresis* **2005**, 26 (12), 2409-2417.
- (66) Chung, W. G.; Miranda, C. L.; Maier, C. S., *Electrophoresis* **2008**, 29 (6), 1317-1324.

- (67) Temple, A.; Yen, T.-Y.; Gronert, S., *J. Am. Soc. Mass Spectrom.* **2006**, *17*, 1172-1180.
- (68) Artemenko, K.; Mi, J.; Bergquist, J., *Free Radical Res.* **2015**, *49* (5), 477-493.
- (69) Siuti, N.; Kelleher, N. L., *Nat. Methods* **2007**, *4*, 817-821.
- (70) Zinnel, N. F.; Pai, P.-J.; Russell, D. H., *Anal. Chem.* **2012**, *84* (7), 3390-3397.
- (71) Polasky, D. A.; Lermyte, F.; Nshanian, M.; Sobott, F.; Andrews, P. C.; Loo, J. A.; Ruotolo, B. T., *Anal. Chem.* **2018**, *90* (4), 2756-2764.
- (72) Halgand, F.; Habchi, J.; Cravello, L.; Martinho, M.; Guigliarelli, B.; Longhi, S., *Anal. Chem.* **2011**, *83*, 7306-7315.
- (73) Dongré, A. R.; Jones, J. L.; Somogyi, Á.; Wysocki, V. H., *J. Am. Chem. Soc.* **1996**, *118*, 8365-8374.
- (74) Paizs, B.; Suhai, S., *Mass Spectrom. Rev.* **2005**, *24*, 508-548.
- (75) Greer, S. M.; Holden, D. D.; Fellers, R.; Kelleher, N. L.; Brodbelt, J. S., *J. Am. Soc. Mass Spectrom.* **2017**, *28*, 1587-1599.
- (76) Tomášková, N.; Varhač, R.; Lysáková, V.; Musatov, A.; Sedlák, E., *Biochim. Biophys. Acta* **2018**, *1866*, 1073-1083.
- (77) Deng, Y.; Zhong, F.; Alden, S. L.; Hoke, K. R.; Pletneva, E. V., *Biochemistry* **2018**, *57*, 5827-5840.
- (78) Guo, J.; Carta, G., *J. Chromatogr. A* **2015**, *1388*, 184-194.
- (79) Krishna, M. M. G.; Lin, Y.; Rumbley, J. N.; Englander, S. W., *J. Mol. Biol.* **2003**, *331*, 29-36.

## Chapter 4. Delineating Heme-Mediated versus Direct Protein Oxidation Pathways in Peroxidase-Activated Cytochrome *c*

### 4.1. Introduction

Covalent protein modifications by reactive oxygen species (ROS) impact numerous biological functions.<sup>1-6</sup> The presence of ROS is an unavoidable consequence of aerobic cellular respiration.<sup>7</sup> Protein oxidative modifications have been implicated in numerous aging and neurodegenerative pathologies.<sup>6,8-10</sup> Protein oxidation is also involved in sensing and signaling,<sup>11-13</sup> and it plays a major role for the efficacy and storage stability of protein therapeutics.<sup>14-16</sup> Most protein oxidation events culminate in oxygen incorporation into side chains, e.g. Met → MetO (sulfoxide, +16 Da), Tyr → Tyr-OH (+16 Da), Lys-CH<sub>2</sub>-NH<sub>2</sub> → Lys-CHO (carbonylation, -1 Da). Numerous additional oxidation pathways exist, and many residues can form various products (e.g., -2, +4, +16, +32, or +48 Da for Trp).<sup>17-21</sup> In addition to oxidative modifications that occur within living cells, ROS can induce protein oxidation *in vitro*. Experimental strategies have been developed that use this approach for monitoring the solvent accessibility of individual side chains.<sup>20-26</sup> *In vitro* oxidative modifications also provide the opportunity to investigate oxidation-induced changes in protein structure, dynamics, and function.<sup>5,13,25,27-30</sup>

Regardless of context (i.e. in living cells or in the test tube), many aspects of protein oxidation are complex and incompletely understood. For example, side chain oxidation by ·OH can be a relatively simple process that starts with addition to a double bond or hydrogen abstraction, followed by quenching of the protein radical by an oxygen-containing species.<sup>22</sup> However, ·OH can also act via mechanisms that are more convoluted, by producing secondary oxidants which then attack the protein.<sup>3,5,31-32</sup>

Some protein oxidation events are catalyzed by transition metals.<sup>18,33</sup> Fenton-like reactions take place in the presence of peroxides, such as  $\text{Fe(II)} + \text{H}_2\text{O}_2 \rightarrow \text{Fe(III)} + \cdot\text{OH} + \text{OH}^-$ . Subsequent metal reduction regenerates Fe(II) such that the process can continue, generating a steady supply of  $\cdot\text{OH}$  that attack the protein.<sup>20,22,33</sup> The peroxidase activity of some heme proteins represents another indirect metal-catalyzed process.<sup>34-36</sup> In this case  $\text{H}_2\text{O}_2$  reacts with Fe(III) heme to form “Compound I”, a Fe(IV)=O species with an adjacent radical. Hydrogen abstraction from R-H sites then regenerates Fe(III).<sup>37</sup> The R $\cdot$  produced in this way undergo additional transformations which yield the final oxidation products. The aforementioned R-H can either be exogenous substrates or side chains in the vicinity of the heme; the latter scenario results in protein self-oxidation.<sup>5,38-41</sup>

Many protein oxidation studies have focused on  $\text{H}_2\text{O}_2$  and  $\cdot\text{OH}$ ,<sup>20,22</sup> while other common oxidants have received less attention.<sup>2,42-44</sup> Particular knowledge gaps persist for the widely used “mild” oxidant chloramine-T (CT, Figure 4-1).<sup>29-30,43-48</sup> In aqueous solution CT transforms into other reactive species that include  $\text{OCl}^-$ .<sup>44,46</sup> The latter can cause side chain oxidation (e.g.,  $\text{Met} + \text{OCl}^- \rightarrow \text{MetO} + \text{Cl}^-$ ), but alternative CT-induced protein oxidation pathways appear to exist.<sup>46</sup> The exact nature of these pathways remains to be explored.

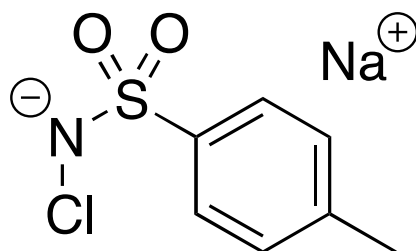


**Figure 4-1.** Structure of the oxidant chloramine-T (N-chloro-4-toluenesulfonamide), referred to as “CT” in this work.



Oxidative modifications of cytochrome *c* (cyt *c*, Figure 4-2) have attracted major attention over the past few years.<sup>25,29-30,41,44,47,49-53</sup> Cyt *c* acts as an electron transporter in the respiratory chain by cycling between its Fe(II)/(III) heme oxidation states.<sup>54</sup> In addition, cyt *c* can act as a peroxidase that catalyzes the oxidation of cardiolipin in mitochondria, a key step during apoptosis.<sup>53,55-58</sup> Interestingly, the peroxidase activity of native cyt *c* is very low because the heme iron is fenced in by a 6-coordinate environment, being ligated by four pyrrole nitrogens, His18, and Met80. To become an active peroxidase cyt *c* must undergo a structural transition that severs the Fe-Met80 bond and generates 5-coordinate heme with an open distal site. This 5-coordinate form is catalytically active because it allows for Fe-peroxide interactions with subsequent formation of reactive Fe(IV)=O species.<sup>34,36,59</sup> This peroxidase activation can be achieved by oxidative modifications of cyt *c*.<sup>27,29,44,47,52</sup> The most common *in vitro* activation method is cyt *c* exposure to CT. The “CT-holo-cyt *c*” generated in this way represents an important model system for apoptosis research.<sup>29-30,44,47</sup>

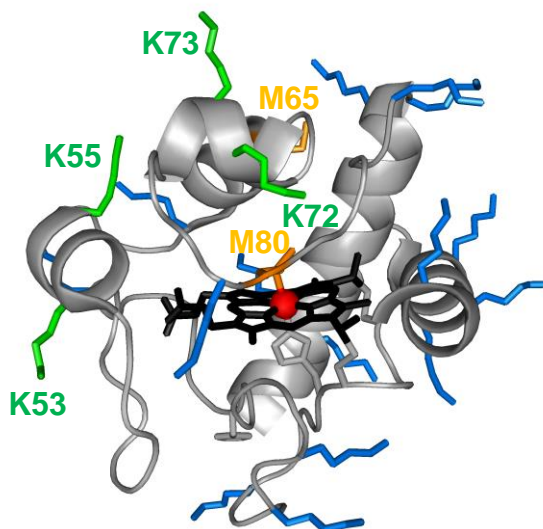


**Figure 4-2.** Crystal structure of equine holo-cyt *c* (PDB 1HRC).<sup>60</sup> Met residues are depicted in orange. Sites of LysCHO formation are depicted in green. All remaining Lys are depicted in blue. The heme cofactor is depicted in black, and the heme iron is shown in red.

We recently conducted a detailed mass spectrometry (MS)-based characterization of CT-holo-cyt *c*, and we found it to be a mixture of structurally and functionally diverse proteoforms.<sup>27</sup> In addition to MetO modifications at residues 80 and 65,<sup>29,44,47,52</sup> CT-holo-cyt *c* carries up to three carbonylated Lys. Both Met80 oxidation and Lys carbonylation are essential for peroxidase activation. The former ruptures the Fe-Met80 bond and generates the vacant coordination site required for catalysis, while the latter ensures that this site remains vacant by preventing Fe-Lys coordination.<sup>27</sup> The presence of LysCHO in CT-holo-cyt *c* and in other oxidation-activated forms of the protein had long been overlooked<sup>27-28</sup> but is now well accepted.<sup>25,41</sup> A key finding of our previous work<sup>27</sup> was that despite cyt *c* possessing 19 Lys that are equally solvent-accessible,<sup>60</sup> only a small Lys cluster (53/55/72/73) was susceptible to LysCHO formation (Figure 4-2). The factors responsible for this unexpected specificity remain unexplored.

Here we tackle the mechanism by which CT induces oxidative modifications in cyt *c*. Specifically, we investigated whether these transformations are mediated by the heme cofactor, keeping in mind the role of transition metal centers during the oxidation of other proteins.<sup>20,22,33</sup> The strategy of our experiments is simple - we compared the effects of CT on holo-cyt *c* and apo-cyt *c* (the heme-free variant of the protein). Our work applied various MS tools. A particularly powerful approach is the fragmentation of intact proteins by top-down MS/MS via collision-induced dissociation (CID), followed by ion mobility (IM) separation and mass analysis of fragment ions. This top-down CID-IM-MS method<sup>61-63</sup> is superior to traditional bottom-up MS in cases where protein modifications such as LysCHO interfere with tryptic digestion, peptide ionization and fragmentation.<sup>27</sup> Our experiments uncovered that Met → MetO conversion in cyt *c* can proceed in a heme-independent fashion. In contrast, LysCHO formation requires heme catalysis, a finding that explains the spatial selectivity of Lys carbonylation.

## 4.2. Methods

### 4.2.1. Materials.

Equine cyt *c*, CT, dithiothreitol (DTT), Girard's reagent T (GRT, (carboxymethyl)trimethylammonium chloride hydrazide), Tris base (2-amino-2-(hydroxymethyl)-1,3-propanediol), guanidinium chloride, and AgCl were supplied by MilliporeSigma (St. Louis, MO). Acetonitrile and ammonium acetate were supplied by Fisher (Nepean, ON). Potassium phosphate was from Caledon (Georgetown, ON). MS-grade modified trypsin was obtained from Promega (Madison, WI). Centrifuge filters (Amicon Ultra 0.5, 10 kDa MWCO) were supplied by Millipore Sigma, and used following manufacturer instructions (15 min at 13,000 G; buffer exchange steps were performed using four cycles). Unless stated otherwise, reactions were performed at  $22 \pm 2$  °C, and solutions contained 50 mM potassium phosphate (pH 7.4).

### 4.2.2. Mass Spectrometry.

MS experiments were conducted on a Waters SYNAPT G2-Si Q-TOF in positive ion mode. MS/MS experiments were performed using CID with Ar as collision gas. Samples were prepared as 5  $\mu$ M protein solutions in 50/50/0.1% H<sub>2</sub>O/acetonitrile/formic acid that were infused directly into the electrospray ionization (ESI) source of instrument at 5  $\mu$ L min<sup>-1</sup>. Top-down CID-IM-MS was performed as described<sup>27</sup> using N<sub>2</sub> as drift gas with trap collision energies between 22 and 25 V. The 16+ charge state served as precursor ion for top-down fragmentation. Bottom-up samples were digested overnight at 37 °C using a 50:1 protein:trypsin ratio. Tryptic peptides were separated on a Waters ACQUITY UPLC BEH C18 column (1.7  $\mu$ m, 2.1  $\times$  10 mm) with a H<sub>2</sub>O/acetonitrile gradient in the presence of 0.1% formic acid. MS/MS data were collected using data-dependent acquisition. Isotope distributions were modeled using Protein Prospector (<http://prospector.ucsf.edu>).

### 4.2.3. Heme Removal: Preparation of apo<sup>ss</sup>-cyt *c*.

Heme in cyt *c* is covalently bound by thioether linkages to Cys14 and Cys17.<sup>60</sup> Heme removal was performed as described<sup>64</sup> with some modifications. Cys-S-heme bonds were initially replaced with Cys-S-Ag bonds. For this purpose, 200  $\mu$ L glacial acetic acid

were added to 1.8 mL of an aqueous solution of 400  $\mu\text{M}$  cyt *c* and 25 mM AgCl, followed by incubation at 40 °C in the dark for 4 h and centrifugation at 13,000 G for 5 minutes. The supernatant was buffer exchanged into 100 mM acetic acid, yielding apo-cyt *c* carrying up to three silver ions (Ag-apo-cyt *c*, Figure 4-3B). For Ag removal, 100  $\mu\text{L}$  Ag-apo-cyt *c* was added to 900  $\mu\text{L}$  of 50 mM pH 5 ammonium acetate containing 6 M guanidinium chloride and 1 M DTT, followed by incubation for 3 h. Samples were then buffer exchanged into 50 mM pH 5 ammonium acetate, yielding apo-cyt *c* ( $\epsilon_{280} = 10.9 \text{ mM}^{-1} \text{ cm}^{-1}$ )<sup>65</sup> with both Cys14 and Cys17 in the thiol form. The absence of heme was confirmed by MS (Figure 4-3C) and UV-Vis (Figure 4-4). The apo-cyt *c* generated in this way underwent a mass shift of -2 Da during storage (Figure 4-5A) that was reversible upon addition of DTT (Figure 4-6). This behavior indicates -SS- bond formation between Cys14 and Cys17. To obtain homogeneous stable heme-free samples we deliberately promoted formation of this -SS- bond by storing 10  $\mu\text{M}$  apo-cyt *c* for 24 h at 22 °C, followed by overnight incubation at 4 °C. The disulfide-containing protein generated in this way is referred to aposs-cyt *c*. Top-down CID-IM-MS confirmed the presence of a disulfide between Cys14 and Cys17 in aposs-cyt *c*, while simultaneously verifying the absence of other covalent modifications (Figure 4-5B, C).

#### 4.2.4. CT-induced Oxidation and GRT Labeling.

50  $\mu\text{M}$  aposs-cyt *c* or holo-cyt *c* were incubated in 2.5 mM CT/50 mM pH 8.4 Tris buffer for 3 h.<sup>66-67</sup> The reaction was halted by buffer exchange into 50 mM pH 5 ammonium acetate, yielding CT-aposs-cyt *c* and CT-holo cyt *c*. We also prepared aposs-cyt *c* samples that were less oxidized by using 0.5 mM instead of 2.5 mM CT (CT<sub>low</sub>-aposs-cyt *c*). Oxidation experiments in the presence of microperoxidase 11 (MP11) were performed using the same procedures, except that 50  $\mu\text{M}$  MP11 was added to the CT/protein reaction mixture. Covalent tagging of reactive carbonyl groups was performed using GRT<sup>15</sup> by incubating 10  $\mu\text{M}$  protein (CT-treated or unoxidized controls) with 80 mM GRT in 50 mM pH 5 ammonium acetate for 3 h. Excess GRT was removed by buffer exchange into 50 mM pH 5 ammonium acetate.

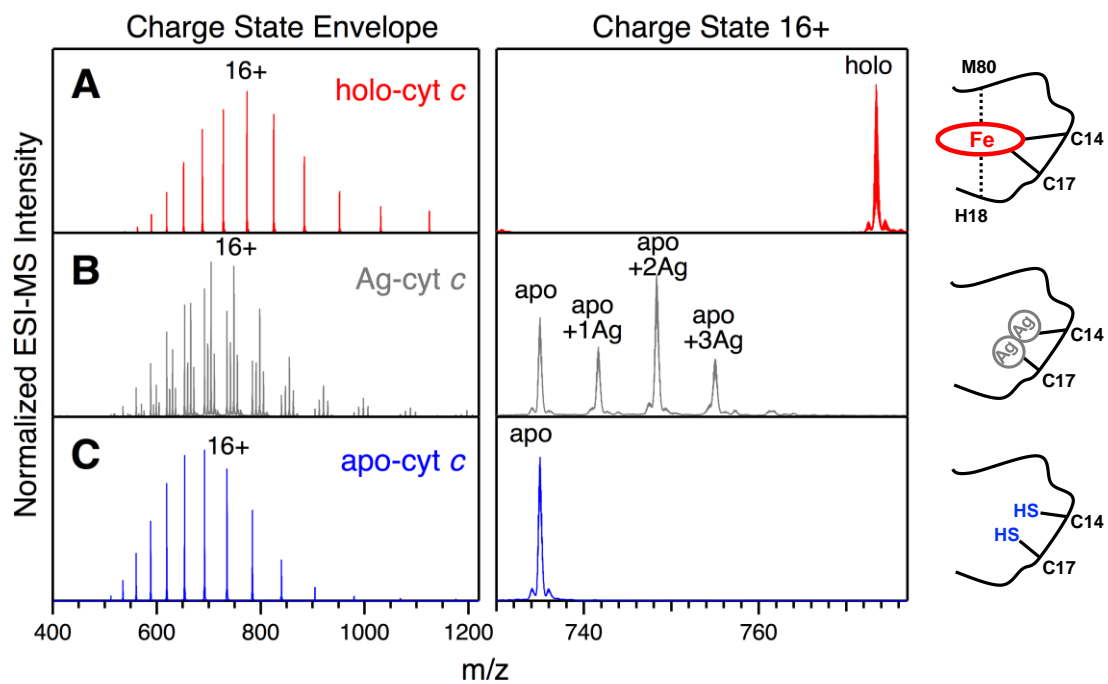


**Figure 4-3.** Left: Intact protein ESI mass spectra of different cytochrome *c* forms. (A) Holo-cytochrome *c* (unmodified control), (B) Ag-cytochrome *c*, (C) apo-cytochrome *c*. Far right: Cartoon representation of each form.

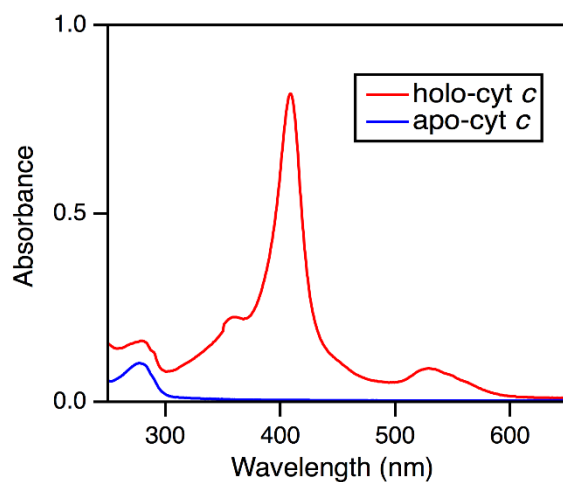


**Figure 4-4.** UV/Vis absorption spectra of cytochrome *c* before and after heme removal: holo-cytochrome *c* (red), apo-cytochrome *c* (blue).

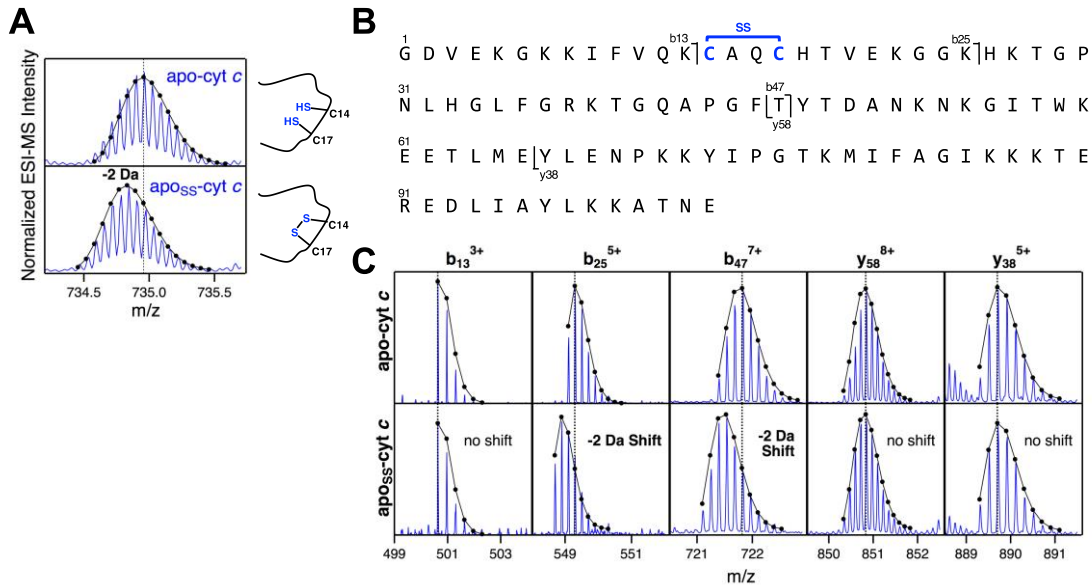


**Figure 4-5.** (A) Mass spectra of apo-cyt *c* highlighting a disulfide-induced mass shift after storage. (B) Aposs-cyt *c* sequence; selected top-down fragmentation sites are indicated. (C) Representative top-down CID-IM-MS fragment ions from apo-cyt *c* (top) and aposs-cyt *c* (bottom). All spectra are overlaid with their modeled isotope distributions (black dots and lines).

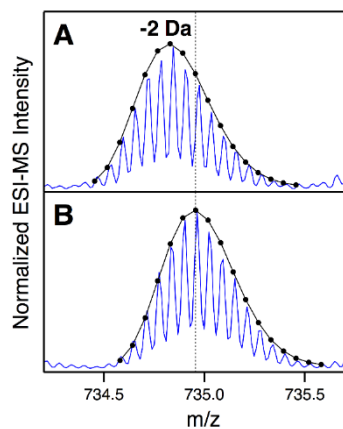


**Figure 4-6.** Mass spectrum (charge state 16+) of aposs-cyt *c* (A) before DTT treatment and (B) following DTT treatment. The vertical dashed line is included as a visual aid. Following DTT treatment, the -2 Da mass shift is lost, and the original (free -SH) mass is recovered.

### 4.3. Results and Discussion

For probing the role of heme during CT-induced cyt *c* oxidation we compared the behavior of the native protein and its heme-free counterpart. To assist readers, we briefly recapitulate the sample types that were used here, and that were prepared as described above: (i) Holo-cyt *c* is the native protein, possessing a covalently attached heme. (ii) Aposs-cyt *c* is devoid of heme, and its Cys14 and Cys17 side chains are linked by a -SS- bond (Figure 4-5). (iii) CT-holo-cyt *c* refers to holo-cyt *c* after oxidation by CT, comprising various proteoforms with MetO formation at residues 80 and 65, and one or more LysCHO in the Lys53/55/72/73 range.<sup>27</sup> (iv) CT-aposs-cyt *c* refers to aposs-cyt *c* after oxidation by CT, under conditions identical to those used for CT-holo-cyt *c*. (v) CT<sub>low</sub>-aposs-cyt *c* was exposed to a five-fold lower CT concentration than CT-aposs-cyt *c*. Oxidative modifications in CT-aposs-cyt *c* and CT<sub>low</sub>-aposs-cyt *c* have not been characterized previously.

#### 4.3.1. Effects of CT-Induced Oxidation.

Intact protein mass spectra of the aforementioned protein species are depicted in Figure 4-7. CT-holo-cyt *c* and CT-aposs-cyt *c* both showed oxidative modifications, with ~16 Da peak progressions that represent the hallmark of +*n*O incorporation. Similar patterns have previously been reported for many other oxidized proteins.<sup>5,20,22</sup> The spectrum of CT-holo-cyt *c* had its maximum at +2 O (Figure 4-7B), while that of CT-aposs-cyt *c* was dominated by signals around +4 O (Figure 4-7E). This observation reveals that heme removal renders cyt *c* more susceptible to oxidation by CT. Comparable oxidation levels to holo-cyt *c* could be achieved only when incubating aposs-cyt *c* samples in five-fold less CT (Figure 4-7D).

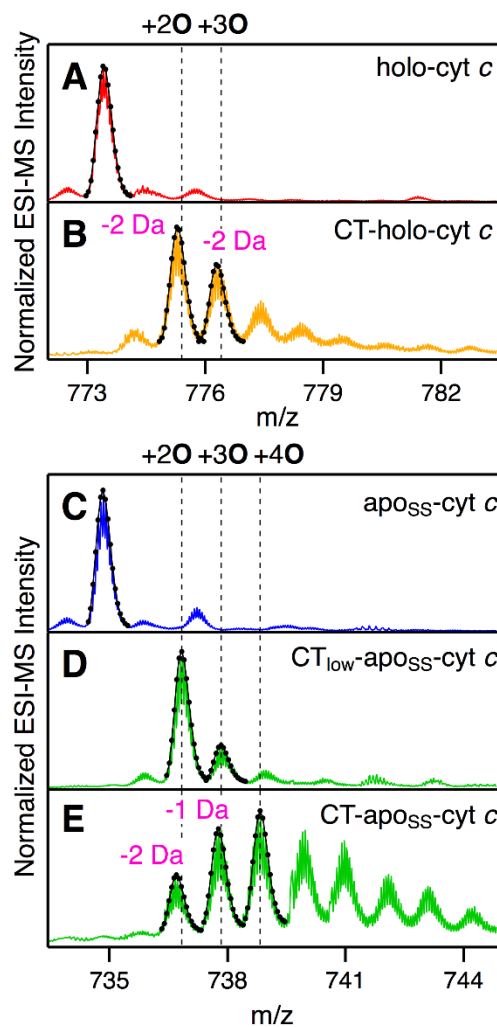


**Figure 4-7.** Intact protein mass spectra (charge state 16+) depicting the effects of cytochrome *c* oxidation by CT. (A) holo-cyt *c* (untreated control). (B) CT-holo-cyt *c*. (C) apo<sub>SS</sub>-cyt *c*. (D) CT<sub>low</sub>-apo<sub>SS</sub>-cyt *c*. (E) CT-apo<sub>SS</sub>-cyt *c*. Black solid lines and dots are modeled isotope envelopes. Vertical dashed lines mark the positions expected for “clean” +*n*O modifications; experimentally observed deviations from these “clean” positions are indicated in pink.



Close inspection of Figure 4-7 reveals deviations from “clean” +*n*O behavior. In CT-holo-cyt *c*, the signals were shifted by -2 Da due to LysCHO formation (Figure 4-7B).<sup>27</sup> CT-apo<sub>SS</sub>-cyt *c* showed a similar negative shift (Figure 4-7E). This -2 Da shift was absent for CT<sub>low</sub>-apo<sub>SS</sub>-cyt *c* (Figure 4-7D). While the -2 Da shift in Figure 4-7E seems to suggest the presence of LysCHO in CT-apo<sub>SS</sub>-cyt *c*, the data discussed below reveal that it has a different origin.

It may seem counterintuitive that heme removal enhances the oxidation susceptibility of cyt *c*, considering the capability of metal centers to catalyze oxidation.<sup>20,22,33-36</sup> However, metal catalysis is not the only factor that is relevant in this context. CD spectroscopy revealed that heme removal causes cyt *c* unfolding (Figure 4-8), confirming earlier reports that the protein structural integrity is contingent on heme.<sup>64</sup> The enhanced oxidation susceptibility of apo<sub>SS</sub>-cyt *c* is attributable to the fact that unfolding renders previously buried side chains sterically accessible to CT. This interpretation is in line with studies on other proteins where unfolding was found to enhance modifications by water-soluble labeling agents.<sup>20,22,68-69</sup>

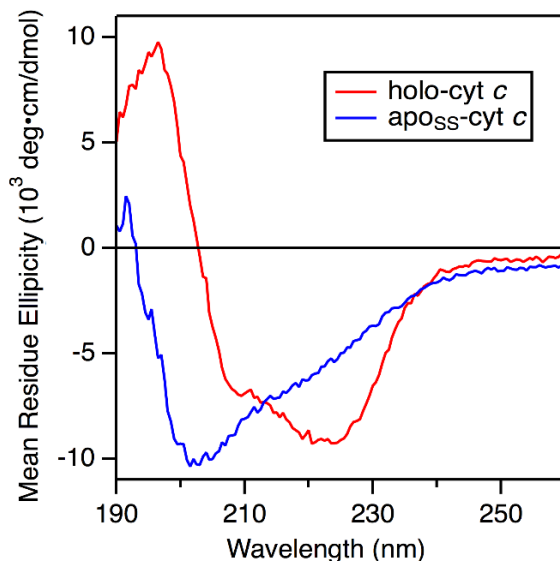


**Figure 4-8.** Far-UV CD spectra of holo-cyt *c* (red) and apo<sub>SS</sub>-cyt *c* (blue). The minimum close to 200 nm for apo<sub>SS</sub>-cyt *c* reveals that heme removal causes the protein to adopt an extensively unfolded conformation.

### 4.3.2. Oxidation Site Mapping.

We performed top-down CID-IM-MS to identify the modifications in CT-aposs-cyt *c* and CT<sub>low</sub>-aposs-cyt *c* (Figure 4-9). Data for CT-holo-cyt *c* were included for comparison (Figure 4-10), although an in-depth analysis of this species has already been reported.<sup>27</sup> All top-down experiments were performed by fragmenting [M + “2 O”] ions. The quotation marks indicate the presence of additional -2 Da modifications in CT-holo-cyt *c* and CT-aposs-cyt *c* that cause deviations from “clean” +2 O (+32 Da) Da mass shifts. Fragment spectra of all three CT-oxidized forms shared a y<sub>24</sub> to [y<sub>25</sub> + O] transition, as well as a [y<sub>39</sub> + O] to [y<sub>40</sub> + 2 O] transition (Figure 4-9 and Figure 4-10). This pattern confirms MetO formation at both Met80 and Met65 for all three species (CT-holo-, CT-aposs-, and CT<sub>low</sub>-aposs-cyt *c*). These observations demonstrate that CT-induced MetO formation can take place without heme catalysis. This conclusion is in line with the fact that Met is one of the most easily oxidizable residues,<sup>20</sup> that is known to be capable of forming MetO without metal catalysis.<sup>45,70-71</sup>

A more intriguing question is the nature of the -2 Da shift in CT-aposs-cyt *c* (Figure 4-7E). As noted, -2 Da shifts in CT-holo-cyt *c* are caused by LysCHO formation in the range of Lys53/55/72/73.<sup>27</sup> Does CT-aposs-cyt *c* contain these modifications as well? The top-down data of Figure 4-9 localize the -2 Da modification in CT-aposs-cyt *c* between residues 49 and 64, ruling out modifications at Lys72/73. The 49-64 range comprises Lys53/55/60 such that LysCHO formation could, in principle, be a possible explanation of the observed -2 Da shift. However, subsequent experiments demonstrate that CT-aposs-cyt *c* is free of LysCHO.

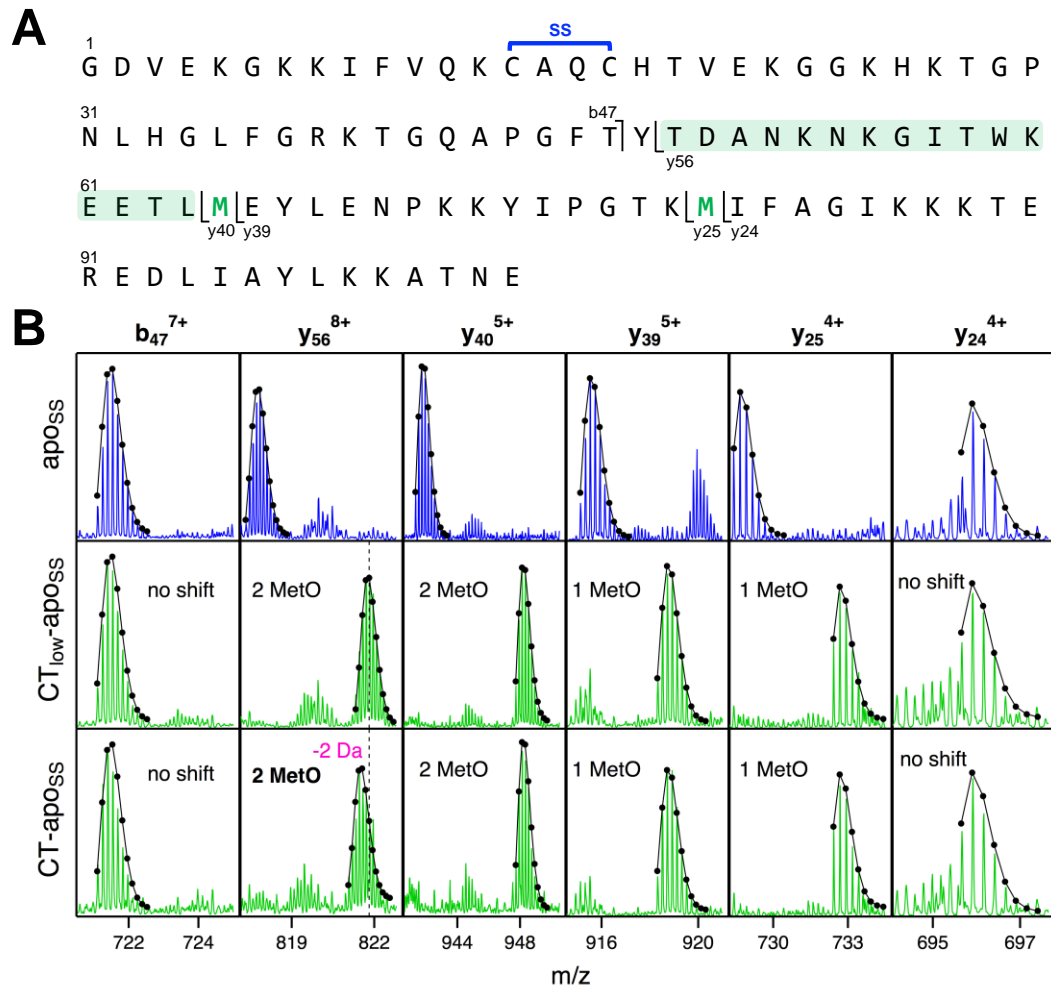


**Figure 4-9.** Top-down CID-IM-MS analysis of CT-apo<sub>SS</sub>-cyt *c*. (A) protein sequence with selected fragmentation sites. The remaining three panels show partial fragment spectra. The two modified Met residues are highlighted in color, along with the sequence range that harbors an additional -2 Da modification. (B) Top: apo<sub>SS</sub>-cyt *c* (untreated control). Center: CT<sub>low</sub>-apo<sub>SS</sub>-cyt *c*. Bottom: CT-apo<sub>SS</sub>-cyt *c*. Each spectrum is overlaid with its theoretical isotopic envelope.

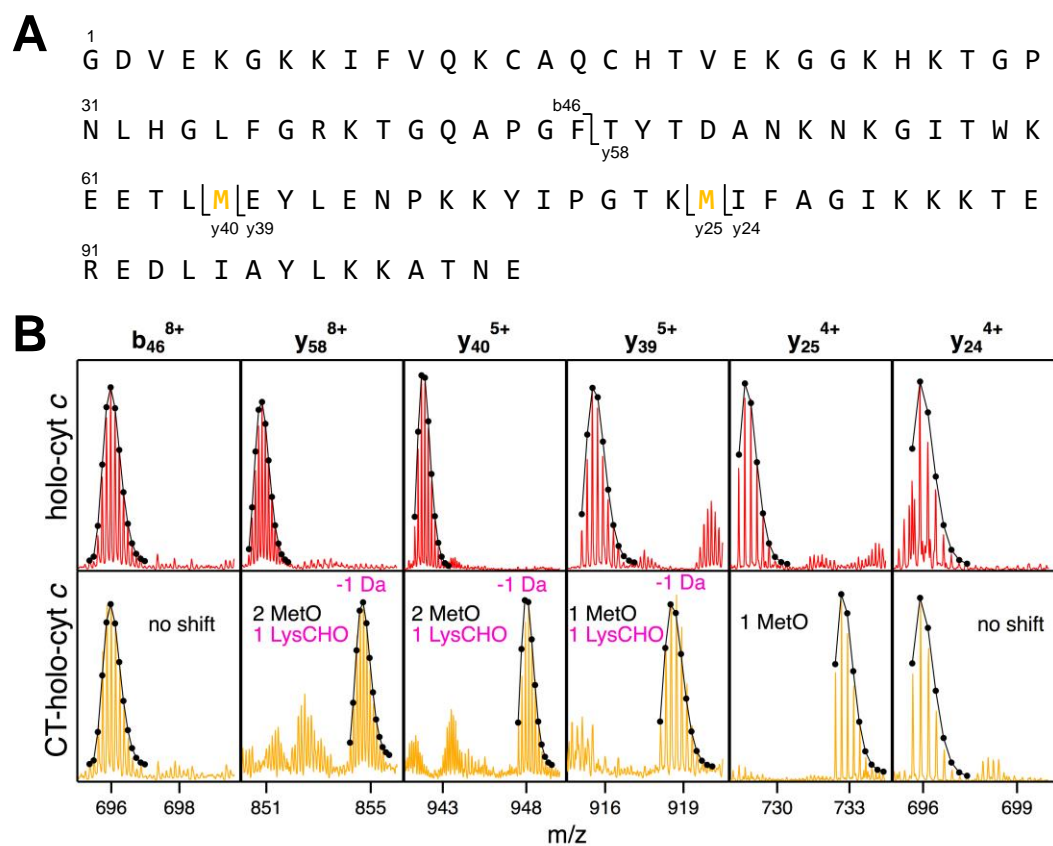


**Figure 4-10.** Top-down CID-IM-MS analysis of CT-holo-cyt *c*. (A) protein sequence with selected fragmentation sites. The two modified Met residues (MetO sites) are highlighted in color. (B) Representative top-down CID-IM-MS fragment ions. Top: holo-cyt *c* (untreated control). Bottom: CT-holo-cyt *c*. Each spectrum is overlaid with its corresponding theoretical isotopic envelope (solid circles and black lines).

### 4.3.3. Confirming LysCHO Sites by GRT Labeling.

GRT is a hydrazide compound that selectively reacts with ketones and aldehydes (such as LysCHO). Other modified side chains that might potentially be present (such as Tyr dimers, -2 Da)<sup>5</sup> do not react with GRT.<sup>15,72-73</sup> GRT labeling of CT-holo-cyt *c* produced satellite peaks corresponding to +1 GRT and +2 GRT, confirming the presence of two LysCHO sites that are responsible for the -2 Da mass shift of CT-holo-cyt *c* (Figure 4-11B).<sup>27</sup> Top-down CID-IM-MS of the most intense GRT adduct confirmed GRT labeling at Lys72/73 (Figure 4-12), in agreement with earlier work.<sup>27</sup>

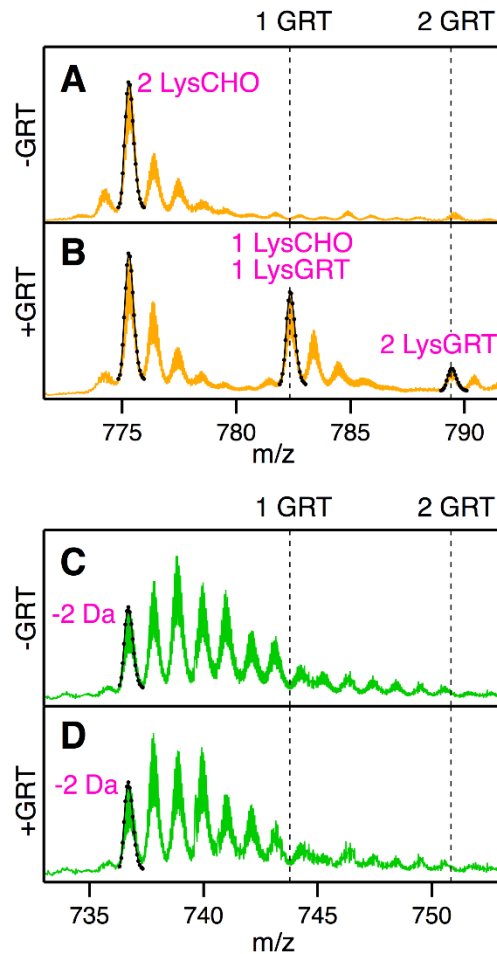


**Figure 4-11.** Intact protein mass spectra (charge state 16+) depicting the effects of GRT labeling. (A) CT-holo-cyt *c* prior to GRT labeling. (B) CT-holo-cyt *c* after GRT labeling. (C) CT-apo-cyt *c* prior to GRT labeling (D) CT-apo-cyt *c* after GRT labeling. Dashed vertical lines mark expected position of GRT-modified species. The first peak of each distribution is overlaid with its theoretical isotopic envelope.

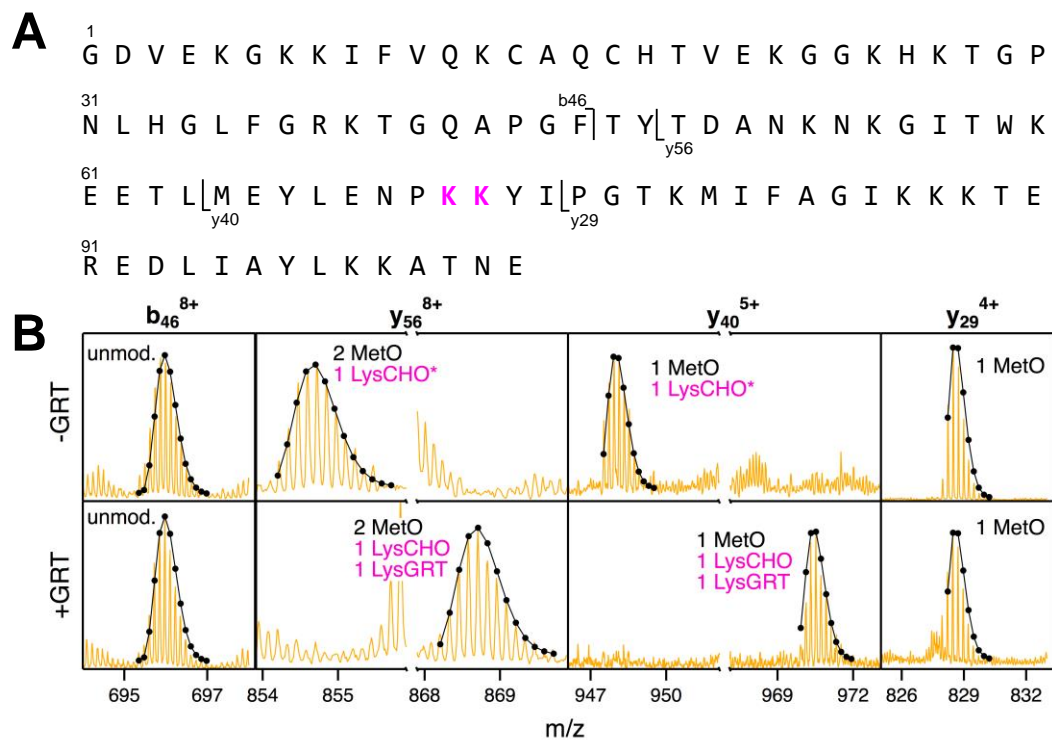


**Figure 4-12.** Top-down CID-IM-MS analysis of GRT-labeled CT-holo-cyt *c*. (A) protein sequence with selected fragmentation sites. The two modified Lys residues are highlighted in colour. (B) Representative top-down CID-IM-MS fragment ions. Top: CT-holo-cyt *c* (no GRT control). Bottom: GRT-labeled CT-holo-cyt *c*, using the [M + 2 O + 1 LysCHO + 1 GRT] peak as precursor. Each spectrum is overlaid with its corresponding theoretical isotopic envelope (solid circles and black lines).

Given the much higher overall oxidation propensity of CT-aposs-cyt *c* relative to CT-holo-cyt *c* (Figure 4-7), one might expect correspondingly more LysCHO sites (and thus more extensive GRT labeling). Surprisingly, CT-aposs-cyt *c* was completely unreactive with GRT (Figure 4-11D). The same was observed for CT<sub>low</sub>-aposs-cyt *c* (Figure 4-13). This lack of GRT reactivity reveals that CT is incapable of forming LysCHO in aposs-cyt *c*. It can be concluded that LysCHO is not a general byproduct of CT-induced oxidation. Instead, Figure 4-11 strongly suggests that CT can induce LysCHO formation in cyt *c* only in the presence of heme.

As LysCHO is absent in CT-aposs-cyt *c*, the -2 Da shift in this protein form must arise from another modification. As noted earlier, top-down CID-IM-MS localized the -2 Da shift to <sup>49</sup>TDANKNKGITWKEETL<sup>64</sup> (Figure 4-9). Scenarios such as ThrCH-OH → ThrC=O (-2 Da) can be excluded by the lack of GRT labeling in CT-aposs-cyt *c*.<sup>20-21</sup> Trp is the residue with the highest intrinsic oxidation propensity in the 49-64 range.<sup>20</sup> Studies on other proteins showed that Trp yields various oxidation products, including -2 Da species.<sup>74</sup> Using bottom-up MS/MS we were able to detect low-level Trp59 oxidation in CT-aposs-cyt *c* (Figure 4-14). Unfortunately, we could not unequivocally attribute the -2 Da mass shift to Trp59 in these experiments. Based on the arguments outlined above, Trp59 nonetheless represents the most likely culprit for the -2 Da modification in CT-aposs-cyt *c*. The unfolded structure of aposs-cyt *c* increases the reactivity of Trp59,<sup>64</sup> while in native holo-cyt *c* this residue is buried.<sup>60</sup> This enhanced solvent exposure renders Trp59 more prone to oxidation in aposs-cyt *c*.<sup>20,22,68-69</sup>

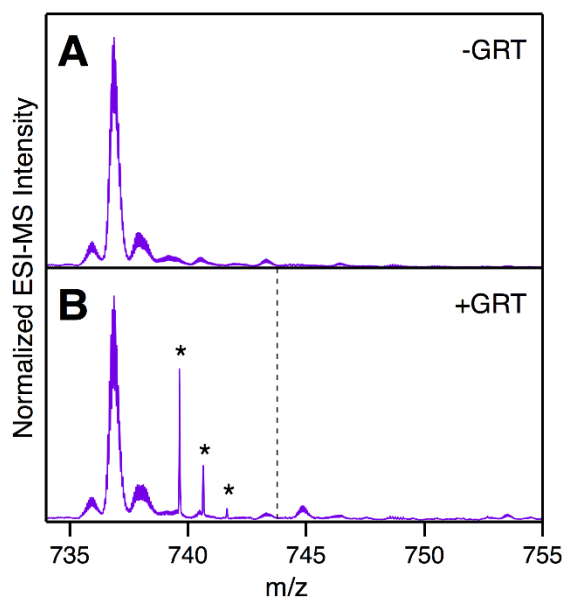


**Figure 4-13.** Intact protein mass spectra (charge state 16+) of CT<sub>low</sub>-aposs-cyt *c*, depicting a lack of GRT labeling due to the absence of LysCHO. (A) Spectrum before GRT exposure. (B) Spectrum after GRT exposure. The vertical line in panel B marks position where the GRT-labeled protein would be expected. The asterisks mark background contaminant signals.

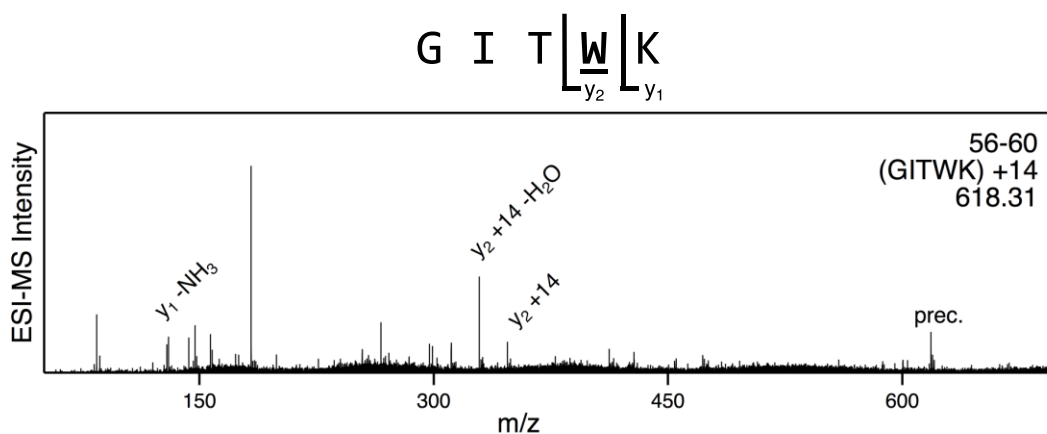


**Figure 4-14.** Bottom-up MS/MS of the tryptic peptide <sup>56</sup>GITWK<sup>60</sup> depicting oxidation of Trp59 (+14 Da) in CT-aposs-cyt *c*. This peptide was not detected in any other sample.



#### 4.3.4. Confirming Heme Catalysis Using MP11.

The absence of LysCHO in CT-aposs-cyt *c* strongly suggests that this type of modification can form only with heme catalysis. However, skeptics might point out that other differences between holo-cyt *c* and aposs-cyt *c* could play a role as well. For example, it could be possible that the absence of LysCHO in CT-aposs-cyt *c* is somehow related to the unfolded structure of this protein form (Figure 4-8). To conclusively test the role of heme, we produced CT-aposs-cyt *c* in the presence of exogenous heme in the form of MP11. MP11 is a heme-containing cyt *c* fragment (residues 11-21). The Fe(III) in MP11 is coordinated by His18 while the distal site remains open, allowing MP11 to catalyze a range of oxidation reactions.<sup>75-76</sup> The covalent thioether linkages in MP11 preclude reconstitution of native holo-cyt *c* upon mixing with aposs-cyt *c*, allowing us to delineate the effects of protein conformation vs. heme involvement on the protein oxidation behavior.

The presence of MP11 during CT-aposs-cyt *c* formation profoundly impacted the mass spectra (Figure 4-15). The most obvious effect was a dramatic shift toward lower charge states (i.e. from maxima around 16+/17+ down to 11+/12+) which indicates the loss of numerous charge-bearing sites (i.e., Lys-CH<sub>2</sub>-NH<sub>3</sub><sup>+</sup> → LysCHO).<sup>77</sup> Abundant LysCHO formation is also apparent from the mass distribution (Figure 4-15F) which shifted by ca. -10 Da, corresponding to ca. 10 LysCHO. We attempted to use GRT labeling of MP11/CT-aposs-cyt *c* for confirming the presence of LysCHO; however, those experiments yielded spectra with low S/N that were difficult to analyze (not shown). Keeping in mind that aposs-cyt *c* is normally unreactive with GRT due to the absence of LysCHO (Figure 4-11F, Figure 4-13B), it is likely that this low S/N arises from over-labeling of MP11/CT-aposs-cyt *c* by GRT. To nonetheless obtain direct confirmation of LysCHO, we performed MP11 experiments under the milder oxidation conditions of CT<sub>low</sub>-aposs-cyt *c*. These experiments yielded the expected GRT-labeled products, confirming the ability of MP11 to induce the conversion of Lys to LysCHO (Figure 4-16B,C).

In summary, our data reveal that LysCHO formation by CT is a heme-dependent process. This finding explains the unusual selectivity of LysCHO formation in CT-holo-cyt *c* which affects only 4 out of the 19 Lys side chains.<sup>27</sup> All of the affected residues (Lys53/55/72/73) are in close spatial proximity to the reactive (distal) heme face,<sup>27</sup> rendering them poised for heme-catalyzed oxidation (Figure 4-2). Other Lys are not targeted because they lack the spatial requirements for interaction with the endogenous heme. This spatial selectivity is reminiscent of metal-catalyzed oxidation events in other proteins.<sup>33</sup> In contrast, the exposure of apo<sub>SS</sub>-cyt *c* to freely diffusible heme (in the form of MP11) removes this geometric requirement, allowing heme to freely sample positions close to any of the 19 Lys and thus resulting in large-scale, non-selective, “global” LysCHO formation (Figure 4-15F). This non-selectivity is also apparent from the multiple fragment ion populations seen after top-down CID-IM-MS fragmentation of GRT-labeled MP11/CT<sub>low</sub>-apo<sub>SS</sub>-cyt *c* (Figure 4-16D).

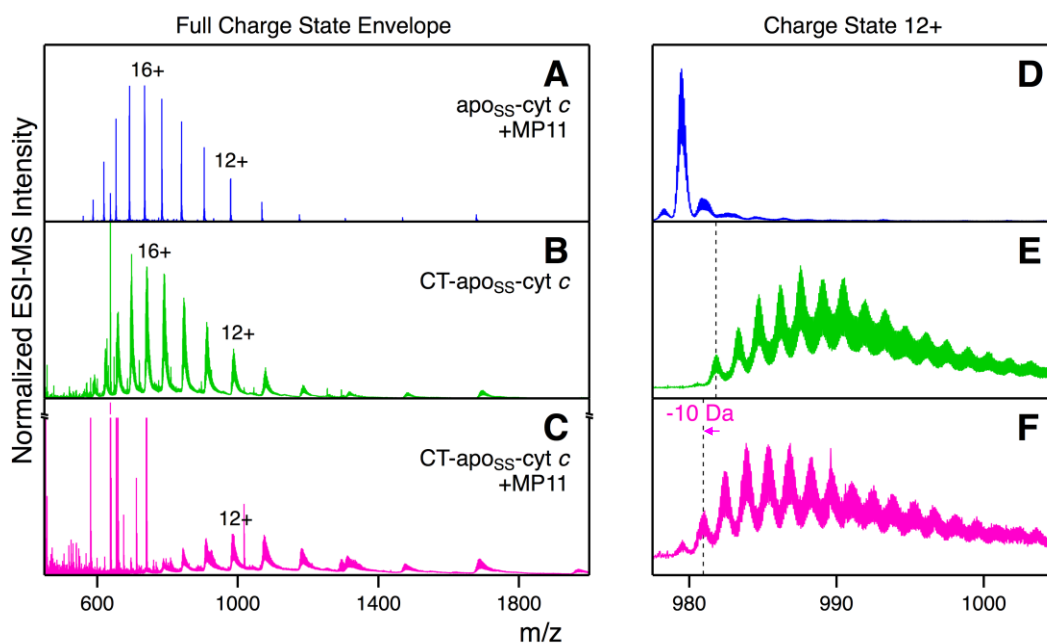


**Figure 4-15.** Intact protein mass spectra, illustrating the effects of MP11 during preparation of CT-apo<sub>SS</sub>-cyt *c*. (A/D) apo<sub>SS</sub>-cyt *c* with MP11 but without CT; (B/E) with CT but without MP11; (C/F) with CT and with MP11. (A-C) depict full charge state envelopes. (D-F) show a magnified view of the 12+ charge state. Vertical lines are present as a visual aid.

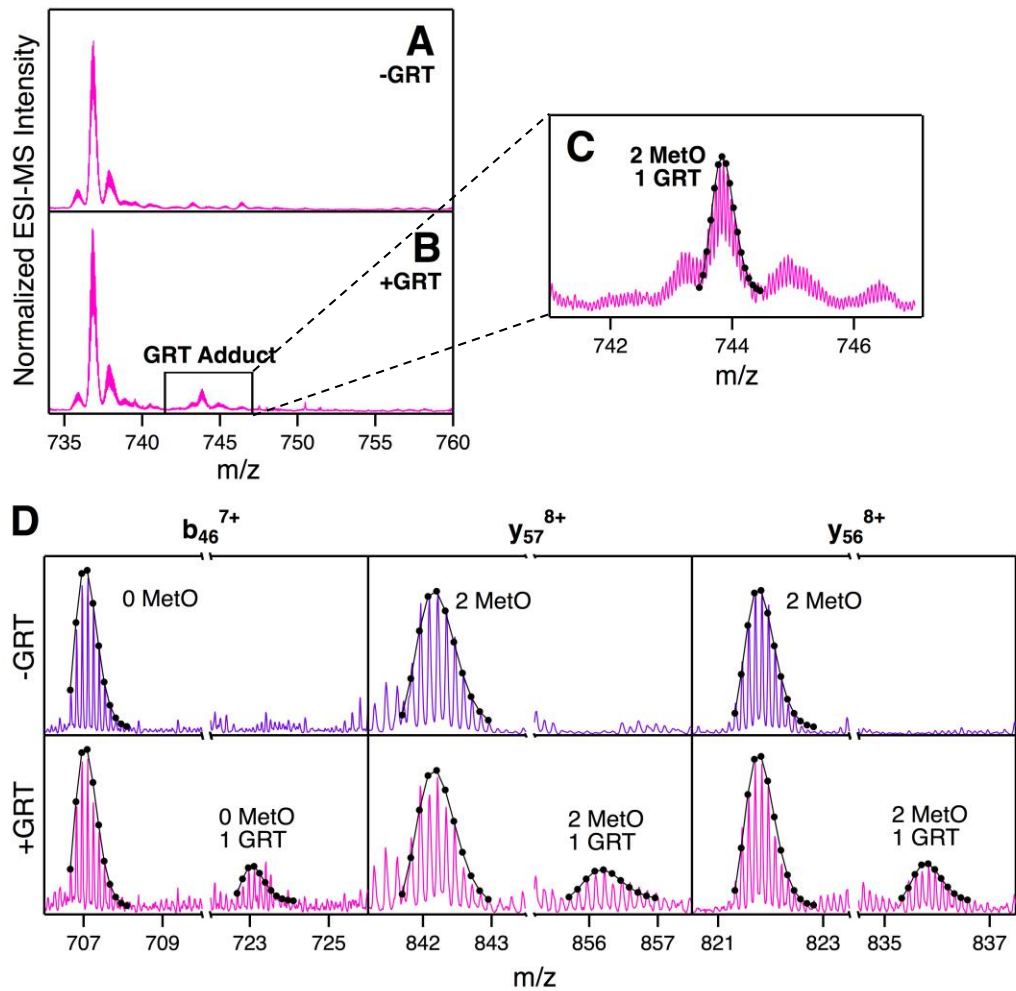


**Figure 4-16.** Mass spectra depicting GRT labeling experiments of MP11/CT<sub>low</sub>-aposs-cyt *c*. Intact protein mass spectra (charge state 16+) are depicted in panels A-C. (A) MP11/CT<sub>low</sub>-aposs-cyt *c* without GRT, and (B) with GRT. (C) Magnified view of (B) highlighting the GRT-labeled protein, overlaid with its simulated isotope distribution. (D) Representative top-down CID-IM-MS fragment ions, highlighting the presence of multiple ion populations in GRT-labeled MP11/CT<sub>low</sub>-aposs-cyt *c*. Top: CT<sub>low</sub>-apossCyt *c* (no GRT treatment). Bottom: GRT-labeled MP11/CT<sub>low</sub>-apossCyt *c*. The b<sub>46</sub> and y<sub>57/56</sub> ions shown in panel D cover mutually exclusive regions of the protein. If the precursor ion were homogeneously modified at a single site, then only one of these complementary fragment ions could contain the modification. The observation of a GRT-containing peak in both fragment ions demonstrates that there is more than one GRT site.

#### 4.4. Conclusions

CT-holo-cyt *c* represents an important model system that mimics the state produced *in vivo* when cells embark on their path towards apoptosis.<sup>27,29-30,44,47</sup> CT-induced oxidation of cyt *c* produces a 5-coordinate Fe(III) that is required for peroxidase activity. These modifications were identified as MetO at residue 80, as well as LysCHO formation in the Lys53/55/72/73 range.<sup>27</sup> The current work provides new insights into the chemistry underlying these transformations. In agreement with previous studies<sup>45,70-71</sup> we found that MetO-formation in cyt *c* can proceed without heme. The key finding of this study is that CT-induced LysCHO formation is heme-catalyzed, and that it only takes place in the direct vicinity of heme. The heme can be endogenous as in the case of holo-cyt *c*, or it can be exogenous as in our MP11 experiments.

The role of metal catalysis during CT-induced oxidation of small organic substrates has been examined previously, e.g. for Os(VIII) oxide and In(III) triflate.<sup>46,78</sup> However, there seems to be no prior work related to the reactivity of CT in the presence of Fe or heme. We consider it most likely that the heme-catalyzed Lys oxidation seen here involves OCl<sup>-</sup>. It is known that CT produces OCl<sup>-</sup>,<sup>44,46</sup> and it is also known that OCl<sup>-</sup> interacts with heme to generate Compound I and related Fe(IV)=O species.<sup>79-81</sup> The formation of such species in our MP11 experiments is favored by the fact that the distal heme face in MP11 is freely accessible.<sup>75-76</sup> In the case of holo-cyt *c*, OCl<sup>-</sup>-Fe interactions require opening of the heme crevice. Such opening events are facilitated by the high flexibility of the 71-85 Ω loop that covers the distal heme face in native cyt *c*.<sup>82-83</sup> Disruption of the Fe-Met80 contact via MetO formation further enhances the tendency of this Ω loop to sample oxidant-accessible conformation.<sup>28,84-85</sup>

It is tempting to speculate on the broader implications of heme-catalyzed LysCHO formation, relative to other oxidation pathways. Compound I-dependent oxidation involves the abstraction of H atoms by radical oxygen species.<sup>34</sup> Analogous H abstraction takes place during other oxidation methods, e.g. Fenton chemistry<sup>33</sup> or direct exposure to  $\cdot\text{OH}$ .<sup>20</sup> Likely, all of these methods generate similar (if not identical) types of oxidation products. It is therefore surprising that LysCHO formation has been observed after Fenton reactions<sup>86</sup> and other metal-catalyzed processes,<sup>18</sup> but not after direct  $\cdot\text{OH}$  exposure.<sup>20-21</sup> One possible explanation is that LysCHO tends to go undetected in conventional bottom-up LC-MS/MS workflows because LysCHO sites interfere with tryptic digestion and collision-induced dissociation of peptides.<sup>27</sup> However, further studies are necessary to explore this possibility.

From a bioanalytical perspective, this work demonstrates that top-down MS is highly suitable for interrogating heterogeneous oxidative modifications, including LysCHO sites which are difficult to track when using traditional bottom-up workflows.<sup>27</sup> Future top-down investigations will be aided by continuing advancements in instrumentation that enable high-resolution analyses of proteins with ever-increasing size and complexity.<sup>87-89</sup> It is hoped that this work will stimulate further top-down MS studies in the exciting field of protein oxidation.

## 4.5. References

- (1) Berlett, B. S.; Stadtman, E. R., *J. Biol. Chem.* **1997**, 272, 20313-20316.
- (2) Radi, R., *Proc. Natl. Acad. Sci. U. S. A.* **2018**, 115 (23), 5839-5848.
- (3) Winkler, J. R.; Gray, H. B., *Q. Rev. Biophys.* **2015**, 48 (4), 411-420.
- (4) Nimse, S. B.; Pal, D., *RSC Adv.* **2015**, 5 (35), 27986-28006.
- (5) Kathiresan, M.; English, A. M., *Chem. Sci.* **2017**, 8 (2), 1152-1162.
- (6) Dalle-Donne, I.; Rossi, R.; Giustarini, D.; Milzani, A.; Colombo, R., *Clin. Chim. Acta* **2003**, 329, 23-38.
- (7) Gray, H. B.; Winkler, J. R., *Accounts Chem. Res.* **2018**, 51 (8), 1850-1857.
- (8) de Graff, A. M. R.; Hazoglou, M. J.; Dill, K. A., *Structure* **2016**, 24 (2), 329-336.
- (9) Pedersen, J. T.; Chen, S. W.; Borg, C. B.; Ness, S.; Bahl, J. M.; Heegaard, N. H. H.; Dobson, C. M.; Hemmingsen, L.; Cremades, N.; Teilum, K., *J. Am. Chem. Soc.* **2016**, 138 (12), 3966-3969.
- (10) Sultana, R.; Boyd-Kimball, D.; Poon, H. F.; Cai, J.; Pierce, W. M.; Klein, J. B.; Markesbery, W. R.; Zhou, X. Z.; Lu, K. P.; Butterfield, D. A., *Neurobiol. Aging* **2006**, 27 (7), 918-925.
- (11) Giorgio, M.; Trinei, M.; Migliaccio, E.; Pelicci, P. G., *Nat. Rev. Mol. Cell Biol.* **2007**, 8 (9), 722A-728.
- (12) Lee, J. W.; Helmann, J. D., *Nature* **2006**, 440 (7082), 363-367.
- (13) Heppner, D. E.; Dustin, C. M.; Liao, C. Y.; Hristova, M.; Veith, C.; Little, A. C.; Ahlers, B. A.; White, S. L.; Deng, B.; Lam, Y. W.; Li, J. N.; van der Vliet, A., *Nat. Commun.* **2018**, 9, 1-11.
- (14) Beck, A.; Wagner-Rousset, E.; Ayoub, D.; Van Dorsselaer, A.; Sanglier-Cianferani, S., *Anal. Chem.* **2013**, 85 (2), 715-736.
- (15) Yang, Y.; Stella, C.; Wang, W. R.; Schoneich, C.; Gennaro, L., *Anal. Chem.* **2014**, 86 (10), 4799-4806.
- (16) Bobst, C. E.; Thomas, J. J.; Salinas, P. A.; Savickas, P.; Kaltashov, I. A., *Protein Sci.* **2010**, 19 (12), 2366-2378.
- (17) Madian, A. G.; Regnier, F. E., *J. Proteome Res.* **2010**, 9 (8), 3766-3780.
- (18) Møller, I. M.; Rogowska-Wrzesinska, A.; Rao, R. S. P., *J. Proteomics* **2011**, 74 (11), 2228-2242.

- (19) Yang, J.; Wang, S.; Liu, J.; Raghani, A., *J. Chromatogr. A* **2007**, *1156* (1-2), 174-182.
- (20) Xu, G.; Chance, M. R., *Chem. Rev.* **2007**, *107*, 3514-3543.
- (21) Johnson, D. T.; Di Stefano, L. H.; Jones, L. M., *J. Biol. Chem.* **2019**, *294* (32), 11969-11979.
- (22) Liu, X. R.; Zhang, M. M.; Gross, M. L., *Chem. Rev.* **2020**, *120*, 4355-4454.
- (23) Li, X. Y.; Grant, O. C.; Ito, K.; Wallace, A.; Wang, S. X.; Zhao, P.; Wells, L.; Lu, S.; Woods, R. J.; Sharp, J. S., *Biochemistry* **2017**, *56* (7), 957-970.
- (24) Fitzgerald, M. C.; West, G. M., *J. Am. Soc. Mass Spectrom.* **2009**, *20*, 1193-1206.
- (25) Chea, E. E.; Deredge, D. J.; Jones, L. M., *Biophys. J.* **2020**, *118* (1), 128-137.
- (26) Sharp, J. S.; Becker, J. M.; Hettich, R. L., *Anal. Chem.* **2004**, *76*, 672-683.
- (27) Yin, V.; Mian, S. H.; Konermann, L., *Chem. Sci.* **2019**, *10*, 2349-2359.
- (28) Yin, V.; Shaw, G. S.; Konermann, L., *J. Am. Chem. Soc.* **2017**, *139*, 15701-15709.
- (29) Capdevila, D. A.; Marmisolle, W. A.; Tomasina, F.; Demicheli, V.; Portela, M.; Radi, R.; Murgida, D. H., *Chem. Sci.* **2015**, *6* (1), 705-713.
- (30) Zhong, F.; Pletneva, E. V., *Inorg. Chem.* **2018**, *57* (10), 5754-5766.
- (31) Vahidi, S.; Konermann, L., *J. Am. Soc. Mass Spectrom.* **2016**, *27*, 1156-1164.
- (32) Saladino, J.; Liu, M.; Live, D.; Sharp, J. S., *J. Am. Soc. Mass Spectrom.* **2009**, *20*, 1123-1126.
- (33) Bridgewater, J. D.; Lim, J.; Vachet, R. W., *J. Am. Soc. Mass Spectrom.* **2006**, *17*, 1552-1559.
- (34) Veitch, N. C., *Phytochem.* **2004**, *65*, 249-259.
- (35) Rodriguez Maranon, M. J.; Mercier, D.; van Huystee, R. B.; Stillman, M. J., *Biochem. J.* **1994**, *301* ( Pt 2), 335-341.
- (36) Volkov, A. N.; Nicholls, P.; Worrall, J. A. R., *Biochim. Biophys. Acta.* **2011**, *1807* (11), 1482-1503.
- (37) Lawrence, A.; Jones, C. M.; Wardman, P.; Burkitt, M. J., *J. Biol. Chem.* **2003**, *278* (32), 29410-29419.
- (38) Florence, T. M., *J. Inorg. Biochem.* **1985**, *23*, 131-141.

- (39) Villegas, J. A.; Mauk, A. G.; Vazquez-Duhalt, R., *Chem. Biol.* **2000**, *7* (4), 237-244.
- (40) Gray, H. B.; Winkler, J. R., *Proc. Natl. Acad. Sci. U.S.A.* **2015**, *112* (35), 10920-10925.
- (41) Barayeu, U.; Lange, M.; Mendez, L.; Arnhold, J.; Shadyro, O. I.; Fedorova, M.; Flemmig, J., *J. Biol. Chem.* **2019**, *294* (6), 1816-1830.
- (42) Keck, R. G., *Anal. Biochem.* **1996**, *236* (1), 56-62.
- (43) Shechter, Y.; Burstein, Y.; Patchornik, A., *Biochemistry* **1975**, *14* (20), 4497-4503.
- (44) Chen, Y.-R.; Deterding, L. J.; Sturgeon, B. E.; Tomer, K. B.; Mason, R. P., *J. Biol. Chem.* **2002**, *277* (33), 29781-29791.
- (45) Pande, J.; Kinnally, K.; Thallum, K. K.; Verma, B. C.; Myer, Y. P.; Rechsteiner, L.; Bosshard, H. R., *J. Protein Chem.* **1987**, *6* (4), 295-319.
- (46) Mushran, S. P.; Agrawal, M. C.; Prasad, B., *J. Chem. Soc. B* **1971**, *0* (8), 1712-1714.
- (47) Parakra, R. D.; Kleffmann, G. N. L.; Jameson, T.; Ledgerwood, E. C., *Dalton Trans.* **2018**, *47*, 9128-9135.
- (48) Campbell, M. M.; Johnson, G., *Chem. Rev.* **1978**, *78* (1), 65-79.
- (49) Lushington, G. H.; Cowley, A. B.; Silchenko, S.; Lukat-Rodgers, G. S.; Rodgers, K. R.; Benson, D. R., *Inorg. Chem.* **2003**, *42* (23), 7550-7559.
- (50) Wang, Z.; Ando, Y.; Nugraheni, A. D.; Ren, C.; Nagao, S.; Hirota, S., *Mol. Biosyst.* **2014**, *10* (12), 3130-3137.
- (51) Birk, A. V.; Chao, W. M.; Liu, S. Y.; Soong, Y.; Szeto, H. H., *Biochim. Biophys. Acta* **2015**, *1847* (10), 1075-1084.
- (52) Nugraheni, A. D.; Ren, C. G.; Matsumoto, Y.; Nagao, S.; Yamanaka, M.; Hirota, S., *J. Inorg. Biochem.* **2018**, *182*, 200-207.
- (53) Diaz-Quintana, A.; Perez-Mejias, G.; Guerra-Castellano, A.; De la Rosa, M. A.; Diaz-Moreno, I., *Oxidative Med. Cell. Longev.* **2020**, *2020*, 1-20.
- (54) Alvarez-Paggi, D.; Hannibal, L.; Castro, M. A.; Oviedo-Rouco, S.; Demicheli, V.; Tórtora, V.; Tomasina, F.; Radi, R.; Murgida, D. H., *Chem. Rev.* **2017**, *117* (21), 13382-13460.
- (55) McClelland, L. J.; Mou, T.-C.; Jeakins-Cooley, M. E.; Sprang, S. R.; Bowler, B. E., *Proc. Natl. Acad. Sci. U.S.A.* **2014**, *111* (18), 6648-6653.



- (56) Kitt, J. P.; Bryce, D. A.; Minter, S. D.; Harris, J. M., *J. Am. Chem. Soc.* **2017**.
- (57) Oemer, G.; Lackner, K.; Muigg, K.; Krumschnabel, G.; Watschinger, K.; Sailer, S.; Lindner, H.; Gnaiger, E.; Wortmann, S. B.; Werner, E. R.; Zschocke, J.; Keller, M. A., *Proc. Natl. Acad. Sci. U.S.A.* **2018**, *115* (16), 4158-4163.
- (58) Belikova, N. A.; Vladimirov, Y. A.; Osipov, A. N.; Kapralov, A. A.; Tyurin, V. A.; Potapovich, M. V.; Basova, L. V.; Peterson, J.; Kurnikov, I. V.; Kagan, V. E., *Biochemistry* **2006**, *45* (15), 4998-5009.
- (59) Hersleth, H.-P.; Ryde, U.; Rydberg, P.; Görbitz, C. H.; Andersson, K. K., *J. Inorg. Biochem.* **2006**, *100* (4), 460-476.
- (60) Bushnell, G. W.; Louie, G. V.; Brayer, G. D., *J. Mol. Biol.* **1990**, *214*, 585-595.
- (61) Zinnel, N. F.; Pai, P.-J.; Russell, D. H., *Anal. Chem.* **2012**, *84* (7), 3390-3397.
- (62) Polasky, D. A.; Lermyte, F.; Nshanian, M.; Sobott, F.; Andrews, P. C.; Loo, J. A.; Ruotolo, B. T., *Anal. Chem.* **2018**, *90* (4), 2756-2764.
- (63) Halgand, F.; Habchi, J.; Cravello, L.; Martinho, M.; Guigliarelli, B.; Longhi, S., *Anal. Chem.* **2011**, *83*, 7306-7315.
- (64) Fisher, W. R.; Taniuchi, H.; Anfinsen, C. B., *J. Biol. Chem.* **1973**, *248* (9), 3188-3195.
- (65) Daltrop, O.; Ferguson, S. J., *J. Biol. Chem.* **2003**, *278* (7), 4404-4409.
- (66) Capdevila, D. A.; Marmisolle, W. A.; Tomasina, F.; Demicheli, V.; Portela, M.; Radi, R.; Murgida, D. H., *Chem. Sci.* **2015**, *6* (1), 705-713.
- (67) Yin, V.; Mian, S. H.; Konermann, L., *Chem. Sci.* **2019**, *10* (8), 2349-2359.
- (68) Mendoza, V. L.; Vachet, R. W., *Mass Spectrom. Rev.* **2009**, *28*, 785-815.
- (69) Jumper, C. C.; Schriemer, D. C., *Anal. Chem.* **2011**, *83* (8), 2913-2920.
- (70) Shechter, Y.; Burstein, Y.; Patchornik, A., *Biochemistry* **1975**, *14* (20), 4497-4503.
- (71) Michel, B.; Proudfoot, A. E. I.; Wallace, C. J. A.; Bosshard, H. R., *Biochemistry* **1989**, *28* (2), 456-462.
- (72) Mirzaei, H.; Regnier, F., *J. Chromatogr. A* **2006**, *1134* (1-2), 122-133.
- (73) Santa, T., *Biomed. Chromatogr.* **2011**, *25* (1-2), 1-10.
- (74) Li, Y. M.; Polozova, A.; Gruia, F.; Feng, J. H., *Anal. Chem.* **2014**, *86* (14), 6850-6857.

- (75) Osman, A. M.; Koerts, J.; Boersma, M. G.; Boeren, S.; Veeger, C.; Rietjens, I., *Eur. J. Biochem.* **1996**, *240* (1), 232-238.
- (76) Spector, A.; Zhou, W.; Ma, W. C.; Chignell, C. F.; Reszka, K. J., *Exp. Eye Res.* **2000**, *71* (2), 183-194.
- (77) Konermann, L.; Metwally, H.; Duez, Q.; Peters, I., *Analyst* **2019**, *144*, 6157-6171.
- (78) Nakahara, K.; Kitazawa, C.; Mineno, T., *Chem. Pharm. Bull.* **2017**, *65* (8), 801-804.
- (79) Schaffner, I.; Hofbauer, S.; Krutzler, M.; Pirker, K. a. F.; Furtmüller, P. G.; Obinger, C., *Arch. Biochem. Biophys.* **2015**, *574*, 18-26.
- (80) Mashino, T.; Fridovich, I., *Biochim. Biophys. Acta* **1988**, *956* (1), 63-69.
- (81) Maitra, D.; Byun, J.; Andreana, P. R.; Abdulhamid, I.; Diamond, M. P.; Saed, G. M.; Pennathur, S.; Abu-Soud, H. M., *Free Radical Biol. Med.* **2011**, *51* (2), 374-386.
- (82) Hu, W. B.; Kan, Z. Y.; Mayne, L.; Englander, S. W., *Proc. Natl. Acad. Sci. U.S.A.* **2016**, *113* (14), 3809-3814.
- (83) Maity, H.; Rumbley, J. N.; Englander, S. W., *Proteins* **2006**, *63* (2), 349-355.
- (84) Deacon, O. M.; Svistunenko, D. A.; Moore, G. R.; Wilson, M. T.; Worrall, J. A. R., *Biochemistry* **2018**, *57* (29), 4276-4288.
- (85) Tomášková, N.; Varhač, R.; Lysáková, V.; Musatov, A.; Sedlák, E., *Biochim. Biophys. Acta* **2018**, *1866*, 1073–1083.
- (86) Requena, J. R.; Chao, C.-C.; Levine, R. L.; Stadtman, E. R., *Proc. Natl. Acad. Sci. U.S.A.* **2001**, *98* (1), 69-74.
- (87) Chen, B. F.; Brown, K. A.; Lin, Z. Q.; Ge, Y., *Analytical Chemistry* **2018**, *90* (1), 110-127.
- (88) Crittenden, C. M.; Novelli, E. T.; Mehaffey, M. R.; Xu, G. N.; Giles, D. H.; Fies, W. A.; Dalby, K. N.; Webb, L. J.; Brodbelt, J. S., *J. Am. Soc. Mass Spectrom.* **2020**, *31* (5), 1140-1150.
- (89) Gomes, F. P.; Diedrich, J. K.; Saviola, A. J.; Memili, E.; Moura, A. A.; Yates, J. R., *Anal. Chem.* **2020**, *92* (4), 2979-2987.

# Chapter 5. Probing the Effects of Heterogeneous Oxidative Modifications on the Stability of Cytochrome *c* in Solution and in the Gas Phase

## 5.1. Introduction

Atomically resolved structural data for proteins in solution or in the solid state can be obtained by X-ray crystallography, NMR spectroscopy and cryo-electron microscopy. Mass spectrometry (MS) and ion mobility spectrometry (IMS) offer complementary avenues. Prerequisite for the application of these vacuum techniques is the capability to generate intact gaseous protein ions.<sup>1</sup> Electrospray ionization (ESI)<sup>2</sup> and matrix-assisted laser desorption/ionization (MALDI)<sup>3</sup> represent key techniques for this purpose, but new ionization methods continue to emerge.<sup>4-8</sup> Particularly interesting is recent work by Trimpin *et al.*<sup>8</sup> which demonstrated that gaseous protein ions can be generated without the aid of lasers, heat, or voltages.

The amino acids in natively folded proteins are closely packed and engaged in H-bonds, salt bridges, van der Waals interactions, and hydrophobic contacts.<sup>9</sup> Covalent modifications can upset this interaction network, destabilize the native state, and render proteins non-functional.<sup>10</sup> One avenue to introduce such modifications involves reactive oxygen species, such as  $O_2^-$ ,  $HO_2\cdot$ ,  $H_2O_2$ , and  $\cdot OH$ .<sup>11-14</sup> Methionine conversion to sulfoxide (MetO) is particularly common,<sup>15-18</sup> but oxidation can also affect many other residues.<sup>19-20</sup> The accumulation of oxidized proteins plays a key role for aging-related pathologies<sup>21</sup> such as Alzheimer's and other neurodegenerative diseases.<sup>22-23</sup> In addition, oxidation compromises the efficacy of protein therapeutics.<sup>16,18,24</sup> Understanding oxidation-related effects on protein structure and stability, therefore, is an important goal with far-reaching repercussions.

Oxidation-induced stability changes in solution can be studied using thermal<sup>15,18,25-26</sup> or chemical<sup>27-28</sup> unfolding experiments. These studies involve protein exposure to heat or chemical denaturants. Optical tools can then be used to probe unfolding profiles, e.g. circular dichroism (CD) spectroscopy at 222 nm which reports on  $\alpha$ -helicity.<sup>29</sup> The melting temperature  $T_M$  marks the unfolding midpoint and is a measure of protein stability.<sup>9,30-31</sup> Oxidative modifications usually destabilize proteins in solution, inducing shifts to lower  $T_M$ .<sup>15,18,25-28</sup>

In addition to the aforementioned solution studies, there is considerable interest in examining proteins in a solvent-free environment. “Native” ESI can generate gaseous biomolecular ions that retain solution-like structures and interactions.<sup>7,32-36</sup> Somewhat analogous to thermal unfolding in solution,<sup>15,18,25-26,30</sup> these gaseous protein ions can be subjected to collisional heating, causing them to undergo collision-induced unfolding (CIU). The structural changes triggered in this way are detectable by IMS.<sup>37-38</sup>

It is an interesting question whether gas phase stabilities correlate with the protein behavior in solution.<sup>39-40</sup> A number of studies indicate that this indeed appears to be the case. For example, enzyme-inhibitor binding stabilities in solution were consistent with trends seen in collision-induced dissociation (CID) studies,<sup>41</sup> ligand-induced stabilization effects were mirrored in the gas phase,<sup>42</sup> and CIU energetics were shown to be correlated with solution structures.<sup>38</sup> Correlation between solution and gas phase behavior was also demonstrated in surface-induced dissociation (SID) experiments on multi-protein assemblies,<sup>36</sup> and blackbody infrared dissociation (BIRD) studies on protein-lipid complexes.<sup>43</sup> On the other hand, the absence of solvent can have profound effects on inter- and intramolecular contacts.<sup>44</sup> Hydrophobic interactions are weakened,<sup>45</sup> while electrostatic contacts are strengthened in the absence of water.<sup>46</sup> These factors can lead to disparities between solution and gas phase stabilities.<sup>46</sup> Overall, much remains to be learned about the relationship between protein stability *in vitro* and *in vacuo*. Particular knowledge gaps persist when it comes to the question how oxidative modifications affect the stability of gaseous proteins.

Oxidative modifications of the heme protein cytochrome *c* (cyt *c*) have attracted a lot of attention in recent years.<sup>47-56</sup> The canonical function of cyt *c* is to shuttle electrons in the respiratory chain.<sup>57</sup> In addition, cyt *c* acts as a peroxidase, i.e. an enzyme that catalyzes the oxidation of organic substrates by H<sub>2</sub>O<sub>2</sub>.<sup>58</sup> Cyt *c*-catalyzed oxidation of cardiolipin in mitochondria plays a key role during apoptosis.<sup>59-62</sup> The peroxidase activity of native cyt *c* is low. It is only after specific oxidation events that the protein becomes fully active.<sup>47-54,63-64</sup> This gain of function contrasts the aforementioned scenarios where oxidation events interfere with protein activity.

The most common method for producing peroxidase-active cyt *c in vitro* is by exposure to chloramine-T (CT),<sup>47,51,53-54</sup> a mild oxidant that releases OCl<sup>-</sup>.<sup>65</sup> We recently conducted a detailed MS characterization of CT-treated cyt *c* (CT-cyt *c*).<sup>63</sup> The protein was found to be highly heterogeneous, with MetO formation at zero, one, or two methionines (Met80 and Met65). In addition, CT-cyt *c* showed Lys carbonylation in the range of Lys72/73 and Lys53/55 (Figure 5-1).<sup>63</sup> Lys carbonylation to amino adipic semialdehyde is associated with  $\Delta M = -1$  Da (LysCH<sub>2</sub>-NH<sub>2</sub> → LysCHO).<sup>66-67</sup> This type of modification is easily missed because of its small mass shift, loss of a charged site, and abrogation of tryptic cleavage. In particular, the presence of LysCHO in CT-cyt *c* had been overlooked until recently.<sup>63</sup> Both MetO and LysCHO are well-known markers for oxidative damage in environmentally stressed proteins and protein therapeutics.<sup>67-68</sup> Therefore, CT-cyt *c* represents as a convenient model system for probing the effects of these modifications on protein structure and stability.

Here we characterize the effects of oxidative modifications in CT-cyt *c* on the stability of the protein in solution and in the gas phase. We find that although the solution stability of the protein is reduced after oxidation, gas phase data show an increase in stability. We conclude that the solution properties of oxidatively modified proteins are not necessarily reflected in their CIU behavior.

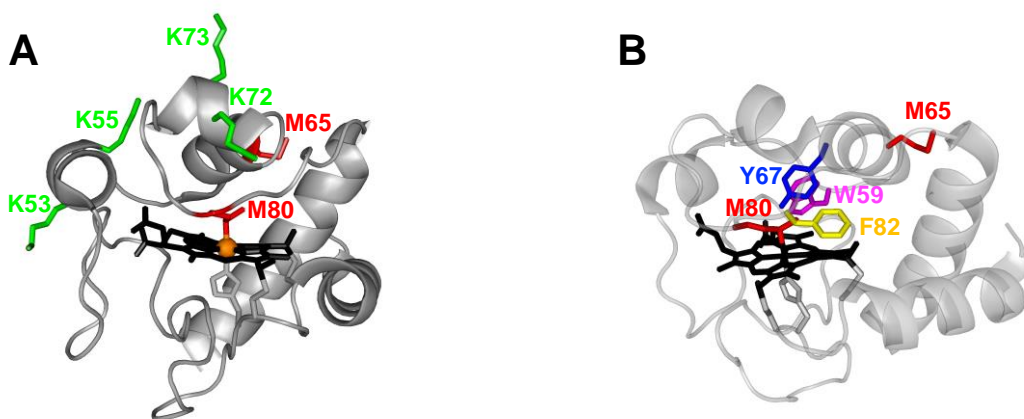


**Figure 5-1.** Crystal structure of horse cyt *c* (PDB 1HRC). (A) Front view with highlighted side chains that are oxidized after CT exposure: Met (red), and Lys (green). The heme iron is shown in orange. (B) Side view with highlighted Met residues and selected aromatic side chains.

## 5.2. Materials and Methods

### 5.2.1. Materials.

Cyt *c* (equine heart), CT (N-chloro-4-toluosulfonamide), and Tris base (2-amino-2-(hydroxymethyl)-1,3-propanediol) were supplied by MilliporeSigma (St. Louis, MO). All other chemicals were supplied by Fisher Scientific (Nepean, ON) or Caledon Laboratories (Georgetown, ON). Centrifuge filters (Amicon Ultra 0.5, 10 kDa MWCO) were supplied by Millipore Sigma, and used according to manufacturer instructions (15 min at 13,000 G).

### 5.2.2. Protein Oxidation.

CT-cyt *c* was prepared as described<sup>63</sup>, with minor modifications. 500  $\mu\text{M}$  cyt *c* was incubated with 2.5 mM CT in 50 mM Tris (pH 8.4) for 60 min at 22 °C. Oxidation was quenched by five serial exchanges into 10 mM ammonium acetate using Amicon filters. The resulting proteoform mixture was fractionated using a 5 mL SCX HiTrap SP cartridge (GE Healthcare). Samples were eluted using a zero to 500 mM ammonium acetate gradient (pH 9).

### 5.2.3. Thermal Unfolding.

Solution phase unfolding was monitored by CD spectroscopy at 222 nm using a J-810 spectropolarimeter (JASCO, Easton, MD). Samples were prepared as 10  $\mu\text{M}$  protein in 50 mM potassium phosphate buffer (pH 7.4). Heating was performed from 20 to 100 °C at a rate of 1 °C  $\text{min}^{-1}$ . The melting temperature ( $T_M$ ) and enthalpy of unfolding ( $\Delta H$ ) were extracted by fitting the  $\text{CD}_{222}$  profiles using<sup>30</sup>

$$\text{CD}_{222} = \frac{(y_N + m_N T) + (y_U + m_U T) \exp(-\Delta G/RT)}{1 + \exp(-\Delta G/RT)} \quad (5.1)$$

where  $T$  is the temperature in Kelvin and  $\Delta G = \Delta H(1 - T/T_M)$ , while  $(y_N + m_N T)$  and  $(y_U + m_U T)$  represent the pre- and post-transition baselines, respectively. The fraction of unfolded protein in solution ( $F_{u_{sol}}$ ) was calculated as<sup>69</sup>

$$F_{u_{sol}} = \frac{\exp(-\Delta G/RT)}{1 + \exp(-\Delta G/RT)} \quad (5.2)$$

There was no evidence of aggregation, as seen from the absence of precipitated protein in the heated samples.

#### 5.2.4. Mass Spectrometry.

MS experiments were performed on a Waters SYNAPT G2-Si instrument in positive ion mode (Waters, Milford, MA). Samples were prepared as 10  $\mu\text{M}$  protein in either 10 mM ammonium acetate for native ESI, or 50/50/0.1 H<sub>2</sub>O/methanol/formic acid for denaturing conditions, and infused at 5  $\mu\text{L min}^{-1}$ . Travelling wave IMS experiments were performed in sensitivity mode with N<sub>2</sub> as buffer gas. Instrument parameters were tuned to maintain minimal ion activation prior to deliberate activation for CIU. CIU was performed by varying the trap collision energy, with Ar as collision gas. IMS profiles of 8+ ions were extracted using TWIMextract.<sup>70</sup> IMS drift times were converted into effective helium collision cross sections ( $\Omega$ ).<sup>71</sup> CIU curves were expressed as fraction unfolded in vacuum ( $F_{u\_vac}$ ), defined as

$$F_{u\_vac} = \frac{\langle\Omega\rangle - \langle\Omega_N\rangle}{\langle\Omega_U\rangle - \langle\Omega_N\rangle} \quad (5.3)$$

where  $\langle\Omega\rangle$  is the average  $\Omega$  at a given trap collision energy.  $\langle\Omega_N\rangle$  and  $\langle\Omega_U\rangle$  are the average  $\Omega$  values measured for minimum (1 V) and maximum collisional excitation (20 V), respectively. All CIU experiments were performed in triplicate, with independent  $\Omega$  calibrations for each replicate. Error bars represent standard deviations. Simulated isotope distributions of Fe(III) cyt *c* were generated using the UCSF ProteinProspector web server.



## 5.3. Results and Discussion

### 5.3.1. Chromatographic Separation of Proteoforms.

Exposure of *cyt c* to CT produces a mix of oxidation products that are modified at Met and Lys side chains.<sup>63</sup> The complexity of these CT-*cyt c* samples can be alleviated by using strong cation exchange (SCX) chromatography. Under the conditions used here, three major SCX fractions were obtained (I, II, and III in Figure 5-2A). The SCX retention time of fraction I (where no Lys is oxidized) was virtually identical to that of unmodified control samples which had not been exposed to CT.

A cursory glance at the mass distributions of the three CT-*cyt c* fractions suggests that they are quite similar to one another. Each fraction showed three dominant signals, corresponding to 0, 1, and 2 MetO modifications (approximately +0, +16, +32 Da, Figure 5-2B-D). The 1 MetO species were previously shown to be oxidized at Met80, while the 2 MetO proteoforms are modified at Met80 and Met65.<sup>63</sup> However, close examination and comparison with modeled isotope distributions reveals additional mass shifts of -2, -1, and -0 Da for fractions III, II, and I. These negative shifts are attributable to the presence of 2, 1, and 0 LysCHO sites. Proteoforms with a -1 Da shift are carbonylated at Lys72/73, while -2 Da species are additionally modified at Lys53/55.<sup>63</sup> The progressive loss of positive charge for these proteoforms is consistent with their SCX retention behavior, keeping in mind that SCX separates proteins based on their cationic character in solution. Specifically, fraction III which has lost the most charge due to two  $\text{Lys}^+ \rightarrow \text{LysCHO}$  conversion events was most weakly retained (Figure 5-2A).

The observation that all three fractions share virtually the same MetO oxidation pattern (Figure 5-2B-D) indicates that Met oxidation and Lys carbonylation occur independently of one another during *cyt c* exposure to CT. The inability of SCX to separate proteoforms with different MetO content reflects the fact that this type of modification does not affect the protein charge.

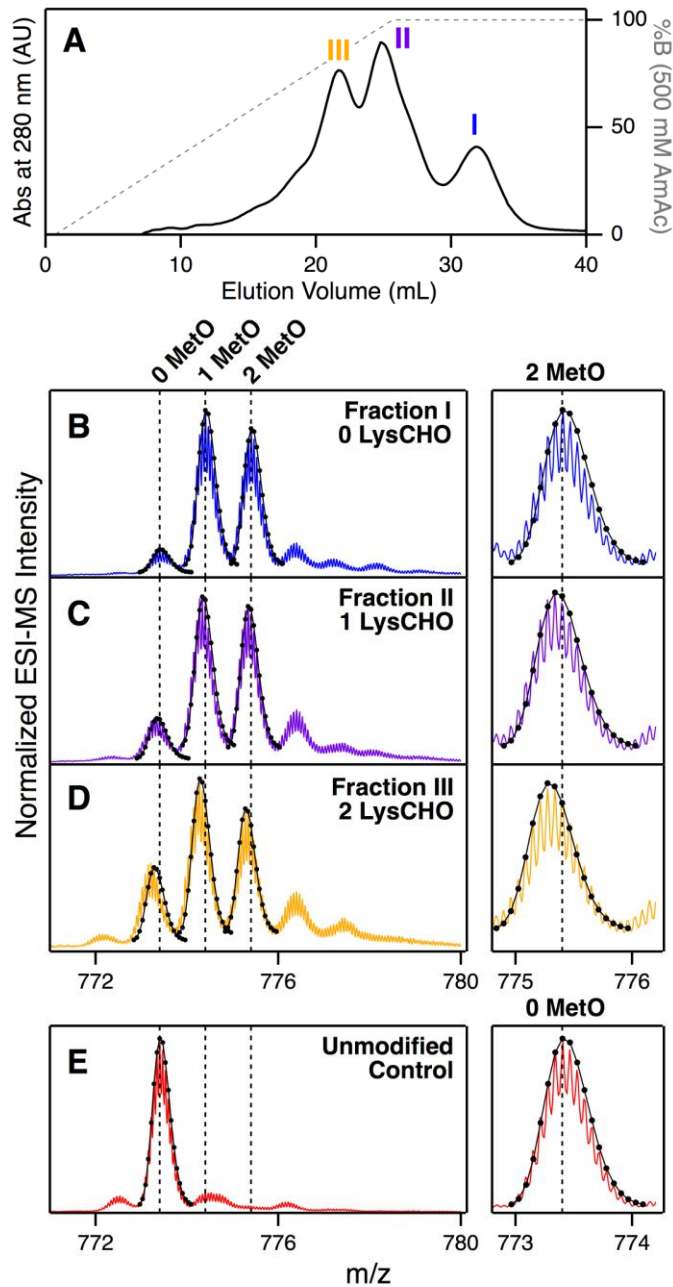


**Figure 5-2.** SCX fractionation of CT-cyt *c*. (A) Chromatogram after CT exposure; three major fractions I, II, and III are highlighted. (B-D) Mass spectra of the 16+ charge state for each fraction (colored lines), overlaid with isotopic models (black solid lines and dots). (E) Unmodified cyt *c*. The number of MetO and LysCHO modifications for each peak is indicated. Vertical dashed lines were included as a visual aid.

In summary, the CT-cyt *c* preparations examined here represent a mix of proteoforms that contain 0, 1, or 2 MetO sites, as well as 0, 1, or 2 LysCHO modifications. SCX allows separation into three fractions that are pure with respect to LysCHO content, but heterogeneous in the number of MetO sites. The separation of CT-cyt *c* into three fractions facilitates the subsequent experiments, compared to investigations on unseparated samples.

### 5.3.2. Stability of CT-cyt *c* in Solution.

Unfolding experiments were performed to establish how CT-induced oxidative modifications affect the stability of cyt *c* in solution (Figure 5-3). Instead of using chemical denaturation<sup>27-28</sup> we chose thermal unfolding assays<sup>15,18,25-26</sup> to allow a direct comparison with gas phase CIU experiments (discussed below), keeping in mind that both techniques probe the protein response to heat. The thermodynamic parameters measured for unmodified cyt *c* were  $T_M = 86.8 \pm 0.2$  °C and  $\Delta H = 493 \pm 20$  kJ mol<sup>-1</sup>. The former agrees with literature data within 1 °C.<sup>72</sup> Previous work reported a somewhat lower  $\Delta H$  (400 kJ mol<sup>-1</sup>)<sup>73</sup> but that earlier study used acidic solutions, while our experiments were performed at pH 7.4. Compared to the unmodified controls, all three CT-cyt *c* fractions showed a substantial decrease in both  $T_M$  (ca. 5 °C) and  $\Delta H$  (ca. 50%), revealing that CT-induced oxidative modifications reduce the stability of the protein in solution (Table 5-1). The stability reduction seen here for CT-cyt *c* is reminiscent of data reported previously for other oxidatively modified proteins.<sup>15,18,25-28</sup>

Interestingly, stability differences between the individual oxidized fractions I, II, and III were small, evident from their almost superimposable unfolding profiles (Figure 5-3). As discussed above, the three fractions only differ in the number of modified Lys residues (0, 1, 2 LysCHO for fractions I, II, III), while they share very similar MetO compositions. From this, one can conclude that LysCHO formation does not significantly affect the protein stability in solution, consistent with the location of these modifications on side chains that protrude into the solvent (Figure 5-1A).

**Table 5-1.** Thermodynamic parameters derived from the thermal unfolding experiments of Figure 5-3.

	$T_M$ (°C)	$\Delta H$ (kJ mol <sup>-1</sup> )
Unmodified Control	86.8 ± 0.2	493 ± 20
Fraction I	81.6 ± 0.1	238 ± 4
Fraction II	82.7 ± 0.1	276 ± 6
Fraction III	82.5 ± 0.2	269 ± 8

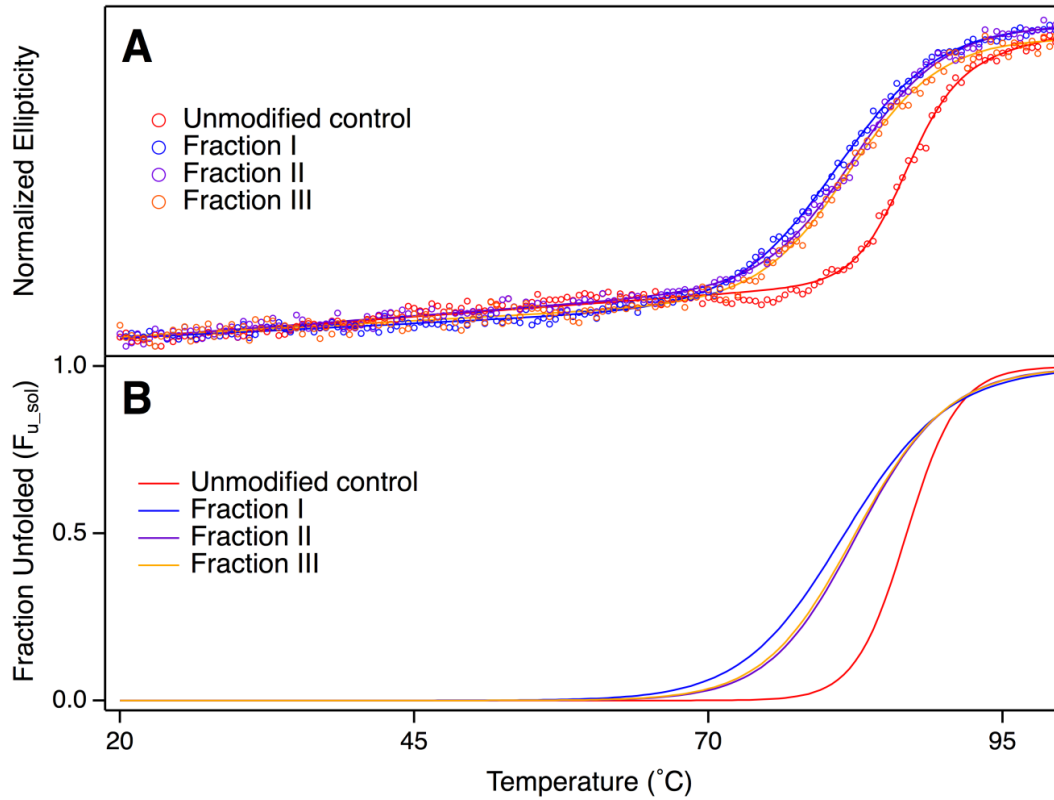


**Figure 5-3.** Solution phase thermal unfolding of cyt *c* monitored by CD spectroscopy at 222 nm. Data are shown for unmodified control protein, and for fractions I, II, III of CT-cyt *c*. (A) Experimental data points (circles) are overlaid with fits (solid lines) according to Equation (5.1).  $T_M$  and  $\Delta H$  values derived from these fits are compiled in Table 1. (B) Fraction of unfolded protein in solution ( $F_{u,sol}$ ) calculated according to Equation (5.2).

Instead, the major stability difference between unmodified *cyt c* and CT-*cyt c* are attributable to MetO formation. Oxidation of the deeply buried Met80 is expected to be particularly disruptive because it ruptures the distal Fe-sulfur bond and interferes with side chain packing in the protein core.<sup>74</sup> Met65 modifications likely affect the protein stability to a lesser extent, because this residue is located close to the protein surface without any critical side chain contacts (Figure 5-1A).

### 5.3.3. ESI Charge States of CT-*cyt c*.

Because the formation of each LysCHO is concomitant with the loss of a basic (protonatable) site, one might expect that the ESI charge state distribution of  $[M + zH]^{z+}$  ions could be affected by LysCHO formation. However, native ESI mass spectra of unmodified controls and fractions I-III were very similar to one another, with charge state distributions dominated by 8+/7+ ions. In contrast, spectra acquired under denaturing conditions exhibited slight shifts to lower charge states, from maxima of 17+/16+ for unmodified *cyt c* and fraction I, down to 16+/15+ for fraction III (Figure 5-4).

Native ESI proceeds according to the charged residue model (CRM), where protein ions are released upon droplet evaporation to dryness. Charge states generated under these conditions are close to those of protein-sized water droplets at the Rayleigh limit ( $z_R \approx 7.9$  for *cyt c*).<sup>75-77</sup> Thus, CRM charge states of globular proteins are governed by their surface area, rather than the number of basic sites.<sup>78</sup> The fact that native ESI generates very similar charge state distributions for unmodified and CT-*cyt c* indicates that the covalent modifications encountered here do not dramatically alter the overall compactness of the protein. This view is consistent with native ESI  $\Omega$  values which are very similar for all proteoforms (see below).

The situation is different under denaturing ESI conditions, where protein ions likely form according to the chain ejection mechanism (CEM).<sup>77</sup> The CEM proceeds with gradual ejection of extended protein chains from the droplet surface, in concert with the equilibration of mobile  $H^+$  between the droplet and its protein appendage. Any factor that

decreases the effective basicity of the protein will compromise the capability of the chain to compete for  $H^+$  during ejection. The slight shift to lower charge states seen for fraction III under denaturing ESI conditions therefore likely reflects the loss of basic sites due to conversion of two Lys to LysCHO (Figure 5-4). In summary, the ESI charge state distributions of the various proteoforms are consistent with current views of the ESI process under native and denaturing conditions.<sup>75-77</sup>

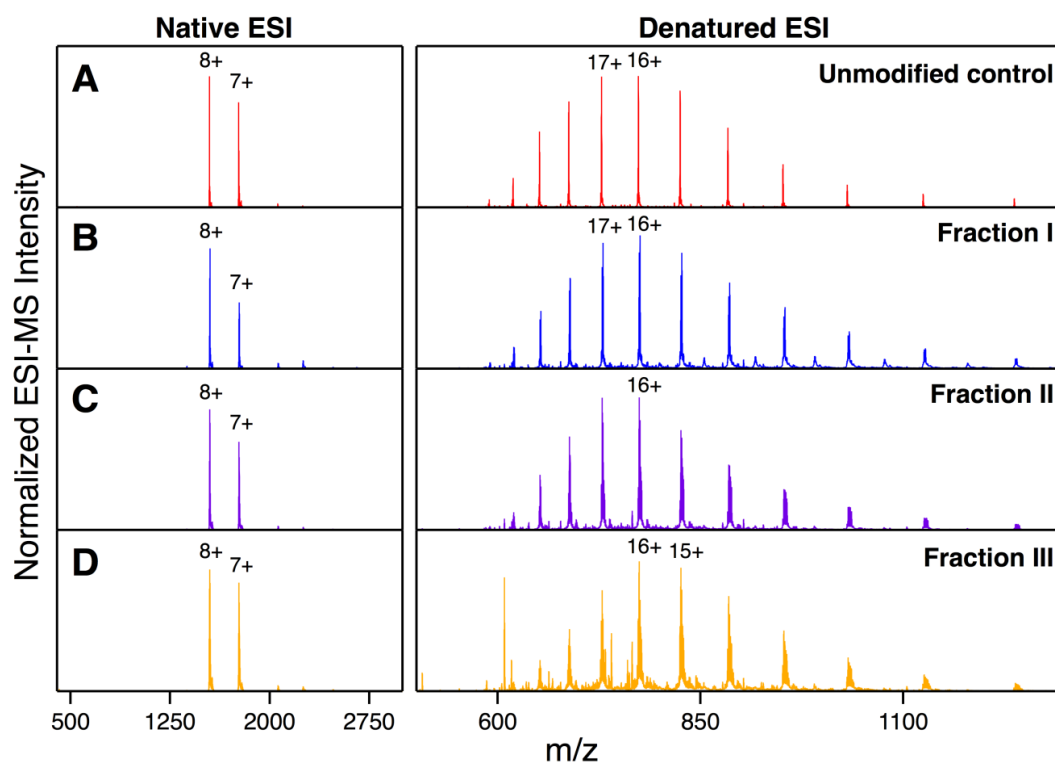


**Figure 5-4.** Mass spectra of unmodified cyt *c* and the three CT-cyt *c* fractions. Data were acquired under native ESI conditions (left) and under denaturing conditions (right).

#### 5.3.4. Native ESI Gas Phase Conformations of CT-cyt *c*.

We initially probed the conformations of unmodified 8+ cyt *c* ions and fractions I-III with minimum collisional excitation (collision energy 1 V) in an effort to preserve solution-like structures in the gas phase.<sup>7,32-36</sup> Figure 5-5A-D displays the resulting IMS data in a MetO-averaged fashion. The unmodified control protein displayed a single dominant feature centered at  $\sim 1350 \text{ \AA}^2$ , consistent with previous reports.<sup>79-82</sup> Virtually the same IMS behavior was seen for fractions I-III (Figure 5-5A-D, Table 5-2). These native ESI data reaffirm that CT-induced oxidation does *not* induce large-scale global alterations of the protein structure, although minor perturbations are known to take place.<sup>54,63</sup> Our IMS data are quite different from those of a recent report<sup>55</sup> where it was concluded that oxidative modifications cause a significant compaction of cyt *c*. The IMS data of ref. 55 showed multiple peaks for both unmodified and oxidized cyt *c*, suggesting that the ions had undergone partial CIU. In contrast, our native ESI-IMS data (and previous studies<sup>79-82</sup>) are dominated by single IMS features, presumably corresponding to solution-like conformations that were not significantly affected by collisional heating. Unfortunately, the IMS data of ref. 55 were not  $\Omega$ -calibrated, rendering a direct comparison with our results difficult.

#### 5.3.5. Gas Phase Stability of CT-cyt *c*.

While the aforementioned IMS experiments avoided collisional excitation, we will now discuss the CIU behavior of the various CT-cyt *c* proteoforms to assess their gas phase stabilities. Similar to unfolding in solution, the extent of structural perturbation in these CIU experiments can be expressed as a fraction unfolded ( $F_{u\_vac}$ , Equation (5.3)). IMS/MS is capable of tracking the IMS profiles of each individual MetO and LysCHO species (see below). In contrast, the solution unfolding experiments of Figure 5-3 could only probe the behavior of fractions I-III in a MetO-averaged fashion. To allow a direct comparison with those solution data, we initially compiled MetO-averaged CIU data (Figure 5-5).

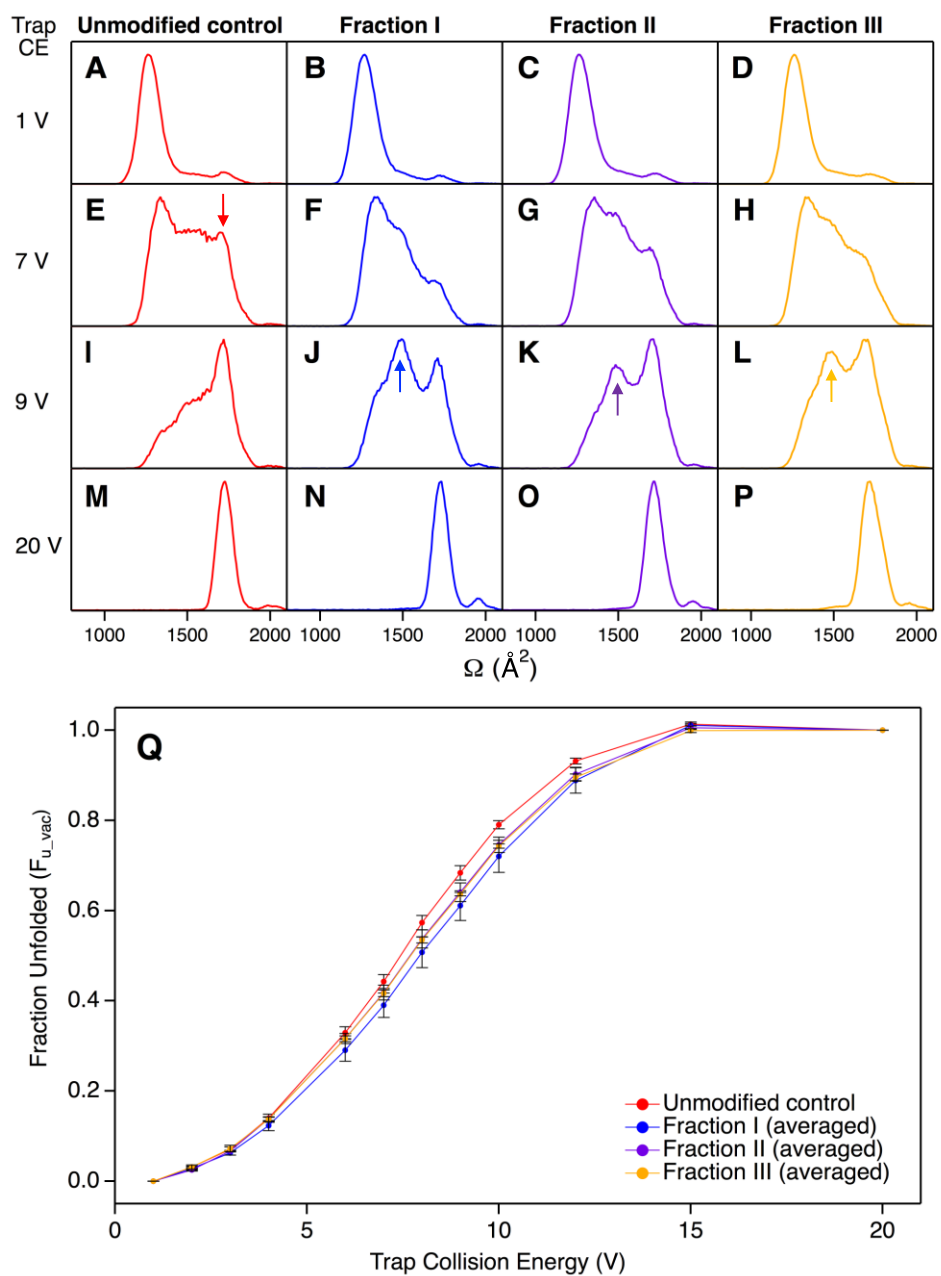


**Figure 5-5.** CIU of unmodified *cyt c* and CT-*cyt c* fractions I-III for 8+ ions generated by native ESI. The data shown here represent an average of all the MetO isoforms in each fraction. (A-P) IMS profiles acquired at different trap collision energy (Trap CE) values, as indicated along the left. Arrows indicate notable features that are discussed in the text. (Q) CIU unfolding profiles for each type of sample, expressed as  $F_{u\_vac}$ .



**Table 5-2.** Collision cross sections ( $\Omega$ ) measured for unmodified *cyt c* and CT-*cyt c* under various conditions. All values in  $\text{\AA}^2$  are for 8+ ions generated by native ESI.

<b>Unmod control</b>	1347	$\pm$	10	<b>MetO-averaged <math>\Omega</math></b>
<b>Fraction I</b>	1348	$\pm$	15	
<b>Fraction II</b>	1337	$\pm$	5	
<b>Fraction III</b>	1347	$\pm$	8	

		<b>MetO (+16 Da)</b>						<b>Native <math>\Omega</math></b>		
		0		1		2				
<b>LysCHO (-1 Da)</b>	0	1347	$\pm$	10	1351	$\pm$	15	1348	$\pm$	15
	1	1345	$\pm$	6	1343	$\pm$	6	1337	$\pm$	6
	2	1358	$\pm$	7	1354	$\pm$	8	1347	$\pm$	8

		<b>MetO (+16 Da)</b>						<b>Unfolded <math>\Omega</math> (after CIU)</b>		
		0		1		2				
<b>LysCHO (-1 Da)</b>	0	1729	$\pm$	4	1732	$\pm$	3	1735	$\pm$	3
	1	1720	$\pm$	3	1724	$\pm$	4	1726	$\pm$	4
	2	1724	$\pm$	2	1725	$\pm$	2	1724	$\pm$	3

Raising the collision energy from 1 V to 20 V resulted in significant gas phase unfolding for all 8+ species, transforming the “native” ( $\sim 1350 \text{ \AA}^2$ ) IMS distributions into unimodal profiles centered at  $\sim 1730 \text{ \AA}^2$  (Figure 5-5, Table 5-2). Although the  $\langle \Omega \rangle$  values of CT-cyt *c* at the lowest and highest collision energies were very similar to the unmodified protein, there were clear differences in the intermediate energy regime. At 7 V all of the IMS profiles had maxima around  $1400 \text{ \AA}^2$ . In addition, the unmodified control exhibited a major feature at  $\sim 1700 \text{ \AA}^2$ , which is close to the fully unfolded protein (marked by the red arrow in Figure 5-5E). This unfolded feature was also seen for fractions I-III, but at much lower intensities (Figure 5-5F-H). Upon raising the collision energy to 9V the IMS distribution of the unmodified control was completely dominated by this  $\sim 1700 \text{ \AA}^2$  feature (Figure 5-5I), while more compact conformers (around  $1500 \text{ \AA}^2$ ) persisted for fractions I-III (see arrows in Figure 5-5J-L). No major differences are seen when comparing the CIU data for fractions I-III among each other.

Overall, our data reveal that the unmodified control protein is more susceptible to CIU than fractions I-III. This effect is also apparent from the  $F_{u\_vac}$  profiles (Figure 5-5Q) which have a midpoint at 0.5 V – 1 V lower collision energies for unmodified cyt *c* than for fraction I-III. Based on these  $F_{u\_vac}$  profiles alone it might be difficult to discern the differences between unmodified cyt *c* and fractions I-III; however, the dissimilarities seen in the IMS distribution for intermediate collision energies are striking (Figure 5-5E-L). The observed oxidation-induced *stabilization* of cyt *c* in the gas phase (Figure 5-5) contrasts the *destabilization* observed in solution (Figure 5-3).

### 5.3.6. Proteoform-Resolved CIU Analysis.

More detailed insights into the role of each modification can be obtained by extracting IMS profiles of individual proteoforms. The three MetO variants are separable by their mass differences (+0, +16, +32 Da), while the LysCHO variants (0, -1, -2 Da) can be resolved using SCX fractionation. To facilitate the following discussion, we will identify proteoforms as  $KmMn$ , where  $m$  and  $n$  are the number of LysCHO and MetO, respectively. For example, K0M0 represents unmodified cyt *c*, while K2M1 refers to the proteoform containing 2 LysCHO and 1 MetO.

To investigate the effects of MetO in the absence of LysCHO modifications we probed the K0M $n$  series ( $n = 0, 1, 2$ , Figure 5-6). At intermediate collision energies, both K0M1 and K0M2 had structures that were significantly more compact than for K0M0, evident from the features highlighted with arrows in Figure 5-6D-I. Also, the midpoints of the K0M1 and K0M2 CIU profiles are  $\sim 1$  V higher than that of K0M0, while the former two are virtually superimposable (Figure 5-6M). From these data it can be concluded that oxidation of Met80 (in K0M1) enhances the gas phase stability of the protein, while the additional oxidation of Met65 (in K0M2) has no discernible effect.

A similar analysis was conducted to investigate the effects of LysCHO modifications by focusing on the  $KmM1$  series ( $m = 0, 1, 2$ , Figure 5-7). The IMS distributions (Figure 5-7A-L) and CIU profiles (Figure 5-7M) for these three species were very similar across all collision energies, suggesting that LysCHO formation only has minor effects on the gas phase stability of cyt *c*. The last aspect is consistent with the behavior in solution (Figure 5-3), where the number of LysCHO also has a negligible effect on stability. This is in stark contrast to MetO formation at residue 80 which greatly affects the properties of cyt *c*, giving rise to opposing stability trends in solution and in the gas phase.

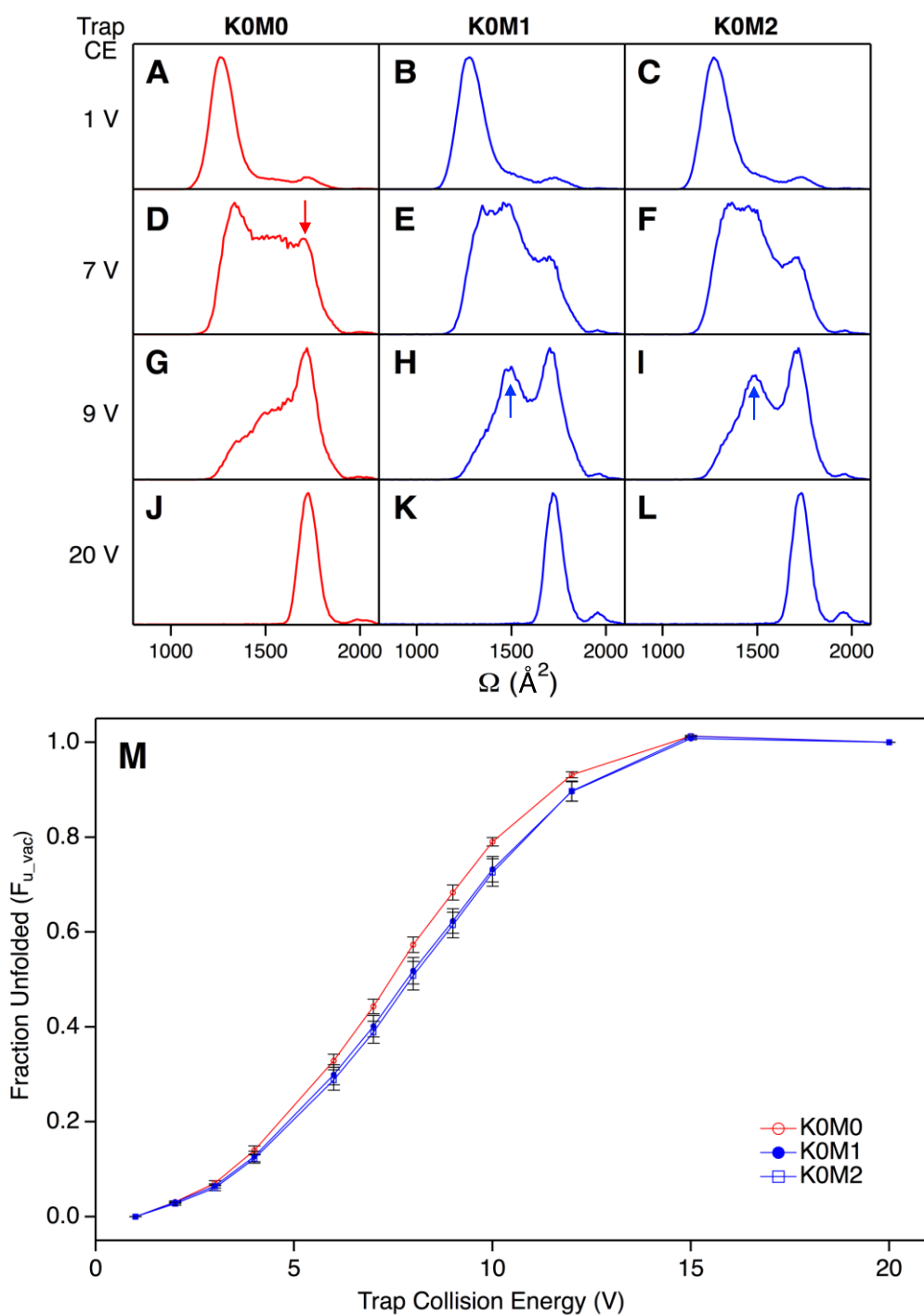


**Figure 5-6.** CIU of KOM $n$  proteoforms (zero LysCHO;  $n = 0, 1, 2$  MetO) for 8+ ions generated by native ESI. (A-L) IMS profiles for each sample at different trap collision energies. (M) CIU unfolding profiles.

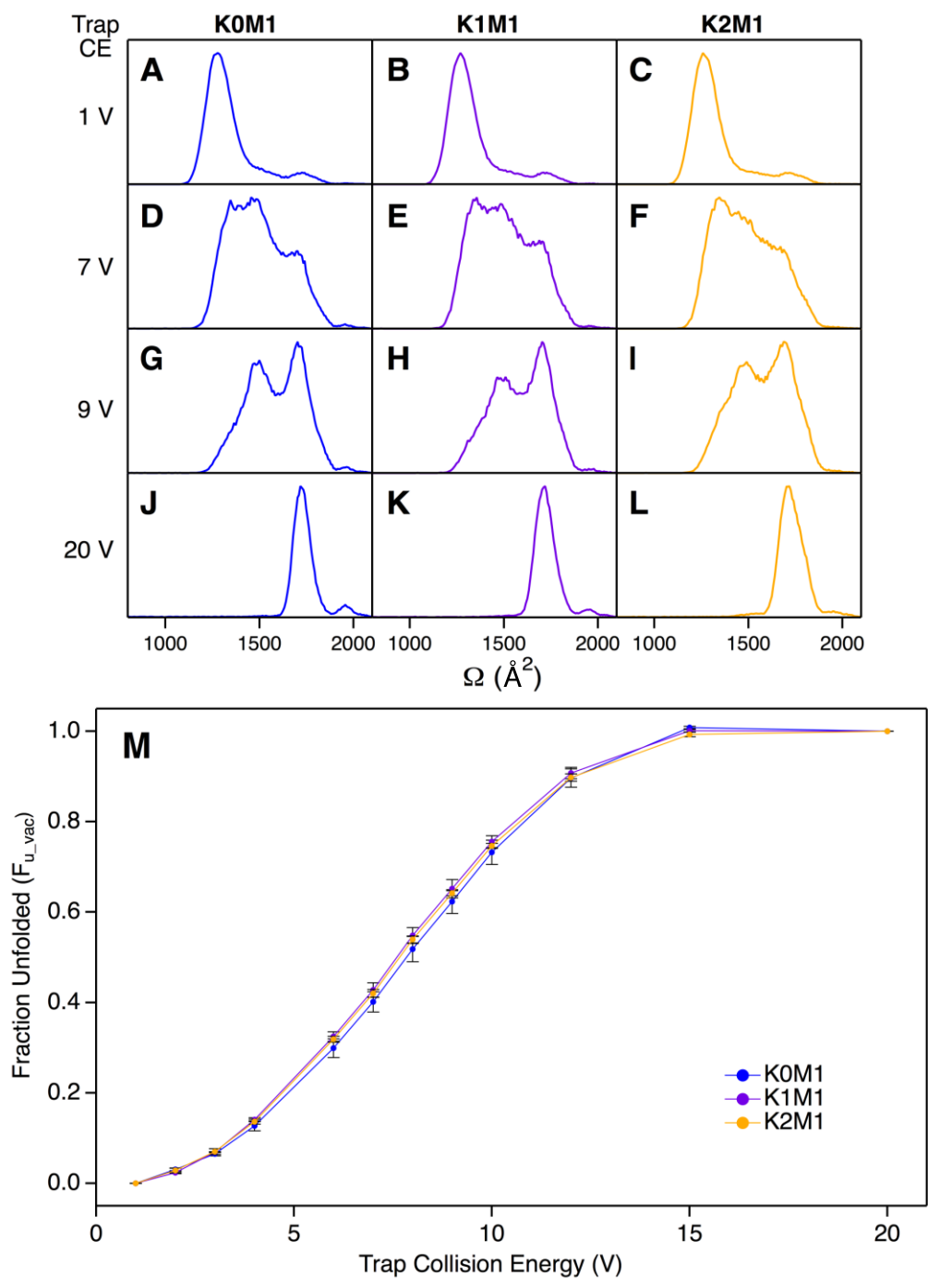


**Figure 5-7.** CIU of  $K_mM_1$  proteoforms ( $m = 0, 1, 2$  LysCHO; 1 MetO) for 8+ ions generated by native ESI. (A-L) IMS profiles for each sample at different trap collision energies. (M) CIU unfolding profiles.

## 5.4. Conclusions

Our results reveal that CT-induced oxidation affects the cyt *c* stability in solution and in the gas phase quite differently. In solution, CT-cyt *c* has a melting point that is ~5 °C lower than that of unmodified cyt *c*, implying large-scale destabilization. In the gas phase, oxidative modifications cause a small but distinct stabilization, evident from a ~1 V shift to higher CIU voltages. Our results indicate that both of these effects can be attributed largely to MetO formation of Met80, a residue that is deeply buried and represents the distal heme ligand in the native state.<sup>74</sup> The effects of other CT-induced oxidative modifications on protein stability are less pronounced (MetO formation at Met65, and LysCHO formation at Lys72/73 and Lys53/55). The lack of major changes following modification of these other sites is consistent with their solvent-exposed locations which allow covalent modifications to be accommodated without disrupting the side chain packing in the core (Figure 5-1A).

The observation that Met80 oxidation reduces the protein stability in *solution* is consistent with a wide range of observations on other oxidatively modified proteins, reflecting the fact that oxidation events usually perturb steric interactions, polarity, hydrophobicity, etc.<sup>15,18,25-28</sup> In cyt *c* the conversion of Met80 to MetO additionally ruptures the distal Met-Fe bond.<sup>47,51,53-54</sup> It seems surprising, therefore, that this modification would render the protein more resilient to CIU in the gas phase. One possible explanation is the formation of new bonds after conversion of Met80 to MetO. Recent work has shown that the partially positive sulfur atom in MetO can noncovalently bind to the partially negative  $\pi$  electron clouds of aromatic rings.<sup>83</sup> Several aromatic residues are relatively close to Met80 (Trp59, Tyr67, Phe82, Figure 5-1B), and thus it seems conceivable that the enhanced gas phase stability could be rooted in newly formed contacts of MetO with one of these sites. Interestingly, computer simulations predict that such MetO-aromatic contacts will be disfavored in water.<sup>84</sup> This could explain our observation of MetO-induced destabilization in solution vs. stabilization in the gas phase.

It is also somewhat surprising that Lys carbonylation does not have a destabilizing effect in the gas phase, keeping in mind the role of strengthened electrostatic contacts *in vacuo* and the likely involvement of Lys<sup>+</sup> in salt bridges at the protein surface.<sup>46</sup> It is possible that the loss of basic sites due to LysCHO formation is compensated by other factors, such as dipole interactions of -CHO sites with positively charged moieties on the protein surface.

Overall, the results of this work highlight the fact that protein stability trends observed in solution are not always mirrored by the corresponding gaseous ions, consistent with the findings of several previous studies.<sup>44-46</sup> Investigating the origin of these different trends offers exciting opportunities to better understand the complex interplay of electrostatic and other noncovalent contacts in native and covalently modified proteins. It is hoped that future comparative solution/gas phase investigations will provide further insights into the molecular foundation of oxidation-induced alterations on protein function and stability.

## 5.5. References

- (1) Covey, T. R.; Thomson, B. A.; Schneider, B. B., *Mass Spectrom. Rev.* **2009**, *28*, 870-897.
- (2) Fenn, J. B., *Angew. Chem. Int. Ed.* **2003**, *42*, 3871-3894.
- (3) Karas, M.; Hillenkamp, F., *Anal. Chem.* **1988**, *60*, 2299-2301.
- (4) Frey, B. L.; Damon, D. E.; Badu-Tawiah, A. K., *Mass Spectrom. Rev.* **2020**, *in press*.
- (5) Brown, H. M.; Pirro, V.; Cooks, R. G., *Clin. Chem.* **2018**, *64* (4), 628-630.
- (6) Susa, A. C.; Lippens, J. L.; Xia, Z.; Loo, J. A.; Campuzano, I. D. G.; Williams, E. R., *J. Am. Soc. Mass Spectrom.* **2018**, *29* (203-206).
- (7) Chorev, D. S.; Baker, L. A.; Wu, D.; Beilsten-Edmands, V.; Rouse, S. L.; Zeev-Ben-Mordehai, T.; Jiko, C.; Samsudin, F.; Gerle, C.; Khalid, S.; Stewart, A. G.; Matthews, S. J.; Gruenewald, K.; Robinson, C. V., *Science* **2018**, *362* (6416), 829-834.
- (8) Peacock, P. M.; Zhang, W. J.; Trimpin, S., *Anal. Chem.* **2017**, *89* (1), 372-388.
- (9) Fersht, A. R., *Structure and Mechanism in Protein Science*. W. H. Freeman & Co.: New York, 1999.
- (10) Balchin, D.; Hayer-Hartl, M.; Hartl, F. U., *Science* **2016**, *353* (6294), 42.
- (11) Winkler, J. R.; Gray, H. B., *Q. Rev. Biophys.* **2015**, *48* (4), 411-420.
- (12) Nimse, S. B.; Pal, D., *RSC Adv.* **2015**, *5* (35), 27986-28006.
- (13) Kathiresan, M.; English, A. M., *Chem. Sci.* **2017**, *8* (2), 1152-1162.
- (14) Dalle-Donne, I.; Rossi, R.; Giustarini, D.; Milzani, A.; Colombo, R., *Clin. Chim. Acta* **2003**, *329*, 23-38.
- (15) Sigalov, A. B.; Stern, L. J., *Chem. Phys. Lipids* **2001**, *113* (1-2), 133-146.
- (16) Mo, J. J.; Yan, Q. R.; So, C. K.; Soden, T.; Lewis, M. J.; Hu, P., *Anal. Chem.* **2016**, *88* (19), 9495-9502.
- (17) Strickland, E. C.; Geer, M. A.; Tran, D. T.; Adhikari, J.; West, G. M.; Dearmond, P. D.; Xu, Y.; Fitzgerald, M. C., *Nat. Protocols* **2012**, *8* (1), 148-61.
- (18) Buecheler, J. W.; Winzer, M.; Weber, C.; Gieseler, H., *J. Pharm. Sci.* **2019**, *108* (3), 1236-1245.



- (19) Xu, G.; Chance, M. R., *Chem. Rev.* **2007**, *107*, 3514-3543.
- (20) Saladino, J.; Liu, M.; Live, D.; Sharp, J. S., *J. Am. Soc. Mass Spectrom.* **2009**, *20*, 1123-1126.
- (21) de Graff, A. M. R.; Hazoglou, M. J.; Dill, K. A., *Structure* **2016**, *24* (2), 329-336.
- (22) Pedersen, J. T.; Chen, S. W.; Borg, C. B.; Ness, S.; Bahl, J. M.; Heegaard, N. H. H.; Dobson, C. M.; Hemmingsen, L.; Cremades, N.; Teilum, K., *J. Am. Chem. Soc.* **2016**, *138* (12), 3966-3969.
- (23) Sultana, R.; Boyd-Kimball, D.; Poon, H. F.; Cai, J.; Pierce, W. M.; Klein, J. B.; Markesbery, W. R.; Zhou, X. Z.; Lu, K. P.; Butterfield, D. A., *Neurobiol. Aging* **2006**, *27* (7), 918-925.
- (24) Bonnington, L.; Lindner, I.; Gilles, U.; Kailich, T.; Reusch, D.; Bulau, P., *Anal. Chem.* **2017**, *89* (16), 8233-8237.
- (25) Mulinacci, F.; Capelle, M. A. H.; Gurny, R.; Drake, A. F.; Arvinte, T., *J. Pharm. Sci.* **2011**, *100* (2), 451-463.
- (26) Jayaraman, S.; Gantz, D. L.; Gursky, O., *Biochemistry* **2008**, *47* (12), 3875-3882.
- (27) Walker, E. J.; Bettinger, J. Q.; Welle, K. A.; Hryhorenko, J. R.; Ghaemmaghami, S., *Proc. Natl. Acad. Sci. U. S. A.* **2019**, *116* (13), 6081-6090.
- (28) Kim, Y. H.; Berry, A. H.; Spencer, D. S.; Stites, W. E., *Protein Eng.* **2001**, *14* (5), 343-347.
- (29) Greenfield, N. J., *Anal. Biochem.* **1996**, *235*, 1 - 10.
- (30) Swint, L.; Robertson, A. D., *Protein Sci.* **1993**, *2* (12), 2037-2049.
- (31) Geer, M. A.; Fitzgerald, M. C., *J. Am. Soc. Mass Spectrom.* **2016**, *27*, 233-243.
- (32) Leney, A. C.; Heck, A. J. R., *J. Am. Soc. Mass Spectrom.* **2017**, *28*, 5-13.
- (33) Osterlund, N.; Moons, R.; Ilag, L. L.; Sobott, F.; Graslund, A., *J. Am. Chem. Soc.* **2019**, *141* (26), 10440-10450.
- (34) Kaddis, C. S.; Loo, J. A., *Anal. Chem.* **2007**, *79*, 1779-1784.
- (35) Ashcroft, A. E., *J. Am. Soc. Mass Spectrom.* **2010**, *21*, 1087-1096.
- (36) Harvey, S. R.; Seffernick, J. T.; Quintyn, R. S.; Song, Y.; Ju, Y.; Yan, J.; Sahasrabudde, A. N.; Norris, A.; Zhou, M. W.; Behrman, E. J.; Lindert, S.; Wysocki, V. H., *Proc. Natl. Acad. Sci. U. S. A.* **2019**, *116* (17), 8143-8148.

- (37) Clemmer, D. E.; Jarrold, M. F., *J. Mass Spectrom.* **1997**, *32*, 577-592.
- (38) Zhong, Y.; Han, L.; Ruotolo, B. T., *Angew. Chem.* **2014**, *53* (35), 9209-12.
- (39) Nouchikian, L.; Lento, C.; Donovan, K. A.; Dobson, R. C.; Wilson, D. J., *Journal of the American Society for Mass Spectrometry* **2020**, *31* (3), 685-692.
- (40) Donor, M. T.; Shepherd, S. O.; Prell, J. S., *J. Am. Soc. Mass Spectrom.* **2020**, *31* (3), 602-610.
- (41) Tesic, M.; Wicki, J.; Poon, D., K. Y.; Withers, S. G.; Douglas, D. J., *J. Am. Soc. Mass Spectrom.* **2007**, *18*, 64-73.
- (42) Hopper, J. T. S.; Oldham, N. J., *J. Am. Soc. Mass Spectrom.* **2009**, *20*, 1851-1858.
- (43) Liu, L.; Michelsen, K.; Kitova, E. N.; Schnier, P. D.; Klassen, J. S., *J. Am. Chem. Soc.* **2012**, *134* (6), 3054-3060.
- (44) Wolynes, P. G., *Proc. Natl. Acad. Sci. U.S.A.* **1995**, *92*, 2426-2427.
- (45) Peschke, M.; Verkerk, U. H.; Kebarle, P., *J. Am. Soc. Mass Spectrom.* **2004**, *15*, 1424-1434.
- (46) Yin, S.; Xie, Y.; Loo, J. A., *J. Am. Soc. Mass Spectrom.* **2008**, *19*, 1199-1208.
- (47) Chen, Y.-R.; Deterding, L. J.; Sturgeon, B. E.; Tomer, K. B.; Mason, R. P., *J. Biol. Chem.* **2002**, *277* (33), 29781-29791.
- (48) Lushington, G. H.; Cowley, A. B.; Silchenko, S.; Lukat-Rodgers, G. S.; Rodgers, K. R.; Benson, D. R., *Inorg. Chem.* **2003**, *42* (23), 7550-7559.
- (49) Wang, Z.; Ando, Y.; Nugraheni, A. D.; Ren, C.; Nagao, S.; Hirota, S., *Mol. Biosyst.* **2014**, *10* (12), 3130-3137.
- (50) Birk, A. V.; Chao, W. M.; Liu, S. Y.; Soong, Y.; Szeto, H. H., *Biochim. Biophys. Acta* **2015**, *1847* (10), 1075-1084.
- (51) Capdevila, D. A.; Marmisolle, W. A.; Tomasina, F.; Demicheli, V.; Portela, M.; Radi, R.; Murgida, D. H., *Chem. Sci.* **2015**, *6* (1), 705-713.
- (52) Nugraheni, A. D.; Ren, C. G.; Matsumoto, Y.; Nagao, S.; Yamanaka, M.; Hirota, S., *J. Inorg. Biochem.* **2018**, *182*, 200-207.
- (53) Parakra, R. D.; Kleffmann, G. N. L.; Jameson, T.; Ledgerwood, E. C., *Dalton Trans.* **2018**, *47*, 9128-9135.
- (54) Zhong, F.; Pletneva, E. V., *Inorg. Chem.* **2018**, *57* (10), 5754-5766.

- (55) Chea, E. E.; Deredge, D. J.; Jones, L. M., *Biophys. J.* **2020**, *118* (1), 128-137.
- (56) Baraye, U.; Lange, M.; Mendez, L.; Arnhold, J.; Shadyro, O. I.; Fedorova, M.; Flemmig, J., *J. Biol. Chem.* **2019**, *294* (6), 1816-1830.
- (57) Alvarez-Paggi, D.; Hannibal, L.; Castro, M. A.; Oviedo-Rouco, S.; Demicheli, V.; Tórtora, V.; Tomasina, F.; Radi, R.; Murgida, D. H., *Chem. Rev.* **2017**, *117* (21), 13382-13460.
- (58) Veitch, N. C., *Phytochem.* **2004**, *65*, 249-259.
- (59) McClelland, L. J.; Mou, T.-C.; Jeakins-Cooley, M. E.; Sprang, S. R.; Bowler, B. E., *Proc. Natl. Acad. Sci. U.S.A.* **2014**, *111* (18), 6648-6653.
- (60) Kitt, J. P.; Bryce, D. A.; Minter, S. D.; Harris, J. M., *J. Am. Chem. Soc.* **2017**.
- (61) Oemer, G.; Lackner, K.; Muigg, K.; Krumschnabel, G.; Watschinger, K.; Sailer, S.; Lindner, H.; Gnaiger, E.; Wortmann, S. B.; Werner, E. R.; Zschocke, J.; Keller, M. A., *Proc. Natl. Acad. Sci. U.S.A.* **2018**, *115* (16), 4158-4163.
- (62) Belikova, N. A.; Vladimirov, Y. A.; Osipov, A. N.; Kapralov, A. A.; Tyurin, V. A.; Potapovich, M. V.; Basova, L. V.; Peterson, J.; Kurnikov, I. V.; Kagan, V. E., *Biochemistry* **2006**, *45* (15), 4998-5009.
- (63) Yin, V.; Mian, S. H.; Konermann, L., *Chem. Sci.* **2019**, *10*, 2349-2359.
- (64) Yin, V.; Shaw, G. S.; Konermann, L., *J. Am. Chem. Soc.* **2017**, *139*, 15701–15709.
- (65) Mushran, S. P.; Agrawal, M. C.; Prasad, B., *J. Chem. Soc. B* **1971**, *0* (8), 1712-1714.
- (66) Bachi, A.; Dalle-Donne, I.; Scaloni, A., *Chem. Rev.* **2013**, *113* (1), 596-698.
- (67) Møller, I. M.; Rogowska-Wrzesinska, A.; Rao, R. S. P., *J. Proteomics* **2011**, *74* (11), 2228-2242.
- (68) Yang, Y.; Stella, C.; Wang, W. R.; Schoneich, C.; Gennaro, L., *Anal. Chem.* **2014**, *86* (10), 4799-4806.
- (69) Konermann, L., Protein Unfolding and Denaturants. In *Encyclopedia of Life Sciences (eLS)*, John Wiley & Sons, Ltd: Chichester, 2012.
- (70) Haynes, S. E.; Polasky, D. A.; Dixit, S. M.; Majmudar, J. D.; Neeson, K.; Ruotolo, B. T.; Martin, B. R., *Anal. Chem.* **2017**, *89* (11), 5669-5672.
- (71) Sun, Y.; Vahidi, S.; Sowole, M. A.; Konermann, L., *J. Am. Soc. Mass Spectrom.* **2016**, *27*, 31-40.

- (72) Bagel'ova, J.; Antalík, M.; Tomori, Z., *Biochem. Mol. Biol. Int.* **1997**, *43* (4), 891-900.
- (73) Kuroda, Y.; Kidokoro, S.; Wada, A., *J. Mol. Biol.* **1992**, *223*, 1139-1153.
- (74) Bushnell, G. W.; Louie, G. V.; Brayer, G. D., *J. Mol. Biol.* **1990**, *214*, 585-595.
- (75) de la Mora, F. J., *Anal. Chim. Acta* **2000**, *406*, 93-104.
- (76) Kebarle, P.; Verkerk, U. H., *Mass Spectrom. Rev.* **2009**, *28*, 898-917.
- (77) Konermann, L.; Metwally, H.; Duez, Q.; Peters, I., *Analyst* **2019**, *144*, 6157-6171.
- (78) Kaltashov, I. A.; Mohimen, A., *Anal. Chem.* **2005**, *77*, 5370-5379.
- (79) Mao, Y.; Woenckhaus, J.; Kolafa, J.; Ratner, M. A.; Jarrold, M. F., *J. Am. Chem. Soc.* **1999**, *121* (12), 2712-2721.
- (80) Allen, S. J.; Schwartz, A. M.; Bush, M. F., *Anal. Chem.* **2013**, *85*, 12055–12061.
- (81) Theisen, A.; Black, R.; Corinti, D.; Brown, J. M.; Bellina, B.; Barran, P. E., *J. Am. Soc. Mass Spectrom.* **2019**, *30* (1), 24-33.
- (82) Zhao, Q.; Schieffer, G. M.; Soyk, M. W.; Anderson, T. J.; Houk, R. S.; Badman, E. R., *J. Am. Soc. Mass Spectrom.* **2010**, *21* (7), 1208-1217.
- (83) Lewis, A. K.; Dunleavy, K. M.; Senkow, T. L.; Her, C.; Horn, B. T.; Jersett, M. A.; Mahling, R.; McCarthy, M. R.; Perell, G. T.; Valley, C. r. C.; Karim, C. B.; Gao, J.; Pomerantz, W. C. K.; Thomas, D. D.; Cembran, A.; Hinderliter, A.; Sachs, J. N., *Nat. Chem. Biol.* **2016**, *12* (10), 860-866.
- (84) Orabi, E. A.; English, A. M., *Phys. Chem. Chem. Phys.* **2018**, *20* (35), 23132-23141.

## Chapter 6. Summary and Future Work

### 6.1. Summary

The peroxidase activity of cyt *c* plays a critical role in triggering programmed cell death (apoptosis). However, the hexacoordinated heme cofactor present in native cyt *c* should render this activity impossible. Despite the central biological importance of this peroxidase function, the molecular mechanisms underlying this structural paradox are poorly understood. The work detailed in this dissertation fills this knowledge gap by deciphering the central role of protein oxidative modifications and their associated structural changes in activating the peroxidase function of cyt *c*.

In Chapter 2, the critical role of *in situ* structural changes in triggering the peroxidase activity of cyt *c* was uncovered. These changes were triggered by multiple oxidative modifications induced by H<sub>2</sub>O<sub>2</sub>. Using top-down MS, we established that the initial oxidative modifications occur sequentially, yielding a stepwise model to peroxidase activation. A key modification in this capacity was the oxidation of Lys into its corresponding aldehyde (LysCHO).

In Chapter 3, we extensively characterized the oxidized cyt *c* proteoforms produced by treatment with CT. We discovered that this purportedly well-characterized model system represents a mixture of structurally and functionally distinct proteoforms that differ primarily by the extent of LysCHO formation at key sites.

In Chapter 4, we established the causal factors underlying the observed specificity in the formation of LysCHO and other oxidative modifications by comparing the oxidation behaviour of cyt *c* with its heme-free counterpart (apo-cyt *c*). These experiments revealed that LysCHO is formed by heme-mediated catalysis, while other modifications (e.g. MetO) proceed via direct interaction with the oxidant.

In Chapter 5, we utilized CT-treated cyt *c* as a model system to test the compatibility of protein stability measurements in the gas phase to their counterparts in solution. Unlike many other reported systems, for which good qualitative agreement was observed, we discovered that oxidized cyt *c* shows opposite stability trends in the gas phase and in solution.

## 6.2. Future Work

### 6.2.1. Peroxidase Activation *In Vivo*

The work described in Chapter 2 and Chapter 3 constitutes *in vitro* approaches to studying the peroxidase activation of cyt *c* that were designed to emulate oxidative conditions present *in vivo*, such as those at the onset of apoptosis and other biological states.<sup>1,2</sup> While some previous studies have attempted to directly map how cyt *c* may be modified by ROS *in vivo*, such reports remain scarce, and structural details remain lacking.<sup>3</sup> To the best of our knowledge, there does not yet exist any systematic reports detailing the types of oxidized proteoforms cyt *c* may form *in vivo*.

It is interesting to note that studies of cyt *c* and apoptosis in a cellular context commonly employ protein immunoblotting (i.e. Western blotting) using anti-cyt *c* antibodies.<sup>4-6</sup> It is unclear whether these antibodies possess sufficient specificity to differentiate unmodified cyt *c* from its oxidized variants. The presence of oxidized cyt *c* proteoforms *in vivo* may explain some unusual observations in the literature. For example, Ott and coworkers reported that cyt *c* in mitochondria exists in two “pools”, which differ by the strength of their interaction to the inner mitochondrial membrane.<sup>7</sup> The first pool could be dislodged by increasing ionic strength, while the second pool required both increasing ionic strength and addition of an oxidizing agent. While the authors attributed this behaviour to the existence of two distinct cyt *c* conformers, it seems plausible that the first “pool” may instead correspond to oxidatively modified cyt *c*. The MS-based experiments described in this dissertation would be amenable to analyze these potential protein variants.

### 6.2.2. Cyt *c* / Cardiolipin Interactions

Interactions between cyt *c* and the membrane lipid cardiolipin (CL) play a key role in the apoptosis-triggering function of cyt *c*.<sup>8-11</sup> CL is thought to be the primary target of the peroxidase activity of cyt *c* that initiates apoptosis. Although a large body of work has attempted to uncover how cyt *c* interacts with CL,<sup>12-18</sup> the precise nature of 1) how cyt *c* binds to CL, and 2) how (and if) the structure of cyt *c* changes in response to CL binding remains contentious. A major hurdle to the structural elucidation of the cyt *c* / CL complex is that the “complex” is likely a mixture of multiple conformations and/or binding modes, rendering spectroscopic characterization difficult.<sup>13</sup> MS-based experiments, particularly HDX-MS, may be an alternative technique to study these conformational ensembles.<sup>19</sup> The multiple protein conformations may be discernable via HDX-MS by the appearance of multiple isotopic envelopes following deuterium labeling. Moreover, as ligand-binding commonly manifests itself as a decrease in the rate of exchange, HDX-MS could also elucidate the locations of the CL binding site(s).

Given our elucidation of an H<sub>2</sub>O<sub>2</sub>-induced pathway of peroxidase activation<sup>1</sup> (Chapter 2), an alternative question could be: how does CL binding affect the oxidative modifications induced by H<sub>2</sub>O<sub>2</sub>? Recent work by Barayeu and coworkers using bottom-up MS found that cyt *c* is extensively oxidatively modified by H<sub>2</sub>O<sub>2</sub> in the presence of CL.<sup>20</sup> However, the direct link between these reported modifications and their effects on peroxidase activity currently remains unknown. Top-down MS of the cyt *c*/CL/H<sub>2</sub>O<sub>2</sub> system would provide insight on the interplay between these factors.

### 6.2.3. Oxidation Mapping in Other Systems

The work described in Chapter 4 describes the causal factors behind the origin of specific oxidative modification products such as LysCHO. Due to the difficulty of detecting LysCHO by the standard bottom-up MS approach, it seems possible that LysCHO is a general, underreported protein oxidative modification that is also produced by other oxidation sources (e.g. direct ·OH attack). However, this remains to be verified experimentally. Experiments described in this dissertation (e.g. GRT labeling) would aid

in the detection of such species. The verification of LysCHO formation is of particular importance for techniques that require accurate quantitation of all oxidative modification products, such as hydroxyl radical-based protein footprinting.<sup>21,22</sup>

Bottom-up MS is currently the *de facto* standard for identifying protein oxidative modifications.<sup>21-23</sup> However, the current dissertation demonstrates the feasibility of top-down MS approaches for this task, even for complex mixtures of oxidized proteoforms. The primary advantage of top-down MS is the ability to detect modifications at the proteoform level, allowing any correlations between the various modifications to be directly observed. We anticipate that this will be particularly impactful for studying oxidative damage pathways in proteins.<sup>24-28</sup> Top-down MS would allow these pathways to be directly mapped via the observed distributions of oxidized proteoforms. Moreover, information such as the temporal relationships between the pathways (or even of specific modifications along each pathway) can in theory be readily obtained.

Another application of top-down MS that we envision is for time-resolved hydroxyl-radical based protein footprinting. Techniques such as Fast Photochemical Oxidation of Proteins (FPOP) rely on rapid labeling (ideally in the  $\mu\text{s}$  regime) to footprint rapid kinetic processes such as protein folding.<sup>29-31</sup> Two prominent challenges in these experiments are 1) controlling the labeling timescales such that only the transient species of interest is being footprinted, and 2) ensuring the protein is only labeled once to minimize label-induced structural perturbations (“single-shot” labeling). While much work has been invested at addressing these challenges (e.g. radical scavengers, rapid-mixing, single-pulse lasers), their success has been controversial.<sup>32</sup> Top-down MS has the capacity to resolve proteoforms with different extents of oxidative labeling by their different masses. Using top-down MS, single-shot conditions could in theory be guaranteed, irrespective of labeling kinetics, by selecting only the singly-labeled proteoforms for analysis. The top-down MS work described in this dissertation set the stage for such proteoform-resolved oxidation experiments.



### 6.3. References

- (1) Yin, V.; Shaw, G. S.; Konermann, L. *J. Am. Chem. Soc.* **2017**, *139* (44), 15701–15709.
- (2) Yin, V.; Mian, S. H.; Konermann, L. *Chem. Sci.* **2019**, *10* (8), 2349–2359.
- (3) Birk, A. V.; Chao, W. M.; Liu, S. Y.; Soong, Y.; Szeto, H. H. *Biochim. Biophys. Acta-Bioenerg.* **2015**, *1847* (10), 1075–1084.
- (4) Liu, X.; Kim, C. N.; Yang, J.; Jemmerson, R.; Wang, X. *Cell* **1996**, *86* (1), 147–157.
- (5) Goshorn, S. C.; Retzel, E.; Jemmerson, R. *J. Biol. Chem.* **1991**, *266* (4), 2134–2142.
- (6) Godoy, L. C.; Muñoz-Pinedo, C.; Castro, L.; Cardaci, S.; Schonhoff, C. M.; King, M.; Tórtora, V.; Marín, M.; Miao, Q.; Jiang, J. F.; Kapralov, A.; Jemmerson, R.; Silkstone, G. G.; Patel, J. N.; Evans, J. E.; Wilson, M. T.; Green, D. R.; Kagan, V. E.; Radi, R.; Mannick, J. B. *Proc. Natl. Acad. Sci.* **2009**, *106* (8), 2653–2658.
- (7) Ott, M.; Robertson, J. D.; Gogvadze, V.; Zhivotovsky, B.; Orrenius, S. *Proc. Natl. Acad. Sci.* **2002**, *99* (3), 1259–1263.
- (8) Kagan, V. E.; Tyurin, V. A.; Jiang, J.; Tyurina, Y. Y.; Ritov, V. B.; Amoscato, A. A.; Osipov, A. N.; Belikova, N. A.; Kapralov, A. A.; Kini, V.; Vlasova, I. I.; Zhao, Q.; Zou, M.; Di, P.; Svistunenko, D. A.; Kurnikov, I. V.; Borisenko, G. G. *Nat. Chem. Biol.* **2005**, *1* (4), 223–232.
- (9) Kagan, V. E.; Bayır, H. A.; Belikova, N. A.; Kapralov, O.; Tyurina, Y. Y.; Tyurin, V. A.; Jiang, J.; Stoyanovsky, D. A.; Wipf, P.; Kochanek, P. M.; Greenberger, J. S.; Pitt, B.; Shvedova, A. A.; Borisenko, G. *Free Radic. Biol. Med.* **2009**, *46* (11), 1439–1453.
- (10) Santucci, R.; Sinibaldi, F.; Cozza, P.; Polticelli, F.; Fiorucci, L. *Int. J. Biol. Macromol.* **2019**, *136*, 1237–1246.
- (11) Díaz-Quintana, A.; Pérez-Mejías, G.; Guerra-Castellano, A.; De la Rosa, M. A.; Díaz-Moreno, I. *Oxid. Med. Cell. Longev.* **2020**, *2020*, 6813405.
- (12) Alvarez-Paggi, D.; Hannibal, L.; Castro, M. A.; Oviedo-Rouco, S.; Demicheli, V.; Tórtora, V.; Tomasina, F.; Radi, R.; Murgida, D. H. *Chem. Rev.* **2017**, *117* (21), 13382–13460.
- (13) Hanske, J.; Toffey, J. R.; Morenz, A. M.; Bonilla, A. J.; Schiavoni, K. H.; Pletneva, E. V. *Proc. Natl. Acad. Sci.* **2012**, *109* (1), 125–130.
- (14) Oellerich, S.; Lecomte, S.; Paternostre, M.; Heimburg, T.; Hildebrandt, P. *J. Phys. Chem. B* **2004**, *108* (12), 3871–3878.

- (15) Sinibaldi, F.; Howes, B. D.; Piro, M. C.; Polticelli, F.; Bombelli, C.; Ferri, T.; Coletta, M.; Smulevich, G.; Santucci, R. *JBIC J. Biol. Inorg. Chem.* **2010**, *15* (5), 689–700.
- (16) Milazzo, L.; Tognaccini, L.; Howes, B. D.; Sinibaldi, F.; Piro, M. C.; Fittipaldi, M.; Baratto, M. C.; Pogni, R.; Santucci, R.; Smulevich, G. *Biochemistry* **2017**, *56* (13), 1887–1898.
- (17) Simon, M.; Metzinger-Le Meuth, V.; Chevance, S.; Delalande, O.; Bondon, A. *J. Biol. Inorg. Chem.* **2013**, *18* (1), 27–38.
- (18) O’Brien, E. S.; Nucci, N. V.; Fuglestad, B.; Tommos, C.; Wand, A. J. *J. Biol. Chem.* **2015**, *290* (52), 30879–30887.
- (19) Konermann, L.; Pan, J.; Liu, Y.-H. *Chem. Soc. Rev.* **2011**, *40* (3), 1224–1234.
- (20) Barayeu, U.; Lange, M.; Méndez, L.; Arnhold, J.; Shadyro, O. I.; Fedorova, M.; Flemmig, J. *J. Biol. Chem.* **2019**, *294* (6), 1816–1830.
- (21) Johnson, D. T.; Di Stefano, L. H.; Jones, L. M. *J. Biol. Chem.* **2019**, *294* (32), 11969–11979.
- (22) Xu, G.; Chance, M. R. *Chem. Rev.* **2007**, *107* (8), 3514–3543.
- (23) Møller, I. M.; Rogowska-Wrzesinska, A.; Rao, R. S. P. *J. Proteomics* **2011**, *74* (11), 2228–2242.
- (24) Winkler, J. R.; Gray, H. B. *Q. Rev. Biophys.* **2015**, *48* (04), 411–420.
- (25) Gray, H. B.; Winkler, J. R. *Proc. Natl. Acad. Sci.* **2015**, *112* (35), 10920–10925.
- (26) Weisz, D. A.; Gross, M. L.; Pakrasi, H. B. *Sci. Adv.* **2017**, *3* (11), eaao3013.
- (27) Kathiresan, M.; English, A. M. *Chem. Sci.* **2017**, *8* (2), 1152–1162.
- (28) Kathiresan, M.; English, A. M. *J. Am. Chem. Soc.* **2018**, *140* (38), 12033–12039.
- (29) Hambly, D. M.; Gross, M. L. *J. Am. Soc. Mass Spectrom.* **2005**, *16* (12), 2057–2063.
- (30) Hambly, D.; Gross, M. *Int. J. Mass Spectrom.* **2007**, *259* (1–3), 124–129.
- (31) Vahidi, S.; Stocks, B. B.; Liaghati-Mobarhan, Y.; Konermann, L. *Anal. Chem.* **2013**, *85* (18), 8618–8625.
- (32) Vahidi, S.; Konermann, L. *J. Am. Soc. Mass Spectrom.* **2016**, *27* (7), 1156–1164.

# Appendix I – Permissions



RightsLink®



Home



Help



Email Support



Sign in



Create Account

## Cytochrome c as a Peroxidase: Activation of the Precatalytic Native State by H<sub>2</sub>O<sub>2</sub>-Induced Covalent Modifications



**Author:** Victor Yin, Gary S. Shaw, Lars Konermann

**Publication:** Journal of the American Chemical Society

**Publisher:** American Chemical Society

**Date:** Nov 1, 2017

*Copyright © 2017, American Chemical Society*

### PERMISSION/LICENSE IS GRANTED FOR YOUR ORDER AT NO CHARGE

This type of permission/license, instead of the standard Terms & Conditions, is sent to you because no fee is being charged for your order. Please note the following:

- Permission is granted for your request in both print and electronic formats, and translations.
- If figures and/or tables were requested, they may be adapted or used in part.
- Please print this page for your records and send a copy of it to your publisher/graduate school.
- Appropriate credit for the requested material should be given as follows: "Reprinted (adapted) with permission from (COMPLETE REFERENCE CITATION). Copyright (YEAR) American Chemical Society." Insert appropriate information in place of the capitalized words.
- One-time permission is granted only for the use specified in your request. No additional uses are granted (such as derivative works or other editions). For any other uses, please submit a new request.

[BACK](#)

[CLOSE WINDOW](#)

## Lysine carbonylation is a previously unrecognized contributor to peroxidase activation of cytochrome c by chloramine-T

V. Yin, S. H. Mian and L. Konermann, *Chem. Sci.*, 2019, **10**, 2349

**DOI:** 10.1039/C8SC03624A

This article is licensed under a [Creative Commons Attribution-NonCommercial 3.0 Unported Licence](#). Material from this article can be used in other publications provided that the correct acknowledgement is given with the reproduced material and it is not used for commercial purposes.

Reproduced material should be attributed as follows:

- For reproduction of material from NJC:  
[Original citation] - Published by The Royal Society of Chemistry (RSC) on behalf of the Centre National de la Recherche Scientifique (CNRS) and the RSC.
- For reproduction of material from PCCP:  
[Original citation] - Published by the PCCP Owner Societies.
- For reproduction of material from PPS:  
[Original citation] - Published by The Royal Society of Chemistry (RSC) on behalf of the European Society for Photobiology, the European Photochemistry Association, and RSC.
- For reproduction of material from all other RSC journals:  
[Original citation] - Published by The Royal Society of Chemistry.

Information about reproducing material from RSC articles with different licences is available on our [Permission Requests page](#).

### Probing the Effects of Heterogeneous Oxidative Modifications on the Stability of Cytochrome c in Solution and in the Gas Phase



**Author:** Victor Yin, Lars Konermann

**Publication:** Journal of the American Society for Mass Spectrometry

**Publisher:** American Chemical Society

**Date:** May 1, 2020

*Copyright © 2020, American Chemical Society*

#### PERMISSION/LICENSE IS GRANTED FOR YOUR ORDER AT NO CHARGE

This type of permission/license, instead of the standard Terms & Conditions, is sent to you because no fee is being charged for your order. Please note the following:

- Permission is granted for your request in both print and electronic formats, and translations.
- If figures and/or tables were requested, they may be adapted or used in part.
- Please print this page for your records and send a copy of it to your publisher/graduate school.
- Appropriate credit for the requested material should be given as follows: "Reprinted (adapted) with permission from (COMPLETE REFERENCE CITATION). Copyright (YEAR) American Chemical Society." Insert appropriate information in place of the capitalized words.
- One-time permission is granted only for the use specified in your request. No additional uses are granted (such as derivative works or other editions). For any other uses, please submit a new request.

[BACK](#)

[CLOSE WINDOW](#)

# Curriculum Vitae

1. **NAME:** Victor Yin

2. **EDUCATION:**

<u>Degree</u>	<u>University</u>	<u>Department</u>	<u>Year</u>
Ph. D.	University of Western Ontario	Chemistry	Current
B. Sc. Hon.	University of British Columbia	Chemistry	2015

3. **TA and OTHER RESEARCH or TEACHING RELATED EMPLOYMENT HISTORY:**

<u>Date</u>	<u>Position</u>	<u>Course</u>	<u>Supervisor</u>	<u>Department and Institution</u>
2017	TA	CHEM3370B	K. Baines	Chemistry, UWO
2017	TA	CHEM1302A	J. Mathers	Chemistry, UWO
2016	TA	CHEM3370B	K. Baines	Chemistry, UWO
2016	TA	CHEM1302A	J. Mathers	Chemistry, UWO
2015	TA	CHEM3391B	M. Suchy	Chemistry, UWO
2015	TA	CHEM1302A	J. Mathers	Chemistry, UWO

4. **HONORS AND AWARDS:**

CSC 2004 UWO Student Travel Award, 2018 - \$900  
CSMS Student Travel Award to ASMS, 2018 - \$2000  
Lefevre Medal and Prize in Honours Chemistry (UBC), 2015 - \$500  
Undergraduate Summer Research Award (UBC), 2014 - \$5740

5. **SCHOLARSHIPS RECEIVED:**

<u>Scholarship type and Organization</u>	<u>Years awarded</u>	<u>Amount awarded</u>
Alexander Graham Bell CGS-D (NSERC)	2	\$35000/yr
Queen Elizabeth II GSST 2019	1	\$15000 (Declined)
Queen Elizabeth II GSST 2018	1	\$15000
Ontario Graduate Scholarship 2016,2017	2	\$15000/yr

6. **COURSES TAKEN:**

<u>Date</u>	<u>Course Number and Title</u>	<u>Instructor</u>	<u>Grade</u>
2018	CHEM9494B (Biophysical Chemistry)	L. Konermann	99
2016	CHEM9544A (Mass Spectrometry)	L. Konermann	97
2015	CHEM9522A (Analytical Separations)	K. Yeung	90

## 7. PUBLICATIONS:

Sever, A.; Yin, V.; Konermann, L. Interrogating the Quaternary Structure of Noncanonical Hemoglobin Complexes by Electrospray Mass Spectrometry and Collision-Induced Dissociation. **Submitted.**

Yin, V.; Holzschere, D.; Konermann, L. Delineating Heme-Mediated versus Direct Protein Oxidation in Peroxidase-Activated Cytochrome *c* by Top-Down Mass Spectrometry. **Submitted.**

Yin, V.; Konermann, L. (2020) Probing the Effects of Heterogeneous Oxidative Modifications on the Stability of Cytochrome *c* in Solution and in the Gas Phase. *J. Am. Soc. Mass Spectrom.*, **In Press**. doi: 10.1021/jasms.0c00089.

Yin, V.; Mian, S. H.; Konermann, L., Lysine Carbonylation is a Previously Unrecognized Contributor to Peroxidase Activation of Cytochrome *c* by Chloramine-T. *Chem. Sci.*, **2019**, 10, 2349-2359.

Yin, V.; Shaw, G. S.; Konermann, L., Cytochrome *c* as a Peroxidase: Activation of the Pre-Catalytic Native State by H<sub>2</sub>O<sub>2</sub>-Induced Covalent Modifications. *J. Am. Chem. Soc.*, **2017**, 139, 15701-15709.

McGregor, N.; Yin, V.; Tung, C.-C.; Van Petegem, F.; Brumer, H., Crystallographic insight into the evolutionary origins of xyloglucan endo-transglycosylases and endo-hydrolases. *Plant J.*, **2017**, 89, 651-670. Featured Article.

McGregor, N.; Morar, M.; Fenger, T. H.; Stogios, P.; Lenfant, N.; Yin, V.; Xu, X.; Evdokimova, E.; Cui, H.; Henrissat, B.; Savchenko, A.; Brumer, H., Structure-function analysis of a mixed-linkage Beta-glucanase/xyloglucanase from key ruminal Bacteroidetes *Prevotella bryantii* B14. *J. Biol. Chem.*, **2015**, 291, 1175-1197.

## 8. SELECTED PRESENTATIONS:

Yin, V.\*, Holzschere, D., and Konermann, L. (2019) Delineating Heme-Mediated vs. Direct Protein Oxidation Pathways: Cytochrome *c* as a Model System. 32nd Annual Lake Louise Tandem Mass Spectrometry Workshop. International Conference, Poster Presentation.

Yin, V.\* and Konermann, L. (2019) Cytochrome *c* / Cardiolipin Interactions in Apoptosis: The Roles of Protein Auto-Oxidation and In Situ Covalent Modifications. 67th Annual conference of the American Society of Mass Spectrometry. International Conference, Poster Presentation.

Yin, V.\* and Konermann, L. (2018) Top-down CID-IM-MS Reveals Lysine Carbonylation as a Hidden Activator in the Apoptotic Peroxidase Activity of Met-Oxidized Cytochrome *c*. 31st Annual Lake Louise Tandem Mass Spectrometry Workshop. International Conference, Poster Presentation.

Yin, V.\* and Konermann, L. (2017) Relationship Between Oxidative Modifications and Peroxidase Activity of Cytochrome *c*: A Combined Bottom-up and Top-down Investigation. 30th Annual Lake Louise Tandem Mass Spectrometry Workshop. International Conference, Poster Presentation.

Yin, V\*, Shaw, G., Konermann, L. (2017) Cytochrome *c* As A Peroxidase: Covalent Labeling and Oxidation Site Mapping Uncovers the Mechanism of Catalytic Activation by H<sub>2</sub>O<sub>2</sub>. 65th Annual Conference of the American Society of Mass Spectrometry. International Conference, Poster Presentation.

Yin, V\* and Konermann, L. (2016) Investigating the Effects of *In situ* Oxidation on the Structure and Non-Canonical Functions of Cytochrome *c* using Electrospray Mass Spectrometry. 29th Annual Lake Louise Tandem Mass Spectrometry Workshop. International Conference, Poster Presentation.

Yin, V\* and Konermann, L. (2016) Exploring the Peroxidase Activation and Deactivation of Cytochrome *c* by Heme-catalyzed Oxidative Labeling and ESI-MS. 64th Annual Conference of the American Society of Mass Spectrometry. International Conference, Poster Presentation.

Yin, V\*, McGregor, N., and Brumer, H. (2015) Inhibition of a plant glycoside hydrolase using xyloglucan-derived affinity labels. 29th Annual Western Canadian Undergraduate Chemistry Conference. National Conference, Oral Presentation (Undergraduate Work)